DEPARTMENT OF THE NAVY
NAVAL INTELLIGENCE SUPPORT CENTER
TRANSLATION DIVISION
4301 SUITLAND ROAD
WASHINGTON, D.C. 20390

3

B.S.

CLASSIFICATION: UNCLASSIFIED

APPROVED FOR PUBLIC RELEASE, DISTRIBUTION UNLIMITED

(6)

TITLE: Methods of the Dimensional Analysis and Similarity Theory in Problems of Ship Hydromechanics

(Metody teorii razmernostey i podobiya v zadachakh gidromekhaniki sudov)

AUTHOR(S): Epshteyn, Leonid Abramovich (Epshteyn)

(10)

(21)

PAGES: 234

SOURCE: Translation of Sudostroyeniye [redacted] 1970

[redacted]08

(USSR) P1-297 1976

ORIGINAL LANGUAGE: Russian

TRANSLATOR: C

NISC TRANS[redacted] - 3973

APPROVED: P.T.K.

DATE: 21 Sep[redacted] 1977

(11)

(12) 246 p.

467662

UNCLASSIFIED

NISC 3615/bjp
2 June 1976
C/N 361-76

MEMORANDUM

UNCLASSIFIED

FROM: NISC 30

TO: NISC 60 B

SUBJ: Russian Book "Methods of the Theory of Degrees and Similarity in the Problems of the Hydromechanics of Ships", request for translation

ENCL: (1) "Metody Teorii Razmernostey I Podobiya V Zadachakh Gidromekhaniki Sudov", Leningrad Sudostroyeniya 1970 206 pgs (2 xeroxed copies)

1. Enclosure (1) is forwarded for translation. It is requested that 3 paper copies of the final translation be sent to NISC 3615 (Mr. John Bogus) upon completion of the translation.

E. W. Dietzen, Jr.

Standing
T. M. No
19333
19324

7606/93
16 Jun 76

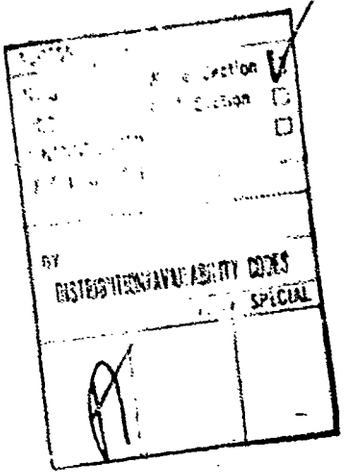

UNCLASSIFIED

METHODS OF THE DIMENSIONAL ANALYSIS AND SIMILARITY THEORY IN PROBLEMS OF SHIP HYDROMECHANICS

[Epshteyn, Leonid Abramovich; Metody teorii razmernostey i podobiya v zadachakh gidromekhaniki sudov; Publishing House "Sudostroyeniye," Leningrad, 1970, 208 pp.; Russian]

ABSTRACT [2*

The basic concepts of the theory of dimensional analysis and similarity are presented, on the basis of which a number of problems related to the hydromechanics of ships are solved; a group of problems with respect to water-displacing ships are analyzed. The major part of the book is dedicated to the problems that arise in connection with the development of high-speed craft. To these belong: steady and non-steady planing, various aspects of cavitational phenomena, motion of hydrofoil and air-cushion craft, deformations of the free surface and spray formation.

This book is intended for personnel in scientific-research institutes, engineers, design bureaus of the shipbuilding industry and students.

FOREWORD [3

The book by L. A. Epshteyn is devoted to application of the methods of the theory of dimensional analysis and similarity to certain problems of hydromechanics which are primarily related to the motion of submerged bodies, as well as the motion of bodies along the water surface. These methods are widely used during the formulation, processing and analysis of the experiments. At the present, an educated approach and understanding of laboratory as well as actual experiments would be impossible without application of the theory of dimensional analysis.

In practice, applications of the methods of similarity are not linked with cumbersome, complicated mathematical analysis; however, they always require a deep penetration into the physical nature of processes, which, in turn,

---

*Numbers in the right margin indicate pagination in the original text.

provides the proper insights to the simulation of the basic factors which determine the phenomenon and its characteristics.

The simplicity of the conclusions and of the final formulas often conceal the logical scheme of the adopted simulation method which must include the basic features of the determining processes. As a result, for many specialists the basic concept of the conclusions becomes emasculated and only the formal way of obtaining them remains.

It should be noted in this respect that in this manuscript, along with many practical applications and examples in the use of the theory of dimensional analysis and similitude, there are also included useful materials in regard to the methodology of formulation of the required laws in question. Much of the presented experimental and theoretical data is the result of many years of creative work performed by the author of this book. The reader will find examples of analysis and solutions for many important specific problems related to the fundamental problems of ship hydromechanics.

Academician L. I. Sedov

FROM THE AUTHOR [4

This book touches upon many quite different problems of ship hydromechanics. These problems are considered to be common only because in their formulation, solution and analysis the methods of the theory of dimensional analysis and similitude are employed. The first chapter contains fundamentals of the theory of dimensions and similitude in a presentation which follows L. I. Sedov's ideas, which he has developed in his well-known monograph "The Methods of Similitude and Dimensional Analysis in Mechanics." These ideas are later adapted to the theory and simulation of problems which are primarily related to questions of high-speed vessels.

Steady and unsteady planing, various aspects related to the utilization of submerged hydrofoils, the processes of formation and development of cavitation, air entry to the body moving near the surface or intersecting it, the processes of spray formation, problems related to the motion of air-cushion vehicles, action of gas jets on the water surface--such is the scope of questions dealt with in the third, fourth, fifth and sixth chapters. Chapter II includes some considerations and material in regard to

ordinary water-displacing craft (wave formation, drag, rolling and pitching, propellers).

These separate problems are presented in the book in various degrees of detail. In some instances it was possible to present an exclusive account of the problems considered, in other cases the arising difficulties are only listed and analyzed and the means for their solution are outlined. The selection of the material for the book, to a certain degree, is related to the author's works in the various fields of ship hydromechanics.

The purpose of this book is to provide the engineer and researcher with information about some of the seldom-analyzed problems in this field, and also to inspire interest and to provide experience in the implementation of simple methods of the theory of dimensional analysis and similitude. From the material presented in the book it is clear that these methods are especially effective if they are considered along with additional mathematical, and especially physical, considerations. In order to explain one or another phenomenon it is necessary to scrutinize the essence of this phenomenon, to construct its rational scheme and by adopting the methods of the theory of dimensional analysis and similitude, to be able to formulate and to analyze a minimum number of experiments.

The author will be grateful for comments and suggestions with respect to the form and the essence of the problems under consideration.

INTRODUCTION [5

Experimentation is the starting point of our knowledge. Often experiments in the study of some phenomenon or structure cannot be conducted under "full-scale" conditions. In some cases, it is too complicated and expensive, in others it is simply impossible because of the remoteness or unavailability of the object which is to be studied.

For example, in the field of our study, covering the theory of a ship before the craft is built, it is necessary to create its design and determine its drag and seaworthiness.

In connection with this problem, the method of model experimentation is widely employed in the most diverse fields of engineering. The correct formulation of such an experiment, and the laws of transition from model to full

size, are determined by the theory of dimensional analysis and similitude.

In combination with additional considerations of physical or mathematical nature, the theory of dimensional analysis is a simple and fruitful method of experimentation.

A great deal of attention has been devoted to the problem of simulation and dimensionality by such great scientists as Newton, Fourier, Rayleigh, Reynolds, and others.

In Russian technical literature there is an excellent account of separate questions and examples of the employment of the methods of dimensional analysis and similitude [13, 15], but unfortunately this theory, which in spite of its apparent simplicity, requires a deep understanding, is presented in a number of textbooks and even in specialized technical presentations inaccurately and unclearly on some points. Some authors in their presentation use pseudo-scientific form and terminology, which obscures the question for them as well as for the reader.

All this, to a certain extent, has interfered with the acceptance of the theory of dimensional analysis and similitude by a large number of specialists.

The appearance of the book by L. I. Sedov, "The Methods of Similitude and Dimensional Analysis in Mechanics" [33], gave a great impetus toward mass development and applications of these methods. In this book, along with clear-cut presentation of the basics of the methods of the theory of dimensional analysis and similitude are given a large number of original new solutions, which include a number of urgent problems in the fields of hydromechanics, strength, combustion theory, explosion and astrophysics.

Below, the employment of methods of the theory of dimensional analysis and similitude for the formulation and solution of a number of problems of ship hydromechanics is analyzed. In some examples these methods will be used for simplification of the theoretical solution; in others the effective results will be obtained due to the combination of the theory of dimensional analysis and similitude with experimental data. A number of examples are devoted to the utilization of the theory of dimensional analysis and similitude for the purposes of proper simulation and for recalculation of the results obtained for the model to the full-size prototype.

Let us note that the term simulation [modeling] is

applied at the present time to a wide variety of concepts. Sometimes it is referred to modeling of the environment and phenomena, meaning by this the creation of certain conditional schemes which are adopted to replace the actual environment and phenomena. For example, as a model for liquid and gas we consider the continuum that possesses the specified properties (ideal fluid, viscous fluid, etc.). The same concept is applied to the study of planetary motion, where the planets are considered as points of mass, thus becoming a study of a model of a real process. [6

By simulation is also meant a method of analysis of a given phenomenon by means of substituting it by another which is defined by differential equations common with the given phenomenon. This type of simulation is used particularly for analysis of fluid flow by the method of electromechanical analogy or for analysis of dynamic processes in mechanical systems by means of their replacement by electrical systems. At present we can often encounter the term simulation by means of computers, where it is understood that the computations of the numerical solutions for some problem are conducted with various parameters. Here, when we say simulation we will mean the analysis of the conditions of similitude and of the laws of recalculation for identical physical phenomena which differ only in scale.*

---

*Let us note that the difference in scale is not necessarily related to geometry only. In a general case the models can be smaller, equal or larger than full size, and, for example, differ by the scales of some other parameters (velocity, density, viscosity, etc.).

It is important hereby to introduce clarity into the meaning of the expression "identical physical phenomena."

All of this is related with the use, even in the latest literature (for example, [2], pp. 128, 134, 148, etc.), of terms like complete similarity and partial or approximate similarity. It should be realized that complete similarity does not exist, just as it is impossible to analyse a real phenomenon or process in its entirety. Any analysis, including analysis with the aid of models, is conducted on the basis of schematization and on the basis of elimination from the analysis of the factors which are secondary, nonessential for the purpose of the given analysis. For example, when experimenting with a ship model in order to determine its drag, only its exterior outline is reproduced, while the design of the hull is not simulated. This

formulation is based on the assumption that the affect of hull deformations under the action of hydrodynamic forces is negligible.

At this point we can clarify the term identical physical phenomena, keeping in mind that identity is ascribed only to those features which are essential for a given precision for the analysis of the problem. Let us note that it follows from the above discussion that for simulation a certain minimum amount of information with regard to the analysis of the problem is required. One should be able to select from the numerous related conditions those which determine the results which we are trying to obtain; obviously, in analyses of new problems and new phenomena this is not always possible.

In a number of cases the partiality of similarity is additionally stipulated by the technical difficulties of simulating even those factors which, as is known a priori, can affect the results being sought. From numerous examples of similar conditions let us indicate the classical case of the difference between the Reynolds numbers of the model and full size in aerodynamic studies. Thus, without mentioning this again in the future, we will consider that the similitude is always partial, while the sum of the effects of factors not modelled for various reasons will produce the so-called scale effect. Into the methods of experimentation with models enter not only the determination of the conditions of similitude and the laws of recalculating the experimental results from the model to full size, but also an estimate of the value of the scale effect, and, when necessary, the development of appropriate corrections.

Let us discuss the question of determining the conditions or criteria of similitude. In a number of cases these criteria are drawn from analysis of the equations of motion, and of initial and boundary conditions. According to existing opinion, this approach is of a more strict and general nature, if not the only reliable one, and its principal advantages, as compared to the "formal" considerations of the dimensional theory, are noted here. These widely circulated views are clearly formulated in [21], [7
from which the following quotation is taken: "The theory of similitude and dimensional analysis determines the conditions under which the phenomena become either exactly or approximately similar. In the theory of similitude this problem is solved by analysis of the related equations, i.e., the equations which describe the phenomena under consideration, for example, the equations of fluid flow or the rolling and pitching of ships. The dimensional theory,

however, is based on the formal concepts based on the dimensional analysis of the physical parameters which are characteristic for the given phenomenon." And further, "...From the principal point of view it is more correct to approach the establishment of the criteria of similitude on the basis of analysis of the operational relationship."

In reality the search for the criteria does not require knowledge of the equations for the process being studied, and the relationships obtained only from the concepts of the dimensional theory are just as general as those which are formed from analysis of the equations.

In order to establish the dimensionless criteria which define the phenomenon, it is necessary and also sufficient to know on which parameters this phenomenon is dependent (see Sedov [33], pp. 39-40). In a number of cases these parameters can be selected from analysis of the phenomenon based on the general physical concepts, even though the equations which relate these parameters cannot be composed. In other cases the same criteria of similitude will correspond to different equations.

It is possible to say that on the basis of the equations of a certain problem we will not neglect any essential factor; however, we should not forget that the equation of the problem itself is also never exact and is constructed on the basis of a certain schematization. If this scheme omits anything essential for the phenomenon under consideration, then the analysis itself, based on these equations, will also be in error. If, however, the phenomenon is properly schematized, i.e., when all the effects of actually secondary importance are excluded, then accounting of the defining values always precedes the formulation of equations. To formulate the equations, in addition to knowledge of the parameters themselves, it is necessary to mathematically define the laws of their interrelations. This particular determination of the laws of the interrelationships for a specific problem is not necessary for determination of the criteria of similitude.

In conclusion of these introductory remarks, let us indicate that in a number of problems the practical impossibility of simulation can be eliminated if the phenomenon under consideration can be subdivided into its elements, for each of which it becomes possible to meet the requirements of similitude or to perform an evaluation by calculation. One of this type of examples is the Froude method for determining a ship's drag, when only those factors are simulated which are related to the residual drag, while the

frictional drag is taken into account with the aid of some additional considerations. The reader will become acquainted with other examples in the chapters where the entry of atmospheric air to the hydrofoil, the simulation of spray, etc., are discussed.

TABLE OF CONTENTS

CHAPTER I. FUNDAMENTALS OF THE THEORY OF DIMENSIONAL ANALYSIS [8

1.1. Concerning the Dimensionality of Quantities

The measurement of some quantity is in reality a comparison of that quantity with another quantity taken as a standard of measure, or, in other words, as a unit of measurement.

If, in the case of the problem under consideration, various standards are being considered or are being used, then our quantity is called dimensional.

If it is stipulated or follows from the definition of the quantity that the standard can be only one, then the quantity will be dimensionless.

Dimensionality is nothing else but the indication of the standard with which the comparison was conducted.

If the standard remains the same at all times it becomes unnecessary to refer to it repeatedly.

The dimensionless state of a quantity means that it is not necessary to additionally indicate the standard for its computation.

Let us clarify these statements by some examples.

We measure the length of some circumference and say: it is equal to 2 meters, or 200 centimeters, or 6.55 feet. We compare the length with various standards--linear lengths--and by indicating a number that represents our length, we have at the same time to indicate the standard used. The length of the circumference in this concept is the dimensional quantity.

We can state the following: the relationship of the length of a circumference to the radius is equal to 2π (2π is a dimensionless quantity). Why, when we have taken the relationship of the length of the circumference to the length of an iridium plate which is preserved in the bureau of standards, and related the length of the circumference to this dimension, have we called it a dimensional quantity, while when we have taken the relationship of the length of the circumference to the length equal to its radius, the length of the circumference became dimensionless?

The reason is found in the statement of the problem of measurement: in the second case the unit of measurement

was defined as the length of the radius, while in the former case the meter, centimeter, the foot as well as other measurements were all possible as the units of measurement.

In a number of cases it is convenient to state the singleness of the adopted standard and consider the corresponding quantities dimensionless. For example, by stating that all the measurements of a body will be compared to its length, we can consider them (width, height, etc.) as dimensionless quantities. The convenience here is derived from the ability to relate all measurements of similar bodies, which when expressed in this manner will remain constant, and probably independent from the type of units in which the lengths are measured. The above examples were in regard to geometric values, however, the above statements apply equally to any other physical quantities. For example, the quantity A--the relationship of two velocities [9

($A = \frac{v_1}{v_2}$ --indicates by its structure that the value v_1 is compared to v_2. The quantity A indicated the number of times v_1 is greater than v_2. Obviously, this quantity can not be dependent on the type of general units by which we will measure v_1 and v_2. The quantity A is a dimensionless quantity.

In the aviation and shipbuilding industries there exists the term "overload." By overloads we mean the relationships between the accelerations that occur during flight or motion through waves and accelerations due to gravity. In this type of expression the overload is a dimensionless quantity, because the definition itself contains information about the standard used for the evaluation of its quantities.

We have called the standard with which the given quantity is measured the dimensional value. It is said: the dimension of this quantity is a meter, or the dimension of this quantity is a kilogram.

The concept of dimensional analysis is also considered in a somewhat expanded form, when the reference is made not to the single standard only, but rather to a category of standards. In such a case, we can state that this quantity has the dimension of length, while the other, the dimension of force.

Below we will record the dimensions of some quantity a by putting its designations into brackets: [a].

In further discussion we will proceed from the following axiom: in a relationship which reflects physical phenomena, the equality signs or the expressions for an algebraic sum can only be made among quantities of similar nature.

Forces can be compared and added only to forces, velocities compared to velocities, lengths compared to lengths, etc. The addition or the comparison of unrelated physical quantities is meaningless.

From the above axiom and the possibility of quantitative comparison, we see that it is imperative that for a relationship which has a physical concept, all of the members which are connected by summation or equality signs should have the same dimension.

Utilizing the above-mentioned condition and designating the units of measurement for certain quantities, which are called basic or primary, we can express the values of all other quantities related to the basic quantities by definitions or by physical laws. These quantities are known as derivative, or secondary quantities.

Thus, for example, designating the units for length L, time T, and force K, we can express through them the units of velocity, acceleration, mass, etc.

Actually the velocity is defined as a relationship of [10
some distance to a corresponding interval of time (it is unimportant whether the quantities are finite or infinitesimal). The dimensions of the right-hand part are the distance divided by the time; hence the left side, i.e., velocity, must have the same dimensions:

$$[v] = LT^{-1}.$$

Similarly for acceleration we find the following:

$$[j] = LT^{-2}.$$

The mass is related to force F and acceleration j by Newton's law, according to which

$$m = \frac{F}{j};$$

with the dimensions of the right side being $KL^{-1}T^2$, it follows that the dimensions of the mass are the same:

$$[m] = KL^{-1}T^2.$$

In a similar way the dimensions of an area, a density, a coefficient of viscosity, work and other quantities can be found. The dimensional expressions for some of these values, using the basic independent values (in this case length, time and force), are called formulas of dimension. In other words, a formula of dimension can be viewed as a relationship which indicates by how much the derived value will change when the basic units of measurement are changed.

The unit of measurement for secondary values will be obtained when in the dimensional formula instead of L, T, and K, we substitute corresponding units (for example, meter, second, kilogram).

Instead of the basic units of length, time and force we can use some other physical values. Specifically, in the adopted physical system of units, instead of the basic dimension of force the mass is selected.

If, for example, we take as the basic value the velocity v, acceleration j, and density ρ, then the length, time, and force will be the derivative secondary values; their dimensions will be expressed through v, j and ρ as follows:

$$L = \frac{[v]^2}{[j]};$$

$$T = \frac{[v]}{[j]};$$

$$K = \frac{[\rho][v]^4}{[j]^3}.$$

The derivation of these dimensional values is based on the same concepts which were previously used in determining the dimensions of velocity, acceleration and mass using the basic dimensions of L, T and K. Let us obtain, for example, the second of these relations. [1

Acceleration is the rate of change of velocity in the unit of time, i.e., some velocity divided by the corresponding time,

$$j = \frac{v}{t};$$

from here

$$t = \frac{v}{j}.$$

And since the dimensional similarity of both sides is a requirement we obtain

$$T = \frac{[v]}{[l]}.$$

The number of basic units is not restricted to three. We can consider each physical quantity (velocity, density, viscosity, area, etc.) as basic and introduce for them their own units of measurement. However, in introducing each new basic dimension (in addition to the basic three) it is necessary to introduce at the same time a new dimensional constant beyond the regularly adopted one in order to secure the necessary condition of similarity among dimensions on both sides of the equality which reflect the relationship of the physical quantities with the new basic dimension.

Let us demonstrate this by examples.

Suppose that along with the length we would like to consider an area as an independent basic dimension that has an independent unit of measurement. Then the expression for the area of a rectangle we would have to write in the following form:

$$S = c_1 lb$$

and consider c_1 as a quantity that has the dimension

$$[c_1] = \frac{[S]}{L^2}.$$

If we do not do this, there will be values of different unrelated dimensions on both sides of the equality.

We can continue farther and consider two linear quantities--let us say, x and y--possessing independent dimensions. In order to place the equality sign between these values it is again necessary to introduce the coefficients of proportionality

$$y = c_2 x,$$

while

$$[c_2] = \frac{[y]}{[x]}.$$

Let us note that this at first glance paradoxical example (dimensional independence of two linear quantities) can be observed, especially in everyday actions, when we are using different systems of measurements. In the

expression 1 foot = 0.305 meter we utilize this coefficient and should actually have written 1 in feet = $(\frac{1}{0.305}\frac{\text{foot}}{\text{meter}})$1 in meters.

Now the dimensions of both parts of the equality are similar.

In the available physical and technical systems of units and measurement the force and mass are related by Newton's law, and if one of them is made as a fundamental unit the other becomes a derivative.

In reality, Newton's law establishes not the equality, but the proportionality, between the force and the product of the mass and the acceleration, and in this form the mass and the force can be considered as the independent fundamental values, but a coefficient of proportionality c appears

$$[c] = KL^{-1}T^{2}[m]^{-1}.$$

Upon Gausse's recommendation it was agreed to consider this coefficient as being dimensionless and equal to unity; as the result of this the dimensions of the mass and of the force became dependent values.

It becomes evident that by introducing a new fundamental unit of measurement we can simplify the process of writing this unit; however, this also leads to the appearance of a new dimensional constant which must be introduced into corresponding relationships. As a rule this complicates the form of the formula and therefore is quite often not done. However, in some instances the introduction of the additional fundamental units is justified. Thus, for example, in thermodynamics along with units of length, time and force, units are chosen for the amount of heat (calorie) and temperature (degree Celsius). In accordance with this conclusion two quantitative constants are introduced, namely: the mechanical heat equivalent I = 427 kg-m/kcal and the universal gas constant R = 1.99 kcal/kg-mole·deg.

The appearance of the new dimensional constants adds to the number of fundamental units and, vice versa, a reduction in the number of dimensional constants leads to a reduction in the number of fundamental units.

Let us consider some constant physical value, such as

the length of the earth's meridian, and for simplicity let us consider it to be unity; then all linear measures will become become dimensionless, and their measuring quantities will indicate the number of times the length of the earth's meridian is contained in this or that distance. The number of fundamental units has been reduced by one. Only the time and force have remained.

We can consider the velocity of light in a vacuum as [13
a dimensionless constant, thus any velocity will become dimensionless, while dimensions of length and time will become interdependent.

If we consider one of them as a fundamental value, the other will be expressed by the equality

$$L = T.$$

The equality between the dimensions of length and time may appear strange at first glance. A question arises: how can a length of distance be determined in seconds, for example? There is nothing unusual in this type of definition, and often to the question, "How far is it to a certain place?" the answer is, "A five-minute walk," or "Two hours' flying time." In this manner, the distance for a known velocity can be characterized by the time. In astronomy one of the units of length is the light year, i.e., the distance which light travels in one year.

Designation of two independent physical constant dimensions as dimensionless will lead to a single basic dimension, while a designation of three will make all values dimensionless.

In reality, if, for example, we consider lengths, times and forces as dimensionless by introducing for each its own unit of measurement, then it becomes obvious that all the other values of interrelated dimensions will become dimensionless, because their values were expressed through the dimensions of quantities which became dimensionless.

In regard to the formation of dimensionless quantities as a condition of unit standards of measurement, we can note the following. If the adopted standards correspond in essence to the question under consideration, then their introduction is justified because the characteristics of all similar systems, by becoming dimensionless, also become constant at the same time. In the opposite case such a constancy does not occur and the introduction of the unit standard usually will not be justified.

Let us clarify the above by an example. Suppose the motion of some body in a fluid is considered. The adoption of the length of this body as a standard (unit of length) makes all of the distances between the points in space and the object and all other dimensions of this body dimensionless values, and for the similar motion of a similar object of twice the length, it is obvious that all corresponding dimensions will also double. A different relation will take place, if instead of the unit standard a value which has no relationship to the considered question is taken. Assume in our sample that a certain part of the earth's meridian was adopted as a unit standard. Here, according to our stipulation, the linear dimensions will also be dimensionless values; however, the values that characterize the dimensions of similar objects will not remain constant. Let us include the earth into our system, that is, let us consider that during simulation not only the dimensions of our object but also the dimensions of the earth will change; as a result, the constancy of the dimensions of similar bodies will hold again.

From the above discussion it is evident that the adoption of unit standards (earth's diameter, velocity of light, water density) will not produce any significant advantages in the majority of practical problems, because these standards will not participate in the similitude and will not provide the characteristics of the dimensionless constancy for similar phenomena. Thus, the number of fundamental units is limitless. The variation of that number is related to the corresponding change in the number of dimensional constants. Usually, in mechanical problems three values are considered to be independent dimensions. [14

1.2. On the Structure of the Dimensionality Formula

Every physical dimensional value a is described by two elements: dimension, i.e., the standard with which it is compared, and the numerical representation that indicates how many times our value is greater than the standard. Designating the numerical value of the quantity a by A, we can write as follows:

$$a = A[a]. \tag{1.1}$$

It is evident that a change in the dimensionality (standard) will lead to a change in the numerical value as well. An increase in the standard will produce a decrease in A, and vice versa. If the length of some segment in centimeters was expressed by a numerical value A = 100, then the same length expressed in meters (the standard has

increased 100 times) will be expressed by a value one hundred times smaller, i.e., A = 1.

As was already noted, the units of dimension [a], i.e., the value of the adopted standard, can depend on the dimensional units (standards) of other values. Thus, for example, units of velocity (meters per second or kilometers per hour) are established by the choice of the dimensional units of distance and time.

For a general case we can write that

$$[a] = f([a_1], [a_2], \ldots, [a_k]), \qquad (1.2)$$

where $a_1, a_2, \ldots, a_k$ are the magnitudes with the basic units which define the dimension a analagously to the way in which the units of distance and time defined the value of velocity. Let us clarify the form of this functional dependence. Suppose, at the beginning, that one of the arguments of the right portion of (1.2) changes, for example $[a_1]$, while $[a_2], \ldots, [a_k]$ remain constant values. Designating for brevity

$$[a_1] = x, \qquad (1.3)$$

we obtain instead of (1.2)

$$[a] = f(x) \qquad (1.4)$$

and instead of (1.1)

$$a = Af(x). \qquad (1.5)$$

Let us increase by μ times the standard for the value of a, i.e., substitute x by μx; then in accordance with (1.4) the dimensional units of the value a, as well as its numerical value, will change. This numerical value will become equal to $\frac{A}{k}$, where k will depend on μ only. For example, with $\mu = 1$ it is obvious that $k = 1$ also. Let us write the expression a in the old and the new dimensional units: [15

$$a = Af(x) = \frac{A}{k} f(\mu x). \qquad (1.6)$$

From (1.6) we obtain

$$\frac{f(\mu x)}{f(x)} = k(\mu). \qquad (1.7)$$

The right side is independent of x and, therefore, the derivative of the left side with respect to x has to be equal to zero.

Denoting

$$\mu x = u \tag{1.8}$$

and performing differentiation, we find

$$\frac{\partial f(u)}{\partial u}\mu f(x) - f(u)\frac{\partial f(x)}{\partial x} = 0, \tag{1.9}$$

from which

$$\mu \frac{1}{f(u)}\frac{\partial f(u)}{\partial (u)} = \frac{1}{f(x)}\cdot\frac{\partial f(x)}{\partial x}; \tag{1.10}$$

since the given calculations are true for any value of μ, we can assume u = 1, i.e., select $\mu = \frac{1}{x}$. Also f(u) and $\frac{\partial f(u)}{\partial u}$ will become constant and instead of (1.10) we obtain

$$\frac{1}{f(x)}\cdot\frac{\partial f(x)}{\partial x} = \frac{a_1}{x}, \tag{1.11}$$

where

$$a_1 = \left[\frac{1}{f(u)}\cdot\frac{\partial f(u)}{\partial u}\right]_{u=1}. \tag{1.12}$$

Integrating (1.11) we find

$$\ln f(x) = a_1 \ln x + \ln C_1,$$

from where

$$f(x) = C_1 x^{a_1},$$

or in accordance with (1.3) and (1.4)

$$[a] = C_1 [a_1]^{a_1}. \tag{1.13}$$

In this case C_1 is a function of $[a_2], \ldots, [a_k]$, [16 which we until now have maintained constant. By similar reasoning for $[a_2], \ldots, [a_k]$ we obtain

$$[a] = C[a_1]^{a_1}[a_2]^{a_2}\ldots[a_l]^{a_l}. \tag{1.14}$$

The dimensionless constant C can be dropped.

Thus, it is established that for a general case the dimension of the value a is expressed by the formula of form (1.14) by the dimensional units that define its basic values. If the units of measurement for the basic dimensional values $a_1, \ldots, a_k$ are increased correspondingly by $\mu_1, \ldots, \mu_k$ times, then according to (1.1) and (1.14) the quantity that measures the derived value a will be A' instead of A:

$$A' = \frac{A}{\mu_1^{\alpha_1}\mu_2^{\alpha_2}\ldots\mu_k^{\alpha_k}}. \qquad (1.15)$$

This expression is convenient for the transition from one set of units to others.

Let us observe the changes in A in the following examples. The speed of an airplane v = 300 m/sec

$$[v] = LT^{-1} = \text{m/sec},$$

i.e., $\alpha_1 = 1$ and $\alpha_2 = -1$.

Let us go to the new set of standards (units of length and time) 1 km = 1000 m; 1 hr = 3600 sec, i.e., $\mu_1 = 1000$ and $\mu_2 = 3600$.

The value of velocity with our new set of units according to (1.15) will be

$$v = 300 \text{ m/sec} = \frac{300}{(1000)^1(3600)^{-1}} \text{ km/hr} = 1080 \text{ km/hr}.$$

Another example: the density of water $\rho = 102$ kg·$\cdot$sec^2/m^4

$$\rho = KT^2L^{-4},$$

i.e., $\alpha_1 = 1$, $\alpha_2 = 2$, $\alpha_3 = -4$.

Let us go to the following new set of units: grams, seconds and centimeters. The values of μ_i will be as follows: $\mu_1 = 10^{-3}$, $\mu_2 = 1$, $\mu_3 = 10^{-2}$. The density of water in the new system becomes

$$\rho = 102 \text{ kg}\cdot\text{sec}^2/\text{m}^4 = \frac{102}{(10^{-3})^1(1)^0(10^{-2})^{-4}} = 1.02\cdot10^{-3} \text{ g}\cdot\text{sec}^2/\text{cm}^4.$$

1.3. Utilization of Dimensional Concepts in Search of a Law for the Relation Among Dimensional Values

As has been stated previously, an equality which expresses some relationship among physical quantities must satisfy the following condition: the dimension on both sides of the equality sign must be the same, or in other words, the values must possess dimensional homogeneity.

This seemingly trivial statement of a condition plays [17
a significant role in the analysis of various problems.

For example, let us say we are interested in the question of the period of oscillations of a mathematical pendulum T and we possess neither theoretical nor experimental information about the process of its motion. We only know that the pendulum has a definite length l and mass m, concentrated at the point at the end of the pendulum, that it swings from the point of equilibrium to the greatest angle φ_0 and remains in the field of gravitational attraction g. We can say that generally speaking

$$T = f(l, m, \varphi_0, g). \tag{1.16}$$

This mathematical expression does not at this point provide us with the nature of the interrelationship of the period and the other listed quantities. At this stage, let us apply the above-formulated condition.

The left side of equation (1.16) represents the period of motion, i.e., the quantity which has the dimension of time; it follows, then, that the right side must also have the dimensions of time.

This condition already defines the form of the function $f(l, m, \varphi_0, g)$ to a great extent. In the first place, it indicates the necessity for the elimination of the quantity m from the number of our terms; otherwise, none of their functional dependence can eliminate the dimension of force or mass (depending on the adopted system), which are included in the value of m but are excluded from other parameters. Secondly, the values l and g must be included in the right side of a completely defined relation containing the dimensions of time, that is $\sqrt{\frac{l}{g}}$.

Thus, we can write that

$$T = \sqrt{\frac{l}{g}} f(\varphi_0). \tag{1.17}$$

Now, using only the most general concepts about the values which define the phenomenon and the above formulated general condition of the dimensional homogeneity of both parts of any equality that expresses the correlation among the physical quantities, we are able to make the following important conclusions from this analyzed example:

1. The period of oscillations of a mathematical pendulum is independent of its mass.

2. The period of oscillations of a mathematical pendulum is directly proportional to the square root of its length and inversely proportional to the square root of its gravitational acceleration.

It can happen that on one side of the equality sign which indicates the interrelationship among physical quantities there will be a dimensionless quantity; it is obvious that in this case the other side of the equality sign must also be dimensionless. This type of expression is usually more convenient for the analysis of any phenomenon.

It is not difficult to prove that any physical correlation among the dimensional quantities can be reduced to a dimensionless correlation of various combinations of these quantities. [18

Let some value a depend on n values

$$a = f(a_1, a_2, \ldots, a_k, a_{k+1}, \ldots, a_n). \qquad (1.18)$$

Among $(a_1, a_2, \ldots, a_n)$ there can exist constants and variables, dimensional and dimensionless values. Suppose in the case under consideration the values $a_1, a_2, \ldots, a_k$ have independent dimensions, i.e., that they form such a group of values, from which it is impossible to obtain a dimensionless value. (Length, velocity, and density will be independent values; the length and the volume are the dependent values, because the relationship of the volume to the length cubed is a dimensionless quantity.)

We define $a_1, a_2, \ldots, a_k$ as the basic values.

If we assume them to be primary unit quantities, that is, if we consider them to be basic dimensionless values, then according to the above discussion all of the derived quantities $a, a_{k+1}, \ldots, a_n$, the dimensions of which are expressed through the basic values, will also become dimensionless, i.e., they will convert into dimensionless

combinations which we can call respectively π, π_1, π_2, ..., π_{n-k}.

Our correlation will become as follows:

$$\pi = f(1, 1, \ldots, 1, \pi_1, \pi_2, \ldots, \pi_{n-k}). \tag{1.19}$$

Let us clarify this by an example. Suppose there exists a correlation which defines a velocity at a point in space with a steady-state fluid flow around the body. The velocity or its projection v_x, for example, will be a function of the dimensions and the shape of the body, the projections of velocity V_x, V_y and V_z of the advancing stream, and the coordinates x, y and z of a point in space

$$v_x = f(l_1, l_2, \ldots, l_n, x, y, z, V_x, V_y, V_z). \tag{1.20}$$

Here l_1, l_2, ..., l_n are the linear quantities which characterize the dimensions and the position of the body in relation to the coordinate axes.

Let us consider the length of the body l_1 and the velocity projection V_x as the principal quantities equal to unity, i.e., we increase the units of measurement correspondingly by l_1 and V_x times, where all the rest of the linear and velocity dimensions will simply be the independent quantities showing by how many times a certain value is greater or smaller than the principal corresponding value. The correlation of (1.20) will become

$$\frac{v_x}{V_x} = f\left(1, \frac{l_2}{l_1}, \ldots, \frac{l_n}{l_1}, \frac{x}{l_1}, \frac{y}{l_1}, \frac{z}{l_1}, 1, \frac{V_y}{V_x}, \frac{V_z}{V_x}\right).$$

Thus, any relation (equality) among the dimensional quantities can be expressed in a series of dimensionless combinations of these quantities. The number of variables in this case decreases by the number of values which have had independent dimensions, i.e., by the number of principal values. This decrease in the number of variables substantially simplifies the analysis. The result (1.19) is known as the π-theorem. [19

In the transition to the dimensionless form we can select any values with independent dimensions as the principal quantities. Thus, in the above example, instead of l_1 and V_x we could have adopted, say, l_2 and V_z. The

dimensionless combinations will also change in such cases.

Let us show what type of form will be obtained for a general case for dimensionless combinations π, π_1, ..., π_{n-k}.

We start by writing the dimensions for our values

$$[a] = [a_1]^{\alpha_1}, [a_2]^{\alpha_2}, \ldots, [a_k]^{\alpha_k};$$
$$[a_{k+1}] = [a_1]^{\beta_1}, [a_2]^{\beta_2}, \ldots, [a_k]^{\beta_k};$$
$$[a_n] = [a_1]^{\gamma_1}, [a_2]^{\gamma_2}, \ldots, [a_k]^{\gamma_k}.$$

Since we have adopted the values a_1, a_2, ..., a_k as our units, i.e., we have increased the units of measurement of these dimensions correspondingly by a_1, a_2, ..., a_k, the numerical values of the derived quantities will decrease in accordance with the dimensional formula, i.e., they will be

$$\left.\begin{aligned} \pi &= \frac{a}{a_1^{\alpha_1} a_2^{\alpha_2} \ldots a_k^{\alpha_k}}; \\ \pi_1 &= \frac{a_{k+1}}{a_1^{\beta_1} a_2^{\beta_2} \ldots a_k^{\beta_k}}; \\ \pi_{n-k} &= \frac{a_n}{a_1^{\gamma_1} a_2^{\gamma_2} \ldots a_k^{\gamma_k}}. \end{aligned}\right\} \qquad (1.21)$$

Let us cite several examples which will illustrate some techniques and the effectiveness of the dimensional analysis method.

Suppose we are interested in the problem of drag of a small body moving slowly through a viscous fluid. Since the forces of inertia (forces of mass) decrease proportionally to the cube of the linear dimensions, while the friction forces (surface forces) are proportional to the square of the linear dimensions, we should expect that for sufficiently small bodies the inertia forces can be made as small as we wish in comparison to forces of a viscous nature; then the density of the fluid as such will not be one of the defining parameters and the resistive force X will only depend on the linear values of l_1, l_2, ..., l_n, which determine the dimensions, shape and position of the body, the velocities of its motion v and the coefficient of dynamic viscosity μ:

$$X = f(l_1, l_2, \ldots, l_n, v, \mu). \qquad (1.22)$$

Let us write the dimensions for our values [20

$$[X] = K;$$
$$[l] = L;$$
$$[v] = LT^{-1};$$
$$[\mu] = KL^{-2}T.$$

Let us compose from X and from our other values a dimensionless combination. For the composition of such a combination there exist various techniques. We can look for this combination in the form of

$$A = Xl^{\alpha}v^{\beta}\mu^{\gamma}. \tag{1.23}$$

Considering the dimensions of the values that enter into the right side of the equality we can write the dimensions of A in the following form:

$$[A] = K^{1+\gamma}L^{\alpha+\beta-2\gamma}T^{\gamma-\beta}.$$

Since we want A to be a dimensionless combination, it then follows that we should equate the power exponents of K, L and T to zero. This condition provides us with three equations for the determination of α, β and γ:

$$\left.\begin{aligned} 1+\gamma &= 0;\\ \alpha+\beta-2\gamma &= 0;\\ \gamma-\beta &= 0. \end{aligned}\right\} \tag{1.24}$$

We immediately obtain from the first equation $\gamma = -1$; substituting this result in the last equation we obtain $\beta = -1$ and finally, from the second equation, we determine $\alpha = -1$.

Thus, expression (1.22) will have the final form

$$A = \frac{X}{l\nu\mu}. \tag{1.25}$$

We can approach this problem in another way. In the combination of type (1.22), besides the quantity which we wish to reduce to the dimensionless state there can enter, as cofactors with different powers, as many values included in the function as there are basic units of measurement. These values must have independent dimensions.

We must obtain a dimensionless combination in which the force X is present. In order to exclude the dimension of the force K, this combination must include the relation $\frac{X}{\mu}$. However, the dimension of this relationship is L^2T^{-1}

and, therefore, in order to exclude the time we must include into the denominator the velocity; the obtained combination will have the dimension of length and then $\frac{X}{l_1 v \mu}$ will be the dimensionless value. It can only depend on the same values as the resistance itself

$$\frac{X}{\mu v l_1} = f_1(l_1, l_2, \ldots, v, \mu). \tag{1.26}$$

However, in the right-hand part there must now be a function of dimensionless combinations consisting only of the above-listed values.

Obviously, the value μ cannot enter into these combinations, since it contains the dimension K, which does not exist in the other values; we must eliminate the velocity v, which contains T, for the same reasons. From the remaining n linear dimensions we can compose n-1 dimensionless combinations, relating all dimensions, for example, to l_1.

Finally we obtain

$$\frac{X}{\mu v l_1} = f_1\left(\frac{l_2}{l_1}, \frac{l_3}{l_1}, \ldots, \frac{l_n}{l_1}\right). \tag{1.27}$$

The number of parameters has been decreased by three, i.e., by the number of values with independent dimensions.

For all similar bodies the arguments of the function f_1 and, consequently, the function itself will be constant. Thus, for the bodies of a given form

$$X = C\mu v l_1, \tag{1.28}$$

where C = const, i.e., the resistance becomes proportional to viscosity, velocity, and to the linear dimensions in the first power. If the body represents a sphere with radius r, then according to the exact calculation

$$X = 6\pi\mu v r, \tag{1.29}$$

i.e., the constant becomes equal to 6π.

We could have approached the solution to this problem in a different way, repeating in this case the general discussion about the possibility of assigning unit values

with independent dimensions. Let us select as the principal values the length l_1, the velocity v and the dynamic coefficient of viscosity μ.

In such a case, the value of force will be a derived value. Using Newton's law of friction we have

$$\frac{X}{S} = \tau = \mu \frac{\partial v}{\partial y},$$

where τ is the frictional stress, i.e., the frictional force per unit area.

We will find*

---

*For dimensional analysis we can assume that the dimension dv/dy is [v]/L.

$$X = \mu S \frac{\partial v}{\partial y},$$

i.e.,

$$[X] = K = [\mu][v]L. \tag{1.30}$$

Let us increase the unit of measurement of length by l_0 times, the velocity by v_0 and the viscosity by μ_0 times. As the result, all the values will decrease in correspondence to the dimensional formula; taking into account (1.30), we can write (1.22) in the new dimensional units: [2

$$\frac{X}{\mu_0 v_0 l_0} = f\left(\frac{l_1}{l_0}, \frac{l_2}{l_0}, \ldots, \frac{l_n}{l_0}, \frac{v}{v_0}, \frac{\mu}{\mu_0}\right). \tag{1.31}$$

Assuming now that

$$l_0 = l_1; \quad v_0 = v; \quad \mu_0 = \mu,$$

and (1.31) will become

$$\frac{X}{\mu v l_1} = f\left(1, \frac{l_2}{l_1}, \ldots, \frac{l_n}{l_1}, 1, 1\right), \tag{1.32}$$

thus we arrive an an expression identical with (1.27).

We could have directly adopted

$$l_1 = 1,\ v = 1 \text{ and } \mu = 1$$

and on the basis of (1.30) and (1.22) written (1.32) directly.

Let us now omit the restriction with respect to the smallness of the inertia forces as compared to the frictional forces, i.e., we will analyze the problem of the motion of a body in an infinite, viscous, incompressible fluid without any restrictions. Then, into the numbers of arguments of the function (1.22) we must introduce density ρ

$$X = f(l_1, l_2, \ldots, l_n, v, \mu, \rho). \tag{1.33}$$

Analyzing the same dimensionless combination for the force

$$\frac{X}{\mu v l_1} = f(l_1, l_2, \ldots, l_n, v, \mu, \rho), \tag{1.34}$$

we observe that on the right side, besides the dimensionless quantities of the $\frac{l_i}{l_1}$ form, a combination must appear that is related to μ and ρ, ($[\rho] = KL^{-4}T^2$); in order to eliminate the dimensions of the force from this combination, it has to be in the form of μ/ρ. The dimension of this relationship is $T^{-1}L^2$. Therefore, $\frac{\mu}{\rho v l_1}$ is a dimensionless quantity. Taking into account that $\mu = \rho\nu$, where ν is the kinematic coefficient of viscosity, we can write

$$\frac{X}{\mu v l_1} = f\left(\frac{l_2}{l_1}, \ldots, \frac{l_n}{l_1}, \frac{\nu}{v l_1}\right) = f\left(\frac{l_2}{l_1}, \ldots, \frac{l_n}{l_1}, \frac{1}{\mathrm{Re}}\right);$$

here $\mathrm{Re} = \frac{v l_1}{\nu}$ is the so-called Reynolds number. For all similar bodies the ratios $\frac{l_i}{l_1}$ will be constants and

$$X = \mu v l_1 f(\mathrm{Re}). \tag{1.35}$$

We would obtain analogous results by proceeding from the definition $l_1 = 1$, $v = 1$, $\mu = 1$. In this system ρ would have been transformed into Re.

Instead of (1.35) we can write [23

$$X = \rho\nu \frac{v^2 l_1^2}{\nu l_1} f(\mathrm{Re}) = \rho v^2 l_1^2 \frac{f(\mathrm{Re})}{\mathrm{Re}} = \rho v^2 l_1^2 F(\mathrm{Re}). \qquad (1.36)$$

The same result would have been obtained if we had adopted the units l_1, ν and ρ instead of l_1, ν and μ.

For a nonviscous (ideal) fluid the second choice of units would have been the only one, but the absence of viscosity would not have provided the possibility to form the combination for Re, and instead of (1.36) we would have had for similar bodies

$$X = C_1 \rho v^2 l_1^2, \qquad (1.37)$$

where

$$C_1 = \text{const.}$$

In a general case (when both μ and ρ play a role) both forms (1.35) and (1.36) are equivalent. The rationality of the practical use of either system is related to the intensity of the dependences f(Re) and F(Re).

It is always advantageous to have the weak dependence that approaches the constant along the substantial interval. For that reason, the form (1.35) is preferred for small values of Re, while (1.36) is for large values of Re (with $\nu \to \infty$ $\mathrm{Re} \to 0$ we arrive at (1.28), while the form (1.37) responds to large values of Re, because $\nu \to 0$ corresponds to $\mathrm{Re} \to \infty$). It is evident from the given example that by selecting different dimensionless combinations (or, which is the same, different units of dimensions) we can obtain different forms of dependences between dimensionless values; however:

1) the nature of the interrelationship is preserved (the dimensionless force--the coefficient of resistance--is a function of the Reynolds number);

2) the different forms can be transformed from one into another (as was done, for example, in obtaining (1.36) from (1.35).

Using the methods of dimensional analysis and some physical concepts, we have established that for bodies with small dimensions (small Re) the drag in high-viscosity liquids is proportional to the dynamic coefficient of viscosity, velocity and the linear dimensions of the body. For the case with low viscosity it has been found that the

drag is proportional to the density, to the square of the velocity, and to the square of the linear dimension.

It was found for a general case that the drag coefficient for the given body* is a function of the Reynolds number.

---

*Among the parameters l_1 there exist ones that define not only the shape, but the orientation of the body.

All these results were found without any analysis or solutions of hydrodynamic equations.

The combination of the theory of dimensional analysis with the additional physical and mathematical considerations increases its effectiveness. [24

Let us analyze the question of drag X and lifting force Y of a rectangular wing with a symmetrical profile. The problem in regard to the lifting force acting on the body (wing) in a viscous incompressible fluid actually does not differ from that of the previously analyzed problem. Using the formulas derived for the motion with large values of Re, we can write the expressions for dimensionless forces (force coefficients) in the following form:

$$\frac{Y}{\rho v^2 l_1^2} = f_1\left(\frac{l_2}{l_1}, \frac{l_3}{l_1}, \ldots, \frac{l_n}{l_1}, \mathrm{Re}\right);$$
$$\frac{X}{\rho v^2 l_1^2} = f_2\left(\frac{l_2}{l_1}, \ldots, \frac{l_n}{l_1}, \mathrm{Re}\right). \qquad (1.38)$$

Let us select out of parameters l_i the principal ones, like: the chord of the wing $l_1 = b$, span l and angle of incidence α. For the time being we will omit the remaining parameters, which describe the shape of the profile, considering that the dimensionless combinations for similar wings are constant. Then

$$\frac{Y}{\rho v^2 b^2} = f_1\left(\frac{l}{b}, \alpha, \mathrm{Re}\right);$$
$$\frac{X}{\rho v^2 b^2} = f_2\left(\frac{l}{b}, \alpha, \mathrm{Re}\right). \qquad (1.39)$$

Multiplying both expressions by $2\frac{b}{l}$ and denoting $\frac{l}{b} = \lambda$ (span-chord ratio of the wing) and $lb = s$ (area of the wing), we obtain

$$C_y = \frac{Y}{\frac{\rho v^2}{2} S} = F_1(\lambda, \alpha, \mathrm{Re});$$

$$C_x = \frac{X}{\frac{\rho v^2}{2} S} = F_2(\lambda, \alpha, \mathrm{Re}). \tag{1.40}$$

In the future we will consider the dependence on Re as insignificant; this is especially true for C_y within the limits of the critical angles of incidence. Then, eliminating Re and expanding F_1 and F_2 with respect to powers of the small angle α, we obtain [25

$$C_y = a_0(\lambda) + a_1(\lambda)\alpha + a_2(\lambda)\alpha^2 + a_3(\lambda)\alpha^3 + \ldots;$$
$$C_x = b_0(\lambda) + b_1(\lambda)\alpha + b_2(\lambda)\alpha^2 + b_3(\lambda)\alpha^3 + \ldots$$

Due to the symmetry the value of the lifting force must change for every change in sign of α; the drag, in contrast, is an even function of α. At this point, eliminating terms of α^2 too small as compared to those being considered, we obtain

$$C_y = a_1(\lambda)\alpha; \tag{1.41}$$
$$C_x = b_0(\lambda) + b_2(\lambda)\alpha^2.$$

For the span-chord ratio $\lambda > 2$ formulas (1.41) are in good agreement with experimental results. Excluding α from these formulas we obtain

$$C_x = b_0(\lambda) + \frac{b_2(\lambda)}{a_1^2(\lambda)} C_y^2,$$

i.e., within the precision of the coefficients which depend on λ, it becomes the well-known wing theory formula

$$C_x = C_{x_p} + \frac{C_y^2}{\pi\lambda}. \tag{1.42}$$

in which the first term is called the profile coefficient and the second is known as the induced drag coefficient.

Wherein lies the essence of the fact that by adopting the methods of dimensional analysis we can establish a relationship among values, without writing equations of

motion, without looking into the essence of the problem, and limiting the analysis to the listing of the factors which define the phenomenon under consideration?

This question is often raised by individuals who use the theory of dimensional analysis and similitude.

The answer to this question is explained by the fact that the formulas of dimensional analysis were obtained from basic laws of nature or from determinations. For example, the relationship of the dimensions of force, mass and acceleration has been established on the basis of Newton's second law. The dimensional formula for the coefficient of friction was obtained from Newton's law of friction. The dimension of the heat conductivity coefficient was a consequence of Fourier's law, the dimension of the modulus of elasticity, of Hooke's law, etc.

Earlier, we analyzed the problem of a body moving slowly through a viscous, incompressible fluid in which the inertia forces could be ignored and it seemed like without a thorough study of the essence of the problem, just utilizing the necessary expressions for the dimensional values, we established that the drag on the body is proportional to the coefficient of viscosity, to the linear dimensions and to the velocity. However, using the dimensional formula for the coefficient of viscosity μ, which we have obtained from Newton's law of friction, and operating with the dimensional formula for μ, we have basically operated with this law, and the result obtained is but a different form of it. Actually, according to Newton's law all stresses are proportional to $\mu\frac{dv}{dy}$ or in similar systems are proportional to μ, v_0 and $\frac{1}{l}$, where v_0 and l are the given velocity and the given linear measurement respectively. Also, because the acting force is proportional to the product of the stress times the area, which in turn is proportional to the square of the linear dimension, we can write $X \div \mu v_0 l$. [26

1.4. The Relationship Between Dimensional Analysis and Similitude

Let us define the conditions of similitude for two phenomena. Let us consider phenomena similar if they fulfill the two following conditions:

1) for every period of time of one phenomenon there exists a similar period of time for the second phenomenon, and for all the corresponding points in space the scale

constancy for each quantity (force, length, viscosity, etc.) which is part of the analyzed phenomena will remain. Generally speaking, the scales are different for different values. These periods of time will be called conforming; by conforming points of space we mean the points whose coordinates satisfy the laws of geometrical similitude for our phenomena;

2) the scale of intervals between any conforming periods of time is unchanged.

Thus, all the numerical values of any quantity in one phenomenon can be derived from the corresponding values of the second phenomenon simply by multiplying them by the constant coefficient for each of them--the so-called scale ratios.

We can analyze, then, our two similar phenomena as being the result of the application of two systems of units of measurement to the same phenomenon, since the numerical values of each type of values, which define the phenomenon when the system of units is changed, must be multiplied by some constant coefficient, i.e., by the same scale ratio which we utilized in analysis of similar phenomena.

Thus, the change of the scale ratio of the phenomenon and the change of the system of units of measurement are equivalent.

The dimensional formula can now be analyzed as a condition of interrelationship which exists between the scales of dimensional values for the two similar phenomena. As has already been noted repeatedly, the dimensionless values will, in similar cases, be simply constant. Let us analyze these problems in more detail. Suppose there are two similar processes. We will designate the values relative to one of them by the index H (nature), and of the other by the index M (model). Let us designate by the letter k with an appropriate index a scale ratio of some quantity. [27
For example, the scale ratio of length

$$k_l = \frac{l_H}{l_M};$$

of velocity

$$k_v = \frac{v_H}{v_M};$$

of density

$$k_\rho = \frac{\rho_H}{\rho_M}$$

etc.

In accordance with the definition of similitude the scale ratios k are constant at all of the corresponding points in space for the respective moments of time. Not all scale ratios are unrestricted. Some of them are interrelated.

For example, in the process of the "natural" case some particle passes the segment $\Delta l_н$ in a time $\Delta t_н$, and consequently will be moving with the velocity

$$v_н = \frac{dl_н}{dt_н} = \lim\left(\frac{\Delta l_н}{\Delta t_н}\right)_{\Delta t_н \to 0}.$$

A corresponding particle in the process of the "model" case passes the segment $\Delta l_м$ within the time $\Delta t_м$ and will have the velocity

$$v_м = \frac{dl_м}{dt_м} = \lim\left(\frac{\Delta l_м}{\Delta t_м}\right)_{\Delta t_м \to 0}.$$

According to definition the scale ratio of velocities will be

$$k_v = \frac{v_м}{v_н} = \frac{\frac{dl_м}{dt_м}}{\frac{dl_н}{dt_н}} = \lim\left(\frac{\Delta l_м}{\Delta l_н} \cdot \frac{\Delta t_н}{\Delta t_м}\right)_{\Delta t_{н,м} \to 0}.$$

However, the ratio of any length and of any time intervals for similar cases is the constant value and equal to k_l and k_t, respectively, while the limit of the constant value is the value itself. Thus

$$k_V = k_l k_t^{-1}, \qquad (1.43)$$

Comparing this formula to the dimensional formula for velocity

$$[v] = LT^{-1},$$

we see that they are identical if we take into account that the role of the units of measurement is assumed by the scale values.

It becomes evident, from further similar discussions, [28
that we can find formulas with interrelated scale ratios for various values and that these interrelated formulas will be identical to the corresponding dimensional formulas. The scale ratios of those values, through which other scale ratios are expressed, are analogous to the principal dimensions, and the scale ratios of these "other" values will respond to the derived values. The relationship of the scale ratios, just as with dimensional relationships, is found either from the determination of the values or from physical laws. As an exercise, let us find several relationships among scale ratios. The relationship between the scale ratios of inertia forces and between the scale ratios of the velocity and density we can find from Newton's law. For simplicity, let us analyze one projection of the inertia forces only, for example, its projection on the normal to the trajectory. As is known, this projection is in the form of

$$R = \frac{\Delta m v^2}{r},$$

where Δm is the mass of our particle or body and r is the radius of trajectory curvature. Obviously

$$k_R = \frac{R_н}{R_м} = k_m k_v^2 k_l^{-1}.$$

Because $\Delta m = \rho \Delta V$, where ΔV is the volume of the particle, we have

$$k_R = k_\rho k_l^2 k_v^2. \qquad (1.44)$$

since the relationship between the volumes of similar elements is proportional to the cube of the linear scale factors.

Let us recall that the dimension of force [see (1.37)] is expressed through the dimensions of length, density and velocity by an analogous formula

$$K = [\rho][v^2]L^2.$$

Let us now find the relation among the scale ratios of forces of viscous friction and the scale ratios of length, velocity and the coefficient of viscosity. Writing Newton's law for viscous friction force F

$$F = \mu S \frac{\partial v}{\partial y}$$

and proceeding in a similar manner as previously, we find

$$k_P = k_\mu k_l k_v$$

or, considering that $\rho\nu = \mu$,

$$k_P = k_\rho k_\nu k_l k_v. \tag{1.45}$$

The scale ratio for gravitational force G will be derived from the condition

$$G = mg$$

and will be

$$k_G = k_\rho k_l^3 k_g. \tag{1.46}$$

In similar systems the scale ratios of similar values must be constant. Consequently, if forces of a different nature are acting in similar phenomena, the scale ratios of these forces must be identical. It follows from this condition that [29

$$k_R = k_G = k_P,$$

substituting instead of k_R, k_P and k_G their expressions (1.44), (1.45) and (1.46), we find that

$$k_l k_v = k_\nu \tag{1.47}$$

and

$$k_l k_g = k_v^2. \tag{1.48}$$

If in any obtained scale ratio we will revert back to the initial designations and arrange all terms with subscript M on one side of the equation and terms with subscript H on the other side, we obtain an equation that states the following: for similar phenomena the dimensionless quantities are constant. This condition has been already noted from other considerations.

Let us perform the indicated operation, for example, on (1.44), (1.47) and (1.48):

$$\frac{R_M}{\rho_M l_M^2 v_M^2} = \frac{R_H}{\rho_H l_H^2 v_H^2}; \tag{1.49}$$

$$\frac{v_M l_M}{\nu_M} = \frac{v_H l_H}{\nu_H}; \tag{1.50}$$

$$\frac{v_м}{\sqrt{g_м l_м}} = \frac{v_н}{\sqrt{g_н l_н}}. \qquad (1.51)$$

The dimensionless quantities which appear in equality (1.49) are known as Newton numbers Nw, those in equality (1.50) are known as Reynolds numbers Re, and in equality (1.51) as Froude numbers Fr. Equations (1.49), (1.50) and (1.51) indicate that in the event of similarity the dimensionless combinations Nw, Re and Fr for a model and an actual case are the same.

If we had analyzed the forces of some other phenomenon, then according to the above discussion we would have obtained relationships like (1.49), (1.50) and (1.51). For example, consideration of the surface forces which are represented by the coefficient σ would lead us to

$$\frac{\sigma_м}{\rho_м v_м^2 l_м} = \frac{\sigma_н}{\rho_н v_н^2 l_н}. \qquad (1.52)$$

Let us emphasize once again that all of these conditions of similitude represent dimensionless combinations which define the process being considered and can be found from the dimensional theory. In the previous paragraph we encountered two such combinations, the Newton and Reynolds numbers, where a detailed outline was presented for their derivation using the dimensional theory. [30

Let us analyze a case when it is not possible to maintain equality between the essential dimensionless quantities (conditions of similitude) for the phenomenon under consideration for the model and the real [natural] case. For example, let π_i be one of those combinations, and $\pi_{iм} \neq \pi_{iн}$. It is obvious that under these conditions the similitude will be violated to a greater degree, the more essential are the values in our phenomenon which define π_i, and the greater is the difference between $\pi_{iм}$ and $\pi_{iн}$. The violation of similitude will lead to errors in determining the desired real quantities which were determined on the basis of model testing. The combination of errors of this type is known as the scale effect. In practical cases it becomes very important to estimate the order of the scale effect, and if it is significant, to find a method of introducing the appropriate corrections, or else to arrange the experiment in a way that will minimize the scale effect.

As was noted in the introduction, one of the ways to solve this problem is to break up the complicated phenomenon under consideration into a series of less complicated systems, which can be subjected to modelization more easily or can be analyzed with the aid of some other methods.

Let us discuss some concepts which in a number of cases allow us to estimate the magnitude of the scale effect and to simplify analysis. For better clarity we will adopt concepts which are applicable to the following, frequently encountered case. Let it be assumed that some desired dimensionless value A (for example, the depth of a cavity behind a planing boat relative to its depth, or the drag coefficient of a vessel) depends primarily on dimensionless combinations which describe geometric similitude and on the Froude number, as well as on the viscosity and the surface tension, i.e., depending also on the Reynolds and Weber numbers:

$$A = f\left(\frac{l_1}{l}, \ldots, \frac{l_n}{l}, \mathrm{Fr}, \mathrm{Re}, \mathrm{We}\right). \qquad (1.53)$$

Here l, l_1, ..., l_n are linear dimensions which define the shape and the location of the elements of an object for our problem (the dimensions of our vessel, its immersion, etc.);

$\mathrm{Fr} = \frac{v}{\sqrt{gl}}$, $\mathrm{Re} = \frac{vl}{\nu}$, $\mathrm{We} = \frac{\sigma}{\rho v^2 l}$ are correspondingly the Froude, Reynolds and Weber numbers,

where v - characteristic velocity;
g - acceleration of the force of gravity;
ρ - density of the medium;
ν - its kinematic coefficient of viscosity; [31
σ - coefficient of surface tension.

Since experiments with the model system and the prototype are very often conducted with the same set of values ρ, ν, g, and σ, the Froude number is the only similarity that is satisfied, while it is not possible to retain the similarities of the Re and We numbers. As a result, the scale effect emerges, i.e., the value A_M, which was determined from model experiments, is different from the value A_H of the corresponding prototype. If the influence of ν and σ could be neglected, then there would be no scale effect.

Rewriting (1.53) in a somewhat different form

$$A = f_1\left(\frac{l_1}{l}, \ldots, \frac{l_n}{l}, \mathrm{Fr}, \mathrm{K}, \Pi\right), \qquad (1.54)$$

where

$$\mathrm{K} = \sqrt[3]{\left(\frac{\mathrm{Fr}}{\mathrm{Re}}\right)^3} = \sqrt[3]{\frac{\nu^2}{gl^3}}; \qquad (1.55)$$

$$\Pi = \sqrt{\mathrm{Fr}^3\mathrm{We}} = \sqrt{\frac{\sigma}{\rho g l^2}}.$$

The new parameters K and Π were formed in such a way that the velocity was excluded and the values ν and σ have entered into the numerator. In order to simplify further calculations the degree of the dimensionless arrangement is selected in such a way that the linear dimension l included into the denominator will be in the first power.

In the future we will assume that the geometric similitude based on the Froude number is valid, i.e., we will assume the values $\frac{l_1}{l}$, ..., $\frac{l_n}{l}$ and Fr to be constant, then

$$A = F(\mathrm{K}, \Pi). \qquad (1.56)$$

If $\nu = \sigma = 0$, then $\mathrm{K} = \Pi = 0$. Expanding $F(\mathrm{K}, \Pi)$ into an exponential series of small values of K and Π

$$A(\mathrm{K}, \Pi) = A(0, 0) + \mathrm{K}\frac{\partial A}{\partial \mathrm{K}}(0, 0) + \Pi\frac{\partial A}{\partial \Pi}(0, 0) + \ldots; \qquad (1.57)$$

limiting to small values of the first order, we can designate

$$\Delta A = A(\mathrm{K}, \Pi) - A(0, 0) = \mathrm{K}\frac{\partial A}{\partial \mathrm{K}}(0, 0) + \Pi\frac{\partial A}{\partial \Pi}(0, 0) =$$

$$= \frac{1}{l}\left[\sqrt[3]{\frac{\nu^2}{g}}\frac{\partial A}{\partial \mathrm{K}}(0, 0) + \sqrt{\frac{\sigma}{\rho g}}\frac{\partial A}{\partial \Pi}(0, 0)\right] = \frac{C}{l}. \qquad (1.58)$$

If ν, ρ, g and σ are known, derivatives $\frac{\partial A}{\partial \mathrm{K}}(0, 0)$ and $\frac{\partial A}{\partial \Pi}(0, 0)$ are finite, and the range of K and Π values permits us to be confined to the linear approximation, then with the known constant C the scale effect will be defined as a difference

$$\Delta A_m - \Delta A_n = C\left(\frac{1}{l_m} - \frac{1}{l_n}\right). \qquad (1.59)$$

For the calculation of C it is necessary to perform two experiments with models which have specific dimensions l_{M_1} and l_{M_2}. As the result of these experiments it was found that

$$\begin{aligned} A_1 &= A(0, 0) + \Delta A_1; \\ A_2 &= A(0, 0) + \Delta A_2. \end{aligned} \tag{1.60}$$

Replacing A_1 and A_2 with their values from formula (1.58), we find from (1.60)

$$C = \frac{A_2 - A_1}{\left(\frac{1}{l_{M_2}} - \frac{1}{l_{M_1}}\right)}. \tag{1.61}$$

Substituting C into (1.59), we determine the correction specified by the scale effect. Assuming $l_{M_1} > l_{M_2}$ we find the desired value of A_H by formula

$$A_H = A_1 + [\Delta A(l_H) - \Delta A(l_M)] = A_1 + (A_1 - A_2)\frac{l_{M_1}(l_H - l_{M_1})}{l_2(l_{M_1} - l_{M_2})}. \tag{1.62}$$

We can assume that the expansion of the series is not done in the region of K = 0 and $\overline{\Pi}$ = 0, but in the region corresponding to real* values of K and $\overline{\Pi}$.

---

*K = 0 holds for two types of flow, the flow of an ideal fluid, defined by the condition $\nu = 0$, and turbulent flow with very large values of Re ($Re \to \infty$). Obviously, for our problem we have to adopt the latter. The expansion in the region of K_H and $\overline{\Pi}_H$ eliminates the necessity for analysis of limiting cases.

Expanding $A(K, \overline{\Pi})$ into a series of differences

$$\begin{aligned} \Delta K &= K_H - K_M = \left(\frac{1}{l_H} - \frac{1}{l_M}\right)\sqrt[3]{\frac{\nu^2}{g}}; \\ \Delta\Pi &= \Pi_H - \Pi_M = \left(\frac{1}{l_H} - \frac{1}{l_M}\right)\sqrt{\frac{\sigma}{\rho g}}. \end{aligned} \tag{1.63}$$

we again arrive at equations (1.59), (1.61) and (1.62). The suggested assumption for the scale effect and for the value of A for the real case, based on data from tests of two models*, will produce correct results if within the

*If we perform experiments with a greater number of models, we will be able to find the coefficients which will be related to terms of the expansion of the form of (1.58).

range of differences $l_{M_2}-l_H$ no crisis phenomena occur and there are no basic changes in $\frac{\partial A}{\partial K}$ and $\frac{\partial A}{\partial \Pi}$.

Let us note that for cases similar to the one analyzed [33
it is advisable to choose a system of parameters of the K and Π type, instead of Re and We, because the effect of constants ρ, ν, σ and g can be replaced only by the effect of one linear dimension l, i.e., instead of (1.54) we can write

$$A=f\left(\frac{l_1}{l}, \ldots, \frac{l_n}{l}, \mathrm{Fr}, l\right).$$

This type of reduction in the number of terms (in some problems l can represent not just two but a larger number of parameters) is convenient during the processing and analysis of experimental data; in particular, dependence A(l), based on the results of experiments (with given $\frac{l_1}{l}, \ldots, \frac{l_n}{l}$, Fr, ρ, ν, g, σ), allows us to directly evaluate the order of magnitude of the scale effect while preserving the constancy of those values. In order to achieve this, a graph $\Delta A_i = A_i - A_{i+1}$ depending on l is plotted using graph $\Delta(l)$, which has been plotted within the range of $l_{M_1}-l_{M_2}$. The abscissa ΔA_i is equal to the abscissa of the median of the interval being considered. $\Delta A(l)$ is extrapolated in the region $l_{M_1} - l_H$ so that $\Delta A \to 0$ with $\to\infty$. Along this curve we find values of $\Delta A(l_H)$; the scale effect will equal $\Delta A(l_{M_1}) - \Delta A(l_H) < \Delta A(l_{M_1})$.

1.5. Utilization of Concepts of the Theory of Dimensional Analysis for the Theoretical Solution of Problems

Up to now, we have basically related the theory of dimensional analysis to questions of similitude and modeling, i.e., to experimental methods of analysis. The utilization of concepts of dimensional analysis made it possible particularly to reduce the number of parameters, and hence to reduce the course of experiments. The reduction in the number of parameters also simplifies substantially

the theoretical solutions of many problems. Many examples of the utilization of the theory of dimensional analysis with this purpose can be given [15, 33]. As an illustration, we will present a solution of a two-dimensional, unidirectional, unsteady flow of a viscous fluid along the x axis in the xoy plane. For this case v = v(y, t). The equations of motion in this case will be in the form

$$\frac{\partial v}{\partial t} = \nu \frac{\partial^2 v}{\partial y^2}. \tag{1.64}$$

The initial conditions can be written as follows:

$$v(y, 0) = F(y). \tag{1.65}$$

We assume initially that F(y) is different from zero [34
in the vicinity of y = 0 only, while

$$\int_{-\infty}^{\infty} F(y)\, dy = Q. \tag{1.66}$$

It is evident that in this formulation

$$v(y, t) = Qf(y, t, \nu). \tag{1.67}$$

This equality is valid with any system of dimensional units. Adopting as our units of measurement ν and t and designating with an upper line the numerical values in this new system, we can rewrite (1.67) as follows:

$$\bar{v} = \bar{Q} f(\bar{y}, 1, 1). \tag{1.67'}$$

The relationship of the numerical values in the old and the new systems is derived from their dimensions. Using one of the methods given in Section 1.3 we find

$$\bar{v} = v\sqrt{\frac{t}{\nu}};\quad \bar{Q} = \frac{Q}{\nu};\quad \bar{y} = \frac{y}{\sqrt{\nu t}}.$$

Substituting these values into (1.67'), and taking into consideration (1.67), we obtain

$$f(y, t, \nu) = \frac{1}{\sqrt{\nu t}} f\left(\frac{y}{\sqrt{\nu t}}, 1, 1\right). \tag{1.68}$$

In the future, let us adopt the following value as

our argument

$$\xi = \frac{y^2}{\nu t}. \tag{1.69}$$

Then, taking into consideration (1.67) and (1.68), we can write

$$v(y, t) = \frac{Q}{\sqrt{\nu t}} F(\xi). \tag{1.70}$$

Substituting this equation into (1.64), after simple transformations we obtain

$$-\frac{1}{2}[F(\xi) + 2\xi F'(\xi)] = 2[F'(\xi) + 2\xi F''(\xi)]. \tag{1.71}$$

Thus, utilization of the methods of the theory of dimensions made it possible to replace the equation in terms of partial derivatives (1.64) with a simple differential equation which can be easily integrated.

Dividing (1.71) by $\sqrt{\xi}$, we obtain

$$\frac{1}{2\sqrt{\xi}} F + \sqrt{\xi} F' + 4\left[\frac{F'}{2\sqrt{\xi}} + \sqrt{\xi} F''\right] = 0$$

or

$$\frac{d}{d\xi}[\sqrt{\xi} F + 4\sqrt{\xi} F'] = 0,$$

from whence [35

$$\sqrt{\xi}(F + 4F') = \text{const}.$$

Since with $\xi = 0$ and limited values of F and F' the left part becomes zero, hence const = 0 and consequently

$$F(\xi) + 4F'(\xi) = 0;$$

integrating this equation, we obtain

$$F(\xi) = Ae^{-\frac{\xi}{4}}.$$

Returning to the values v, y, t and ν, we obtain

$$v(y, t) = \frac{AQ}{\sqrt{\nu t}} e^{-\frac{y^2}{4\nu t}}.$$

To determine A we set up the following expression

$$\int_{-\infty}^{\infty} v(y, t)\,dy = \frac{AQ}{\sqrt{vt}} \int_{-\infty}^{\infty} e^{-\frac{y^2}{4vt}}\,dy.$$

Since it is known that $\int_{-\infty}^{\infty} e^{-u^2}\,du = \sqrt{\pi}$, then, assuming $\frac{y}{2\sqrt{vt}} = u$, we find

$$\int_{-\infty}^{\infty} v(y, t)\,dy = 2AQ\sqrt{\pi}.$$

Specifically, this is also valid with t = 0 and according to condition (1.65) the right side is equal to Q and therefore $A = \frac{1}{2\sqrt{\pi}}$. Thus,

$$v(y, t) = \frac{Q}{2\sqrt{\pi vt}} e^{-\frac{y^2}{4vt}}. \qquad (1.72)$$

Subdividing the axis oy into small intervals and analyzing the interval $\eta < y < \eta + d\eta$, we will assume that v(y, 0) = = 0 outside of the segment $\eta < y < \eta + d\eta$, and $v(y, 0) = F(\eta)$ in the segment $\eta < y < \eta + d\eta$, then by formula (1.66) we will find Q in the form

$$\int_{\eta}^{\eta+d\eta} F(y)\,dy = F(\eta)\,d\eta.$$

Since equation (1.64) is linear and the sum of its solutions is also a solution, then, by obtaining from formula (1.72) (substituting y - η for y for the element dη) the value

$$v(y, t) = \frac{1}{2\sqrt{\pi vt}} e^{-\frac{(y-\eta)^2}{4vt}} F(\eta)\,d\eta,$$

we will find an expression for the velocity which will satisfy equation (1.64) and the initial condition of (1.65) in the form of [36

$$v(y, t) = \frac{1}{2\sqrt{\pi vt}} \int_{-\infty}^{\infty} e^{-\frac{(y-\eta)^2}{4vt}} F(\eta)\,d\eta.$$

As another example, let us analyze the problem of steady-state motion of a body at the free surface of an

ideal, heavy, incompressible fluid. The velocity potential of such a flow will be satisfied by the Laplace equation, while there will be a condition of constant pressure at the free surface of the body and at infinity in addition to the usual boundary conditions.

Analyzing the converted motion and adopting Bernouli's equation to the line of flow which coincides with the free surface, we can write

$$\frac{p_0}{\gamma}+\frac{v_0^2}{2g}=\frac{p_1}{\gamma}+\frac{1}{2g}\left[(v_0+v_x)^2+v_y^2+v_z^2\right]+\eta_1,$$

where p_0 and v_0 are the pressure and velocity at infinity, while η_1 is the localized elevation of the free surface above the level of undisturbed fluid.

If the disturbances are small, the square values of the small produced velocities v_x^2, v_y^2 and v_z^2 can be neglected, and then remembering that $p_1 = p_0$, we will obtain

$$v_0 v_x + g\eta_1 = 0.$$

Differentiating this equality with respect to x and taking into account that in the line of flow $\frac{d\eta_1}{dx}=\frac{v_y}{v_0+v_1}\approx\frac{v_y}{v_0}$ we obtain

$$v_0\frac{\partial v_1}{\partial x}+g\frac{v_y}{v_0}=0. \tag{1.73}$$

Adopting some characteristic dimension of the body l (length of a ship, chord of a wing) as a unit, we can convert relationship (1.73) to a dimensionless form

$$\frac{\partial\bar{v}_1}{\partial\bar{x}}+\frac{\bar{v}_y}{Fr^2}=0, \tag{1.74}$$

where

$$\bar{v}_x=\frac{v_x}{v_0};\quad \bar{v}_y=\frac{v_y}{v_0};\quad \bar{x}=\frac{x}{l};\quad Fr=\frac{v_0}{\sqrt{gl}}.$$

If we are dealing with the condition of small Froude numbers $Fr \to 0$, then for fulfillment of condition (1.74) it is necessary that at the free surface $v_y \to 0$, i.e., transferring the boundary conditions to the undisturbed

surface, we will find that it can be replaced by a solid wall; therefore, our problem will become equivalent to the problem of infinite fluid flow around the body under consideration and the mirror image of that body. Specifically, [37 the flow around a ship can be studied by means of experiments with its model placed in a wind tunnel, while the design of the submerged hydrofoil, which is moving in the range of small Froude values near the free surface, will be developed by the biplanar theory, where the upper wing represents the mirror image of the lower and which is moving in an infinite fluid.

In general, if we substitute for the flow around a body the properties of vortices and sources, then, as follows from boundary conditions with $Fr \to 0$, we can obtain the influence of the free surface by placing at the points of the mirror reflection the properties of the same particular values and by analyzing the flow of this arrangement as an infinite flow. In the case of the reflected sources, the signs remain the same, while in the case of the vortices the signs should be reversed.

If the Froude numbers are large $Fr \to \infty$, then according to (1.74) $\frac{\partial \bar{v}_x}{\partial x} \to 0$, and because far upstream from the body $v_x \approx 0$, then in general on the free surface $v_x \approx 0$. This boundary condition indicates that the mirror reflected sources* must have opposite sign, while vortices the same sign.

---

*In reality, the problem of fluid flow around a body is more complicated, since the properties introduced to fulfill the conditions on the free surface disturb to some extent the boundary conditions on the surface of the body.

CHAPTER II. SOME APPLICATIONS OF THE THEORY OF DIMENSIONAL ANALYSIS AND SIMILITUDE TO PROBLEMS OF WATER-DISPLACING VESSELS

2.1. Determination of Relationships Among the Elements of Two-Dimensional Gravity Waves

Let us analyze the problem of a relationship among the length l, velocity v and the period τ for two-dimensional, steady-state waves on the surface of an ideal incompressible fluid with infinite depth.

Among the values of l, v and τ there exists, based on their definition, an equation of relationship

$$v = \frac{l}{\tau}, \tag{2.1}$$

which allows us to find one of these values when the other two are known. Let us try, applying the method of dimensional analysis, to establish the relationship of interdependence among l and v, for example, and consequently to enable us to obtain with one of our values known the other two.

Let us establish on what the velocity of wave propagation may depend. Obviously, this velocity can depend on the wave dimensions--length l and height h--and on the constants which determine the properties of the medium and the field of external forces*, i.e., on the density ρ

---

*Capillary and viscosity forces are being ignored here.

---

and gravitational acceleration g

$$v = F(l, h, \rho, g). \tag{2.2}$$

Using one of the approaches shown in Sect. 1.3 we can write a dimensionless relationship corresponding to equation (2.2), for example

$$\frac{v}{\sqrt{gl}} = f_1\left(\frac{h}{l}\right). \tag{2.3}$$

It is evident that the velocity of wave propagation cannot depend on ρ, since it is not possible to form a dimensionless equation into which the density would enter.

We had a similar case in regard to mass in the pendulum example in Sect. 1.3. According to (2.3)

$$v = \sqrt{gl} f_1\left(\frac{h}{l}\right), \qquad (2.4)$$

i.e., the velocity of two-dimensional gravity wave propagation, with the imposed limits, is proportional to the square root of the wave length and the gravitational acceleration. The coefficient of proportionality depends on the ratio of the height of the wave to its length only.

In further discussion we will limit ourselves to the linear representation of the problem, which is usually applied to the wave theory.

In the linear representation, the velocity and all the characteristic horizontal dimensions are independent of the wave height, and therefore

$$v = \text{const}\sqrt{gl}. \qquad (2.5)$$

The value of the constant cannot be determined from the dimensional theory; in the wave theory it can be proven that

$$\text{const} = \frac{1}{\sqrt{2\pi}},$$

thus, the relationship of the velocity and wave length is given by formula

$$v = \sqrt{\frac{gl}{2\pi}}. \qquad (2.6)$$

We can state some simple concepts which would clarify the applied independence of the length and velocity of waves from their height. Since the Laplace equation is linear, with the linear boundary conditions on the free surface the sum of the particular solutions will also be a solution.

Adding the solutions which contain similar wave forms, [39
we probably will obtain a wave of the same length, propagating with the same velocity, but with ordinates arbitrarily stretched in the vertical direction.

2.2. Waves Produced By Ships [62]

During the motion of a ship the two following wave systems are formed: one in the region of the bow and the

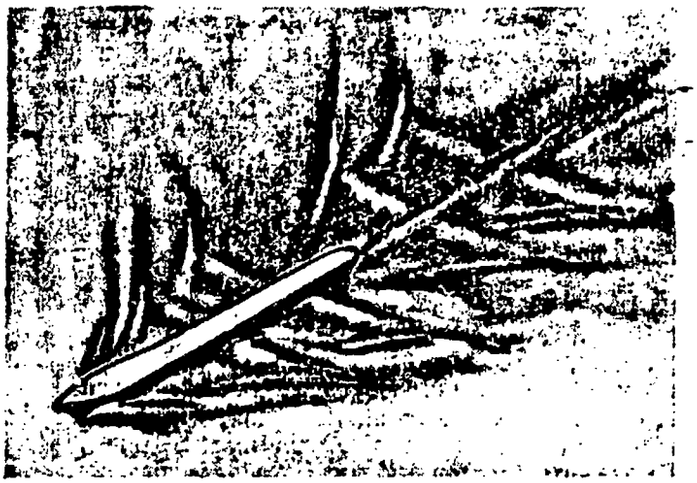

Fig. 1. Wave system near a moving ship.

other in the region of the stern. Each wave system consists of transverse and divergent waves; the latter propagate along rays which emanate from the place of their origin (bow and stern) and which form an angle $\alpha = \sim 20^\circ$ with the diametral plane of the ship's hull. The wave crests themselves form an angle on the order of 2α with the same plane (Fig. 1).

A wave system that resembles a ship's wave system was theoretically developed and calculated by Thompson, based on the representation of the ship's end conditions as point sources of disturbances.

The elements of circular waves formed by an initial pulse acting at a point are found from Laplace's equation

$$\frac{\partial^2 \varphi}{\partial x^2} + \frac{\partial^2 \varphi}{\partial r^2} + \frac{1}{r}\frac{\partial \varphi}{\partial r} = 0,$$

the solution of which must satisfy the boundary conditions of the undisturbed state at infinity as well as the constancy of pressures at the free surface with the initial condition of no disturbance anywhere, except for a small region near the origin of coordinates. The solution of this problem, which is derived from the wave theory, can be found in the courses of Kochin, Kibel' and Roze [15] and Pavlenko [23]. [40

Let us show how to arrive at the ship's wave system without solving Laplace's equation, but by using concepts of the theory of dimensional analysis instead.

Let us assume a disturbance created by a point-type pulse on the surface. From the condition of axial symmetry it follows that circular waves would form which will move out from the center to the periphery. Let us establish the dependence of the radius of any crest or trough on time t. Taking into consideration the concepts discussed in Sect. 2.1, we can write that

$$r = F(t, g).$$

The radius does not depend on the magnitude of the pulse, or in other words, on the magnitude of the disturbance, in the linear presentation. This was explained in the previous example. The dimensionless combination is made up from these variables,

$$\frac{r}{gt^2} = C = \text{const}, \tag{2.7}$$

since it is not possible to form a dimensionless parameter from the values of t and g under the function sign. From equation (2.7) it follows that

$$r = k_1 t^2, \tag{2.8}$$

i.e., the distance of a specific point under consideration (the crest of a wave, for example) from the origin of the coordinate system varies in direct proportion to the square of time. A system of spreading circular waves will be formed from the action of a point source (a stone thrown into the water). The various values of the constant will correspond to its various crests

$$k_1 = Cg. \tag{2.9}$$

Substituting a point force of disturbances for the end of a ship, we can imagine the wave system as a superimposed system of circular waves, formed by a pulse moving with the same velocity v as the ship.

For visualization it is advantageous to initially replace the continuous motion with intermittent motion of the finite pressure pulse

$$I = \int_0^t p dt$$

by an amount Δx and increments of time that follow one after another through small intervals τ, whereupon

$$\frac{\Delta x}{\tau} = v.$$

In Fig. 2 a series of sequential locations of a pulse and of the corresponding positions of the crests of one of the circular waves is shown whose radius, according to (2.8), varies proportionally to the square of time. [41

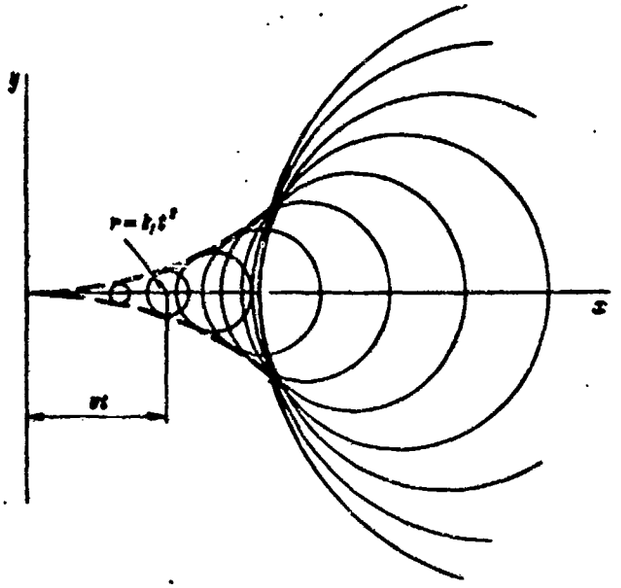

Fig. 2. Diagram of the wave formation produced by a moving pressure pulse. The wave is an envelope of a system of circular waves.

The equation of the circle (of the crest) whose center is $x_0 = vt$ from the source of the disturbance will be (Fig. 2)

$$(x-x_0)^2+y^2=kx_0^2. \tag{2.10}$$

where

$$k=\frac{k_1^2}{v^2}. \tag{2.11}$$

By increasing the number of intervals infinitely and correspondingly decreasing their magnitudes, and thus decreasing the magnitude of the pulse, we also decrease the wave heights, which will remain finite only in the region of their repeated application, i.e., along the contour of the envelope of our group of circles.

In order to determine the envelope we take the derivative of equation (2.10) with respect to parameter x_0

$$-2(x-x_0)=4kx_0. \tag{2.12}$$

and, solving simultaneously (2.10) and (2.12), obtain the equation of the envelope in parametric form:

$$x = x_0(1 - 2kx_0^2);$$

$$y = \pm x_0 \sqrt{kx_0^2 - 4(kx_0^2)^2}. \qquad (2.13)$$ [42

Our curve will lie within an angle whose tangent corresponds to the maximum of the expression

$$\operatorname{tg}\alpha = \frac{y}{x} = \pm \frac{\sqrt{kx_0^2 - 4(kx_0^2)^2}}{1 - 2kx_0^2}.$$

The maximum value $(\operatorname{tg}\alpha)_{max} = \pm \frac{1}{2\sqrt{2}}$.

The corresponding angle $\alpha_{max} = \pm 19^{\circ}28'$. Figure 3 shows a wave system produced by a moving pressure pulse; each curvilinear triangle can be calculated from formulas (2.13); it corresponds to its value k, i.e., to the different crests which are formed from the action of the point pulse.

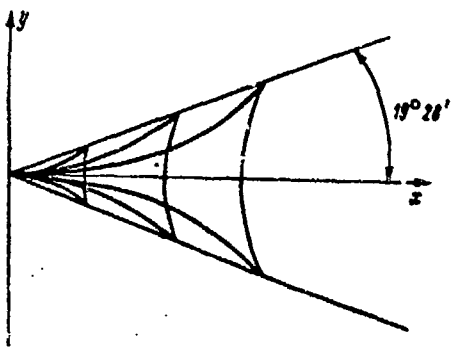

Fig. 3. Wave system produced by a moving pressure pulse.

The sides of the curvilinear triangles correspond to the divergent ship waves, while the base corresponds to transverse ship waves.

Comparison of Fig. 3 with Fig. 1 indicates a great similarity between actual and theoretical wave profiles.

If we apply the assumption that these transverse waves have the length of the corresponding plane waves propagating with the velocity of the ship v, we will able to determine the constant in formula (2.8).

In an actual case, equating the value y to zero in the second formula (2.13), we will find that the position of the transverse crest at the point of its intersection with the diametral plane will be determined by the coordinate

$$x_1 = \frac{1}{2\sqrt{k}}.$$

Taking formulas (2.9) and (2.11) into consideration, we find

$$x_1 = \frac{v^2}{g} \cdot \frac{1}{2C}. \qquad (2.14)$$

The wave length l will be found from the difference of two adjacent values of x_1 that correspond to the two values of constant C.

Let us designate

$$\frac{1}{C} = 2m. \qquad (2.15)$$

Then, designating the adjacent values of m by primes m' and m", we will find from (2.14) and (2.15) [43

$$l = \frac{v^2}{g}(m'' - m'). \qquad (2.16)$$

On the other hand, the length of two-dimensional waves propagating with velocity v will be

$$l = \frac{2\pi v^2}{g}. \qquad (2.17)$$

Combining formulas (2.16) and (2.17), we obtain

$$m'' - m' = 2\pi, \qquad (2.18)$$

i.e.,

$$m = 2n\pi + \delta, \qquad (2.19)$$

where n is any whole number, while δ defines the phase of the initial disturbance.

At this time, considering (2.15), we can finalize the formula for wave propagation from a point source in the form

$$r = \frac{gt^2}{4n\pi + 2\delta}. \qquad (2.20)$$

Let us compare these results with the solution of the hydrodynamic problem of waves formed by a point pulse. This solution produces an equation of a free surface in the form

$$\zeta = \frac{1}{2\pi^2 g}\left[\int_0^{\pi} d\lambda \int_0^{\infty} \sigma \sin(kr\cos\lambda - \sigma t)\, dk - \right.$$
$$\left. - \int_0^{\pi} d\lambda \int_0^{\infty} \sigma \sin(kr\cos\lambda + \sigma t)\, dk \right],$$

where

$$\sigma = gk.$$

An approximate integration of this equation leads us to the formula

$$\zeta = \frac{gt^2}{2^{7/2}\pi r^{3/2}} \sin\frac{gt^2}{4r}.$$

This result is valid for large values of $\frac{gt^2}{4r}$. The locations of crests and troughs can be found as a result of finding the limits of the ζ values and leads us to the following expression:

$$r_i = \frac{gt^2}{4m_i}, \qquad (2.21)$$

where m_i is the root of the equation [44

$$\operatorname{tg} m = -\frac{m}{4},$$

whereby the roots alternately correspond to a crest and a trough.

The interval between the roots, corresponding to the crests (or the troughs), happens to be somewhat smaller than 2π initially, then in the region of large values of m_i it approaches 2π, when the result of the approximated integration is valid.

For large values of m_i the following approximation is valid:

$$m_i = \frac{2n+1}{2}\pi,$$

i.e., according to (2.21)

$$r = \frac{gt^2}{2\pi(2n+1)}. \qquad (2.22)$$

The same result can be obtained from (2.20) if we assume $\delta = \pi$.

Thus, the solution (2.20), which was found with the theory of dimensions and some other simple concepts, happened to be similar to expression (2.22), which was obtained from the linearized hydrodynamic problem. Besides, the difficulty of computations in this solution made it necessary to employ methods of approximated integration, as a result of which the small values of roots m_i contained

errors; the large values of m_i are in agreement with the given simple solution, where the methods of dimensional analysis and certain physical considerations were used.

In the examples given above, and also in examples of Sect. 1.3, the effectiveness of the dimensional theory and the possibilities of obtaining with it a number of important results which clearly establish the dependencies among the values under consideration have been illustrated. These results are accomplished with an extremely simple mathematical technique; however, for their derivation additional physical or mathematical concepts in regard to the analyzed phenomena are necessary. They include, in addition to the selected specific parameters which define the problem, the concepts of linearization, symmetry, etc.

If only the determining parameters are known and their number is greater than the number of principal dimensional units, the dimensional analysis theory does not allow us to establish a clear dependence among these parameters. However, it will always provide an opportunity to decrease the number of variables, and it also helps in rational preparation of a scientific experiment and its correct simulation. Below, we will examine several similar examples.

2.3. The Resistance of Water to Ship Motion, and Ship Propellers [45

In Sect. 1.3 we have already analyzed the drag X on a body in an infinite, viscous, incompressible fluid, and have established that for all geometrically similar bodies

$$X = \rho v^2 l^2 f(\mathrm{Re}). \qquad (2.23)$$

For a vessel moving along the free surface, it is also necessary to consider the weight which is related to the wave processes and is determined by the gravitational acceleration g. The value g must be introduced into the terms of the function which is in the right part of (1.33). The appearance of the new term will force an introduction of a new dimensionless combination which can be found by one of the methods described in Ch. I. It is easy to see that such a combination can be chosen in the form of the already known Froude number

$$\mathrm{Fr} = \frac{v}{\sqrt{gl}}.$$

Instead of (2.23) we must now write

$$X = \rho v^2 l^2 f(\mathrm{Re},\ \mathrm{Fr}). \qquad (2.24)$$

Let us note that neither (2.23) nor (2.24) allow us to establish the relationship between drag, length l and velocity v, and even though the first co-factor of the right part of the equation shows proportionality between the drag and the squares of the velocities and linear dimension, this proportionality is valid only if Fr = const and Re = const are preserved. In general, without this restriction, formulas (2.23) and (2.24) do not indicate any specific relationship between X, l and v because l and v enter into the terms of function f.

However, formula (2.24) indicates that instead of five terms (ρ, v, l, ν, g) on which the drag depends, for geometrically similar vessels it is necessary to find a function of only two terms Re and Fr, and if this function is known, then by (2.24) the value X can be determined.

Specifically, if we build a model geometrically similar to the prototype and test it for arbitrary values of v, but keep Fr and Re the same as for the prototype, then the function f can be found from the obtained measurements with a formula which is obvious from (2.24):

$$f(\mathrm{Re},\ \mathrm{Fr}) = \frac{X_M}{\rho_M l_M^2 v_M^2}, \qquad (2.25)$$

and, consequently,

$$X_H = \rho_H v_H^2 l_H^2 \frac{X_M}{\rho_M l_M^2 v_M^2}. \qquad (2.26)$$

Here, as was done previously, we denote by subscripts M and H the corresponding values for the model and the real ship, respectively.

It should be noted that in literature and even in the specific books about the dimensional theory we can encounter statements that some of the criteria of similitude are "incompatible." Specifically, this is stated with respect to the Reynolds and Froude numbers. For example, in the book by L. M. Nogid [21], on p. 18 it is stated* "...It may, [46

---

*Emphasis ours (L.E.).

---

however, turn out that some of the found criteria are incompatible, and due to this it is not possible to satisfy all values of π in

$$\pi = \text{idem.}$$

"In such instances it is not possible to simulate the phenomenon to full extent. Specifically, for example, as will be shown below, the wave drag and the skin-friction drag exerted on a ship can be defined by phenomena that are incompatible with the criteria of similitude for the model. Therefore, two noted components of the total drag cannot be determined together experimentally."

Actually, the claim of incompatibility of similitude criteria, or in other words of dimensionless combinations, is in principle wrong. Since these criteria (combinations) are independent, their compatibility can always be assured by means of proper selection of variables and formulation of the experiment.

The other problem that arises in this respect is the difficulty of fulfilling the requirements for a given experiment, high cost, or sometimes it may even be dangerous, etc. Let us analyze this in more detail based on a previously given example of "compatibility" of quantities

$$\mathrm{Re} = \frac{vl}{\nu}$$

and

$$\mathrm{Fr} = \frac{v}{\sqrt{gl}}.$$

Usually, accepting this as unalterable fact, we can consider that for a model and a prototype ν and g are constant and we can say that it is not possible to make, at the same time, the velocity inversely proportional to the length of the model (the condition for Re = const) and directly proportional to the square root of this length (the condition for Fr = const).

The second condition is incompatible with the first. The essence of "compatibility" is contained not in the dimensionless criteria, but rather in the postulation of the condition that ν = const and g = const for the model and the prototype.

The theory of dimensional analysis indicates the concrete ways by which the similitude should be achieved; specifically, it indicates the necessity to adopt fluids with lower viscosity* for models that are smaller than the prototype.

*Let us note that the constancy of acceleration is not obligatory, and in a number of analyses (in the case of centrifugal machinery, for example) g is varied.

Of course, in this respect we encounter serious technical difficulties, but the presence of these difficulties does not provide us with the basis to claim incompatibility of the criteria. [47

Let us see whether the Froude criterion really does disrupt satisfaction of similitude by using Re.

If, for example, the model of some ship which has a speed of 12 knots is made to a scale of 1:20 of the prototype, then to preserve the constancy of the Re number for the same medium (water), it becomes necessary to conduct the experiments at a speed v = 240 knots, whereupon the forces acting on the model would be equal to the forces acting on the prototype.

In order to eliminate the phenomenon of cavitation at such high speeds, it would be necessary to increase the pressure in the room where the experiment is conducted to several tens of atmospheres.*

*Actually, in order to maintain the same number for the cavitation (see below) it would be necessary to have ~400 atm. pressure.

We used an example of a low-speed ship, but if, however, we consider a high-speed ship, say a destroyer with a speed of 40 knots, then it would be necessary to produce a velocity of 800 knots for the same scale of model, and the pressure would have to be brought up to 400 atmospheres.

Thus, even in the absence of the requirement to maintain the Froude number, the technical difficulties for achieving similitude with respect to Re are probably insurmountable; in any case, these difficulties are no less than those that are related to conducting the experiments in a different medium.

If we combine the possibilities in principle with technical difficulties, then we should insist that Reynolds' criterion is in itself incompatible with the requirements

of similitude.

Thus, all the criteria of similitude (independent dimensionless combinations) are compatible, and the problem of the analyst narrows down to the selection and the organization of such an experiment which can preserve the equality of the dimensionless parameters for both the model and the prototype.

In our case, we should select velocities in agreement with Froude's law, and the viscosity should be based on the condition that will keep the Reynolds number constant. Then, by formulas (1.47) and (1.48) $k_\nu = k_l^{3/2}$ (we have assumed that $k_g = 1$).

Thus, the viscosity would have to be varied according to the linear scale of three halves. For commonly employed scales we need a fluid 20-200 times less viscous than water.

Unfortunately, water is a fluid with low viscosity; therefore, it is difficult to find a medium with lower viscosity. We can, however, indicate a group of esters or pentane, whose kinematic viscosity is one-fifth that of water. As is known, liquid helium has infinitely small viscosity at temperatures approaching absolute zero.

It is possible that progress in modern chemistry will develop a more convenient fluid with the required viscosity for hydrodynamic analysis. [48

Of course, in any preparation of an experiment it should be considered to what degree any complication that guaranties similitude of various factors is necessary.

Questions as to whether certain complications of an experiment are worthwhile have to be resolved individually for the specific problems; however, the questions of worthiness and fundamental possibilities should not be mixed up. It seems to us that in the case under consideration the use of models of hydrodynamic phenomena in fluids with low viscosity is sufficiently urgent and is unjustly ignored.

In addition to the above, let us note that some experiments which seemed to be very complex and impossible to fulfill at a certain stage of technical development later on became well developed. Without going into any remote regions of applications, we can indicate the use of wind tunnels with variable density, in which in accordance

with Maxwell's paradox regarding the independence of μ from ρ, experiments are conducted under pressures up to 20 atm in order to decrease the corresponding values of the coefficient of viscosity. In these wind tunnels, by reducing ν significantly high Reynolds numbers are obtained at relatively low velocities. The following example of modeling of screw propellers provides another case of surmounting similar difficulties.

At the present time, when there is still no possibility of maintaining the same Reynolds values for the models of ships and the prototypes, the determination of the total drag becomes a problem in two parts, namely: skin friction drag, which is dependent on the Reynolds number; and residual drag, which is independent of the Reynolds number, since it includes wave drag and pressure drag. Although the pressure drag is specified by viscosity, its values are assumed, starting with certain values of $Re_{кр}$, to be self-similar, i.e., the pressure drag coefficient is assumed to be independent of Re values. A geometrically similar (in outer outline) model is tested with Froude numbers which are equal to the prototype; from the measured total drag we subtract the surface friction drag, which is determined as the friction drag of a flat plate, the wetted area and length of which are equal to the corresponding area and length of the model. The residual drag that is obtained is recomputed with respect to Froude's law of similitude (since according to the statement above it is assumed to be independent of Re). To the ship's residual drag that has been found in this manner we add its surface friction drag, which was determined just as for the model, but with real-case Reynolds numbers.

We have presented here only the principal scheme. The problem of determining the drag of a ship by analyzing its model is widely described in literature, handbooks, and textbooks (see [8, 9] for example). Let us also note that the detailed analysis of this problem depends on the consideration of a whole series of additional conditions, of which we will indicate only a few: the surface drag of the model and of the prototype are somewhat different from the "equivalent" flat plate. In order to determine the surface friction drag of a model, it is necessary to create a turbulent state of flow in the boundary layer (for small models this can be achieved by placing a special turbulence attachment at the bow). It is necessary to introduce corrections which take into account the effect of the surface roughness of the real ship on its drag. Even in the event of the use of large models, for which Reynolds numbers correspond to the supercritical state of flow around the

[49

hull, characteristics of flow for relatively small parts--like protruding parts--will remain subcritical. This condition can lead to noticeable errors in the presented methods of recomputation. In a number of cases, more accurate results can be obtained when a model without any protruding small parts is tested, later adding their drag, which has been previously determined from tests with the same or similar materials and with high Reynolds numbers. Certainly, here too, errors due to the failure to consider the mutual action of the hull and protruding parts can arise.

It becomes evident from the given examples that in order to obtain results which closely duplicate the actual conditions, we knowingly make pronounced deviations, even in geometric similarity (roughness, positioning of turbulence attachments, removal of protruding parts from the model).

Let us now examine the modeling of screw propellers and the factors that may have an effect on the thrust P and the moment M of a submerged screw propeller. Obviously, P and M will depend on the diameter of the propeller D, its pitch H, disc relationship δ, number of blades z, and a number of linear dimensions $l_1, \ldots, l_n$, which determine the geometry of the propeller; further, we must list the following kinematic characteristics: forward velocity v and propeller rpm n.

For given geometry and kinematics the thrust and the moment will be determined by the properties of the medium --its density ρ and viscosity ν.

If we examine the operating conditions in the absence of cavitation, the amount of external static pressure will not be a determining factor; static pressure produces a resultant equal to zero and therefore its changes cannot reflect on the characteristics of the propeller. The weight of the fluid, i.e., the value g, also has virtually no effect if the propeller is submerged to a sufficient depth below the free surface.

In a general case, when cavitation may be present, the amount of static pressure p_0 plays a significant role, since by changing the pressure and keeping all other conditions the same, we can either induce or eliminate cavitation, i.e., make the conditions for separation of the continuity of fluid either easier or more difficult. Since the conditions that establish the existence of sufficiently deep cavities are determined by the difference between the external pressure and the pressure of saturated vapors p_d, [50

then instead of the outer pressure p_0 and pressure p_d, we can introduce the following difference into the parameters which determine the performance of the screw propeller:

$$p_0 - p_d.$$

Taking cavitation into account, it is necessary to reintroduce the weight of the fluid, in addition to the pressure difference $p_0 - p_d$, because for a given pressure at some level, for example at the level of the propeller axis, the weight determines the pressure at various points of the propeller's disc. Thus, we have enumerated the main factors and consciously avoided a number of secondary ones, such as the presence of diluted air in the water, its contamination, etc.

In accordance with the above discussion, we can write

$$\begin{aligned} P &= F_1(D, H, \theta, z, l_1, \ldots, l_n, v, n, \rho, \nu, p_0 - p_d, g); \\ M &= F_2(D, H, \theta, z, l_1, \ldots, l_n, v, n, \rho, \nu, p_0 - p_d, g). \end{aligned} \qquad (2.27)$$

Let us emphasize that in order to adopt the methods of dimensional analysis, it was necessary to form expressions (2.27) as the initial condition, and this, in turn, required definite physical representations in regard to the phenomenon under consideration.

Let us write expressions (2.27) in a dimensionless form, taking D, n and ρ as principal values.* The dimen-

*It is recommended to the reader, as an exercise, to take other groups for principal values, for example D, n, $p_0 - p_d$ or ν, ρ, g or ν, g, $p_0 - p_d$, etc., and with the derived expressions to again come up with (2.33) or (2.34).

sions of all other values are expressed through [D], [n] and [ρ] by the following formulas (see Ch. I):

$$\begin{aligned} &[P] = [\rho][n^2][D^4]; \quad [p_0 - p_d] = [\rho][n^2][D^2]; \\ &[H] = [l_i] = [D]; \quad [g] = [D][n^2]; \\ &[v] = [D][n]; \quad [M] = [\rho][n^2][D^5]. \\ &[\nu] \quad [D^2][n]; \end{aligned} \qquad (2.28)$$

Making D, n and ρ equal to unity, i.e., increasing

their units of measurement by D, n and ρ times, we will decrease the numbers which measure other values in accordance with their dimensional formulas, and as a result, instead of (2.27) we obtain

$$\frac{P}{\rho n^2 D^4} = f_1\left(1, \frac{H}{D}, \vartheta, z, \frac{l_1}{D}, \ldots, \frac{l_n}{D}, 1, 1, \frac{v}{nD}, \right.$$
$$\left. \frac{\nu}{nD^2}, \frac{p_0 - p_d}{\rho n^2 D^2}, \frac{g}{Dn^2}\right);$$
$$\frac{M}{\rho n^2 D^5} = f_2\left(1, \frac{H}{D}, \vartheta, z, \frac{l_1}{D}, \ldots, \frac{l_n}{D}, 1, 1, \frac{v}{nD}, \right. \qquad (2.29)$$
$$\left. \frac{\nu}{nD^2}, \frac{p_0 - p_d}{\rho n^2 D^2}, \frac{g}{Dn^2}\right). \qquad [51$$

For all geometrically similar propellers only the last four terms will remain and formulas (2.29) will be as follows:

$$\frac{P}{\rho n^2 D^4} = f_1\left(\frac{v}{nD}, \frac{\nu}{nD^2}, \frac{p_0 - p_d}{\rho n^2 D^2}, \frac{g}{n^2 D}\right);$$
$$\frac{M}{\rho n^2 D^5} = f_2\left(\frac{v}{nD}, \frac{\nu}{nD^2}, \frac{p_0 - p_d}{\rho n^2 D^2}, \frac{g}{n^2 D}\right). \qquad (2.30)$$

The so-called coefficients of thrust k_1 and moment k_2 stand on the left:

$$k_1 = \frac{P}{\rho n^2 D^4}; \qquad (2.31)$$
$$k_2 = \frac{M}{\rho n^2 D^5}.$$

The terms of the function are:

1) advance ratio of the propeller

$$\lambda = \frac{v}{nD}; \qquad (2.32)$$

2) a value inverse to the Reynolds number, which has been determined by the circumferential velocity at the ends of the propeller blades u and the diameter of the propeller,

$$\frac{\nu}{nD^2} = \frac{\pi}{\frac{\pi nDD}{\nu}} = \frac{\pi}{\frac{uD}{\nu}} = \frac{\pi}{\mathrm{Re}_u};$$

3) cavitation number $\varkappa_u$, defined by the same velocity,

$$\frac{p_0 - p_d}{\rho n^2 D^2} = \frac{p_0 - p_d}{\rho u^2} \pi^2 = \frac{\pi^2}{2} x_u;$$

4) a value inverse to the square of the Froude number, defined by the diameter of the propeller and velocity, and

$$\frac{g}{n^2 D} = \frac{gD}{n^2 D^2} = \pi^2 \frac{gD}{u^2} = \frac{\pi^2}{Fr_u^2}.$$

The last three terms contain the still constant multipliers, which we will drop later on, and we will write (2.30) as follows:

$$k_1 = f_3(\lambda, Re_u, x_u, Fr_u);$$
$$k_2 = f_4(\lambda, Re_u, x_u, Fr_u). \qquad (2.33)$$

Instead of (2.33) we can write

$$k_1 = \Phi_1(\lambda, Re, \varkappa, Fr);$$
$$k_2 = \Phi_2(\lambda, Re, \varkappa, Fr), \qquad (2.34)$$

where Re, $\varkappa$ and Fr are defined by the axial velocity v. [52
Actually, for example

$$Re_u = \frac{uD}{\nu} = \frac{\pi n D^2}{\nu} = \pi \frac{nD}{v} \frac{vD}{\nu} = \frac{\pi}{\lambda} Re.$$

Since λ already enters into the number of terms and the terms f_3 and f_4 are replaced by Φ_1 and Φ_2, we can obviously replace (2.33) with (2.34).

If the Re numbers are not too small, specifically

$$Re > 10^5 \frac{\pi\lambda}{8},$$

then the influence of the Re number can be disregarded, and

$$k_1 = \Phi_1(\lambda, \varkappa, Fr);$$
$$z_2 = \Phi_2(\lambda, \varkappa, Fr).$$

In the absence of cavitation and with sufficient depth of submergence of the propeller, according to the above discussion, the terms $\varkappa$ and Fr are dropped simultaneously from the number of expressions and we arrive at the following conclusion, that the coefficients of the thrust k_1 and moment k_2 are functions of the advance ratio λ only.

All these conclusions also pertain to the efficiency of the propeller η, since it is expressed by k_1, k_2 and λ,

$$\eta = \frac{k_1}{k_2}\frac{\lambda}{2\pi}.$$

In the absence of cavitation the dependencies $k_1(\lambda)$, $k_2(\lambda)$ and $\eta(\lambda)$ can be obtained experimentally by testing geometrically similar models of a propeller with independent values of velocity and revolutions, but maintaining the required λ values. These tests are usually performed in test basins. The propeller and the measuring apparatus are placed on a tow-cart; by varying the speed of the tow-cart and the number of propeller rpm, different values of advance ratio are obtained. Experiments in air can be substituted for experiments in water. The problem for determining propeller properties becomes considerably more complex if cavitation is taken into consideration.

Since the pressure p_0 is basically the atmospheric pressure, which, like p_d, remains the same for actual and simulated conditions, it follows from the equality of the cavitational numbers that water testing of the model should be performed at natural forward velocities and this, in turn, requires (in order to satisfy λ = const) that the number of revolutions of the model should exceed the number of revolutions in reality by as many times as the model is smaller than the real propeller. In addition, from the [53
conditions of maintaining constancy of the Froude number, forward velocities of the model must be smaller than natural by the square root of the scale of the model. Again, we are met by "incompatibility" in the requirements of similitude; however, just as in the example analyzed above, this incompatibility refers not to the criteria of the similitude, but rather to the arbitrarily established condition of constancy of external pressure and pressure of saturated vapor for the model and the real case. If we neglect this constancy, then the requirements of similitude are satisfied.

Of course, variation of pressures p_0 and p_d is linked to surmounting technical difficulties. Practically, this is resolved through the installation of special cavitation tunnels in which the static pressure as well as the saturated vapor pressure (by heating the water) can be varied within a wide range.

It is not possible to obtain small cavitation numbers

Fig. 4. Photograph of a propeller in a cavitation tunnel with the free stream surrounded by rarefied gas. [52

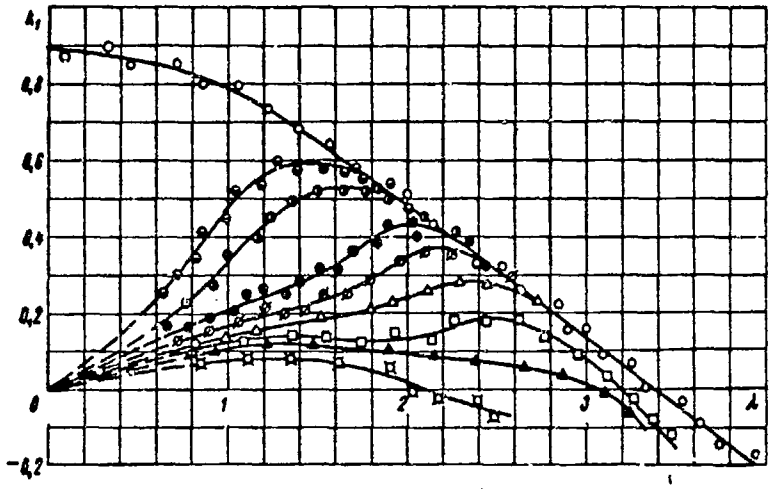

[53

Fig. 5. Example of the dependence of the coefficient of screw propeller thrust k_1 on the advance ratio λ and the cavitation number $\varkappa$. Tests in a cavitation tunnel with a free stream.

o - without cavitation; ● - x = 3; ⊙ - x = 2; ● - x = 1; ∅ - x = 0.7; Δ - x = = 0.5; □ - x = 0.3; ▲ - x = 0.2; ⊠ - x = 0

in ordinary cavitation tunnels, due to the beginning of cavitation on tunnel and pump surfaces. These difficulties can be surmounted by way of special design of the tunnels with a free stream of water surrounded by rarefied gas. Figure 4 is a photograph of a propeller test in this type of tunnel. The tunnel was built at TsAGI in 1947 [51]. In this tunnel cavitation numbers of $\varkappa = 0$ could be reached. Figure 5 shows an example of the dependence of the coefficient of thrust k_1 on the advance ratio λ and the cavitation number $\varkappa$.

Relatively small dimensions of working cross sections (the biggest tunnel at the University of Pennsylvania has a working cross section diameter of 1.2 m) make experimentation with ship models fitted with screw propellers more [55

difficult, although the presence of the hull of the ship can have a significant effect on the characteristics of a cavitational propeller. In order to obtain the necessary experimental data and in order to eliminate the influence of the walls of the tunnel, at the present time, according to information in available literature, hermetically tight model testing basins with variable pressures are being built.

Analysis of screw propellers under conditions of highly developed cavitation with small values of advance ratio λ and cavitation number $\varkappa$ can also be performed, by the method of induced cavitation developed by the author [50] at TsAGI, whereby the cavity is formed by feeding air or some other gas into the region of rarefaction. In this method, in the formula for the cavitation number the role of pressure of saturated vapors p_d is played by p_k, the gas pressure in the cavity. By regulating and measuring p_k, it is possible to obtain very small cavitation numbers at relatively low velocities. Experiments of this type can be performed in ordinary model testing basins. Especially developed procedures and apparatuses make it possible to supply air and make dependable pressure measurements in cavities rotating together with propeller blades [51]. The design scheme of such a system is shown in Fig. 6; Fig. 7 is a photograph of a propeller for one of the conditions with a well developed cavity.

2.4. Concerning Modeling of Rolling and Pitching and the Maneuverability of Ships

In contrast to the previously analyzed problems with respect to modeling for analysis of ship drag and screw propeller characteristics, for analysis of rolling and pitching and of the maneuverability of ships the motion of the object under study is not defined by the given kinematic conditions (speed, number of revolutions). This motion is stipulated by hydrodynamic forces, as well as the inertia forces of the body itself. Therefore, in addition to the geometric dimensions of the body, the properties of the medium and the field of external forces, the defining parameters will include values which characterize the inertia properties of the object, namely: its mass, moments of inertia relative to respective axes, coordinates of the center of gravity, etc. The so-called dynamically similar model, i.e., a model which, besides being geometrically similar to the prototype also has similar characteristics of mass distribution, would be required for the experiments.

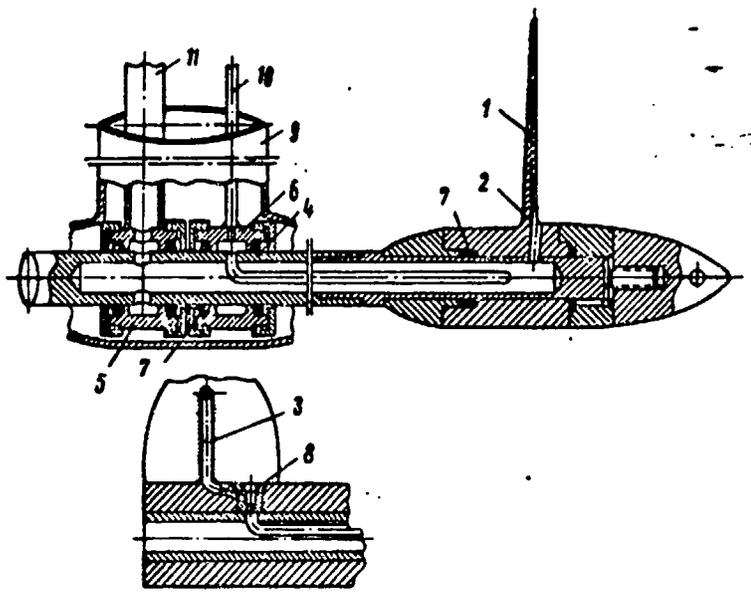

Fig. 6. Design scheme of a device for testing screw propellers with an air supply to form conditions of artificial cavitation.
1. blade; 2. channel for air supply; 3. pipe for pressure measurements in the cavity; 4. tubular shaft; 5. air supply collector; 6. collector for pressure measurement in the cavity; 7. stuffing box seal; 8. device for sealing the air intake for pressure measurements; 9. propeller cone; 10, 11. pipes leading to the manometer and the air blower.

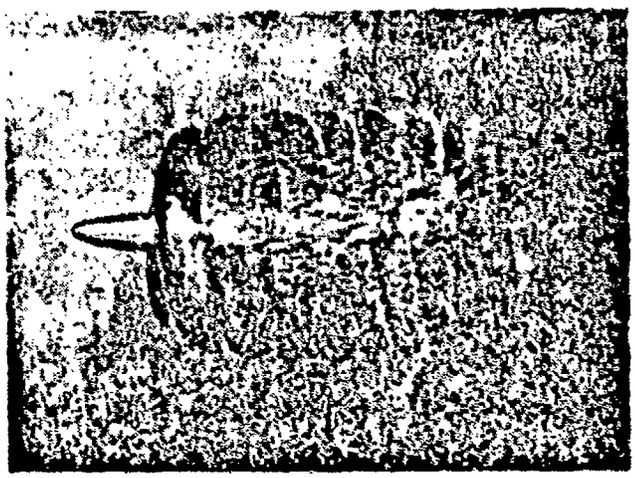

Fig. 7. Photograph of a propeller with the condition $\lambda = 0.63$, $\varkappa = 0.065$ in tests with an air supply in a test basin.

It has already been mentioned above that due to various considerations it becomes necessary to study schematized phenomena. In the problems under consideration with respect to the rolling or the maneuverability of a ship in swells, a number of simplifications must be made. Let us note some of them: the actual ship moves under conditions of irregular three-dimensional seas and contains all degrees of freedom; its speed is determined by the operation of screw propellers whose revolutions in turn depend not only on the speed, but on oscillations of the ship, shift of the rudder and the angle of drift. The dependence of revolutions on loads on the propeller is determined by a machine located on the ship, which is not identical to the motor, and which usually puts the self-propelled model into motion--the form of testing closest to reality and differing from it, besides the already noted condition, primarily by the Reynolds numbers and errors in simulating the given irregular waves. Instead of experiments with self-propelled ships on irregular seas, quite often the behavior of a model is studied on regular two-dimensional waves created by a wave-producing mechanism. In a number of cases further simplifications are made, as for example, examining the rolling of the ship's model moving at a constant speed, equal to the speed of the tow cart, or even the rolling of the ship's model with a limited freedom of all horizontal displacement. And finally, in isolated cases, only two or even one degree of freedom is retained.

Naturally, all of the listed deviations from similitude lead to errors in the evaluation of the ship's behavior. The magnitude of these errors may be determined as a result of the motion analysis of a specific model, since the errors will particularly depend on the distribution of mass, the coordinates of the towing point or the suspension of the model and on the hull lines.

For simulation of the problems under analysis from the formal point of view, in addition to geometric similarity of model and wave motion and to equality of the Froude, Reynolds and Weber numbers for the model and the full-size ship, it is also necessary, as was mentioned before, to preserve the dimensionless values for mass, moments of inertia and coordinates of the center of gravity. Without carrying out the computations here, which are identical to those used in previous problems, let us indicate that the expressions for the dimensionless mass $\bar{m}$ and the dimensionless moment of inertia $\bar{I}$ with respect to some axis or a point are usually written as follows:

$$\bar{m} = \frac{m}{\rho l^3} \text{ and } \bar{I} = \frac{I}{\rho l^5}, \qquad (2.35)$$

where m, I - mass and moment of inertia;
ρ - density of the fluid;
l - typical dimension.

Let us indicate that due to the additional parts of the assembly under conditions of the simulation experiment, the mass in horizontal motion could differ from the mass in vertical motion (see Fig. 8). This also contributes to deviations from similarity.

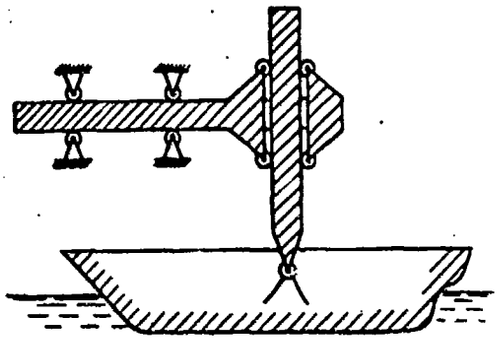

Fig. 8. Schematic diagram of a towing attachment where the mass differs for horizontal and vertical motion [57

The study of rolling and pitching and maneuverability of a ship is in some cases performed analytically, with the aid of the coefficients found during experimentation with a model on calm water, coefficients which characterize the rotary derivatives, added inertia and damping. It should be noted that in contrast to the motion of a body in an infinite ideal fluid, such quantities as, for example, coefficients of the added inertia, are defined not just by the shape of the body alone, but rather they depend on the type and on the history of motion, primarily on the dimensionless frequency of oscillations and the decrement of damping. This, in turn, is related to the influence of weight and viscosity. Data on the influence of weight on the added inertia of the system can be found in [38, 37]. [56 [57

The effect of viscosity is especially pronounced with smaller models, and for these cases an estimate of the degree of the scale effect should be performed, dependent on the difference of the Reynolds numbers between the full size and the model. Some elements of such an estimate, based on the calculations of a problem [41] concerning the rotary oscillations of a cylinder in a viscous fluid, can be cited here. This problem corresponds to the case of transverse rolling of the cylindrical hull of a submarine,

and to a certain degree is close to the problem of transverse rolling of a half-cylinder with frames in calm water. It should be mentioned, however, that the previously indicated solution is based on the common theory of viscous fluid without considering the effects of turbulence.

For exponentially decreasing or increasing rotary oscillations of a cylinder in a viscous fluid the moment of drag forces can be expressed in the form

$$M_{\tau} = -I_1 \frac{d\omega}{dt} - 2N\omega, \tag{2.36}$$

where ω is the angular velocity and N is the coefficient of energy dissipation of the fluid that surrounds the cylinder.

If we consider the rotary oscillations of a cylinder in a viscous fluid, we can express them in an equation in the form

$$I \frac{d\omega}{dt} = M + M_{\tau}, \tag{2.37}$$

where I is the moment of inertia of the cylinder itself and M is the moment of the external forces from which the moment M_τ is removed. The coefficient I_1 with $\frac{d\omega}{dt}$ in the expression M_τ will play the role of added moment of inertia. The magnitude of the added moment of inertia I_1 will depend on the parameters of motion, in this case, on the value of λ and ω, which define angular oscillations of a cylinder by the following law:

$$\varphi = \varphi_0 e^{-\lambda t} \cos(\omega t + \delta). \tag{2.38}$$

Coefficient N will also depend on λ and ω.

Utilizing the theory of dimensions and the theoretical solution [41], we will produce here general relationships for the determination of I_1 and N in a two-dimensional problem. The terms on which these values may depend will be as follows: the radius of the cylinder a, the density of the fluid ρ_1 and the coefficient of kinematic viscosity ν, and also the parameters which define the character of the motion, ω and λ.

$$I_1 = F_1(a, \rho, \nu, \omega, \lambda); \tag{2.39}$$
$$N = F_2(a, \rho, \nu, \omega, \lambda).$$

On the basis of the π-theorem, the relationships between dimensional values can be replaced by the relationships between the independent dimensionless groups composed of these values. Using one of the repeatedly adopted methods we can write these relationships in the form*

*The values I_1 and N are taken per unit of cylinder length.

$$\bar{I}_1 = \frac{I\omega}{\rho\nu a^2} = f_1\left(\frac{\omega a^2}{\nu}, \frac{\lambda}{\omega}\right); \qquad (2.40)$$

$$\bar{N} = \frac{N}{\rho\nu a^2} = f_2\left(\frac{\omega a^2}{\nu}, \frac{\lambda}{\omega}\right).$$

Let us note that ρ cannot enter into the dimensionless group of the right side, becuase the remaining four terms have the dimensions of kinematic values. The terms of the right side represent the decrement of damping

$$\chi = \frac{\lambda}{\omega} \qquad (2.41)$$

and the unique Reynolds number analogous, for example, to that which is introduced in the analysis of the similitude of screw propellers

$$\mathrm{Re}_\omega = \frac{\omega a^2}{\nu}. \qquad (2.42)$$

The definite form of the functions $\bar{I}_1(\mathrm{Re}_\omega, \chi)$ and $\bar{N}(\mathrm{Re}_\omega, \chi)$ can be established on the basis of the solution [41] according to which, after some uncomplicated transformations, we obtain

$$\bar{I}_1 = f_1(\mathrm{Re}_\omega, \chi) = \pi\sqrt{\mathrm{Re}_\omega}\sqrt{2\left(\sqrt{1+\chi^2}+\chi\right)}; \qquad (2.43)$$

$$\bar{N} = f_2(\mathrm{Re}_\omega, \chi) =$$

$$= \pi\left[2+\sqrt{\frac{\mathrm{Re}_\omega}{2}}\left(\sqrt{\sqrt{1+\chi^2}-\chi}+\chi\sqrt{\sqrt{1+\chi^2}+\chi}\right)\right].$$

In the case of harmonic oscillations [60

$$\bar{I}_1 = \pi\sqrt{2\mathrm{Re}_\omega}; \qquad (2.44)$$

$$\bar{N} = \pi\left(2+\sqrt{\frac{\mathrm{Re}_\omega}{2}}\right).$$

The dependences of $\overline{I_1}$ and $2\overline{N}$ on Re_ω and χ are given in Fig. 9 and 10.

Formulas (2.43) and the computed graphs based on them (Figures 9 and 10) have been obtained for large Reynolds values Re_ω by means of a series expansion. The remaining members of the series, to which the error of (2.43) is proportional, have the order of $\frac{1}{\sqrt{Re_\omega(1+\chi)}} < \frac{1}{\sqrt{Re_\omega}}$. These conditions are usually satisfied for the cases of the rolling of a ship and its models.

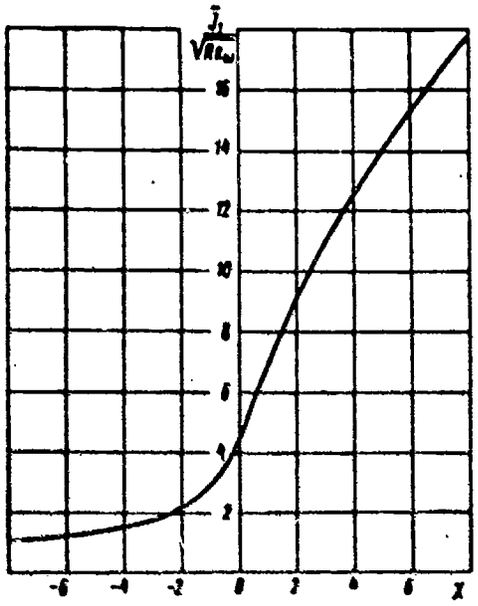

Fig. 9. Graph for determining the dependence of the added dimensionless moment of inertia $\overline{I_1}$ for rotary oscillation of a round cylinder in a viscous fluid on the decrement of damping χ and on the Reynolds number $Re_\omega = \frac{\omega a^2}{\nu}$.

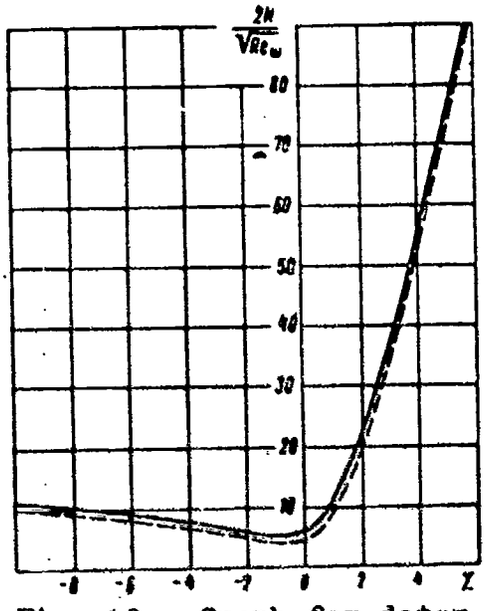

Fig. 10. Graph for determining the dependence of the dimensionless coefficient of the moment of drag $2\overline{N}$ for oscillation of a cylinder in a viscous fluid on the decrement of damping χ and on the Reynolds number $Re_\omega = \frac{\omega a^2}{\nu}$.

– – – Re_ω – –; —— Re_ω = 120.

[59

CHAPTER III. APPLICATION OF THE THEORY OF DIMENSIONAL ANALYSIS IN STUDYING PLANING SHIPS [60

3.1. Steady-State Planing of Flat and Profiled Bottoms

Planing vessels have a rather small draft y (Fig. 11) and they seem to glide along the water surface. The bottom of the vessel, which is oriented at some small angle α to the velocity vector during the process of its motion, continuously ejects fluid masses downward. The reaction of ejected particles creates the lifting force, which basically balances the weight of the vessel. Hydrostatic forces, which are the main forces for the support of ordinary water-displacing ships, play only a secondary role in the case of planing objects. In analyzing the lifting forces of the planing bottom the fluid can be considered as ideal, since according to what has been said, the lifting force is the result of the normal pressure exerted by the bottom on the water surface. The friction drag forces are lower by one order than the weight of the ship.

[61

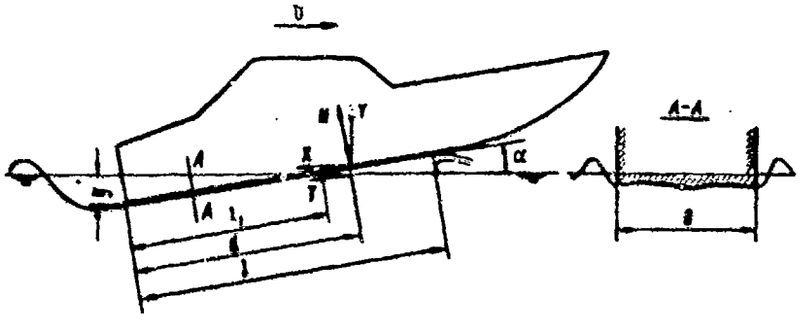

Fig. 11. Schematic diagram of the flow around a planing vessel and the hydrodynamic forces acting on the vessel.

During planing only the bottom is in contact with water. The boards and transom (the stern cut of the ship) remain in the air. The bottom, in a first approximation, can be considered as a flat plate. The circumstances that distinguish the actual shape of the bottom from a flat plate will be analyzed further on. [60

Let us analyze, keeping the previous comments in mind, the relationships which exist for steady-state motion between the coordinates which determine the position of the bottom with respect to water and the forces which act laterally from the latter. Let us select for such coordinates the angle of attack α and the wetted length* l (see Fig. [61

*Because of the backwater that emerges in front of a planing plate, the wetted length l is always greater than the length $l_1 = y/\sin\alpha$, which is formed at the intersection of the plate and the undisturbed water surface.

11). It is obvious that for a single-value definition of these relationships we must also have the width of the bottom B, speed of motion v, density of the medium ρ and acceleration of the force of gravity g. The forces acting on the bottom--on the plate--can be reduced to a normal force N and a moment M with respect, for example, to the edge of the stern or with respect to the force N and the coordinate d of the intersection of its line of action with the plate.

In the future, for simplicity, we will analyze only force N. Hence, we can write

$$N = F_1(B, l, \alpha, g, \rho). \qquad (3.1)$$

Selecting B, v and ρ as the dimensional units, instead of (3.1) we obtain the following dimensionless relationship:

$$\frac{N}{\frac{\rho v^2}{2} B^2} = f_1\left(\frac{l}{B}, \alpha, \frac{gB}{v^2}\right). \qquad (3.2)$$

In studying planing it is customary to refer to the value $\lambda = l/B$ as the wetted elongation (although in wing theory the wetted elongation is known as the reciprocal value), and instead of the parameter gB/v^2 the Froude number $Fr = \frac{v}{\sqrt{gB}}$ is introduced.

Let us substitute the normal force by its vertical projection, i.e., by the lifting force Y or by the load on the water Δ (among the small angles of attack α characteristic for planing vessels we can consider $N \approx Y$), and let us define [62

$$\frac{Y}{\frac{\rho v^2}{2} B^2} = \frac{\Delta}{\frac{\rho v^2}{2} B^2} = C_\Delta. \qquad (3.3)$$

Then*, instead of (3.2) we can write

*Introduction of the coefficient of lifting force in the form $2Y/\rho v^2 B^2$ instead of the coefficient C_y accepted in aerodynamics is specified by the condition that the wetted surface of a planing plate, in contrast to the area of a wing, is not fixed.

$$C_B = f(\alpha, \lambda, Fr). \qquad (3.4)$$

Expanding $f(\alpha, \lambda, Fr)$ by powers of α and taking into account that with finite λ and zero angle of attack the lifting force, and thus also C_B, are equal to zero, we obtain, discarding terms containing α to the second or greater power,

$$C_B = a_1(\lambda, Fr)\alpha. \qquad (3.5)$$

Experimental research has made it possible to establish the relationship [63

$$\frac{C_B}{\alpha} = a_1(\lambda, Fr). \qquad (3.6)$$

[62

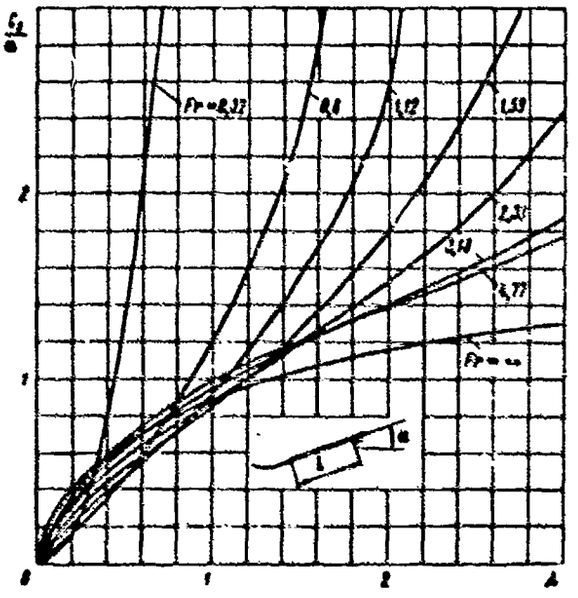

Fig. 12. Dependence of $\frac{C_B}{\alpha}$ on elongation $\lambda = \frac{l}{B}$ and the Froude number

$$Fr = \frac{v}{\sqrt{gB}}$$

Figure 12 gives the graph of $\frac{C_B}{\alpha}(\lambda, Fr)$ obtained in [42, 43]. The dependence $\frac{C_B}{\alpha}(\lambda)$ with $Fr \to \infty$ is shown on the same graph. [63

$$\frac{C_B}{\alpha} = \frac{0{,}7\pi\lambda}{1 + 1{,}4\lambda}. \qquad (3.7)$$

This relation was suggested by L. I. Sedov [27, 35] based on the thorough analogy established by him between the planing plate and the wing. It should be noted that in contemporary literature (for example, [9]), instead of the relations presented in Fig. 12 curves are given which were obtained on the basis of the old experimental works by Zottorf [81]. These curves produce erroneous values of C_B/α in the region of small values of λ, and specifically they contradict the theoretical solution of L. I. Sedov [28] for the two-dimensional problem. According to this solution, in the region of $\lambda \to 0$ with large values of Fr

$$\frac{C_B}{(C_B)_{Fr\to\infty}} = 1 - \frac{\pi^2 + 4}{2\pi\, Fr^2}, \qquad (3.8)$$

i.e., the value C_B/α must decrease with a decrease in the Froude number and will not remain constant as follows from the above-mentioned experiments of Zottorf.

Repeating computations similar to those mentioned above with respect to the moment of hydrodynamic forces, we would obtain analogous results with respect to the coefficient of the moment

$$C_m = \frac{2M}{\rho v^2 B^2} = \alpha b_2(\lambda, Fr). \qquad (3.9)$$

However, it is more convenient to represent the moment by the force N already known to us and by the indicated coordinate point d of the intersection of its line of action with the bottom. In Fig. 13 the dependence $\bar{d} = \frac{d}{B}(\lambda, Fr)$ is presented. Since $\bar{d} = \frac{M}{NB}$, then in accordance with formulas (3.3), (3.6) and (3.9) the value $\bar{d}$ does not depend on angle α.

Application of the theory of dimensions in conjunction with analysis of the physical processes and conditions characteristic to the planing phenomenon made it possible to narrow the problem of determining the lifting force and the moment of the planing bottom to an analysis of the influence of two variables--λ and Fr--only, and for large Froude numbers to only the influence of λ. This has immensely simplified and decreased the volume of experimental analyses and has led to relationships which are simple and

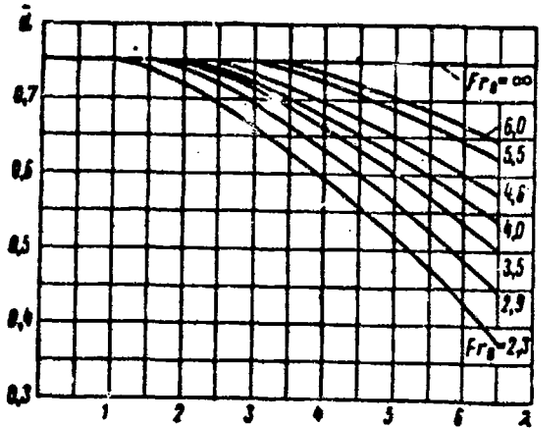

Fig. 13. Dependence of the dimensionless coordinate $\bar{d}$ of the center of pressure of a planing plate on the span-chord ratio $\lambda = \frac{l}{B}$ and on the Froude number $Fr = \frac{v}{\sqrt{gB}}$.

convenient for practical utilization. Specifically, the introduction of the coefficient $C_B = 2\Delta/\rho v^2 B^2$ shows that for large Froude numbers the analysis of planing under conditions of high speeds can be replaced with experiments at moderate speeds easily attainable in test basins, but with a smaller load or a larger width.

Let us note that for planing, of all the geometric values only the angle of attack and the width of the bottom are usually assigned. The wetted length is a value to be found for the given speed and weight. Instead of the angle of attack an external moment may be assigned.

For large span-chord ratios in expression (3.5) it is insufficient to be limited by the first term and it should be written

$$C_B = a_1(\lambda, Fr)\alpha + a_2(\lambda, Fr)\alpha^2 + \ldots \qquad (3.5')$$

Let us proceed to analysis of the drag X during planing. One of the components of the drag X_1 will be the projection of the normal force analyzed above on the direction of motion. For small angles of attack

$$X_1 \approx N\alpha \approx Y\alpha. \qquad (3.10)$$

Another component, not considered until now, will be the drag force of friction T between the water and the bottom. This force is projected almost entirely on the direction of motion and it is of the same order as the force X. Thus, for small values of α

$$X = Y\alpha + T. \qquad (3.11)$$

In practical applications an extensive role is played by the quality K of the planing bottom or its reciprocal value ε, called the coefficient of planing and equal to the ratio of the drag to the lifting force.* Taking (3.11) in- [65

*This coefficient is also introduced for ordinary ships; it is called specific drag and is usually expressed not by a dimensionless value, but by a value whose dimensions are kilograms per ton of water displacement.

to account, we can write that

$$\varepsilon = \frac{X}{Y} = \alpha + \frac{T}{Y}. \qquad (3.12)$$

Let us express the friction force T by the usual formula for the friction of flat plates

$$T = \zeta(\mathrm{Re})\rho\frac{v^2}{2}Bl. \qquad (3.13)$$

The coefficient of surface friction ζ is a function of the Reynolds number

$$\mathrm{Re}_l = \frac{vl}{\nu} = \frac{vB}{\nu}\frac{l}{B} = \mathrm{Re}_B\lambda \qquad (3.14)$$

and can be found*, for example, from the graphs of Prandtl

*For small angles of attack the friction forces of the planing plate approach the values of the friction forces of the plates which are towed along their flat face.

and Schlichting. Substituting in (3.12) the value of Y from formula (3.3) and T from formula (3.13), and taking (3.5) into account, we will find

$$\varepsilon = \alpha + \frac{1}{\alpha}\frac{\zeta(\mathrm{Re})\lambda}{a_1(\lambda, Fr)}. \qquad (3.15)$$

The angle of attack α_H, corresponding to the maximum quality or to the minimum value of ε_{min}, can be found from (3.15) by the usual rules for finding the extremals of the function

$$\alpha_{\text{м}} = \sqrt{\frac{\zeta(\mathrm{Re}_B\lambda)\lambda}{a_1(\lambda, \mathrm{Fr})}}; \qquad (3.16)$$

$$\varepsilon_{\min} = 2\alpha_{\text{м}}. \qquad (3.17)$$

The existence of the optimal angle of attack can easily be clarified by considerations that are given for a certain velocity region and the weight of the ship. In an ideal fluid (with T = 0) the drag force is the projection of the normal force on the direction of motion. For the assigned value of lifting force, which is equal to the weight, this projection will become smaller for decreasing angles of attack. The most advantageous angle is $\alpha = 0^\circ$. However, decrease of the angle of attack for the given width, lifting force and speed (that is, with C_B = const) must be compensated by an increase of the wetted length [see formula (3.7) and Fig. 12] and, therefore, of friction forces. Thus, with small angles the drag increases due to friction, while with large angles due to the projection of the normal pressures. In Fig. 14 is presented the nature of variation of both terms of formula (3.15) and their sum with varying angles of attack α. The problem of the most advantageous relations during planing was thoroughly analyzed in the work of L. I. Sedov [29]. For large Froude numbers, by replacing a_1 with its value from formula (3.7) we obtain instead of (3.16)

$$\alpha_{\text{м}} = \sqrt{\frac{1 + 1{,}4\lambda}{0{,}7\pi}\zeta}. \qquad (3.18)$$

Formulas (3.16) and (3.18) indicate that with λ = = const the most advantageous angle of attack decreases with an increase in the Reynolds number as $\sqrt{\zeta}$.

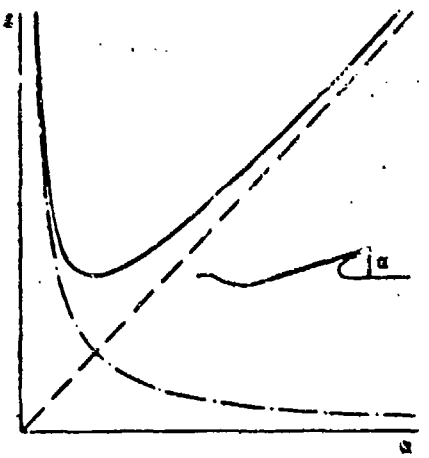

Fig. 14. Dependence of specific drag from normal forces (dotted line) and friction forces (dash-dot line) on the angle of attack α (solid line is combined specific drag ε).

For full-size objects with displacements of several tens of tons the magnitude of the Reynolds numbers is within the range of Re $\sim 10^7$-10^8. Corresponding to the average Reynolds number of Re = $5 \cdot 10^7$ is the value $\zeta = 2.2 \times 10^{-3}$. Assuming the span-chord ratio $\lambda = 2$ we obtain by (3.18) $\alpha_H = 0.06 = 3.5^\circ$.

In simulation with respect to the Froude number the Reynolds numbers vary as the length scale in 3/2 power and therefore for the model made to the scale of $k_1 = B_M/B_H = 10^{-1}$,

$$Re_M = Re_H k_l^{3/2} = 5 \cdot 10^7 \cdot 10^{-3/2} \approx 1{,}6 \cdot 10^6; \quad \zeta = 4 \cdot 10^{-3}.$$

and the most advantageous angle of attack will be $\alpha_H = 4.8^\circ$. Thus, the given example indicates that the optimal angle determined from experimental results will differ significantly from angles for the real object. This difference is explained by the effect of the size factor, i.e., the equality of Reynolds numbers for the model and the prototype is not satisfied.

The influence of the scale effect on the drag, or, what is the same thing, on the value ξ, will be different for different planing objects. From formula (3.15) it follows that ξ for large angles of attack $\alpha \gg \alpha_H$ is determined basically by the first term, which does not produce the scale effect; conversely, with small angles $\alpha \ll \alpha_H$ the main part of ξ is made up of the member which contains the coefficient of friction, which depends on the Reynolds number. For $\alpha = \alpha_H$ the terms of formula (3.15) are equal.

According to the material presented above, the hydrodynamic lifting force and the moment can be calculated from the model to the full size virtually without taking scale [6
effect into account. In addition, starting with sufficiently large Froude numbers Fr > 5-6 and with not too large λ ($\lambda < 1$), we can also avoid modeling by the Froude method, maintaining only the similarity of the angle of attack and the value C_B.

The requirements of seaworthiness (i.e., decrease of impacts and overloads in motion through waves) dictate a bottom design for a planing craft with a wedge-shaped keel (Fig. 15a). The bigger the deadrise, the smaller become impacts and overloads for motion on the wave. However, enlargement of the deadrise leads to substantial increase

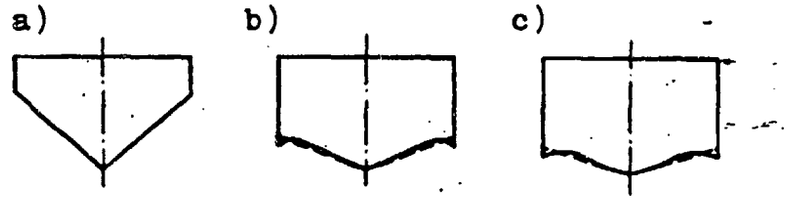

Fig. 15. Cross sections of the bottom shapes of planing boats and hydroplanes: a) flat deadrise bottom; b, c) bottoms with folds at the bilges.

of the wetted surface and drag. A compromise is reached by the special shaping* of frames with variable deadrise, in-

*This shaping also has the goal of reducing spray formation.

creasing toward the bow. In Figures 15b and 15c typical cross-sectional bottom shapes for planing boats and hydroplanes are shown. The variation of deadrise along the length provides for acceptable hydrodynamic properties for motion over calm water and small disturbances. When encountering large waves, the bow portions of the hull, with very pronounced deadrise, enter the water first, reducing the impact. When moving on calm water these portions remain in the air.

The hydrodynamic force characteristics of low deadrise bottoms differ only slightly from those of a flat plate. The results of systematic analysis of various types of profiles are presented in [35]. It is evident that into the right side of relation (3.1) for the shaped bottom there will additionally enter a number of values which describe the geometric shape, specifically the angle of the transverse deadrise β. For similar shapes the dimensionless relationships of the form of (3.2) or (3.4) will remain the same as those for a flat bottom.

As was shown for the first time by L. I. Sedov and A. N. Vladimirov [31], very interesting and effective results can be obtained with the aid of the dimensional theory for the flat deadrise bottom, planing on a partial width, i.e., in the regimes of motion shown in Fig. 16. In this case, for geometrically similar* bottoms it is not [68

*The shape of the flat deadrise bottom is defined by

its angle of transverse deadrise β and the angle between the line of the keel and the plane of the transom.

---

possible to indicate a characteristic dimension, and therefore draft y, wetted width B_{CM}, length l and coordinate of the center of pressure d are defined by single-valued terms

$$\Delta, \alpha, v, g, \rho. \tag{3.19}$$

Due to the considerations mentioned above, the effect of viscosity forces on y, B_{CM}, l and d is negligible and will be pronounced only during determination of the drag through the use of the coefficient of friction.

In the dimensionless form the relations among the mentioned linear values with the parameters of (3.19) will be in the form (for example, for l)

$$\frac{l}{\frac{\rho v^2}{\Delta}} = f\left(\alpha, \frac{v}{\sqrt{g\sqrt[3]{\frac{\Delta}{\rho g}}}}\right). \tag{3.20}$$

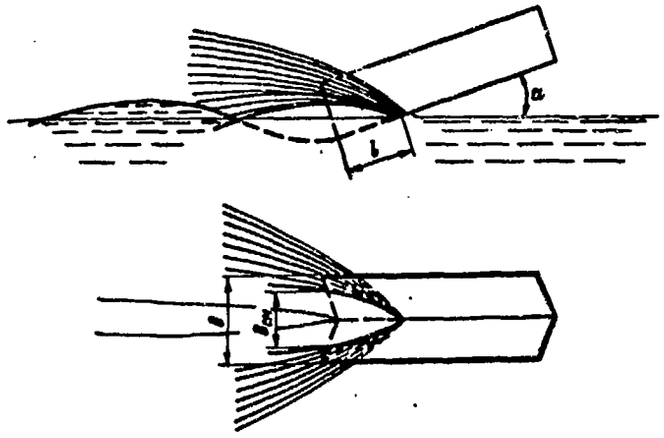

Fig. 16. Schematic presentation of planing of a flat deadrise bottom on a partial width.

The second term of the function (3.20) can be considered as the Froude number with respect to load

$$Fr_{\Delta} = \frac{v}{\sqrt{g\sqrt[3]{\frac{\Delta}{\rho g}}}}. \tag{3.21}$$

If the influence of gravity is unimportant, then according to relationship (3.20)

$$l = \sqrt{\frac{\Delta}{\rho g^2}} f(\alpha). \qquad (3.22)$$

Similar relations, evidently, can also be written for [69
the values of B_{CM}, y and d. From (3.22) it follows that it is sufficient to find the value l for any one of the values ρ, v and Δ with several α in order to be able to compute l for any regime of motion.

Experiments [30] indicate that in the analyzed problem the gravity is unimportant for $Fr_\Delta > 2.5$ (Fig. 17). From

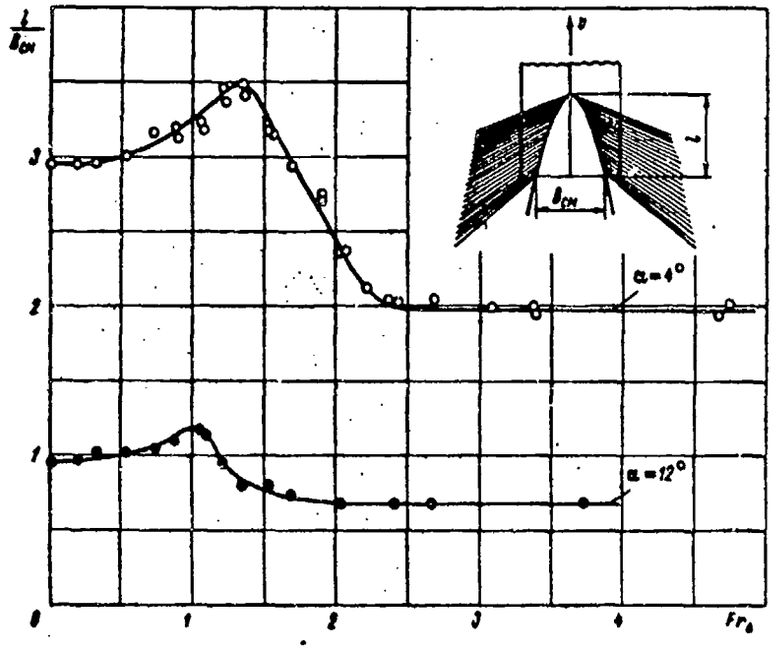

Fig. 17. The dependence of elongation $\lambda_{CM} = \frac{l}{B_{CM}}$ of the wetted surface on the number $Fr_\Delta = \frac{v}{\sqrt{g\sqrt[3]{\frac{\Delta}{\rho g}}}}$ and the angle of attack α.

Fig. 17, formula (3.22) and the similar relations for B_{CM} and y, it follows that for a fixed α and Fr > 2.5, the shapes of wetted surfaces for all values of ρ, v and Δ will be similar. The same result could have been obtained directly if instead of the system (3.19) we would have selected a system of determining parameters, for example,

like the following:

$$l,\ \alpha,\ v,\ g,\ \rho; \tag{3.23}$$

by taking l, v and ρ as the units of measurement and neglecting the effect of g, we would have obtained the following relationship for the wetted width

$$\frac{B_{cm}}{l} = f(\alpha). \tag{3.24}$$

Then we would be able to write for the lifting force Y, which is equal to the load on the water Δ, the following: [70

$$\frac{Y}{\rho v^2 l^2} = \frac{\Delta}{\rho v^2 l^2} = f(\alpha), \tag{3.25}$$

which is formula (3.22) transformed.

3.2. Stability in Planing

For planing objects there exist unstable conditions, i.e., such conditions under which, regardless of the absence of any visible form of external disturbances, spontaneous vertical and angular oscillations occur in the longitudinal plane of the vessel. Figure 18 is a recording of the development of angular and vertical oscillations of a planing vessel on a movie film moving with a constant velocity. Lights attached to the model were photographed. A stroboscope disc was placed in front of the lens. The interval between the points was 0.02 sec. The probability of occurence and the intensity of oscillations increases with the increase of velocity. Actually, it was instability that accounted for the majority of sportsmen's lives lost during their attempts to break speed records on water.

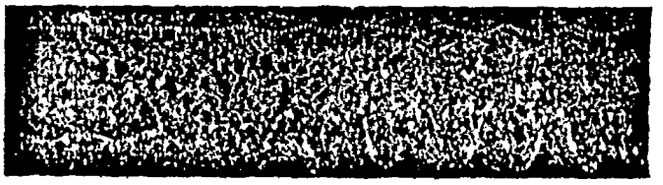

Fig. 18. Recording on constantly moving tape of the development of angular and vertical oscillations of a planing vessel. Interval between points 0.2 sec.

If a model of a planing vessel is tested at various

speeds and with two degrees of freedom--surfacing and trim --and if for each velocity (by assigning proper moments) different trim angles are provided, then the joint effect of all experimental conditions can be presented as a field of points within the coordinates α and v. If on this diagram the points that correspond to the conditions of developing oscillations are darkened, then the picture that is schematically shown in Fig. 19 will be obtained.

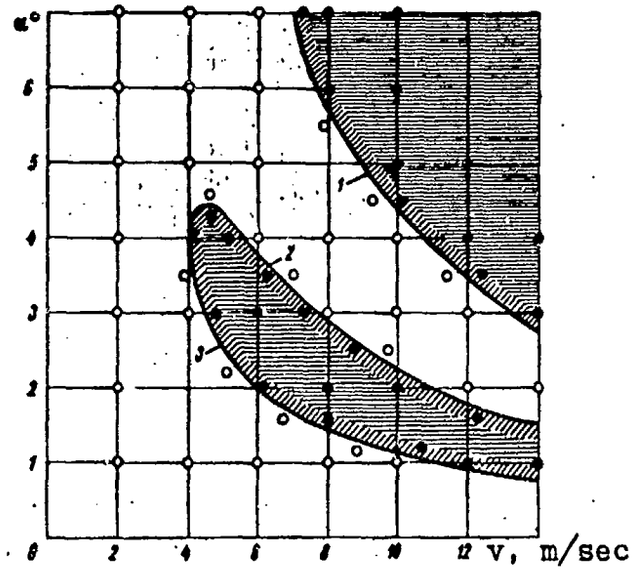

Fig. 19. Zones of stable and unstable regions of a planing vessel of constant weight and different trim angles α.

Points corresponding to the unstable region are darkened. Unstable regions are cross-hatched.

The lines separating the regions of stable and unstable motion are known as the stability boundaries. There are three such boundaries in Fig. 19. The first boundary 1 is characterized by conditions of emergence of vertical oscillations. These oscillations also occur with one degree of freedom (along the vertical). The second 2 and third 3 boundaries are related to the appearance of combined angular and vertical oscillations. The presented diagram is typical; the location of boundaries is determined in each individual case by the geometric and dynamic characteristics of the vessel. For every planing object of a given weight and alignment there corresponds a dependence of the trim angle on travel speed. In order to provide

stability it is necessary that this curve, up to the design velocity, pass within the stability region without intersecting its boundaries.

The stability of planing remained an unsolved problem for a long time. The understanding and development of design methods were primarily achieved as a result of the theoretical and experimental work performed by TsAGI in the period 1938-1943. These studies, which were done under the supervision of L. I. Sedov, were to a great extent based on the dimensional theory. In the general case, when analyzing the stability of a planing vessel, in addition to the values analyzed above, which define the conditions of equilibrium, it is necessary to consider the value and the distribution of masses, which can be represented by a total mass* of the object m, by the moment of inertia I relative

*The mass m and the load Δ are usually related by the expression $\Delta = mg$, but in a number of cases they could and should be considered as independent values. As examples we can cite the aerodynamic unloading of hydroplanes or the unloading by the block and pulley during experiments in a test basin.

to the transverse axis passing through the center of gravity, and by the coordinates of the center of gravity x_T and y_T.

The conditions which characterize the boundary of the stable region may be written in the form of the relationship

$$F(B, \alpha, l_1, \ldots, l_n, \Delta, I, m, v, \rho, g) = 0, \qquad (3.26)$$

in which the values x_T and y_T are included in the value l_i, and the dimensions and position of the plate are defined by its width B, angle of attack α and the load on the water Δ. The viscosity is not taken into account due to the considerations listed in Section 3.1.

With the aid of the usual techniques we can convert to the dimensionless form and instead of (3.26) obtain

$$f\left(\alpha, \frac{l_1}{B}, \ldots, \frac{l_n}{B}, C_\Delta, \frac{m}{\rho B^3}, \frac{I}{\rho B^5}, \mathrm{Fr}\right) = 0. \qquad (3.27)$$

Let us note that in a number of cases it is convenient to utilize the coefficient

$$C_\Delta = \frac{\Delta}{\gamma B^3} = \frac{C_B \mathrm{Fr}^2}{2}. \qquad (3.28)$$

For all geometrically similar hulls with a geometrically similar location of the center of gravity, expression (3.27) is simplified, and solved with respect to α taking into account the substitution of C_Δ for Fr, it will take the form

$$\alpha_{kp} = f_1\left(C_B,\ C_\Delta,\ \frac{m}{\rho B^3},\ \frac{I}{\rho B^5}\right). \qquad (3.29)$$

Expanding (3.29) into an exponential series of C_B we obtain

$$\alpha_{kp} = A_0 + A_1 C_B + A_2 C_B^2 + \ldots, \qquad (3.30)$$

where the coefficients A_0, A_1, ... are functions of $\bar{m} = m/\rho B^3$, $\bar{I} = I/\rho B^5$, C_Δ and of the geometric characteristics of the hull. In Fig. 20 the dependence $\alpha(C_B, C_\Delta)$ is shown, which was obtained in [45] for a flat plate with $\bar{m} \approx 1$ and $\bar{I} = 4$.

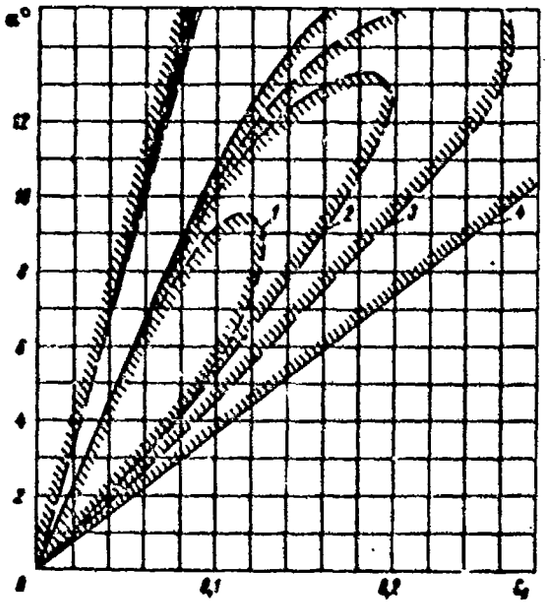

Fig. 20. Typical stability zones of a flat planing plate in the coordinates α and C_B. Unstable regions are dashed.
1. $C_\Delta = 0.93$; 2. $C_\Delta = 0.555$; 3. $C_\Delta = 0.37$; 4. $C_\Delta = 0.185$.

As follows from theoretical analysis and Fig. 20, in the region $C_B < 0.05$ it is sufficient to be limited to the first two terms of the expansion and regard $A_0 = 0$. Thus, the proportionality between α_{kp} and C_B is valid for all the boundaries. Writing that for each boundary

$$a_{кр} = \frac{C_B}{R_i} = \frac{2}{R_i} \frac{\Delta}{\rho a^4 B^3} \qquad (3.31)$$

(i = 1, 2, 3), we will note that the value R_1 for the flat plate does not depend on $\bar{m}$ and $\bar{I}$, and for $C_\Delta > 0.5$ can be approximately assumed as $R \sim 0.35$.

The value R_2 depends only on $\bar{I}$. This dependence is illustrated in Fig. 21. The value R_3 depends substantially on C_Δ and $\bar{m}$. The influence of $\bar{I}$ is relatively weak. The value R_3 can be determined by formula

$$R_3 = R_{3_1} \varphi_1\left(\frac{C_\Delta}{C_{\Delta_1}}\right) \varphi_2\left(\frac{\bar{m}}{\bar{m}_1}\right) \varphi_3\left(\frac{\bar{I}}{\bar{I}_1}\right), \qquad (3.32)$$

where $R_{3_1} = 1.13$ is the value of R_3 with $C_\Delta = 0.37$, $\bar{m}_1 = 1.08$ and $\bar{I}_1 = 4.1$; Φ_1, Φ_2 and Φ_3 are shown on Fig. 22.

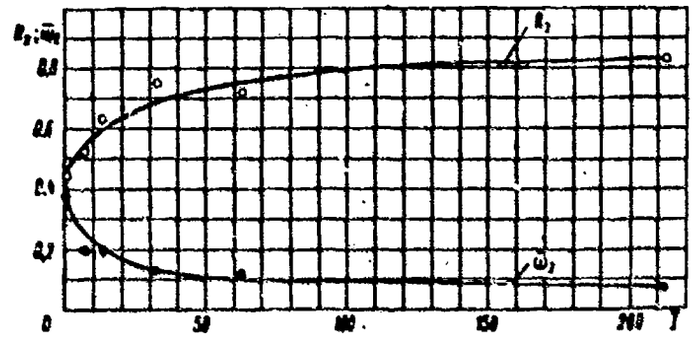

Fig. 21. The dependence of the coefficient R_2 and the dimensionless oscillation frequency $\bar{\omega}_2$ on the dimensionless moment of inertia $\bar{I}$.

To each boundary (on the rectilinear portion) there corresponds a dimensionless oscillation frequency

$$\bar{\omega} = \frac{\omega_1 B}{g}. \qquad (3.33)$$

The frequency $\bar{\omega}_1$ depends only on $\bar{m}$, $\bar{\omega}_2$ on $\bar{I}$. The frequency $\bar{\omega}_3$ is affected by $\bar{m}$ and $\bar{I}$, but is not affected

by C_Δ. A typical character of the frequency variation for increasing inertia is presented in the example for the relationship $\bar{\omega}_2(\bar{I})$ (Fig. 21).

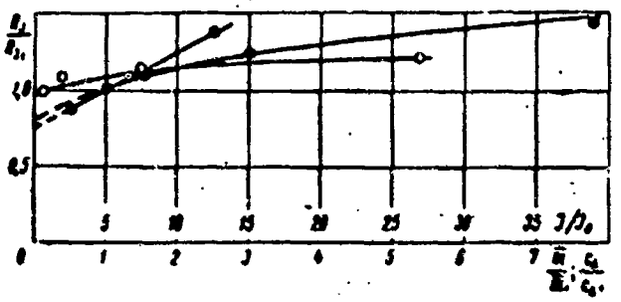

Fig. 22. The functions $\varphi_1\left(\frac{C_\Delta}{C_{\Delta_1}}\right)$; $\varphi_2\left(\frac{m}{m_1}\right)$; $\varphi_3\left(\frac{I}{I_1}\right)$ for the design of the third boundary of stability.

● - C_Δ; ● - I; o - m.

All of the material presented has dealt with flat plates. The transverse profile of the bottom was analyzed in [31] and [48]. In the first approximation the shaped bottom can be substituted by the flat keel as presented schematically by the dotted line in Fig. 15. The effect of the deadrise is pronounced primarily in the first boundary, which in the coordinates α_{kp} and C_B is displaced equidistantly upwards to an angle approximately equal to half the angle of the cross-sectional deadrise β. In other words, in the formula (3.30)

$$A_0 = \frac{\beta}{2}. \qquad (3.34)$$

The transverse shaping is not reflected in the second boundary. Its influence on the third boundary has not been sufficiently studied. [75

Let us analyze in greater detail the mechanism and the conditions of oscillation formation in transition across the first boundary. As has already been stated, the instability in this region originates with preservation of one degree of freedom--the freedom of vertical displacement. As will be shown below, we are dealing here with the case of static instability stipulated by deformation of the

fluid surface, which is characteristic for planing. The planing bottom seems to be pushing the water in front of itself; it creates a "backwater," the hydraulic head, which protrudes above the undisturbed level. The emerging local rise in turn lifts the planing bottom, and as a result it can happen that the draft will become negative, i.e., even the lowest point on the bottom will be above the undisturbed water surface. This condition is shown schematically in Fig. 23.

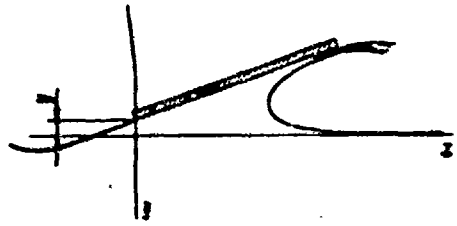

Fig. 23. Schematic presentation of the condition of planing where the trailing edge of the plate is located above the undisturbed water level.

In the two-dimensional problem of planing along the surface of a weightless fluid, the uplift of the trailing edge above the water surface approaches infinity; if, however, we take the weight of the fluid into consideration, the uplift becomes finite. As has been shown for the first time in [42] and [43], the conditions of motion with negative draft are also true for real cases with finite span-chord ratios. We will show that the presence of the condition of negative draft determines the emergence of static instability [45].

Actually, if in the case of planing of a plate at a constant speed v and constant angle of attack α its load is decreased down to the value $\Delta = 0$, then the wetted elongation will tend to approach zero, and the graph of the dependence of the lifting force on the draft will consecutively pass through the points $O_1(\Delta > 0,\ y > 0)$; $O_2(\Delta > 0,\ y = 0)$; $O_3(\Delta > 0,\ y < 0)$; $O_4(\Delta = 0,\ y = 0)$, and will have the characteristics shown in Fig. 24. At the point where the tangent to the curve $\Delta(y)$ becomes vertical, $\partial\Delta/\partial y$ changes from $+\infty$ to $-\infty$ and static instability occurs. The condition of motion and all of the characteristics (draft, wetted length, etc.) are defined for the two-dimensional problem by values α, Δ, ρ, v and g. The condition on the stability boundary can be expressed as follows:

$$F(\alpha, \Delta, \rho, v, g) = 0. \qquad (3.35)$$

The number of parameters can be further reduced if we consider the dependence between Δ and α mentioned above for

[76

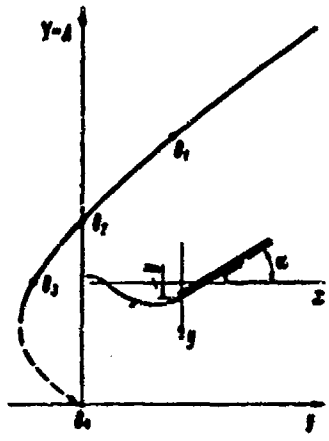

Fig. 24. The dependence of the lifting force $Y = \Delta$ of a planing plate on the draft y of its trailing edge (stabilized motion with a constant angle of attack α and velocity v).

small angles of attack and replace these two values with their ratio. Then, instead of (3.35) we will obtain

$$F_1\left(\frac{\Delta}{a}, \rho, v, g\right) = 0 \tag{3.36}$$

or in a dimensionless form

$$f\left(\frac{v}{\sqrt{g\sqrt[3]{\frac{\Delta}{\rho g^3}}}}\right) = 0, \tag{3.37}$$

i.e., on the boundary of the stability region

$$\frac{v}{\sqrt{g\sqrt[3]{\frac{\Delta}{\rho g^3}}}} = C_1, \tag{3.38}$$

from which we find

$$v_{cr} = C_1^2 \frac{g^2 \Delta}{\rho g^4}. \tag{3.39}$$

The solution of the problem concerning planing of a flat plate along the surface of a heavy fluid was obtained by Yu. S. Chaplygin [40] using a method developed by L. I. Sedov [28]. Let us utilize this solution to find C_1. In order to achieve this, it is necessary to have the relation between the draft, on the one hand, and the lifting force or the load on water, on the other. For small angles of attack the draft, the vertical velocities and the lifting force are proportional to the angle of attack, hence

$$\frac{y}{c} = F\left(\frac{\Delta}{c}, \rho, v, g\right) \qquad (3.40)$$

or in a dimensionless form

$$y^0 = \frac{y}{\sqrt[3]{\frac{\Delta}{\rho g}}} = \Phi\left(Fr_\Delta = \frac{v}{\sqrt{g\sqrt[3]{\frac{\Delta}{\rho g}}}}\right). \qquad (3.41)$$

It is not difficult tc find the value of the Froude number Fr_Δ for which $\partial\Delta/\partial y$ experiences a discontinuity [45]. From (3.41) we obtain

$$\frac{\partial\Delta}{\partial y} = \frac{3\sqrt[3]{\frac{\Delta^2}{c^2}}}{\Phi - \frac{1}{2}\frac{d\Phi}{dFr_\Delta}Fr_\Delta}. \qquad (3.42)$$

Relation (3.41) was determined in [40] and is shown in Fig. 25. The denominator of (3.42) becomes zero with $Fr_\Delta = C_1 = 1.7$, and consequently, in accordance with (3.39), [77

$$\alpha_{kp} \approx 8{,}5\frac{g\Delta}{v^2}. \qquad (3.43)$$

When $\alpha > \alpha_{kp}$ the planing of a flat plate of infinite length becomes unstable.

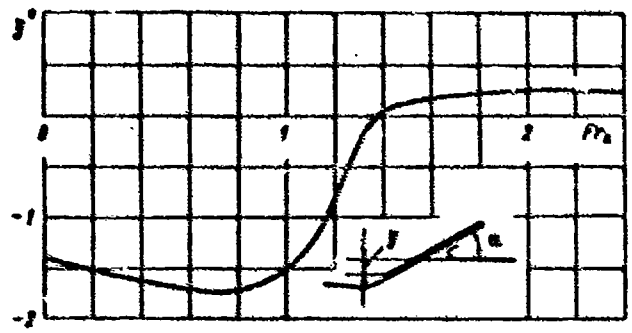

Fig. 25. Dependence of the dimensionless immersion $y^0 = \frac{y}{\sqrt[3]{\frac{\Delta}{\rho g}}}$ on the Froude number $Fr_\Delta = \frac{v}{\sqrt{g\sqrt[3]{\frac{\Delta}{\rho g}}}}$ fcr a flat plate of infinite span.

Returning to the more general case of a planing plate with $\lambda \neq 0$, let us note that finiteness of the span removes the area of emergence of instability to quite large Froude numbers, where their influence becomes of secondary importance, while the influence of the span-chord ratio, which naturally was not present in the two-dimensional case, becomes most important. Comparing formulas (3.30), (3.31) and (3.43), we see that for small Froude numbers and a span-chord ratio $\lambda = \frac{1}{B} \to 0$ the main role is played by the third term of the expansion and α_{kp} is inversely proportional to the square of the velocity [formula (3.31)].

As has already been noted in Sect. 3.1, the absence of a typical linear dimension is valid for planing of flat deadrise plates on partial width. The stability for this case was analyzed by L. I. Sedov and A. N. Vladimirov [31]. [78
For one degree of freedom the determining parameters will be

$$\alpha,\ \beta,\ \Delta,\ m,\ \rho,\ v,\ g,$$

and for the boundary of stability we obtain

$$\alpha_{kp} = f\left(\beta,\ \frac{mg}{\Delta},\ \mathrm{Fr}_{\Delta}\right).$$

Experiments did not indicate any significant influence of the parameter $\frac{mg}{\Delta}$ on α_{kp}, and hence

$$\alpha_{kp} = f(\beta,\ \mathrm{Fr}_{\Delta}).$$

This relationship is supported well by experiments [32].

3.3. Concerning the Scale Effect of Waves and Spray Formed by Planing Bodies

The reasons which may cause changes in the shapes of waves and spray under actual conditions of towing the model should be broken down into two categories. To the first belong all types of external effects, such as wind, waves, etc.; and to the second belongs everything that is understood to be associated with the scale effect. Let us analyze here the magnitude and the direction of the errors which occur in the process of recalculating the wave and spray values from the model to full size under identical external conditions. The formulation of the scale effect problem in modeling in accordance with Froude's law of similitude implies allowance for the effect of viscosity

and surface tension, i.e., exactly those forces which are usually ignored in the calculation of problems which deal with planing, waves and streams. Examining the pattern of the flow around the hull of a planing craft, we see that from the entire variety of wave and stream patterns we can select the following three main types:

a) thin streams that swing off the bow of the model at low speed;

b) the cavity and the wake formed at the stern of the model by the convergence of the stream flow around the model;

c) streams and spray which escape from the bilges in the planing mode.

It can be expected that the role of the factors unaccounted for by similitude on the basis of Froude will be different for each of the listed phenomena, and hence, every one of them will have its own scale effect and will demand individual analysis.

In order to study the scale effect of waves and spray during planing, analyses [44] were performed on a series of four types of models with widths B = 600 mm, B = 300 mm, B = 150 mm and B = 50 mm. The models had bow shapes typical for planing craft and cylindrical stern regions with flat deadrise cross section and bent away bilges. The experiments were performed in a test basin with rigidly mounted models. The draft, trim, and Froude numbers guaranteed the formation of the conditions under which three of the listed types of waves and spray are formed. The water surface relief was captured by the stereophotographic technique. This method turned out to be effective for processes taking place behind the stern. A number of technical difficulties and the limitations of the apparatus of those years did not make it possible to obtain reliable experimental data for "a" and "c". Based on the scale effect of this type of stream we can make some theoretical deductions. Figure 26 is an example of the breakdown of the diametrical cross sections of the water surface behind the stern, while Fig. 27 shows photographs (reduced to the same width) of this region for one of the conditions (Fr = 1.22, $\alpha = 3^0$, H/B = 0.535). [79

In analyzing the problem under consideration, the concepts layed out in Sect. 1.4 can be fully utilized, considering that error in the dimensionless value which interests us, for example the maximum height h of the wave crest

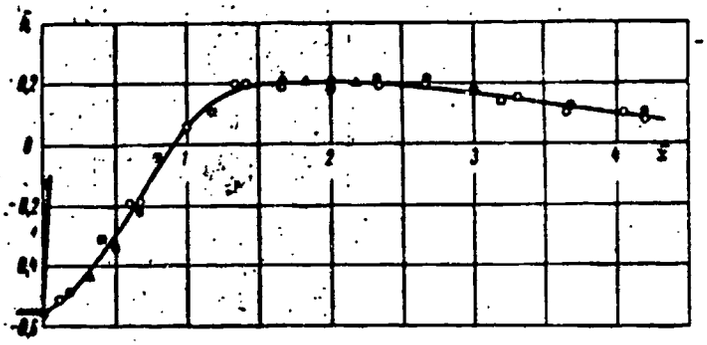

Fig. 26. Results of measuring the diametrical cross section of the water surface profile behind the stern for a series of similar models of a planing bottom ($\alpha = 3^\circ$, $Fr = \frac{v}{\sqrt{gB}} = 1{,}22$). All values are with respect to the model's width B. □ - B = 0.6 m; o - B = 0.3 m; ● = B = = 0.15 m; Δ - B = 0.05 m.

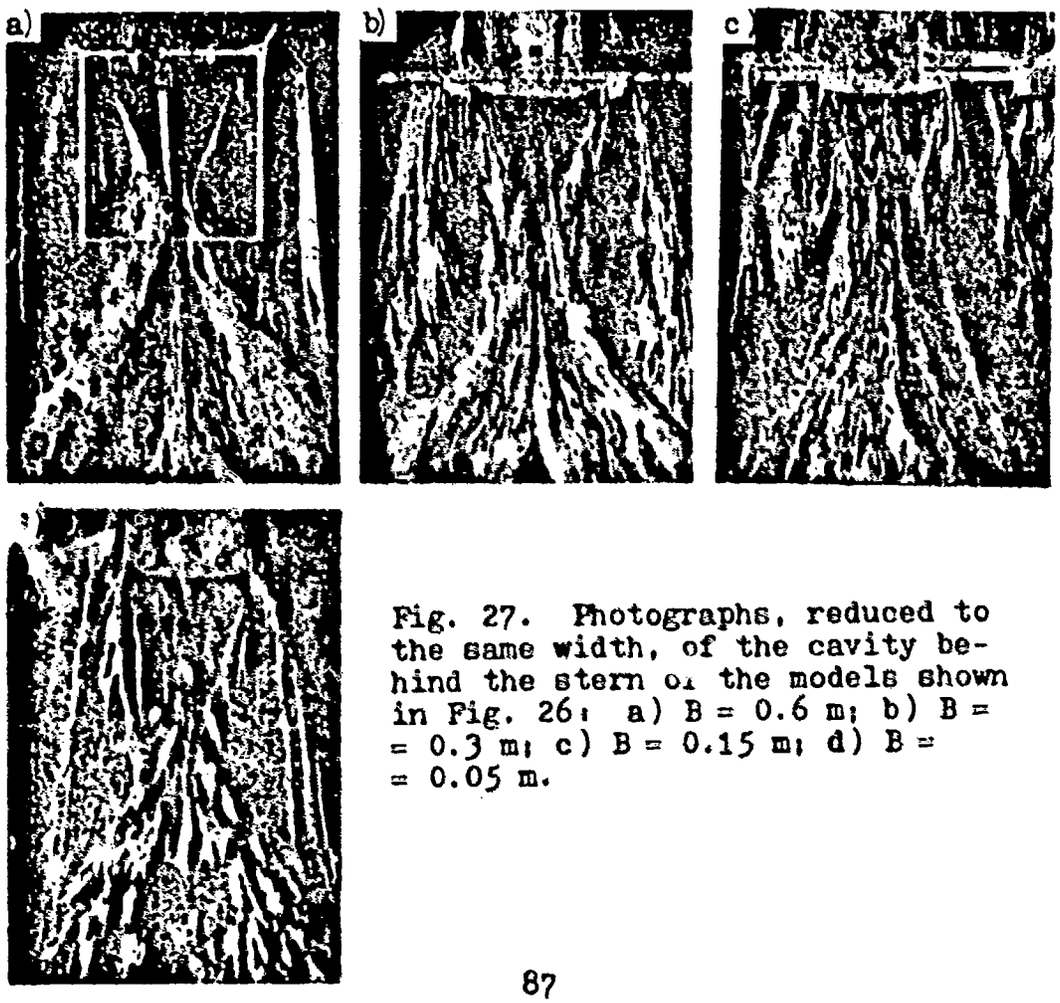

[80

Fig. 27. Photographs, reduced to the same width, of the cavity behind the stern of the models shown in Fig. 26: a) B = 0.6 m; b) B = = 0.3 m; c) B = 0.15 m; d) B = = 0.05 m.

related to the width of the model, becomes, for geometrically similar models with the same Froude numbers, a function of the groups Π and K, i.e., $\Delta h/B = f(\Pi, K)$. The value $\Delta h/B \to 0$ with $\Pi \to 0$ and $K \to 0$. The values Π and K for the given properties of the medium depend only on the typical dimension--width B. From Fig. 26 it follows that for all the tested models, i.e., within the range of $5 \cdot 10^{-3} < \Pi < 6 \cdot 10^{-2}$ and $10^{-4} < K < 10^{-3}$, the value $\Delta h/B \approx 0$; therefore, for $\Pi < 6 \cdot 10^{-2}$ and $K < 10^{-3}$ ($B > 50$ mm) we can ignore the scale effect for the value h. Observations, and particularly analysis of Fig. 27, indicate that certain details of the stream flow change substantially for smaller models. The essence of these changes leads to smoothing of the stream flow, to the disappearance of the typical small details, and to the decrease and disappearance of foam and wave crests. For the smallest model it was not possible to obtain spray for any of the conditions. Thus, in order to form a picture for a typical flow it is necessary to use models with a width of $B > 100$-150 mm. The smaller the part to be analyzed, the larger the model should be.

Let us now present the various considerations entering into the modeling of the thin, arched streams that look like the bubbles escaping from the bow of a ship. Let us analyze a thin flat stream ejected at the angle β_0 with respect to the undisturbed surface and let us assume that in addition to the forces of gravity and inertia, there are forces acting due to the surface tension. Let us assume that the action of these forces is the same as in the undisturbed layer of the fluid with the same curvature as the stream. Projecting the forces acting on the element of the fluid on the tangent and the internal normal line to the thin stream, we can write (Fig. 28) an equation for the motion of an element

$$\Delta m \frac{dv}{dt} = -\Delta mg \sin \varphi; \qquad (3.44)$$

$$\Delta m \frac{v^2}{r} = 2\frac{\sigma}{r} ds + \Delta mg \cos \varphi.$$

Taking into consideration that $\Delta m = \rho h ds$ and

$$r = -\frac{ds}{d\varphi} = -\frac{ds}{dt} \cdot \frac{dt}{d\varphi} = -v\frac{dt}{d\varphi},$$

we can rewrite these equations as follows:

$$\frac{dv}{dt} = -g \sin \varphi;$$

$$\frac{d\varphi}{dt}\left(\frac{2\alpha}{\rho^2}\frac{1}{v}-v\right)=g\cos\varphi. \qquad (3.45)$$

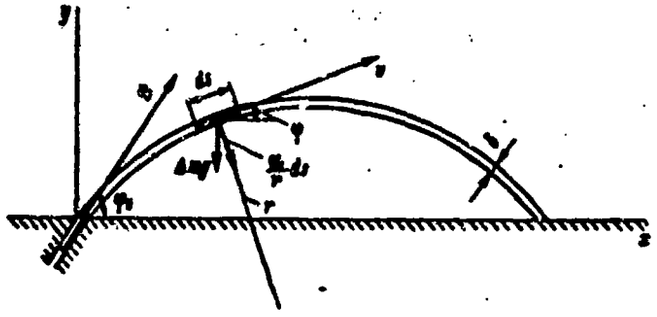

Fig. 28. Diagram for the computation of a two-dimensional stream.

Dividing the first by the second we obtain

$$\frac{vdv}{k^2-v^2}=-\operatorname{tg}\varphi\,d\varphi, \qquad (3.46)$$

where $k^2=\frac{2\alpha}{\rho^2}$.

Integrating (3.46) with the boundary condition of $v = v_0$ with $\varphi = \varphi_0$, we obtain

$$k^2-v^2=\frac{k^2-v_0^2}{\cos^2\varphi}\cos^2\varphi_0. \qquad (3.47)$$

Since

$$\frac{dx}{d\varphi}=\frac{dx}{dt}\frac{dt}{d\varphi}=v\cos\varphi\frac{dt}{d\varphi};$$

$$\frac{dy}{d\varphi}=\frac{dy}{dt}\frac{dt}{d\varphi}=v\sin\varphi\frac{dt}{d\varphi},$$

then substituting into this equation instead of $\frac{dt}{d\varphi}$ its expression from the second equation of (3.45), we obtain

$$\frac{dx}{d\varphi}=\frac{k^2-v^2}{g};\quad \frac{dy}{d\varphi}=\frac{k^2-v^2}{g}\operatorname{tg}\varphi.$$

Integrating with consideration of (3.47) we obtain

$$x=\frac{(v_0^2-k^2)\cos^2\varphi_0}{g}(\operatorname{tg}\varphi_0-\operatorname{tg}\varphi);$$

$$y = \frac{(v_0^2 - k^2)\cos^2\varphi_0}{2g}(\operatorname{tg}^2\varphi_0 - \operatorname{tg}^2\varphi). \qquad (3.48)$$

Excluding φ we obtain an equation of a trajectory, i.e., the equation of the contours of the stream as follows:

$$y = x\operatorname{tg}\varphi_0 - \frac{gx^2}{2(v_0^2 - k^2)\cos^2\varphi_0}. \qquad (3.49)$$

From (3.49) it follows that the action of surface tension forces is equivalent, in a way, to decrease in the initial velocity of the ejected stream. Selecting some typical dimension of the body l and the value g as the dimensional units, we can reduce (3.48) to a dimensionless form

$$\bar{x} = \mathrm{Fr}^2\left(1 - \frac{1}{\bar{\delta}}\frac{K^2}{\mathrm{Fr}^2}\right)\cos^2\varphi_0(\operatorname{tg}\varphi_0 - \operatorname{tg}\varphi);$$

$$\bar{y} = \frac{\mathrm{Fr}^2}{2}\left(1 - \frac{1}{\bar{\delta}}\frac{K^2}{\mathrm{Fr}^2}\right)\cos^2\varphi_0(\operatorname{tg}^2\varphi_0 - \operatorname{tg}^2\varphi), \qquad (3.50)$$

where $\bar{x}$, $\bar{y}$ and $\bar{\delta}$ are used to designate $\frac{x}{l}$, $\frac{y}{l}$ and $\frac{\delta}{l}$; $\mathrm{Fr} = \frac{v_0}{\sqrt{gl}}$ and $K = \sqrt{\frac{2\sigma}{\rho g l^2}}$.

From formulas (3.50) it follows that the scale effect is important for the case when the value

$$\frac{1}{\bar{\delta}}\cdot\frac{K^2}{\mathrm{Fr}^2} = \frac{2\sigma}{\rho\delta v_0^2}$$

can be compared to unity and the dimensions of the stream flow obtained during experiments with models will be relatively smaller than full size. In order to visualize the order of value of the scale effect we can consider the following example: from the bow of the model with a width of B = 0.3 m (the width B is used as the typical dimension l), with a velocity v_0 = 2.5 m/sec, there originate streams of thickness δ = 3 mm. Let us compute [8]

$$\mathrm{Fr}^2 = \frac{v_0^2}{gB} = 2{,}1;\ \bar{\delta} = 10^{-2};\ K^2 = \frac{2\sigma}{\rho g B^2} = 1{,}67\cdot 10^{-3};$$

parameter $\frac{1}{\bar{\delta}}\frac{K^2}{\mathrm{Fr}^2} \approx 0{,}08$. For full size with a width of $B_н$ = = 3 m the applicable value will be one hundred times smaller. Thus, utilizing formula (3.50) for the model and the prototype, we find that the error in the dimensions of the stream flow, for example in the height of the rise, will

constitute ~8%. By decreasing the size of the model this error will increase in inverse proportion to the square of its dimensions. Let us emphasize that the error for the model and the prototype in the same medium and the same gravitational field is defined by the linear dimensions, and specifically by the width of the model B_M, and not by the scale, i.e., the relationship B_M/B_H. If in the given example the width of the prototype would have been not 3 but 30 meters, i.e., if the scale would be not 1:10 but 1:100, the error would remain practically unchanged, while by maintaining the scale 1:10 the dimensions of the model would be 0.1 m rather than 0.3 m, and the error would increase almost tenfold. Let us note that when $\frac{1}{\delta}\frac{K^3}{Fr^3}=1$, the streams completely disappear, which is actually observed for very small models. Let us also point out that the additional distortions can be caused by the effect of wetting, which influences the angles of stream escape for small models.

Let us go to the scale effect which is encountered in determining the dimensions of rise and distance of spray flight that is formed during planing. The spray is the result of the breaking up of the stream flow from around the planing bottom. A schematic diagram of the spray stream reflected from the keeled bottom is shown in Fig. 29.

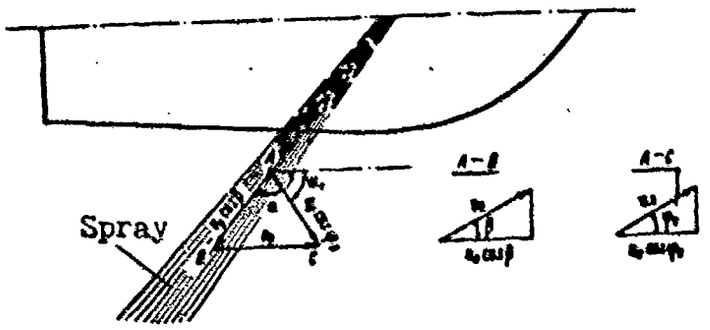

Fig. 29. Schematic diagram of a spray stream reflected from a planing bottom. $v_0 \sin\beta = u_0 \sin\varphi_0$.

It follows from Bernoulli's equation that in the coordinate system connected with a ship, the magnitude of the spray stream velocity is equal to the velocity of its motion v_0.

Let us examine the flight of one of the drops of the

spray jet. Let the plane that contains the vector of the initial velocity of the drop, which is perpendicular to the water surface, form an angle α with the diametral plane of the ship, and let the vector v_0 itself form an angle β with the water surface. Then, the velocity vector of the drop in the fixed coordinate system will have the following modulus

$$u_0 = v_0\sqrt{2(1+\cos\alpha\cos\beta)} \tag{3.51}$$

and forms an angle φ_0 with respect to the water surface, an angle determined by the following equation:

$$\sin\varphi_0 = \frac{\sin\beta}{\sqrt{2(1+\cos\alpha\cos\beta)}}. \tag{3.52}$$

The projection of this vector on the water surface [8
forms an angle α_1 with the diametral plane of the ship:

$$\sin\alpha_1 = \frac{\sin\alpha\cos\beta}{\sqrt{1+2\cos\alpha\cos\beta+\cos^2\beta}}. \tag{3.53}$$

In the fixed system of coordinates the drop flies in the vertical plane defined by the angle α_1 with an initial velocity u_0 and exit angle φ_0, experiencing the drag of the air at rest. The longest flight distance and the highest ascent attained by drops will be experienced by the largest drops, since the inertia forces are proportional to the cube of the linear measurements, and the drag force to their square. The maximum size of the drops is determined by the condition of their stability in the gas stream, while the stability of a drop's shape is determined by the stabilizing forces of surface tension and the aerodynamic forces that act to disintegrate the drop. According to experimental data [10, 25], the boundary of stability can be determined from the expression

$$\frac{\rho' u_0^2 d}{\sigma} \approx 14, \tag{3.54}$$

where ρ' - density of the gas;
u_0 - velocity of the drop with respect to the gas;
d - diameter of the drop;
σ - coefficient of surface tension.

In the table below the values of the velocities and

Table

d, мм	0,1	0,3	1	3	10
u_0, m/sec	92	53	32	17	9
$10^{-4} \cdot Re$	0,92	1,6	3,2	5,1	9

diameters which satisfy relationship (3.54) are given, as are the corresponding Reynolds numbers $Re = \frac{v_0 d}{\nu}$ with $\nu = 10^{-6}$ m^2/sec. For approximately this range of Reynolds numbers is formula (3.54) also valid.

From the table it follows that for all velocities and drop diameters interesting for practical purposes the Reynolds numbers lie within the limits of 10^4-10^5, i.e., in the region where the drag coefficient of the sphere is almost constant and equal to ~0.5. Thus, we can consider the drag on the flying drop proportional to the square of the relative velocity, while the process of flight of drops is independent of the Reynolds number.

Taking as the units of measurement the speed of the ship and some typical dimension 1, we can write the equation for the motion of a drop as projections on a tangent and the interior normal to the trajectory in a dimensionless form

$$\frac{d\bar{u}}{d\bar{t}} = -\frac{\sin\varphi}{Fr^2} - \frac{k}{\bar{d}}\bar{u}^2;$$

$$\frac{\bar{u}^2}{\bar{r}} = Fr^2\cos\varphi. \qquad (3.55)$$

where

$$\bar{u} = \frac{u}{u_0};\ \bar{d} = \frac{d}{l};\ \bar{r} = \frac{r}{l};\ Fr^2 = \frac{u_0^2}{gl};\ \bar{t} = \frac{tu_0}{l};\ k = \frac{3}{4}C_x\frac{\rho'}{\rho}. \qquad (3.56)$$

The solution of equations (3.55), which describe the ballistic trajectory with drag proportional to the square of the velocity, is well known. Introducing a set of dimensionless coordinates $\bar{x}$ and $\bar{y}$ lying in the plane of the trajectory with the origin of the coordinate system at the point of drop ejection, we obtain (see, for example [36])

$$\bar{x} = -\frac{\bar{d}}{k}\int_{\varphi_0}^{\varphi}\frac{d\varphi}{F(\varphi)}; \qquad (3.57)$$

$$\bar{y} = -\frac{\bar{d}}{h}\int_{s_0}^{s}\frac{s\,ds}{F(s)}; \qquad (3.58)$$

$$\bar{t} = -\sqrt{\frac{\bar{d}}{h\,Fr^2}}\int_{s_0}^{s}\frac{ds}{\sqrt{F(s)}}, \qquad (3.59)$$

where

$$F(s) = \frac{\bar{d}\,Fr^2}{\bar{w}_0^2 h\cos^2\varphi_0} + \left(s_0\sqrt{1+s_0^2} - s\sqrt{1+s^2}\right) + \ln\frac{s_0+\sqrt{1+s_0^2}}{s+\sqrt{1+s^2}}; \qquad (3.60)$$

[86

$$s = \operatorname{tg}\varphi; \quad s_0 = \operatorname{tg}\varphi_0. \qquad (3.61)$$

We will transform function F(S), representing it in the form

$$F(s) = \frac{1}{n}[1 + nf(s)], \qquad (3.62)$$

where

$$n = \frac{h\bar{w}_0^2\cos^2\varphi_0}{\bar{d}\,Fr^2} \qquad (3.63)$$

and

$$f(s) = s_0\sqrt{1+s_0^2} - s\sqrt{1+s^2} + \ln\frac{s_0+\sqrt{1+s_0^2}}{s+\sqrt{1+s_0^2}}. \qquad (3.64)$$

Then the formulas (3.58), (3.59) and (3.60) will take the form

$$\bar{x} = -\frac{\bar{w}_0^2\cos^2\varphi_0}{Fr^2}\int_{s_0}^{s}\frac{ds}{1+nf(s)}; \qquad (3.65)$$

$$\bar{y} = -\frac{\bar{w}_0^2\cos^2\varphi_0}{Fr^2}\int_{s_0}^{s}\frac{s\,ds}{1+nf(s)}; \qquad (3.66)$$

$$\bar{t} = -\frac{\bar{w}_0\cos\varphi_0}{Fr}\int_{s_0}^{s}\frac{ds}{\sqrt{1+nf(s)}}. \qquad (3.67)$$

In the absence of drag from the medium n = 0, formulas (3.65), (3.66) and (3.67) determine the flight of a drop along the usual parabolic trajectory, and the corresponding values x, y and t we can denote with a zero subscript. The distortion of this trajectory, and hence the scale effect, are determined by the difference in the value n or, more precisely, by the product nf(s), for the model and the full size.

The integrals entering into (3.57), (3.58) and (3.59) are given in the ballistic tables. Calculation of the trajectory by these formulas, or by the formulas (3.65), (3.66) and (3.67), does not present any difficulties. The values $\bar{u}_0$ and φ_0 are determined by formulas (3.51) and (3.52) from the velocity of the craft or the model and from the angles α and β that define the direction of the emitted streams.

For better visualization, let us bring to a conclusion the computations for the maximum rise of the spray for small angles of ejection φ_0.

For small φ_0

$$s \approx \varphi;\ s_0 \approx \varphi_0;\ f(s) = 2(\varphi_0 - \varphi);\ \cos\varphi_0 \sim 1.$$

Integration is performed from φ_0 to zero [87

$$\bar{y}_{max} = \frac{\bar{u}_0^2}{Fr^2}\int_0^{\varphi_0} \frac{\varphi d\varphi}{1+2n(\varphi_0-\varphi)} = \frac{\bar{u}_0^2}{Fr^2}\left[\left(\frac{\varphi_0}{2n}+\frac{1}{4n^2}\right)\ln(1+2n\varphi_0) - \frac{\varphi_0}{2n}\right]; \quad (3.68)$$

in the absence of drag (n = 0)

$$\bar{y}_{0max} = \frac{\bar{u}_0\varphi_0^2}{2} Fr^2. \quad (3.69)$$

The relationship between the actual maximum height attained by the spray to the same value in the absence of resistance of the medium will be

$$\frac{y_{max}}{y_{0max}} = 2\left[\left(\frac{1}{\delta}+\frac{1}{\delta^2}\right)\ln(1+\delta) - \frac{1}{\delta}\right], \quad (3.70)$$

where

$$\delta = 2n\varphi_0. \quad (3.71)$$

In Fig. 30 the dependence of $\frac{y_{max}}{y_{0max}}$ on δ and $\frac{1}{\delta}$ from formula has been plotted.

Let us examine the following specific example: let a craft with width B = 4 m move with speed v_0 = 25 m/sec, and suppose the spray is being emitted at an angle φ_0 = 0.2. Let us determine n by formula (3.63) with consideration of formulas (3.54) and (3.56). For simplicity in formulas (3.51) and (3.52) we will assume $\cos\alpha \cos\beta = -0.5$, i.e.,

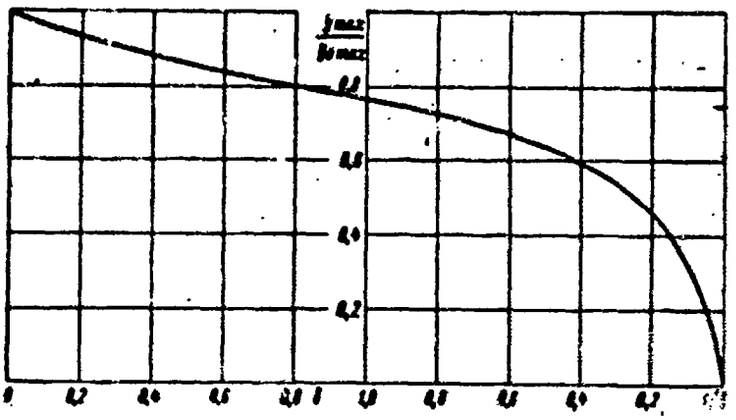

Fig. 30. Dependence of the ratio of the maximum height reached by spray drops y_{max} to the same value in the absence of air resistance y_{0max} on the parameter δ.

$\bar{u}_0 = 1$ and $\beta = \varphi_0$; then

$$n = \frac{3}{4} C_x \frac{\rho'}{\rho} \frac{v_0^2}{gB} \frac{\rho' v_0^2 B}{14\sigma} = \frac{3}{4} C_x \frac{\rho'}{\rho} Fr^4 \frac{\rho' g B^3}{14\sigma}.$$

Assuming $C_x = 0.5$, $\rho' = 0.125$, $\rho = 100$, $\sigma = 0.0075$, [88 we will find

$$n_0 = 22 \text{ and } \delta_0 = 2n\varphi_0 = 8{,}8.$$

From the graph in Fig. 30 or from formula (3.70) we find

$$\left(\frac{y_{max}}{y_{0max}}\right)_0 = 0{,}34.$$

For the model with width B = 0.2 m the value of n will be 400 times smaller, i.e.,

$$n_M = 0.055 \text{ and } \delta_M = 0.022.$$

Thus for the model

$$\frac{y_{max}}{y_{0max}} = 0{,}99 \sim 1,$$

i.e., the height reached by the spray drops recalculated

according to scale from the model to full size will be three times greater than the real one.

Let us note that for spray jets we have obtained results opposite from those obtained for thin, continuous, fluid jets. The drops which make up the spray jets in the full size were smaller in absolute size than those of the model; hence, the height and the distance of the jet became relatively smaller. The scale effect is substantially more pronounced for increasing dimensions of the full size, while with respect to continuous fluid jets and deformations of the fluid surface behind the stern, the scale effect was basically determined by the dimensions of the model and virtually did not depend on the dimensions for the real case.

CHAPTER IV. SIMULATION OF CERTAIN PHENOMENA AND PROCESSES RELATED TO CAVITATION.

4.1. Concerning the Scale Effects in the Initial Stages of Cavitation

Let us examine the cavitation (formation of interruptions of continuity) caused by a decrease in pressure in the steady-state flow around bodies or during their motion in fluid with a constant speed. The phenomena of the formation of cavitation in other cases, such as due to the influence of rising temperature (boiling) or due to the influence of changes in fields of acceleration, will not be discussed here. At the present time, it is known [50, 24] that the process of the origination of cavitation is related not only to local decrease in pressure, but also to such factors as the presence of incipient nuclei, which are tiny gaseous bubbles or solid particles and cracks which have adsorbed gas on their surface. The presence of gas dissolved in the fluid which precipitates in the cavity near the incipient nuclei has a very substantial influence on the origination of cavitation. The process of growth and displacement of bubbles along the surface of the object is also related to the phenomenon of wetting. [8

This brief information is sufficient for the formulation of a system of parameters which determine the conditions of origination of cavitation.

Among these parameters will be the geometric dimensions l, l_1, ..., l_n, which define the size, shape and position of the object or objects, as well as the condition of their surfaces and the size of foreign inclusions in the fluid, such as bubbles, particles, etc. Along with these linear dimensions, among the determining parameters will be the dimensionless functions φ_1, ..., φ_k, which characterize the law of distribution for peaks of surface roughness, particles, etc. dimensionally, as well as the numbers n_1, ..., n_m, which define the overall quantity of particles in a unit of volume or the number of cracks and roughness peaks per unit area of surface. In addition, the following values must obviously be considered: the velocity v of the stream relative to the body; such properties of the medium as its density ρ and viscosity $\mu = \rho\nu$; the surface tension coefficients σ_{12}, σ_{13}, σ_{23} at the boundaries between fluid and gas, fluid and solid object, and gas and solid object, respectively. Also, the pressure p_0 in the

incoming stream; the pressure p_d of the saturated vapors; the specific volume occupied by the dissolved gases δ under pressure p_0 and temperature T_0; and the diffusion coefficient D that characterizes the rate at which the gas is escaping from the solution. The mass of gas which is escaping from the solution can be defined by its volume ΔV_r for certain pressure and temperature. We will consider the temperature equal to the temperature of the fluid T_0; and it is convenient to use as the value of pressure the pressure p_0 of the incoming stream. In accordance with Bohr's formula

$$\Delta V_r = DS\frac{p_н - p_п}{p_0}\Delta t. \qquad (4.1)$$

Here D - diffusion coefficient;
S - surface area through which the gas escapes;
$p_н$, $p_п$ - partial gas pressures in solution and in the space into which the gas is escaping (in the bubble);
Δt - time interval of gas escape.

Obviously, the change in pressure in the bubble due to the escaping of dissolved gases will be

$$\Delta p = \frac{\Delta V_r}{V_п}\cdot p_0, \qquad (4.2)$$

where $V_п$ is the volume of the bubble.

In selecting the parameters which define the system, it is important to consider not only the essential values for the given phenomenon, but also to note and eliminate those factors which have little effect on the outcome. This is often not done, and in a number of works (see, for example, [24, 39]) various factors are entered without sufficient analysis into those which define the origination of cavitation, such factors as the velocity of sound, weight, and values which define the thermodynamic processes in the systems "liquid-gas" and "liquid-wall," etc. Due to this fact, new, unsubstantiated difficulties arise, which interfere with analysis of the already complicated phenomenon.

Since the velocity of sound in water is approximately 1440 meters per second and the velocity v of the motions being studied has the order of several tens of meters per second, it is not necessary to talk about the negligibly

small effect of compressibility at Mach numbers that do not exceed M = 0.1. As far as the velocity of sound in a two-phase medium is concerned, it is not an independent value, but varies at various points of the stream and is determined by the conditions of the flow, by the content of gas in the fluid, by the amount of nuclei, etc. In a specific case, adoptable to a fluid in which the emission of gas follows the Henry-Dalton law, the expression for the sound velocity depending on the specific volume of the dissolved gases is given in [46, 49, 50]. Thus, the inclusion of the sound velocity among the dimensionless parameters which determine the emergence of cavitation is wrong in principle.

For the same reasons, it is incorrect to include among independent parameters such parameters as the specific time from which the Strouhal number is later formed. The specific time, which is understood to mean the time required for the formation of the bubble, the time of its displacement into the various specific positions, etc., is not an independent value and is determined by the elements listed above. The specific time should be introduced only for the processes with given kinematic characteristics (vibrating airfoil, revolving propeller, etc.).

The effect of gravity can be ignored for the type of problems under consideration, since the difference in pressures it causes is negligibly small in small gas bubbles as compared to all other pressures. Even with a 1 mm diameter the difference between the hydrostatic pressures (1 mm of water column) will be 15 times smaller than the pressure caused by surface tension forces, which are usually ignored for this size of bubble. The gravitational effect can become noticeable near the free surface, e.g., in the case of analysis of cavitation for a shallowly submerged hydrofoil; however, such a case does not belong to the essence of the problem being studied.

It is not difficult to show that numerous [39, 85] attempts to relate the origination of cavitation (for ordinary flow in cold--20°--water) to different thermodynamic processes are devoid of any basis. This has already been mentioned by us in [50], where it was indicated that, specifically such types of factors as heat conductivity of the walls of the object, variation in vapor pressure under a curved surface, the rate of evaporation, and the related thermodynamic processes do play a certain role. However, their consideration is just as justified and fruitful as the substitution of Einstein's mechanics for Newtonian mechanics in considering our problem. Depending

on the amount of vapor that will be taken in by the forming bubble in a unit of time, the pressure in it will either be p_d or 20% less than the pressure of the saturated vapors, and the cavitation number will be changed by an amount within the limits of experimental precision. [91

In actual cases, experiments with models are usually conducted with velocities of $v \sim 10$ m/sec, i.e., with dynamic velocity heads $q = \frac{\rho v^2}{2} \approx 5000$ kg/m^2. The pressure of saturated vapors at T = 20°C amounts to $p_d \sim 200$ kg/m^2. If evaporation would not have sufficient time to occur, then it would lead to a change in the cavitation number by the amount of $\Delta x = \frac{p_d}{q} = 0.04$. Variation in the p_d value of 25% would produce a change $\Delta x \sim 0.01$. It is also necessary to consider the small volumes and the heat capacity of the vapors and gases trapped in bubbles and the relatively large surface of heat transfer [50].

Thus, on the basis of the material presented the regime of cavitation emergence can be written in the form of the following relation:

$$F(l, l_1, \ldots, l_n, n_1, \ldots, n_m, \varphi_1, \ldots, \varphi_k, \rho, v, \nu, \sigma_{12}, \sigma_{13}, \sigma_{23}, p_s, p_d, \delta, D). \quad (4.3)$$

In the future, due to the lack of data, we will exclude from the analysis the values $n_1, \ldots, n_m, \varphi_1, \ldots, \varphi_k$ and those l_i which define the cavitation nuclei, the surface roughness, etc. In analyzing the experiments with respect to the scale effect, it is necessary to remember that these characteristics, as a rule, remain constant for various scales of the models. For simplicity, we will retain of all σ_i only $\sigma_{12} = \sigma$; it is evident that σ_{13} and σ_{23} will produce perfectly similar dimensionless relationships as σ_{12}. Substituting for (4.3) at this point the analogous relationship composed from the dimensionless combinations, we obtain

$$f\left(\frac{l_1}{l}, \ldots, \frac{l_n}{l}; x, \mathrm{Re}, \mathrm{We}, \delta, \bar{D}\right) = 0. \quad (4.4)$$

Here

$$x = \frac{p_s - p_d}{\frac{\rho v^2}{2}}; \quad \mathrm{Re} = \frac{vl}{\nu}; \quad \mathrm{We} = \frac{\sigma}{\rho v^2 l}; \quad \bar{D} = \frac{D}{l}. \quad (4.5)$$

Let us note that it would be more accurate to introduce the two Euler values $\frac{p_0}{\frac{\rho v^2}{2}}$ and $\frac{p_d}{\frac{\rho v^2}{2}}$ instead of the cavitation number; however, for the case under consideration of normal temperatures, which correspond to small values of p_d for water, this refinement is unnecessary. Thus, with allowance for the previously made reservations for geometrically similar systems, it follows from (4.4) that the critical value $\varkappa_{kp}$ can be written in the form

$$\varkappa_{kp} = f_1(\mathrm{Re}, \mathrm{We}, \delta, \bar{D}). \qquad (4.6)$$

With the aid of special resorbers it is sometimes possible to achieve similitude with respect to δ (see [50, 78], but in this case, too, there remain the values Re, We, $\bar{D}$, [92 which are, as a rule, different for the model and the prototype.

Let us remember that the model and the prototype are understood to be two systems that differ by some kind of scale: geometric, velocity, etc. The difference in Re and We numbers, and in the coefficient of diffusion $\bar{D}$, as well as the lack of similitude of dimensions and amount and distribution of cavitation nuclei, cracks, surface roughness--all these factors contribute to the emergence of the scale effect, i.e., an ambiguity in $\varkappa_{kp}$ for geometrically similar objects and bodies identically oriented in the stream. Many works have been devoted to the scale effect of cavitation emergence. They are basically discussed and analyzed in the monograph by A. D. Pernik [24] and in the part of the book "Cavitation" written by F. E. Eisenberg and M. P. Tulin [82]. A bibliography on this problem is included in [24] and [82].

Before proceeding to analysis of the theoretical and experimental data, and before making any comments with respect to the question of the magnitude and characteristics of the scale effect during the origination of cavitation, we will clarify what exactly is understood by the origination of cavitation and how one can define such a condition, for example, in testing a series of geometrically similar models. The simplest methods of registering the beginning of cavitation are either visual or sonic evaluation. The appearance of cavitation is accompanied by the formation of a foggy strip and by a characteristic sound. The recording of optical or acoustic phenomena can be conducted either directly or with the aid of special instruments. Regardless of this, the following problem

arises. Let the accuracy of our apparatus be such that we can distinguish the cavitation region if its size reaches the value A or its sound pressure reaches the value B. Suppose we have two models and suppose model No. 1 is ten times larger than model No. 2. Obviously, it is true for both models that we will be able to detect the cavitation region only after it reaches the magnitude A. However, on the other hand, it is obvious that even if the phenomena were completely similar the cavitation area with the magnitude A on model No. 1 would have to correspond with the cavitation area of size 0.1A of model No. 2. In conformance with the adopted assumptions with respect to the accuracy of the apparatus, we are incapable of registering this phenomenon and therefore arrive at a false conclusion with regard to the presence of the scale effect. On the contrary, if with the same cavitation numbers we had noticed with our apparatus emerged cavitation (with an area of size A), then we can state that the scale effect was not pronounced, even though, in reality, the cavitation area of model No. 2 is ten times larger than model No. 1.

The considerations presented above were not taken into account and were not discussed by the authors who analyzed the scale effect. In the experimental works concerning this problem there is also no information about a number of other factors which could substantially affect conclusions with respect to the scale effect. Let us mention only a few examples of undiscussed conditions which, while [93
influencing the result, are not connected to the essence of the problem. With variation of the velocity in the cavitation tunnel the local characteristics of the flow and its degree of vorticity can vary, and change in the dimensions of the models changes the restriction of the working cross section of the tunnel. Sometimes the data with respect to the amount of dissolved gas are entirely absent, and sometimes, as for example in [76], it is indicated that this value varies by a factor of 2. In most of the works there are no experimental data on the distribution of pressures taken from test specimens with tested Reynolds numbers.

All of this suggests a very careful approach toward often contradictory results in the conducted experiments and, therefore, toward their analysis. In Figures 31, 32 and 33, using information contained in [39], we have shown the influence of the Reynolds number on the value of the incipient cavitation for three symmetrical profiles mounted at a zero angle of attack. The relative thickness of all profiles is 12%. Profile No. 1 is the Zhukovskii profile; profile No. 2 has parallel walls, a tip rounded to a semicircle, and a pointed tail; profile No. 3 is NACA-16012

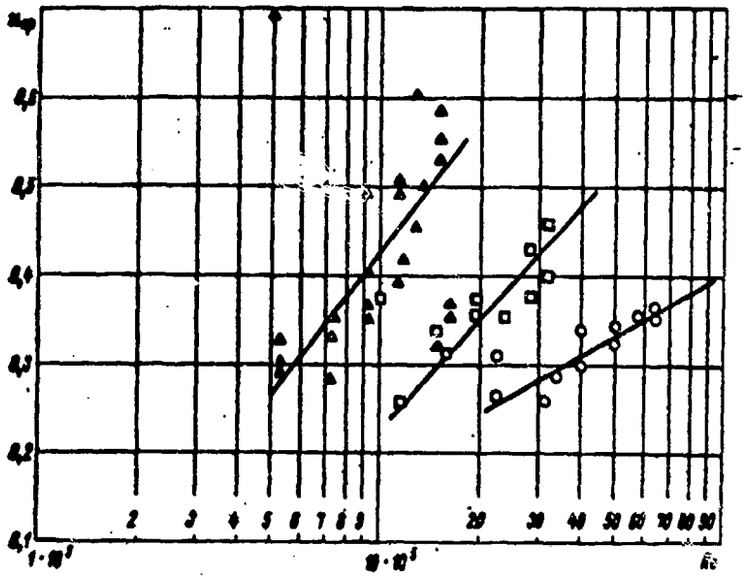

Fig. 31. Dependence of the number of incipient cavitation $\varkappa_{кр}$ on the Reynolds number for the Zhukovskii profile.
Δ - b = 50.8 mm; □ - b = 101.6 mm; o - b = 203.2 mm.

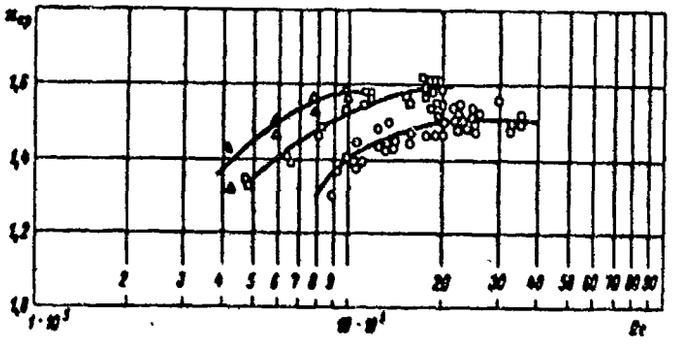

Fig. 32. Dependence of the number of incipient cavitation $\varkappa_{кр}$ on the Reynolds number for a profile of constant thickness with a rounded tip and a pointed tail.
Δ - b = 50.8 mm; □ - b = 101.6 mm; o - b = 203.2 mm.

and represents a contemporary high-speed profile with the maximum thickness at the middle of the chord.

Along with experimental research there have been attempts at theoretical prediction of the scale effect. As

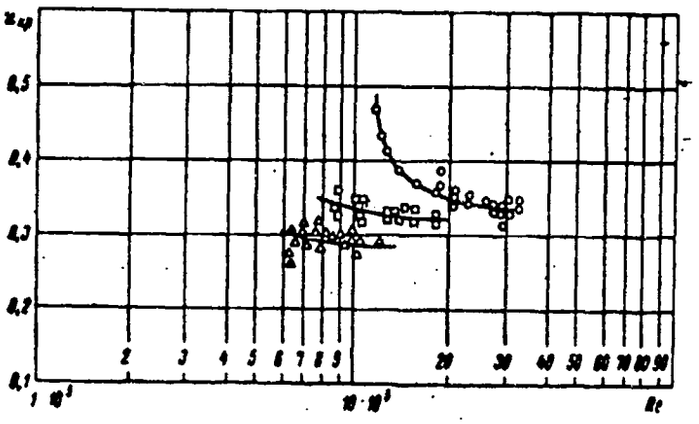

Fig. 33. Dependence of the number of incipient cavitation $\varkappa_{кр}$ on the Reynolds number for the high-speed profile NACA-16012.
Δ - t ~ 10°C, b = 63.5 mm;
□ - t ~ 27°C, b = 63.5 mm;
o - t ~ 25°C, b = 127 mm.

has already been noted, these observations are given in [24] and [82]. At this point we will analyze in greater detail the work of R. Oshima [22], who discusses the motion and the growth of the spherical incipient bubble at the boundary under the following conditions: 1) pressure distribution is similar for similar bodies; 2) the law governing the distribution of velocities at the boundary layer is independent of the Reynolds number; 3) the bubbles move along the paths $y/\delta = \text{const}$; 4) the growth of the incipient bubble up to the radius R, equal to half the thickness δ^* of displacement, starts and ends at corresponding points of geometrically similar bodies. The condition at which $R = \delta^*/2$ is considered to be the condition of the onset of cavitation. Oshima conducts his discussion by using the known equation for bubble expansion

$$\frac{\Delta p}{\rho} = \frac{3}{2}\left(\frac{dR}{dt}\right)^2 + R\frac{d^2R}{dt^2} \qquad (4.7)$$

and the equation which describes its motion along the outline of the body. After a series of transformations he arrives at the expression

$$\left(\varkappa_1 + \bar{p} + \frac{4\sigma_1}{\rho_1 v_1^2 R_1}\right) R_1^2 l_1^2 = \left(\varkappa_2 + \bar{p} + \frac{4\sigma_2}{\rho_2 v_2^2 R_2}\right) R_2^2 l_2^2, \qquad (4.8)$$

where $\varkappa_i$ - the number of the incipient cavitation;

$\bar{p}$ - pressure coefficient;

σ - surface tension coefficient;

ρ - density;

v - velocity of the incoming stream;

R - radius of the bubble;

l - typical dimension of the body.

subscripts "1" and "2" designate two similar bodies. The displacement thickness is determined by boundary layer theory.

Let us show that Oshima's results [22], using his approximations, can be obtained without using the equations of expansion and motion of the bubble, with the aid of dimensional analysis theory.

In reality, the radius R of the bubble that is expanding in an incompressible ideal fluid, from almost the zero dimension, depends on the pressure drop Δp on the inside and on the outside of the bubble (the pressure drop Δp is determined with consideration of the surface tension forces), on the density ρ of the fluid, and on the time of expansion, i.e.,

$$R = F(\Delta p, \rho, t). \tag{4.9}$$

The dimensionless combination

$$\frac{R}{t}\sqrt{\frac{\rho}{\Delta p}} = \text{const}, \tag{4.10}$$

since it is not possible to form the dimensionless value from the terms of the right side of equality (4.9). The time of expansion determined with (4.10) must be equal to the time of displacement of the bubble along the contour of the body, that is, in the region from the point where the expansion has started to the point at which the diameter of the bubble has become equal to the displacement thickness. With Oshima's approximations formulated in points 1-4, this time of displacement is directly proportional to the typical linear dimension of the object and inversely proportional to the velocity of the flow, i.e.,

$$t = \text{const}\frac{l}{v}. \tag{4.11}$$

From (4.10) and (4.11) we find, excluding t,

$$\Delta p = \text{const}\,\frac{\rho v^2 R^2}{l^2}. \qquad (4.12)$$

On the other hand,

$$\Delta p = p_1 - p_d + \frac{2\sigma}{R}, \qquad (4.13)$$

where p_1 is the pressure exerted by the fluid surrounding the bubble.

Since the cavitation number is

$$x = \frac{p_0 - p_d}{\frac{\rho v^2}{2}}, \qquad (4.14)$$

and the pressure coefficient is

$$\bar{p} = \frac{p_1 - p_0}{\frac{\rho v^2}{2}}, \qquad (4.15)$$

then, substituting in (4.13) p_1-p_d by the formula

$$p_1 - p_d = \frac{\rho v^2}{2}(x + \bar{p}),$$

we obtain, considering (4.12), the following:

$$\left(x + \bar{p} + \frac{4\sigma}{\rho v^2 R}\right)\frac{l^2}{R^2} = \text{const}, \qquad (4.16)$$

i.e., an expression equivalent to (4.8).

Even though the recalculations from one scale to another, performed in accordance with (4.8), are in agreement with experiments [76] for cylinders with a spherical head portion, Oshima's theory is inconclusive. Its weakest point is its completely arbitrary, unfounded initial presumption that cavitation begins when the diameter of the bubble becomes equal to the thickness of displacement of the boundary layer. The assumption that the bubble moves along the line $y/\delta = \text{const}$ is also quite arbitrary. It would be much more logical to consider that the bubbles move with the same velocity as the fluid at a distance from the wall equal to the radius of the bubble. The time for displacement of the bubble along the contour would depend then on the Reynold number.

Returning to equation (4.6), let us express some preliminary considerations with respect to the influence on the emergence of cavitation of the terms that enter into the right side of the equation. Let us first examine the influence of the Reynolds numbe. It is advisable to start with the simplest scheme for the emergence of cavitation, by assuming that it emerges when the local pressure becomes equal to the pressure of the saturated gases p_d. In such a formulation the question of the influence of Re on cavitation reduces to the effect of Re on the distribution of pressures along the surface of the body, i.e., it reduces to a problem which has nothing in common with the problem of cavitation.

As a descriptive example, we can examine the emergence of cavitation on a cylinder. The results of such experiments are contained in the works of Martyrer [77], where [97
it is shown that cavitation emerges in complete agreement with pressure distribution along the cylinder for supercritical Reynolds numbers at $\varkappa_{kp} \approx 2.5$ (cylinder diameter $d = 23.7$ mm), and for subcritical Reynolds numbers at $\varkappa_{kp} \approx \approx 1.5$ ($d = 4.98$ mm). These values of $\varkappa_{kp}$ are in agreement*

*The value $\bar{p}_{min} = 2.5$ is greater than the theoretical value in an infinite ideal fluid $\bar{p}_{min} = 9/4 = 2.25$; however, we must also take into consideration the influence of the walls, which tends to increase $\bar{p}_{min}$.

with $\bar{p}_{min}$ for supercritical and subcritical conditions of flow around the cylinder.

Although there is in the given example a direct scale effect, i.e., the influence of Re on $\varkappa_{kp}$, it would be more expedient to consider, as the scale effect of viscosity forces, those changes in $\varkappa_{kp}$ which are directly related to the specific features of the interaction between the viscous flow at the boundary layer and the expansion of cavitation bubbles.

For better clarity let us consider the influence of Re on $\varkappa_{kp}$ as scale effect of the first type, if this influence is determined only by the action of Re on the distribution of pressures along the body. The influence of

Re on $\varkappa_{kp}$ for the same pressures we will consider to be scale effect of the second type.

Obviously, this categorization simplifies understanding and analysis of the corresponding experimental investigations. Particularly, the scale effect of the first type can be determined by wind tunnel tests for the corresponding Reynolds values, and can be separated from the overall scale effect. Unfortunately, this was not done in most of the above-mentioned experimental studies.

To determine the system of defining parameters (4.6) it was sufficient to have general brief information with respect to the values which have an influence on the emergence of cavitation. In order to analyze the influence of scale effects, a deeper understanding of the concepts about the processes of the emergence and development of cavitation is required. We will formulate here certain basic aspects which arise from [50] and also from high-speed photographs made in a somewhat later period and partially published in [56].

In proportion to the pressure drop along the smooth and streamlined contour, two discontinuities characteristic of cavitation appear, the passing bubble type (Fig. 34) and the "boundary cavity" type, attached to the quasi-stationary cavity, which then is carried away by the flow (Fig. 35). For the condition of relatively small degree of vacuum, the cavities appear after a considerable time interval, during which the continuity of the fluid remains undisturbed (Fig. 36). The length of the intervals and the life of the cavity attached to the body are governed by the laws of statics. With an increase of vacuum, the frequency of appearance of discontinuities increases and stationary cavities grow in size and remain longer, while new bubble sources of discontinuities appear before the previous discontinuity has time to collapse (Fig. 37). With [9
further vacuum increase in the area of reduced pressure, a large number of bubbles moves simultaneously away from successive discontinuities, and finally, with further vacuum increase, the cavity attached to the body remains the only one to be stable, starting from the point of greatest vacuum.

In spite of the prevailing views (see [24], for example), bubble and quasi-stationary types of cavitation can occur under the same conditions on the same body. Both types of cavitation can freely replace one another within a span of only a few hundredths of a second, and can even coexist (Fig. 37 and 38).

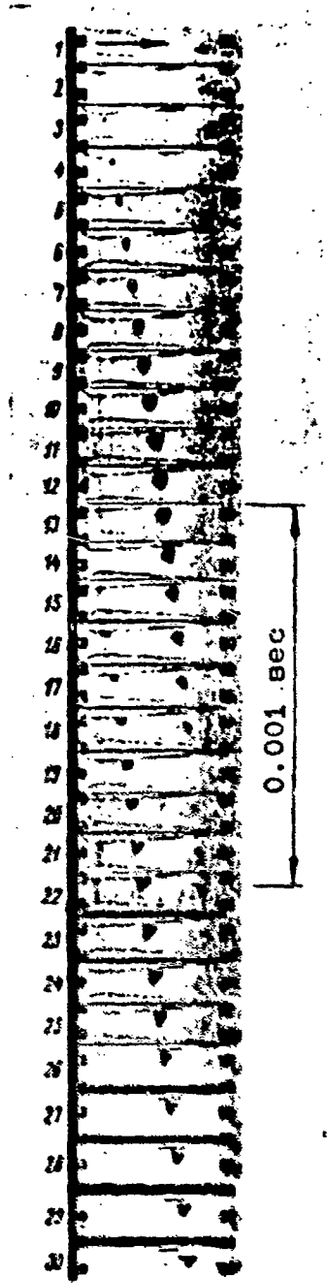

The emergence of one or the other form of cavitation is probably related to two factors: 1) the area through which the emerging nucleus is passing; 2) the conditions of surface-wetting. If the emerging nucleus passes at a certain distance from the wall, then the bubble form of cavitation appears. If the emerging nucleus passes in the immediate vicinity of the wall, a cavity attached to the body may emerge. The free boundary of this cavity is pulsating and if, as the result of these pulsations, the boundary in the region of the origin of cavitation deviates substantially from the current direction, then the cavity becomes detached and is carried away by the flow. We can also detect intermediate cavity forms, when the part of the cavity located closest to the wall moves more slowly and becomes elongated along the stream similarly to the stationary cavity, while the part of the cavity further removed from the wall moves similarly to the bubble (see frames 18-21 in Fig. 37 and 100-102 in Fig. 38). During the process of their motion the bubble type cavities expand on a section larger than the region $p < p_d$ (see [47]), and then collapse. Measurements showed that velocities of collapse reached 100 m/sec and even higher. After collapsing, the bubble regenerates again several times in a disintegrated form.

The length of the stationary cavity pulsates; hollow vortices, spinning in the direction from the center of the stream flow toward the wall, break

Fig. 34. High-speed photography of cavitation in a pipe with constriction. Bubble form. The cavity which disappears in frame 19 reappears in frames 20-23. Slotted pipe No. 3; width of minimum cross section 4.5 mm. (Photographed 8/23/47)

[99

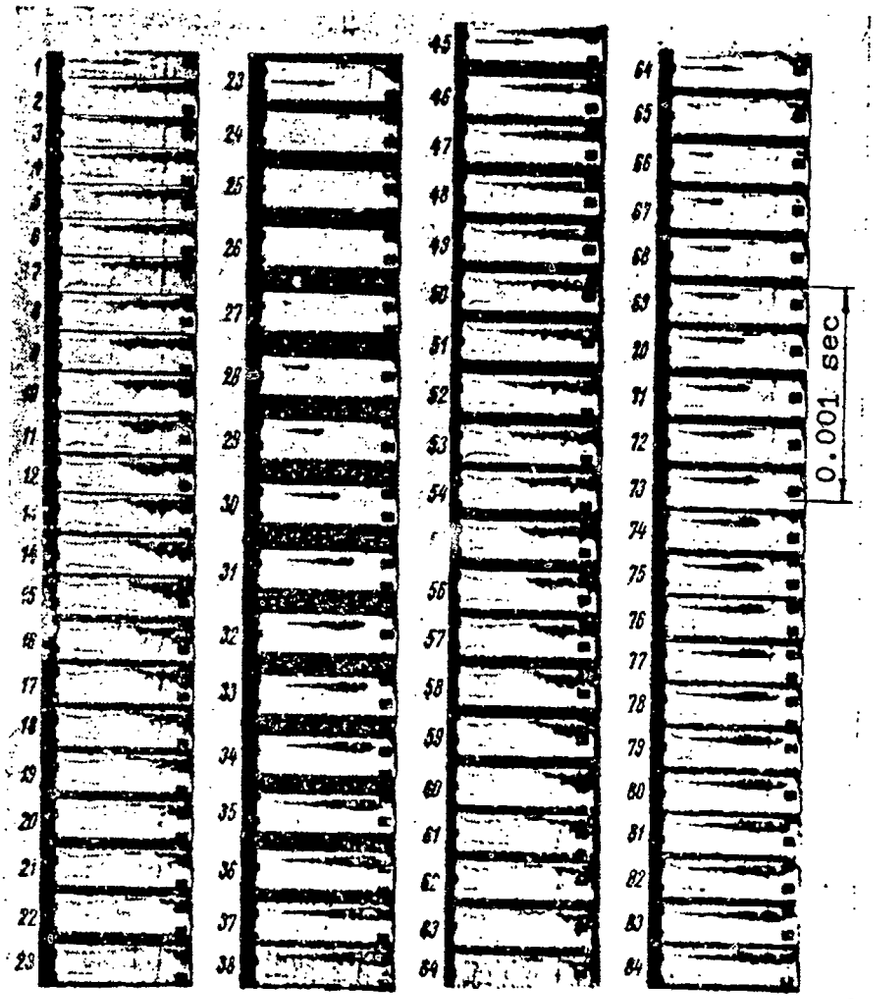

Fig. 35. High-speed photography of cavitation in a pipe with constriction. Boundary form (cavity attached to a body). Cycles of emergence (frames 27 and 65), development and carrying away of the cavity. Slotted pipe No. 3. (Photographed 5/20/47)

[100

off from the tip of the cavity and then are carried away by the stream. The presence of the large projection of surface roughness, notches, etc., greatly contributes to the emergence and preservation of attached cavities. After break-off and departure of the attached cavity, a small nucleus, measuring a few tenths of a millimeter, often remains behind such a projection, out of which a new cavity then develops. The presence of this nucleus probably explains the effect of hysteresis, first discovered in [50, p. 61], which should be absent with the bubble type

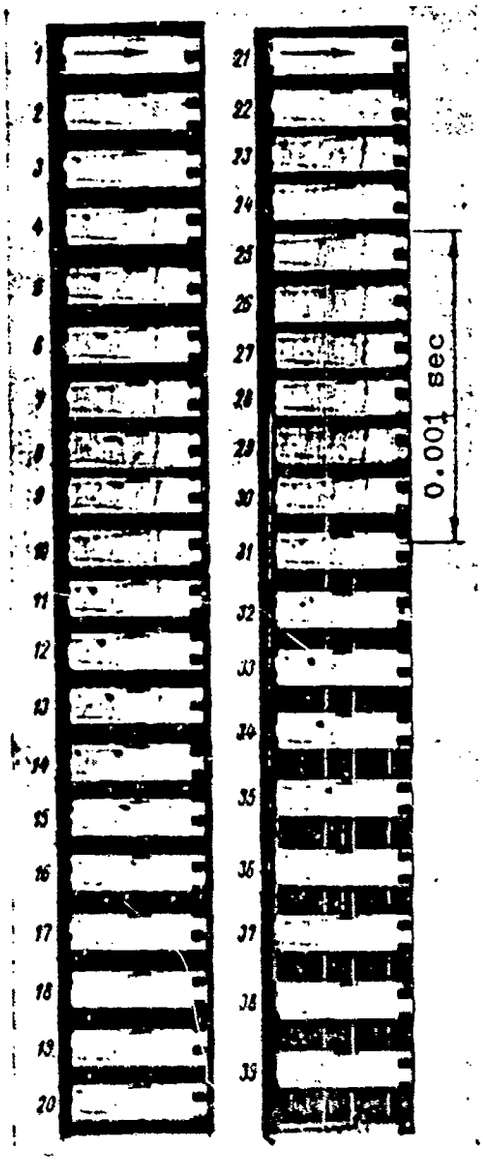

Fig. 36. High-speed photography of the initial stages of cavitation in a pipe with constriction. Illustration of the random nature of cavity formation. In frames 1, 2, 17-28, 36-39 the cavity is absent. Slotted pipe No. 3. (Photographed 8/12/47)

cavitation which emerges near the passing nuclei. The cited materials particularly prove the unfitness of the attempt by Hall and Wislisenus to explain the difference between the relationships in Figures 31-33 by the effect of the shape of a profile on the type of the cavity (bubble or attached). [101

Now we can return to the problem of the scale effect of emerging cavitation (bubble type) under the condition of pressure distribution independent from Re. First of all, let us formulate what type of conditions can be considered to be the beginning of cavitation. In light of the above discussion it is rational to give the following definition: by beginning of cavitation is understood such a condition under which the probability of the appearance of bubbles-cavities of a particular size has the prescribed value. The probability is determined by the ratio of time, for example, during which a certain small portion of the vacuum region is occupied by bubbles, to the time when it is free of them. Obviously, the size of the bubbles and the vacuum region must be proportional to the dimensions of the body. In correspondence with the number of passing bubbles, the cavitation region will appear more or less transparent, because the passing bubbles, refracting and reflecting light, disrupt transparency.

The degree of development of initial cavitation can be

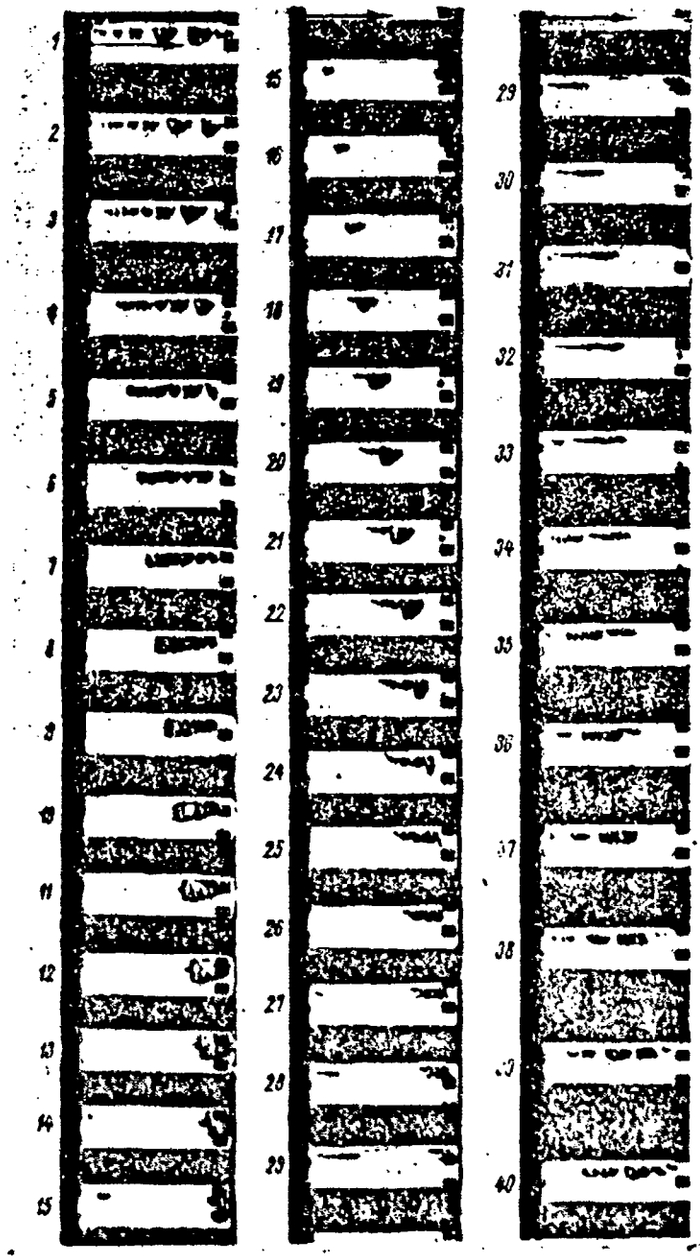

Fig. 37. High-speed photography of the developed cavitation condition in a pipe with constriction. In frames 1, 2, etc., one can observe a large number of emerging cavities within short intervals of time. In frame 27 one can see the emergence [figure and text cont. next page]

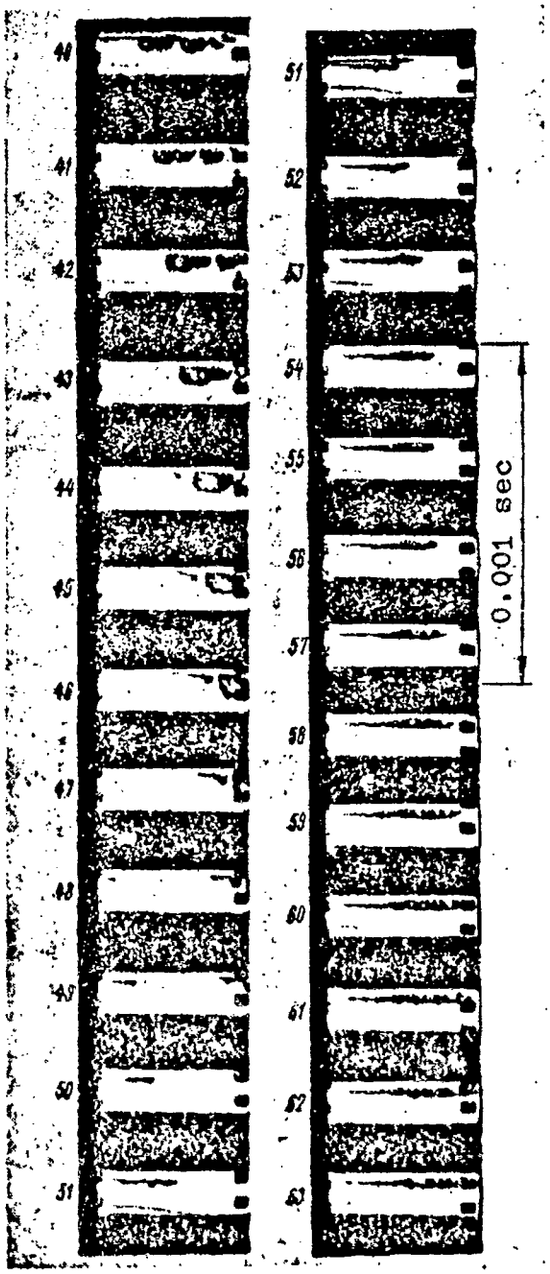

[Fig. 37 cont.] of the cavity attached to the wall; in frames 33 and on we can observe its destruction and carrying away. Frames 44 and 45 show the emergence of cavities in the boundary layer; frames 48-63 show the emergence and the growth of the cavity attached to the wall. (Photographs taken 8/11/47)

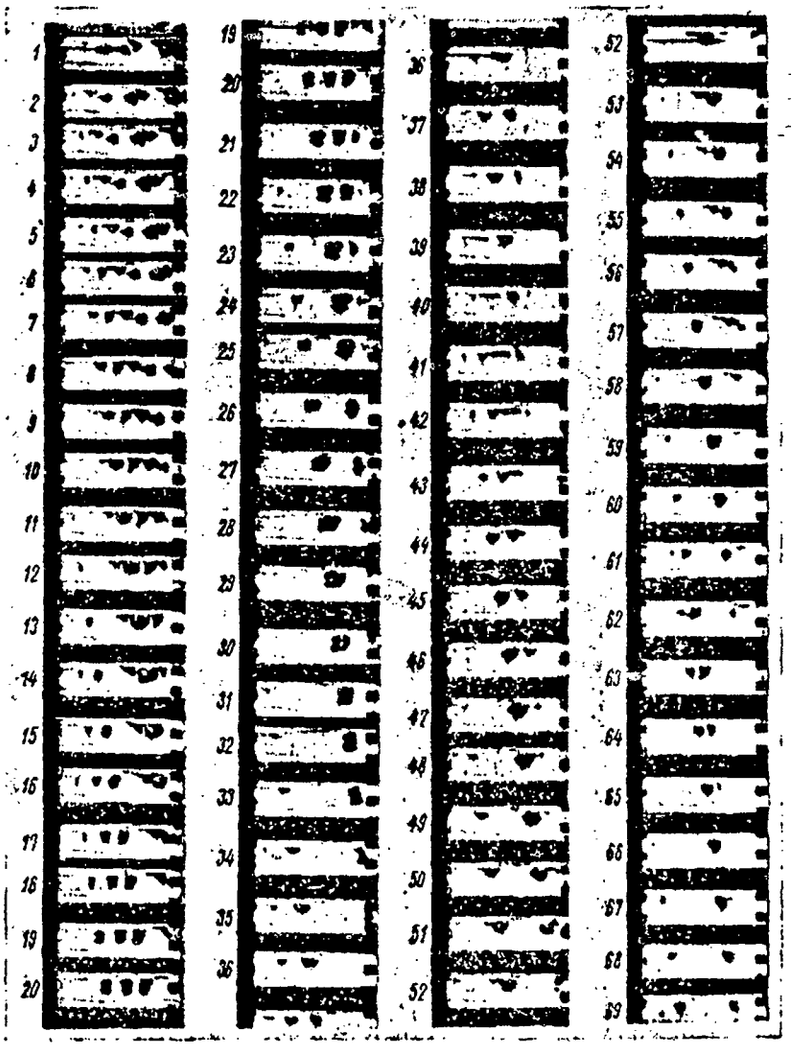

Fig. 38. High-speed photography of the developed cavitation condition for a time interval of ~ 0.03 sec. The figure illustrates spontaneous change in the shape of cavities, their expansion, displacement, destruction and re-emergence. Frames 95-102 show the effect of the boundary layer on the velocities of displacement of various parts of the cavity. Pipe No. 3. (Photographed 8/11/47)
[Figure continued on next page]

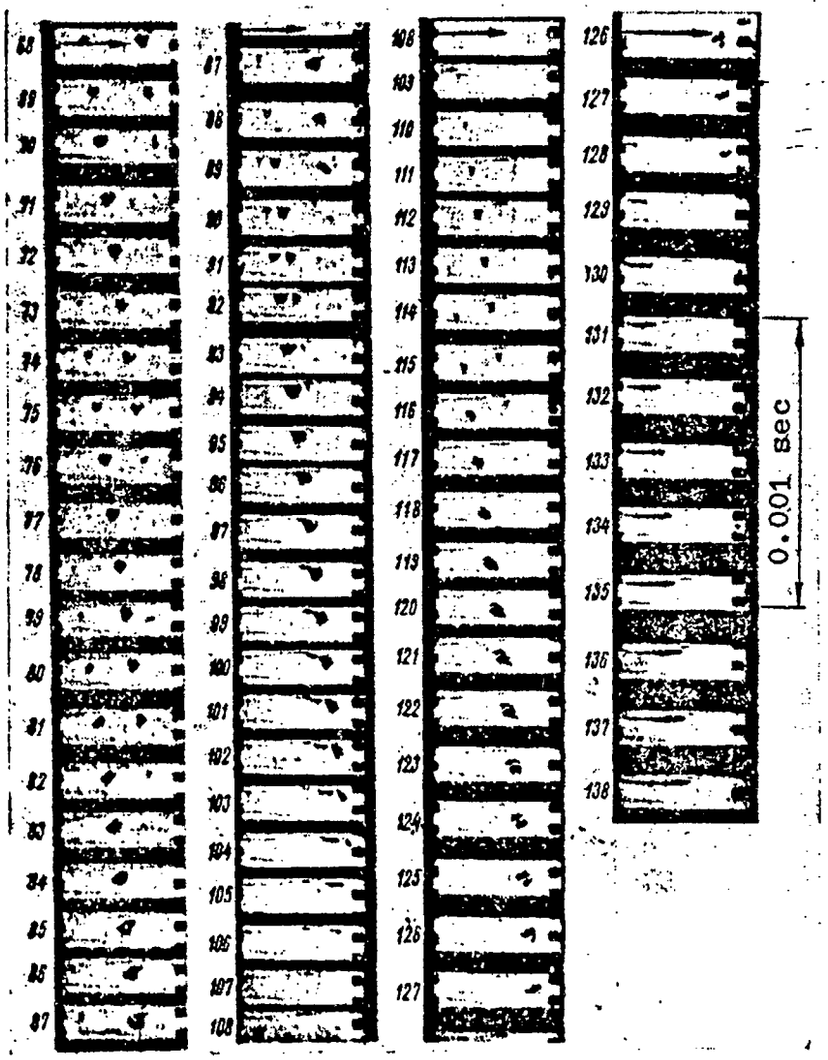

Fig. 38 (cont.)

defined either by statistical measurement of the number of bubbles on similar areas of the body surfaces, or with the aid of optical equipment which is capable of recording the degree of loss of transparency at these same areas. Let us note that the growth of bubbles for identical Δp [see formula (4.13)] does not in practice depend on their radius during the incipient stage, and therefore a difference between the relative dimensions of the nuclei for bodies of different scales will destroy similarity only through variations in the value of Δp. Let us now examine what will occur if the body, the cavitation number, the flow velocity, etc., remain constant while we alternately vary only

ν, only σ and only D.

Let us assume for all of the above cases that the medium that flows around the body retains its properties, gas content, number of particles, etc. Let us also assume that we are located in the region of Reynolds numbers where their effect on $\bar{p}$ can be ignored.

In the first case, with a decrease in viscosity the thickness of the boundary layer will also decrease, and hence the velocity at the same distance from the wall will increase. This increase in velocity leads to a decrease in the time during which the particle remains in the region of the vacuum and to a decrease in the amount (thus also in pressure) of dissolved gas separated into the bubble. Thus, a decrease in viscosity only hinders formation of cavities, especially under the condition when this depends primarily on the amount of gas dissolved in the fluid. Obviously, a qualitatively similar effect will be produced by a decrease in D. A decrease in σ, on the contrary, facilitates the growth of cavities. Taking formulas (4.5) into consideration, we can state that we have established the effect of parameters Re, We and $\bar{D}$, by their alternate change, on the growth of bubbles.

Let us now analyze the case in which the velocity of the flow varies, while the body in the stream, the fluid, and $\varkappa$ remain constant. This problem reduces to the previous problem because the increase in velocity is equivalent to a decrease in the values of ν, D and σ and, consequently, if cavitation bubbles grow primarily due to diffusion of dissolved gas, the size of the cavitation bubbles will decrease, i.e., the cavitation will move further away. If the amount of dissolved gases is small and the principle role is played by surface tension forces, then the intensity of bubble formation will increase, i.e., the cavitation will emerge earlier (with large values of $\varkappa$).

It is not difficult to see that a similar analysis will lead to a similar conclusion with respect to the influence of the linear dimensions of similar bodies on cavitation. Let us analyze one more form of cavitation, which in the literature is often called "cavitation developing in the stream behind a body in the stream." It is usually considered that this type of cavitation occurs in the fluid flow around blunt bodies such as discs, flat plates, circular cylinders, etc., positioned perpendicularly to the flow. In the opinion of most researchers, cavitation of this type occurs not on the wall surfaces, but in the nuclei of the vortices.

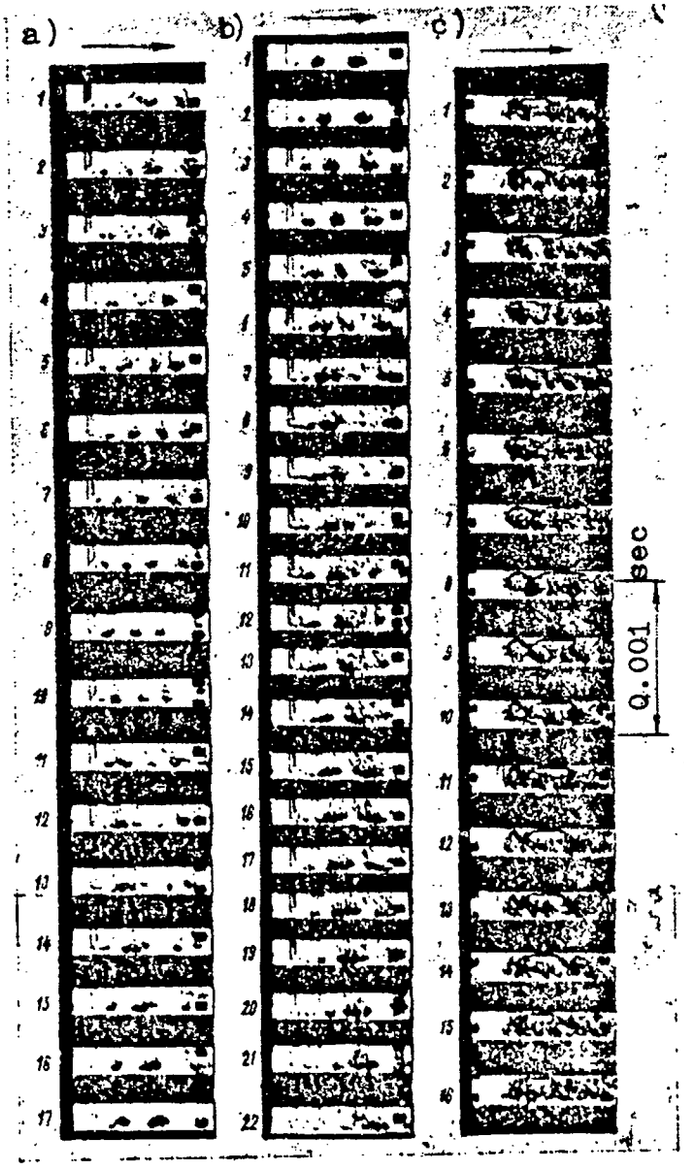

Fig. 39. High-speed photography of the three stages (a, b, c) of cavitation development behind a flat plate with a sharp edge, positioned perpendicularly to flow in a channel. In frame 1 the plate is darkened. A periodic vortex formation and carrying away of vortical cavities can be observed. The third stage precedes the formation of the common cavity. (Photographed 12/25/47)

In reality, as has been demonstrated by our analyses with high-speed photography, cavities in this case too often emerge on the body itself at the boundary between the free flow and the stagnation region. These cavities have the form of thin lines or layers which further turn into the relatively large cavities located inside the vortices' nuclei. The vortices with hollow nuclei are carried away by the stream, interact and pulsate (Fig. 39). As the cavitation number decreases, the dimensions of the cavities increase. This type of cavitation is caused by change in the pressures caused by viscous stresses. The

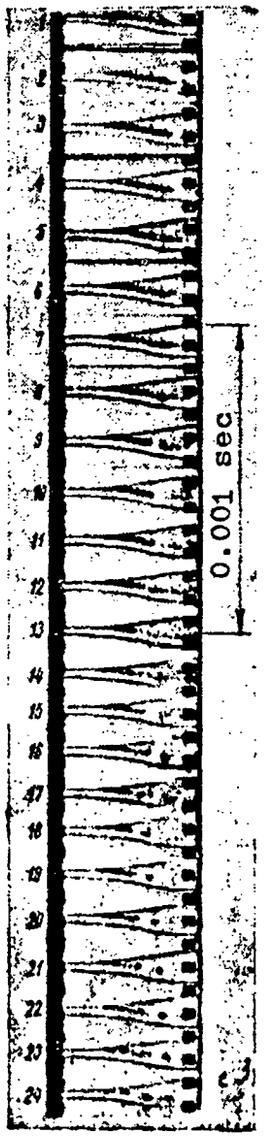

Fig. 40. Formation of cavitation during separation of the boundary layer in the diffuser region. High-speed photographs of cavitation in No. 4 slotted pipe. The width of the least cross section is 2.2 mm. (Photographed 8/25/47)

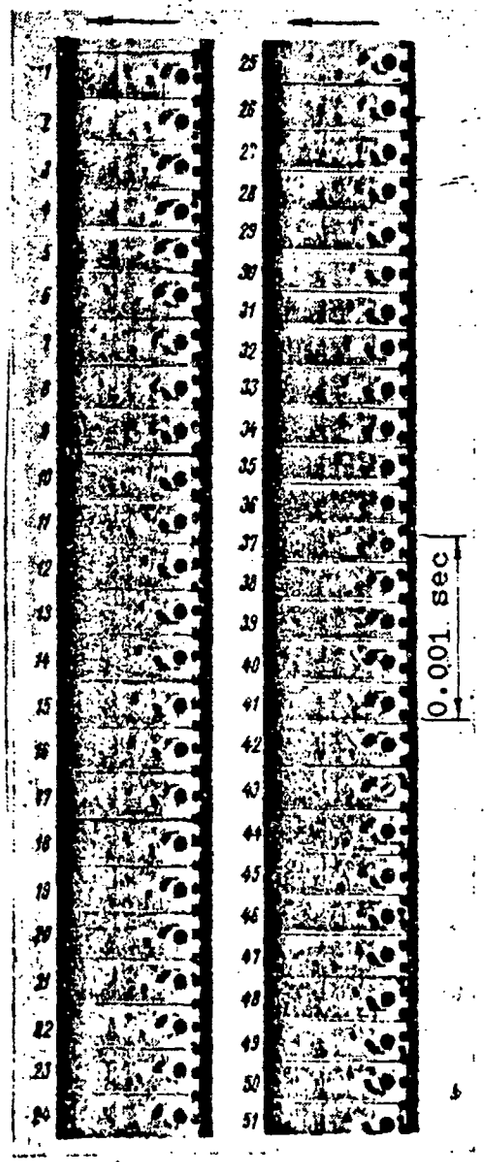

Fig. 41. High-speed photography showing cavitation near a circular cylinder. The emergence of cavitation in the boundary layer, the development, the break off, and the pulsations in the nuclei of vortices are seen. The cylinder is made of plexiglass and appears transparent in the photographs. The black circle is the opaque clamping part. (Photographed 3/25/48)

primary determining parameter is the Reynolds number. [108
Based on existing experimental data (see [39]), it can be considered that the cavitation number for discs that corresponds to its origination will be

$$\varkappa \approx 0{,}06\,\mathrm{Re}^{0.25}. \qquad (4.17)$$

Similar forms of cavitation are also found in the diffuser regions of the flow with separation of the boundary layer. Figure 40 shows high-speed photographs of cavitation in the diffuser, and Fig. 41 in the vortices near the cylinder.

The emergence of cavitation in the nuclei of filaments trailing off a foil of finite span will be studied in the next chapter.

4.2. Scale Effects with Developed Cavitation

By developed cavitational conditions is understood such types of flow around a body when a single cavity, bounded by the free stream and, as a rule, filled with gases or vapors, is formed behind the body. The limiting condition for this type of flow is flow with cavitation number $\varkappa$ of zero. Theoretically, the cavity which corresponds to [10
the values of $\varkappa = 0$ is a cavity that extends to infinity and is of infinite width. For small cavitation numbers the cavity size becomes finite; however, it exceeds by many times the size of the body forming this cavitation. Figure 42 shows a photograph of developed cavitational flow behind a disc.

It should be noted that the model of an ideal incompressible fluid has probably never before responded so correctly to reality, as in the case of developed cavitational flow. Specific qualities of the real fluid are reflected only at the end of the cavity, where the closing of the boundaries forming the cavity occurs and a region filled with foam appears. We were analyzing small cavita- [11
tion numbers, i.e., large cavities; this means that the region of the joining of streams occurs far beyond the body located in the stream flow and in practice does not reflect on the forces acting on the body and the character of fluid flow in front of the middle of the cavity. In this region neither the viscosity nor the surface tension play any significant role*, and therefore it would seem that the scale

*If small models with small stream velocities are not used.

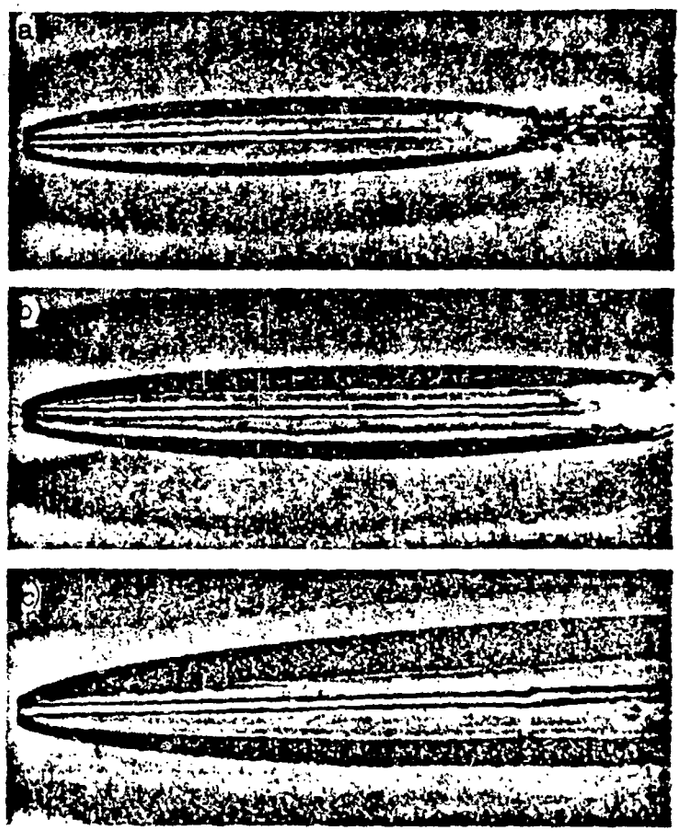

Fig. 42. Photographs of cavities behind a disc; a) $\varkappa = 0.065$; b) $\varkappa = 0.052$; c) $\varkappa = 0.025$.

effect in developed cavitation can be disregarded. However, we shall soon be convinced that such is not the case.

Under real conditions very high velocities correspond to low cavitation numbers. Thus, for example, if the pressure of an incoming flow is close to atmospheric and the pressure of the water vapors at normal temperatures can be ignored, then the value for the velocity which corresponds to the cavitation number $\varkappa = \frac{p_0 - p_d}{\frac{\rho v^2}{2}} = 0.1$ will be v = 45 m/sec, while with $\varkappa = 0.01$, velocity v = 140 m/sec.

As follows from Sect. 2.4, experiments with high velocities under natural conditions can be substituted by tests in the cavitation tunnel at low velocities with the

same cavitation number, which is provided by reducing the pressure p_0 of the incoming flow. However, with this type of simulation we encounter very extensive influence by the walls, since the cross section of the tunnel, which is rather large in comparison to the body producing the cavity, becomes comparable to the dimensions of the cavity, which at a decreased cavitation number, as has been mentioned before, can exceed the dimensions of the body by many times. Since in the vicinity of the real object the flow boundaries are virtually absent, a disruption of geometrical similarity takes place, which creates the scale effect.

In going to lower velocities, simulation with respect to cavitation number requires a simultaneous decrease in linear dimensions in order to preserve the same Froude number for the model and the prototype.

In analysis of the initial stage of cavitation we established that it is not necessary to observe similitude with respect to the Froude number, since for small bubbles-cavities, consideration of hydrostatic pressures results in negligible corrections. In the case of developed cavitations, when the cavities reach very large size, the influence of gravity forces cannot be ignored. Due to reasons that will be discussed below, it is not always possible to achieve similitude with respect to the Froude number. The difference between the Froude numbers for the model and the prototype also leads to demonstration of the scale effect. It has already been mentioned in Sect. 2.4 that similitude among the cavitational flows for the case of developed cavitation can be achieved if a cavity is formed artificially through the introduction of air or gas into the vacuum region at the surface of the body or beyond the body. The cavitation number for the general case will be as follows:

$$\sigma = \frac{p_0 - p_k}{\frac{\rho v_0^2}{2}}, \qquad (4.18)$$

where p_k is the pressure inside the cavity, while p_0, as usual, is the pressure of the incoming stream. Keeping in mind the previously mentioned need to take gravity into consideration, we will in the future designate by p_0 the pressure at the level of the body axis. Experiments in which small cavitation numbers are provided by feeding gas into the cavity [53, 55] can be performed not in cavitation tunnels, but in conventional experimental and circulation basins, troughs, or other installations. The basin

size is usually so big that the influence of the walls can be ignored for practical purposes. Nevertheless, even this type of experiment does not exclude the influence of the free surface, because it is necessary to fasten the towed body to a holder-blade, and then to feed gas along the hollow in this blade into the cavity and measure the pressures in it. The creation of very long blades and experimentation at relatively large depths causes definite difficulties due to which it is not always possible to eliminate the influence by the free surface on the characteristics being studied. This influence can also be relegated to the category of scale effects, i.e., the influence caused by deviations from similitude.

In analysis of bodies with developed cavitational flow, along with the action of flow forces on the body, it is of great practical interest to have information in regard to the shape and dimensions of the cavitation region, as well as on the amount of gas which has to be fed to maintain the required cavitation conditions. Scale effects linked to the carrying away of gases have their own specific characteristics based on the nature of cavity collapse and will be analyzed in the next section. In conclusion to these introductory remarks we can indicate that any further discussion will be basically connected with the flow around axially symmetrical bodies.

Analysis of cavitation as a two-dimensional problem is successfully and accurately performed by methods of the theory of streams [11]. Recently these methods were used to solve problems with consideration of gravity and capillarity [14, 17]. At the same time, there are no precise theoretical computations even for the simplest open-stream problems and in order to obtain the necessary information, especially with respect to the scale effect, the more rational approach is the one which incorporates the general mechanical considerations of the experiment and dimensional analysis theory.

On the basis of the presented material the conditions of the steady-state stream flow are determined by the linear dimensions which define the body in the stream and its position l, l_1, ..., l_n, by the difference in pressures p_0-p_k along the axis of the body and in the cavity, by the stream velocity, by density ρ, v [sic], and by the gravitational acceleration g, i.e.,

$$F(l, l_1, \ldots, l_n; p_0-p_n, v, \rho, g)=0$$

or in a dimensionless form

$$f\left(\frac{l_1}{l}, \ldots, \frac{l_n}{l}, \varkappa, \mathrm{Fr}\right) = 0. \qquad (4.19)$$

In this equation $\varkappa$ is determined by formula (4.18), while $\mathrm{Fr} = \frac{v}{\sqrt{gl}}$. All of the dimensionless characteristics of the flow or forces will be functions of the terms in the left part of the ratio (4.19). Specifically, for similar, similarly positioned bodies the drag coefficient and the typical cavity dimensions with respect to l or to each other will depend on $\varkappa$ and Fr only. Let us first analyze a simpler problem for the case of an infinite, weightless fluid when $\mathrm{Fr} \to \infty$ and only the term $\varkappa$ remains.

If the law of momentum is applied to the developed cavitational flow and the controlling surfaces are located far ahead of the body at the middle plane of the cavity, we can then determine that the relationship between the area of the middle plane of the body S (more precisely, the area at the middle of such a cross section around which the free streams flow) and the area at the middle plane of the cavity S_k depends, for a body of any shape, only on the drag coefficient* of the body C_x and on the cavitation number $\varkappa$ [55]. This dependence has the form

$$\frac{S_k}{S} = \frac{C_x(1+\varkappa)}{k\varkappa}. \qquad (4.20)$$

*The drag coefficient belongs to the same area at the middle plane of the body.

Here, the drag coefficient C_x for the cavitation number $\varkappa$ is expressed through the drag coefficient C_{x0} with $\varkappa = 0$ by the approximate relationship $C_x = C_{x_0}(1+\varkappa)$. This relationship is in close agreement with reality for bodies which are not very pointed. The value k which enters into formula (4.20) is some constant which is close to unity (by different evaluations k = 0.9-0.95). If a dependence on $\varkappa$ can be shown for the area of the middle plane, i.e., for the largest cross-sectional dimension of the cavity D_k, then for the length l_k there is no theoretical data even in the formula's structure. Experimental data with

respect to the axially symmetric bodies with diameter d [53] show that for a relative submergence y/d ~3 and Froude numbers in the range 5-20 (there are no data for Fr = ∞), the relationship $D_к/L_к$ can be expressed by the following approximation:

$$\frac{D_к}{L_к} \approx 0{,}6\sqrt{\varkappa(1+\varkappa)}. \qquad (4.21)$$

For small values of $\varkappa$

$$\frac{D_к}{L_к} \approx 0{,}6\sqrt{\varkappa}. \qquad (4.22)$$

If we assume that the structure of formula (4.21) can be used for a weightless, infinite fluid, then taking (4.20) into consideration we obtain [11

$$\frac{L_к}{d} = \text{const}\frac{\sqrt{C_{x_0}}}{\varkappa}. \qquad (4.23)$$

Expressions (4.20) and (4.23) define an interesting circumstance: for analysis of the principal dimensions of a cavity it is not necessary to produce a model of the body. Bodies having similar middle sections and drag coefficients will have approximately similar dimensions of the diameter and length of cavities.

The difficulties mentioned are even worse in the theoretical study of three-dimensional cavities, due to the necessity of considering additionally the influence of gravity and the nearness of the free surface. The experimental works in this field are rather limited, even though they do provide a number of separate facts. For example, it is known that with Fr ≠ ∞ the axis of the cavity warps and the cavity seems to float up, while its cross section becomes deformed. The first considerations and evaluations in regard to the floating up and the deformation problem were given by G. V. Logvinovich in 1953 [19]. Later on a number of considerations and experimental data in regard to this question were presented in [57, 58].

It should be noted that the derivation of rationally constructed formulas for the dependence of cavity dimensions on the values of $\varkappa$ and Fr, and on the relative submergence of the axis of the body y/d, becomes not only practically important, since real flows occur with Fr ≠ ∞, but also interesting from the theoretical point of view, because any comparison of theoretical flows to experimental

results without regard to gravity is possible only after extrapolations of experimental data from $Fr = Fr_1$ to $Fr = \infty$. Below we will present some views [65] in regard to the structure of formulas relating the basic cavity dimensions to the values of $\varkappa$ and Fr.

Let us analyze the mechanism of the flow around bodies with small cavitation numbers in an infinite, weightless fluid. In the flow approaching the body there develop substantial variations in pressure, from $\rho v^2/2$ at at the critical point to $p_k - p_0$ at points of stream separation. The fluid particles moving far ahead of the body along its axis receive, upon impact with the body, radial velocities directed from the center toward the periphery of the body, in other words, away from the region with pressure $p = p_k$ (cavity) toward the region far away from the body with the pressure $p = p_0$. The expanding portion of the cavity corresponds to this emerged motion. With radial displacement of fluid particles in the direction of the positive pressure gradient, work is produced due to their kinetic energy. When the radial velocities become equal to zero, the cavity dimension approaches its maximum (at the middle section). Furthermore, because the ambient pressure will exceed pressure in the cavity, a reverse process will occur. The cavity will begin to contract until it finally collapses. Obviously, with all conditions being equal (same shape and dimensions of the body, same velocity of its motion, same density of the medium, etc.) the trajectories of the particles will become steeper and the cavities smaller for bigger differences of $p_0 - p_k$. This is exactly what happens in reality: with increase in $p_0 - p_k$ for a given flow velocity v and density ρ, the cavitation number $\varkappa$ increases and the cavity becomes smaller. At the same time the region of the cavity near the body remains practically the same for all cavitation numbers (Fig. 43). The same result also follows from computations of two-dimensional cavitation flows and from experimental results. This is due to the fact that in the region before the cavity the pressure almost has no influence on the character of flow. [114

After these preliminary remarks we can proceed to the evaluation of the effect of gravity on the shape and size of the cavity. It is easy to see that the effect of gravity, i.e., the difference in hydrostatic pressure along the depth, practically will not be reflected on the region of flow in front of the body, and the small portions of

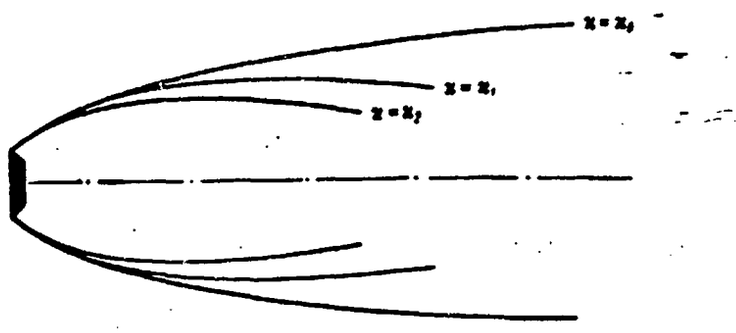

Fig. 43. Schematic diagram of changes in the shape of the cavity with variation in cavitation number.

the cavity near the body will be almost identical in weightless or weighable fluid. Actually, introducing

$$q = p + gy$$

instead of pressure p a new value q (the y axis is directed down), we can consider the fluid as weightless because the equations of its motion will be the same as for weightless fluid, namely

$$\frac{d\bar{v}}{dt} + \frac{1}{\rho}\operatorname{grad} q = 0.$$

The validity of such an approach fails only in the regions of free boundaries, where for real (weighable) fluid $p = \text{const}$ and $q \neq \text{const}$.

Thus, the initial regions of the cavity for real and weightless fluid differ very little; however, according to the above statements the lower boundary, located in layers with higher pressure than in weightless fluid, will deform more extensively, while the upper boundary, on the contrary, will deform less (Fig. 44). As a result the cavity emerges and its cross sections are deformed. The emergence of the cavity, in turn, leads to the relocation of all the points of its contour into the region of lesser submergence, and hence of smaller pressures, which means that any further deformation of the contour will take place under a lower gradient of pressures, the size of which proportional to (p_0-p_k).

The cavity regions located near the body virtually will not "emerge," and hence will not change; on the

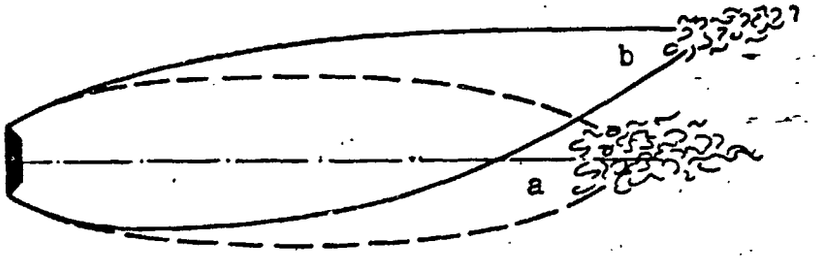

Fig. 44. Nature of cavity deformation under the influence of gravity: a) in an ideal weightless fluid; b) in real fluid.

contrary, the regions near the end of the cavity will be located in the region of substantially lower pressures and the cavity here will expand. It is natural to consider that the cavity will have the same dimensions as in weightless fluid with a cavitation number determined not by pressure p_0 on the axis of the leading body, but by the pressure of the incoming flow at the level of the middle portion of the cavity. This pressure will correspond to the average emergence (ascent) of the distorted axis of the cavity. In the first approximation the average ascent h_{cp} can be considered to be equal to half (or more precisely, to some fraction) of the ascent of the end portion of the cavity h_k. The corresponding cavitation number will be

$$\sigma_1 = \frac{(p_0 - \gamma h_{cp}) - p_k}{\frac{\rho v^2}{2}} = \sigma - \frac{\bar{h}_k}{Fr^2}. \qquad (4.24)$$

Here

$$\bar{h}_k = \frac{h_k}{d} \quad \text{and} \quad Fr = \frac{v}{\sqrt{gd}}.$$

The portion of the cavity below the middle plane will ascend approximately by the distance $h_{cp}/2$. That is why for the determination of the width of the cavity it is necessary to take the cavitation number in the form

$$\sigma_2 = \sigma - \frac{1}{2}\frac{\bar{h}_k}{Fr^2}. \qquad (4.25)$$

From the above discussion it follows that when the gravity is taken into account the middle plane is located not at the center of the length of the cavity, but closer to the body. The above discussion by itself does not provide the means to find the relationship between the dimensions of the cavity, the Froude numbers, and the cavitation

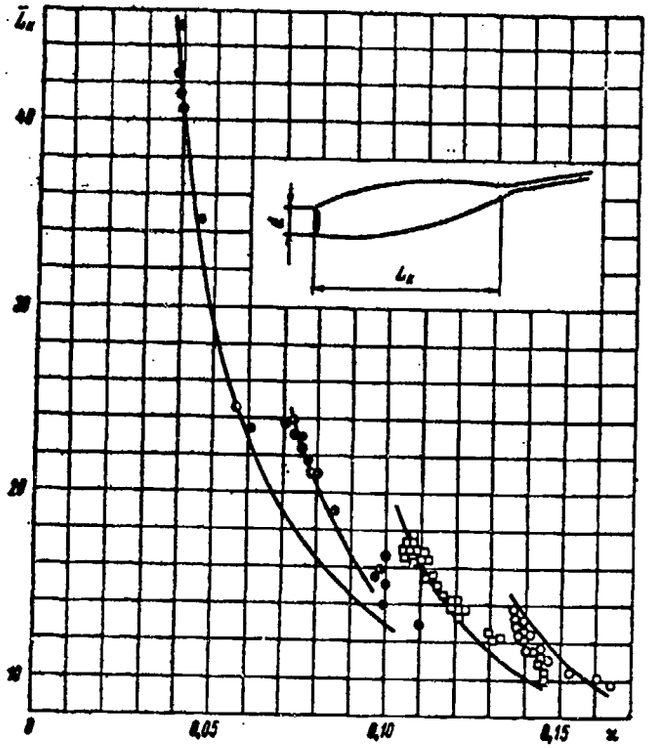

Fig. 45. Dependence of dimensionless length of the cavity $\bar{L}_к = \frac{L_к}{d}$ on the cavitation number $\varkappa$ with Fr = const.
● - Fr = 15.2; □ - Fr = 6.8; ○ - Fr = 5.7.

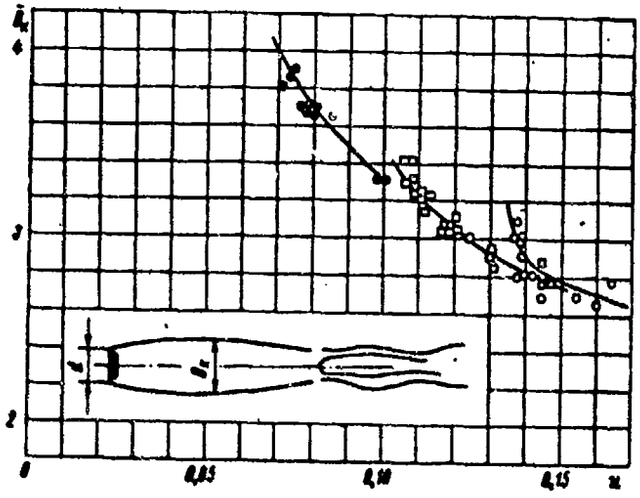

Fig. 46. Dependence of the dimensionless cavity width $\bar{B}_к = \frac{B_к}{d}$ on the cavitation number $\varkappa$ with Fr = = const.
● - Fr = 9;
□ - Fr = 6.8;
○ - Fr = 5.7.

numbers; however, it does make it possible to essentially generalize experimental results and give them a universal character. Let us demonstrate this with an example of processing experimental results [57]. In Figures 45-47 are shown dependences* obtained in this work $L_к/d$ =

*Here, instead of the diameter of the cavity $D_к$ its

width B_k is introduced, since the measurements were made from the photographs of the cavity plan, and in a real fluid B_k is somewhat different from D_k.

$= \bar{L}_k(\varkappa, Fr)$, $B_k/d = \bar{B}_k(\varkappa, Fr)$ and $h_k/d = \bar{h}_k(\varkappa, Fr)$ for the cavities formed behind the disc d = 20 mm submerged to a depth of $y = 4.25d$ ($\bar{y} = 4.25$).

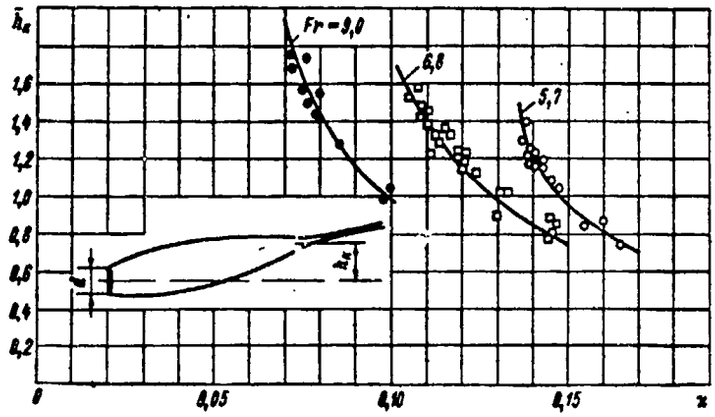

Fig. 47. Dependence of the dimensionless ascent of the end of the cavity $\bar{h}_k = h_k/d$ on the cavitation number $\varkappa$ with Fr = = const.
● - Fr = 9; □ - Fr = 6.8; o - Fr = 5.7.

Also plotted in Fig. 45 are the points for Fr = 15.2 from experimental results with $\bar{y} \approx 4$ in a rotating channel.

It is not by chance that these dependences represent portions of curves within small ranges of $\varkappa$ values. In a real, weighable, fluid, for every Froude number there exists its own limiting small value $\varkappa_{min}$. On the other hand, the range of variations of $\varkappa$ during the free* collapse of

---

*It is meant that the cavity does not collapse on the body or the holder for the disc forming the cavity.

---

the cavity is restricted by the conditions of existence of stable cavities. In Figures 48 and 49 the values $\bar{L}_k$ and $\bar{B}_k$ are plotted with respect to $\varkappa$ and $\varkappa_2$, respectively.

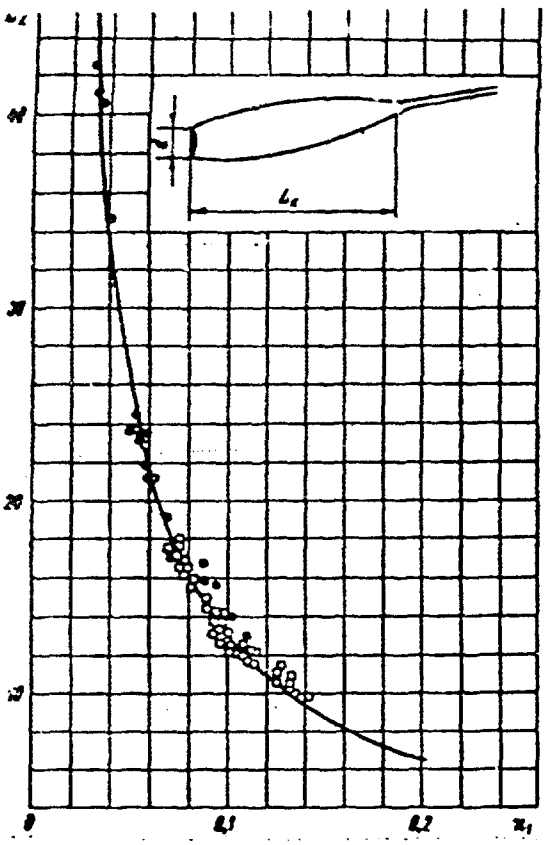

Fig. 48. Experimental data of Fig. 45 plotted on the basis of the generalized cavitation number $x_1 = x - \bar{h}_k/Fr^2$.

● - Fr = 15.2; ● - Fr = = 9; □ - Fr = 6.8; o - Fr = 5.7.

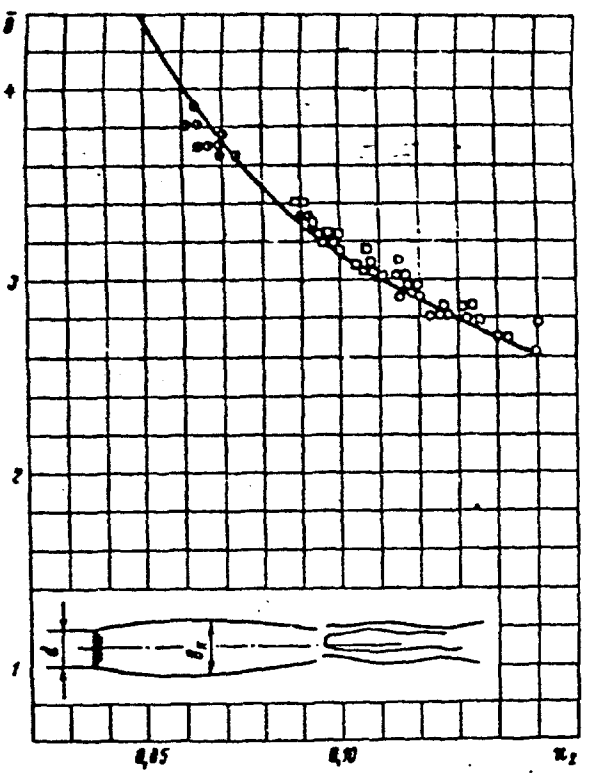

Fig. 49. Experimental data of Fig. 46 plotted on the basis of the generalized cavitation number $x_2 = x - 1/2\ \bar{h}_k/Fr^2$ (dots). The curve represents calculation from formula (4.27) with k = 0.9.

while the values $\bar{h}_k$ were taken from the graph in Fig. 47; for the curve $L_k(\varkappa)$ with Fr = 15.2 the $\bar{h}_k$ values were found with the formula from [58]

$$\bar{h}_k = 0{,}34\left(\frac{I}{Fr}\right)^3 - 0{,}016\left(\frac{I}{Fr}\right)^4. \qquad (4.26)$$

Figures 48 and 49 indicate that the utilization of the values $\varkappa_1$ and $\varkappa_2$ allows us to obtain a singular general dependence for $\bar{I}_k$ and $\bar{B}_k$ for various Froude numbers and with submergence of $\bar{y} = 4$. Since $\bar{h}_k \to 0$ when $Fr \to \infty$, the

values $\varkappa_1$ and $\varkappa_2$ become $\varkappa$ and the dependences in Figures 48 and 49 represent the dependences $\bar{L}_к(\varkappa)$ and $D_к(\varkappa)$ for a weightless fluid. Specifically, in Fig. 49 a theoretical curve has been plotted which was obtained by formula

$$\bar{D}_к = \sqrt{\frac{C_{x_0}(1+\varkappa)}{k\varkappa}}, \tag{4.27}$$

which was derived from formula (4.20). For computations $k = 0.9$ and $C_{x_0} = 0.82$ were assumed.

The dependence in Fig. 48 is approximated by the expression of the type (4.23)

$$\bar{L}_к = \frac{1{,}45\sqrt{C_{x_0}}}{\varkappa_1} \tag{4.28}$$

or by considering the expressions (4.24) for $\varkappa_1$ and (4.26) for $\bar{h}_к$

$$\frac{\bar{L}_к}{Fr} = \frac{1{,}45\sqrt{C_{x_0}}\,Fr}{\varkappa\,Fr^6 - 0{,}34\left(\frac{\bar{L}_к}{Fr}\right)^3 + 0{,}016\left(\frac{\bar{L}_к}{Fr}\right)^5}. \tag{4.29}$$

This equation of the fifth degree with respect to $\bar{L}_к$ can easily be solved with respect to $\varkappa$:

$$\varkappa = \frac{1{,}45\sqrt{C_{x_0}}\,Fr^6 + 0{,}34\bar{L}_к^3\,Fr^2 - 0{,}016\bar{L}_к^5}{\bar{L}_к\,Fr^6}. \tag{4.30}$$

From formula (4.30) we find the dependence $\bar{L}_к(\varkappa)$ for the given Fr value.

In [64] a verification was performed with regard to the validity of the formulas of the type (4.23) for bodies of various shapes, and specifically for a series of cones with apex angles from 30° to 180°. The results of these experiments with a constant relative submergence $\bar{y} = 5$ and $Fr = 12.7$, shown in Fig. 50, actually indicate that the points $\frac{\bar{L}_к}{\sqrt{C_{x_0}}}$ are grouped near the common curve; however, some corrections should be introduced here. As has been previously mentioned, in a weightless infinite fluid the diameter and length of a cavity relative to the diameter

[121

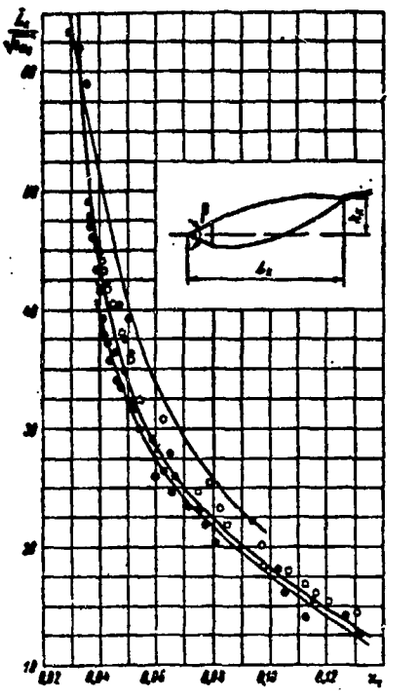

Fig. 50. Dependence of $L_к/\sqrt{C_{x_0}}$ on the generalized cavitation number $\varkappa_1=\varkappa-\bar{h}_к/Fr^2$ for a series of cones.
● - β = 180°; o - β = = 120°; ⊙ - β = 90°; □ - β = 60°; ⊕ - β = 30°.

of the body and $\sqrt{C_{x_0}}$ are functions only of the cavitation [119
number and do not depend on the shape of the body. Since the influence of gravity and the free surface are related [120
to cavity dimensions, and since the latter are determined by the value

$$d_1 = d\sqrt{C_{x_0}}, \qquad (4.31)$$

then it should be expected that the values $L_к/d_1$ and $D_к/d_1$, regardless of the body shape, will be functions of only one cavitation number with constant values of relative submergence and Froude number, calculated with respect to d_1, i.e., with constant $\frac{y}{d\sqrt{C_{x_0}}}$ and $\frac{v}{\sqrt{gd\sqrt{C_{x_0}}}}$.

In [64] the values y/d and $\frac{v}{\sqrt{gd}}$ were maintained constant, therefore the dependence $\frac{L_к}{\sqrt{C_{x_0}}}(\varkappa_1)$ turned out to be not identical for various angles of conicity, which has a major effect on the drag coefficient (Fig. 51). The relative closeness of the points of various cones (a noticeable difference in Fig. 50 can only be observed for β = 30° and

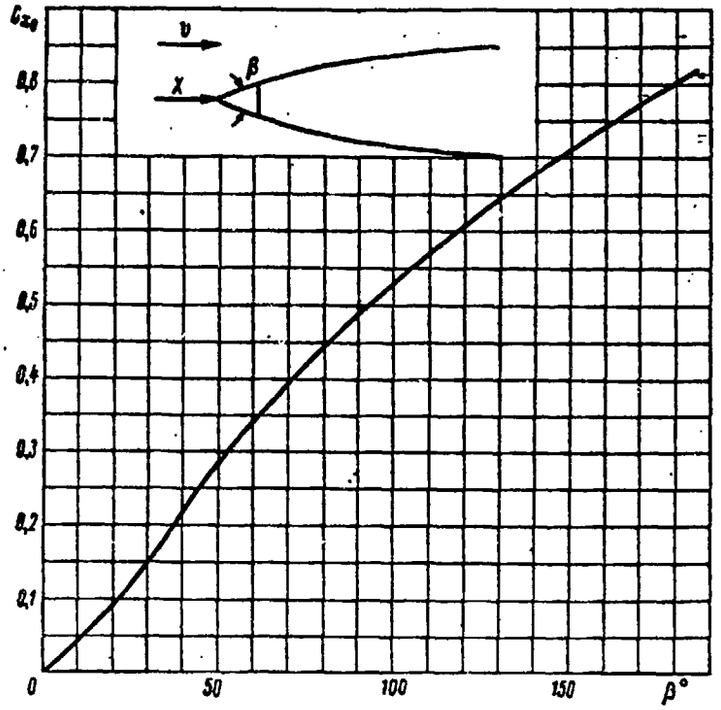

Fig. 51. Dependence of drag coefficient C for cones with zero cavitation number on the cone angle β.

β = 180°) is connected with the fact that the variation of C_{x_0} has the same effect on the values of y/d_1 and $\frac{v}{\sqrt{gd_1}}$, and their effect on $\frac{L_k}{\sqrt{C_{x_0}}}$ is the opposite: with an increase in y/d_1 the value $\frac{L_k}{\sqrt{C_{x_0}}}$ increases, and with an increase in $\frac{v}{\sqrt{gd_1}}$ it decreases.

Thus, if we adopt as a typical linear dimension the value $d_1 = d\sqrt{C_{x_0}}$ instead of the diameter d, and also introduce the cavitation numbers $\varkappa_1$ and $\varkappa_2$ from formulas (4.24) and (4.25), then for determining the dimensions of a cavity formed behind axially symmetrical bodies of various shapes, with different Froude numbers and different relative depths of submergence, the following equations will be valid:

$$\frac{L_k}{d_1} = f_1\left(\varkappa_1, \frac{y}{d_1}\right); \qquad (4.32)$$

$$\frac{B_K}{d_1} = f_2\left(x_3, \frac{y}{d_1}\right). \qquad (4.33)$$

If $Fr \to \infty$, the values $\varkappa_1$ and $\varkappa_2$ turn into $\varkappa$. The formulation of f_1 and f_2 using (4.32) and (4.33) requires, at the present time, additional experimentation to determine the effect of the free surface, i.e., the value y/d_1.

In conclusion let us discuss the effect of channel boundaries on developed cavitation flows in the vicinity of the bodies being tested. For solid parallel walls of the channel which confine two-dimensional and three-dimensional axially symmetrical flows near the bodies this problem has been analyzed in [4, 50, 68, 70] and others. The main conclusions and results with respect to the effect of solid walls in the case of an ideal fluid flow comes to the following.

There exists the minimum cavitation number $\varkappa_{min}$, which is determined by the formula

$$\varkappa_{min} = \frac{1}{\left(1 - \sqrt{C_{x_0}\frac{S}{S_0}}\right)^2} - 1 \approx 2\sqrt{C_{x_0}\frac{S}{S_0}}, \qquad (4.34)$$

where S is the area of the middle section of the body and S_0 is the area of the cross section of the channel. The approximate value $\varkappa_{min}$ corresponds to the small values of S/S_0.

The infinite cavity length and the area of its middle section, determined from the formula

$$S_K = \sqrt{C_{x_0} S S_0}, \qquad (4.35)$$

correspond to the minimum cavitation number.

For any cavitation number $\varkappa > \varkappa_{min}$ the area of the middle section of the cavity is determined by the following relationship:

$$S_K = \frac{1}{2}\left(C_{x_0}\bar{S} + \frac{\varkappa}{1+\varkappa}\right)\left[1 - \sqrt{1 - \frac{4C_{x_0}\bar{S}}{\left(C_{x_0}\bar{S} + \frac{\varkappa}{1+\varkappa}\right)^2}}\right], \qquad (4.36)$$

where a dash above the letter denotes that the corresponding value refers to the area of the cross section of the channel S_0.

For the same values of $\varkappa$ the area of the cavity's middle and its length in the channel will always be greater than the area of the middle and the length of a cavity in an infinite fluid. With small values of $\bar{S}$ in $\varkappa \to \varkappa_{min}$ the area of the cavity's middle in the channel will be two times bigger than in an infinite flow.

The drag coefficient for not very thin bodies C_x with $\varkappa \neq 0$ is related to C_{x_0} with $\varkappa = 0$ by the same relationship as for the infinite fluid flow,

$$C_x = C_{x_0}(1 + \varkappa);$$

this equation corresponds well with the real conditions for a wide range of $\varkappa$ values.

Due to viscosity the size of the cavity decreases because of the drag of fluid near the boundary layer.

The effect of the solid boundaries of the channel and the free stream for the case of two-dimensional flow has been analyzed on the basis of theoretical solutions in [11, 72] and others.

4.3. Carrying Away of Gas from the Cavity and Scale Effects Related to It

In the previous section the possibility of producing small cavitation numbers by feeding gas into the cavity was noted. For a number of applications it is of interest to know what quantity of gas should be supplied in a unit of time in order to provide the prescribed conditions. Obviously, for steady conditions the amount of gas supplied will be equal to the amount being carried away from the cavity. The mechanism of gas removal is related to the processes of closing of cavity boundaries at its end part. These processes, in turn, are determined primarily by the condition of boundary closing--whether it is free or some kind of bodies or devices are located in its vicinity. The material below will concern only the conditions of unobstructed, free closing of a cavity formed by axially symmetrical bodies. [12]

Observations indicate that there are basically two

Fig. 52. Photograph of the cavity behind a disc. Gas is being carried away by circular vortex filaments.

types of cavity closing. With large Froude numbers and large cavitation numbers, when the effect of gravity is almost negligible and the cavity shape approaches the axisymmetric, the end of the cavity is filled with foam which is periodically ejected in the form of circular vortices. A photograph of such a condition is shown in Fig. 52. Some descriptive elements and an analysis of such a condition were given in [59]. The fluid particles flowing around the body in radial planes collide in the region where the cavity closes. If this process were completely ordered, then in an ideal fluid the so-called Efrose's jet, directed into the cavity, would emerge.

In reality the collision of fluid particles occurs in the region occupied by the foam and is accompanied by inelastic impact with a loss of energy. The two-phase medium thereby formed partially fills the cavity and proceeds to move in it in the form of a toroidal vortex. The periphery of this vortex, under the influence of tangential stresses at the boundary of the cavity, shifts into the direction of the incoming flow, while the central part, under the action of the pressure gradient, moves in the opposite direction. The dimensions of the toroidal vortex increase due to the influx into it of the new, two-phase medium, flowing in similarly to the reversed jet that flows into the cavity in an idealized scheme.

As the vortex grows larger its area of contact with [124
the external flow increases, and therefore the frictional forces also increase. At the moment when the value of these forces becomes equal to the impact every second of the reversed jet, an ejection from the cavity of the two-phased vortex or part of it occurs and this process repeats again. The ejected vortex consists of the two-phase liquid, and therefore carries gas away from the cavity. Along with this pulsating ejection of foam, it is also removed

continuously at the expense of the area of foam located behind the critical point.

So far there is no theory for the described process--we will refer to it as the first form of gas removal--but from the above discussion it follows that an important role in this phenomenon is played by both frictional forces, as well as the surface tension forces which are determinant in the processes of bubble formation and fragmentation. With Froude numbers $Fr \to \infty$ the gravity can be disregarded and the dimensionless volume of gases that is being carried away in one second will be a function of the cavitation number $\varkappa = \frac{p_0 - p_k}{\frac{\rho v^2}{2}}$, the Reynolds number $Re = \frac{vd}{\nu}$ and the Weber number $We = \frac{\rho v^2 d}{\sigma}$, i.e.,

$$\bar{Q} = \frac{Q}{vd^2} = f(\varkappa, Re, We). \qquad (4.37)$$

Other characteristics of such a flow will also depend on the same values, such as average length $L_п/d$ of the region occupied by foam, etc.

The pulsating removal and the flow conditions associated with it have been studied very little. With ordinary techniques of experimentation these conditions are unstable (see [59]). The assumed character of the dependence $\bar{Q}(\varkappa)$ is shown in Fig. 53.

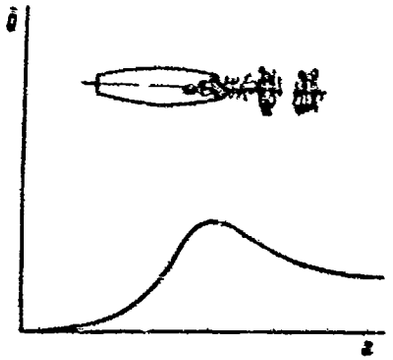

Fig. 53. Probable nature of the dependence of the coefficient of consumption $\bar{Q}$ on the cavitation number $\varkappa$ for the condition in which gas is carried away by circular vortices (weightless fluid).

According to studies by the author [60], conducted in experimental and rotating pools, an increase in the flow velocity with constant body dimensions and cavitation numbers*, i.e., simultaneous increase in the Re and We, leads

*For experiments in the pool the Froude number was

varied. In the rotating pool, the description of which was given in [66], the Froude number was held constant.

to enlargement of the part of the cavity occupied by foam*.

*This condition may be of great importance in simulation problems for cavitation flows. By decreasing the velocity while keeping the cavitation number constant, the effects relative to the action of the oncoming flow of foam in the cavity may be overlooked.

This is illustrated by Fig. 54.

In the general case, when $Fr \neq \infty$, the Froude number should be included into the terms of the right part of equation (4.37), because the gravity not only influences the shape of the cavity, but also leads to an irregular distribution of foam along the height. This can be clearly observed in Fig. 54.

The second form of the process of gas removal from the cavity has an absolutely different character. This takes place with small cavitation and Froude numbers, when the flow at the end of the cavity has become regulated and the cavity terminates in two hollow vortex filaments (Fig. 55) with circulation Γ, equal to the circulation around the diametral cross section of the cavity. As was shown for the first time by G. V. Logvinovich [18], this circulation can be expressed through the area of the diametral cross section S^* of the cavity by the formula

$$\Gamma = \frac{qS^*}{v}. \qquad (4.38)$$

The first attempts to formulate a theory for the process of gas removal along the vortex filaments were made by Cox and Clyden [74]. Although their work contains interesting concepts and conclusions, it is not correct, and therefore the obtained dependence of gas consumption on the Froude and cavitation numbers using their theory neither qualitatively nor quantitatively agrees with experimental results. The theory of gas removal by vortex filaments was given in [59]. The initial conditions and the results of this theory satisfactorily agree with experiments in [74] as well as with a number of other studies [16, 57, 73]. The essence of the process of gas removal is specified by the condition that the gas always fills up the tubes of the vortex filaments, which are formed in proportion to the

[125

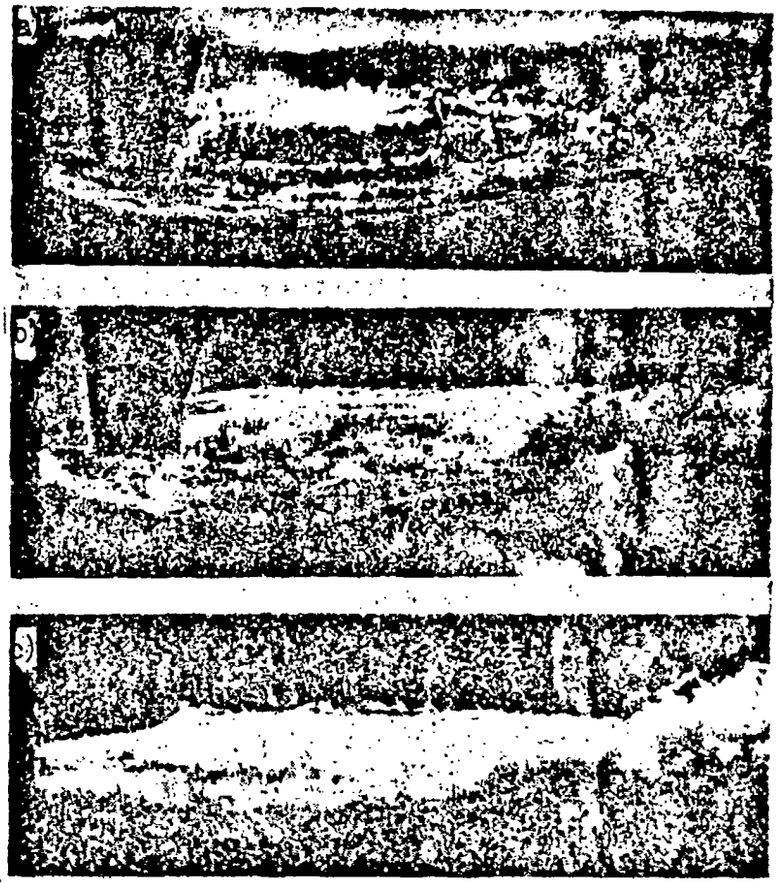

Fig. 54. Photographs of cavities for equal cavitation numbers $\varkappa = 0.1$ and Froude numbers $Fr = \frac{v}{\sqrt{jd}} = 12.8$ at the following velocities:

a) v = 10 m/sec; b) v = 20 m/sec; c) v = = 30 m/sec; j is the centrifugal acceleration. Increase in the velocity leads to the cavity filling up with foam. Experiments in a rotating channel [60].

forward motion of the cavity. Therefore, the amount of [127
volumetric gas consumption is equal to the cross-sectional area of the hollow vortex filaments multiplied by the velocity of the moving body. The mass consumption will be equal to the volumetric consumption multiplied by the density of the gas at a pressure equal to the pressure inside the cavity at the temperature of the fluid.*

*The vortex filament contains foam, drops, etc., i.e., the contact surface between the gas and the fluid is large and gas temperature approaches the temperature of the fluid.

[126

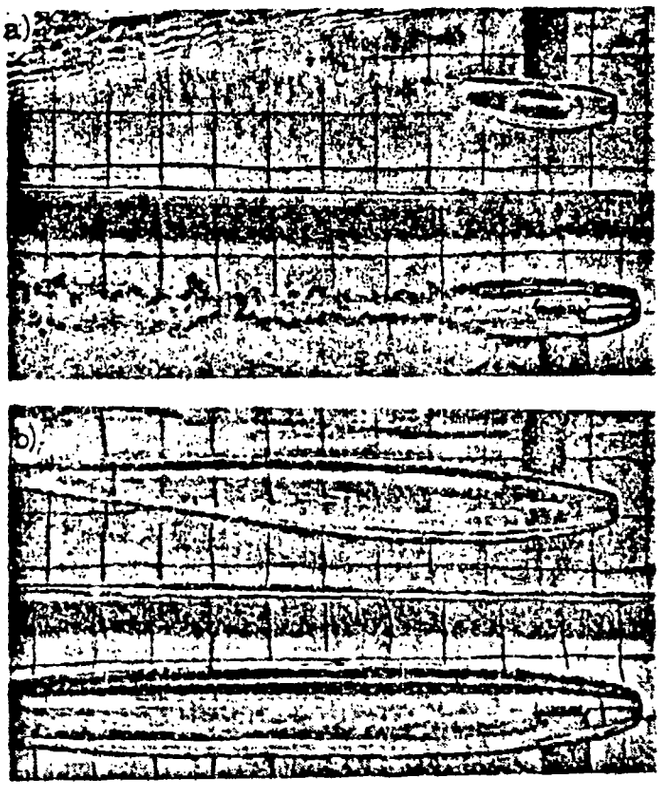

Fig. 55. Photographs of cavities formed behind a disc in two projections: a) $\varkappa \approx 0.15$; Fr = 6.8; b) $\varkappa = 0.072$, Fr = 9.

[127

Since circulation around the vortices is expressed according to (4.38) through the area of the diametral cross section of the cavity, all of the concepts and material related to determining cavity dimensions (Section 2 of this chapter) also concerns the problem of the removal of gas along the vortex filaments. Because of this the consumption coefficient, derived in the form of Q/vd_1^2, can be written as follows:

$$\frac{Q}{vd_1^2} = \frac{Q}{vd_1^2 C_{x_0}} = f\left(\varkappa; \frac{v}{\sqrt{gd_1}}; \frac{\nu}{d_1}; \frac{p_0 d_1}{\rho}\right). \qquad (4.39)$$

moreover, this relationship must be universal for axially symmetrical bodies of various shape. In contrast to the formulas (4.32) and (4.33), in this case we can not combine the effect of $\varkappa$ and Fr expressed by values of the type $\varkappa_1$ or $\varkappa_2$. This is because the values $\varkappa_1$ and $\varkappa_2$ also affect the diametral cross-sectional area; in addition, the hydrostatic pressure in the region of vortex filament formation, i.e., at the end of the cavity, also plays a certain role (see [59]).

The Weber number is also included in the parameters of (4.39) because for relatively thin vortex filaments the pressures which depend on surface tension forces can be significant and can decrease the cross sections of vortex tubes and hence decrease the amount of gas carried away. This is actually observed in reality: with small dimensions of bodies and small velocities, cavitation flows can exist even without gas removal. With values We > 1000 its influence may be ignored. At the present time a universal relationship in the form of (4.39) has not been developed. There only exists experimental data [57, 64, 73] concerning the coefficient of consumption for a disc in the form

$$\overline{Q} = \frac{Q}{\omega d^3} = f\left(\varkappa;\ \frac{v}{\sqrt{gd}};\ \frac{y}{d}\right) \qquad (4.40)$$

and analogous information with respect to cones with y/d = = 5 and y/d = 10 [64]. The typical character of dependences of the (4.40) form is shown in Figures 56 and 57.

It can be expected that the experimentally determined values of the coefficients of consumption represent the sum of the coefficients of consumption caused by both types [128
of gas removal. This is shown schematically in Fig. 58, from which it is seen that the dependence $\overline{Q}(\varkappa)$ with Fr = = const must have a minimum. Studies concerning gas removal processes are usually conducted with Fr < 20; the use of higher Froude numbers meets with a number of difficulties and demands either very high velocities of motion or very small bodies. Thus, in order to obtain Fr = 80 with velocity 10 m/sec the diameter of the body must be d = 1.6 mm. Analyses conducted in the range 20 < Fr < 80 [129
[67] showed that the coefficient of consumption corresponding to the value $\overline{Q}_{min}$ increases considerably with increase of Fr. This can be observed from the relationships $\overline{Q}(\varkappa)$ with Fr = const, shown in Fig. 59.

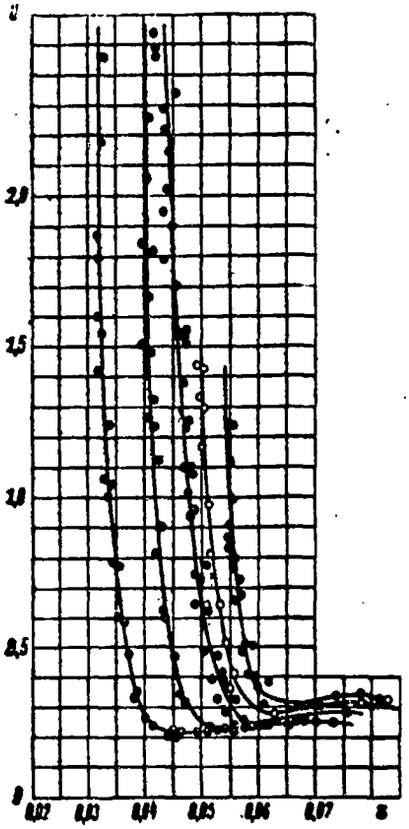

Fig. 56. Dependence of dimensionless consumption $\bar{Q} = \frac{Q}{vd^2}$ on the cavitation number $\varkappa$ for various relative submergences of a disc with Fr = 16.5. Tests conducted in a rotating channel. d = 3.5 mm; v = 30 m/sec; ● - $\bar{y} = \frac{y}{d} = 5$; ● - $\bar{y} = 10$; ● - $\bar{y} = 15$; ○ - $\bar{y} = 20$; ● - $\bar{y} = 26$.

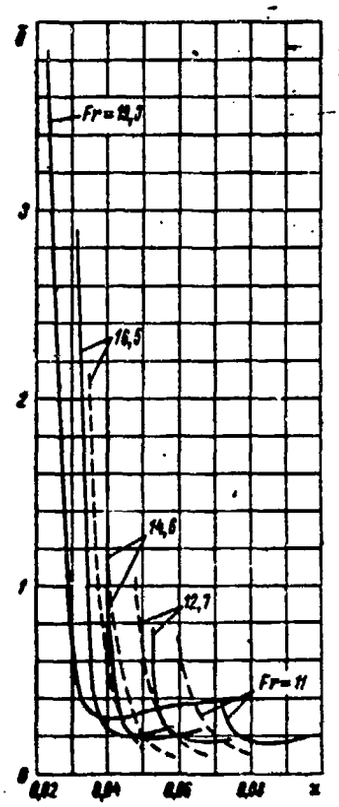

Fig. 57. Dependence of dimensionless consumption $\bar{Q} = \frac{Q}{vd^2}$ on the cavitation number $\varkappa$ for various Froude numbers with relative submergence of the disc $\bar{y} = 5$.

—— Tests in a rotating channel, v = = 30 m/sec;

---- tests in a test basin.

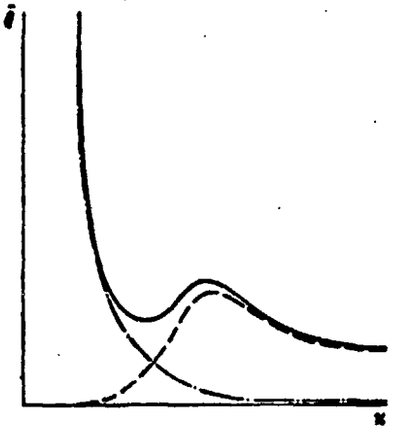

Fig. 58. Character of the dependence of the coefficient of consumption $\bar{Q}$ on the cavitation number $\varkappa$ with a constant Froude number, obtained experimentally.
---- component of gas removal by circular vortices;
-·-·-· component of gas removal by vortex filaments.

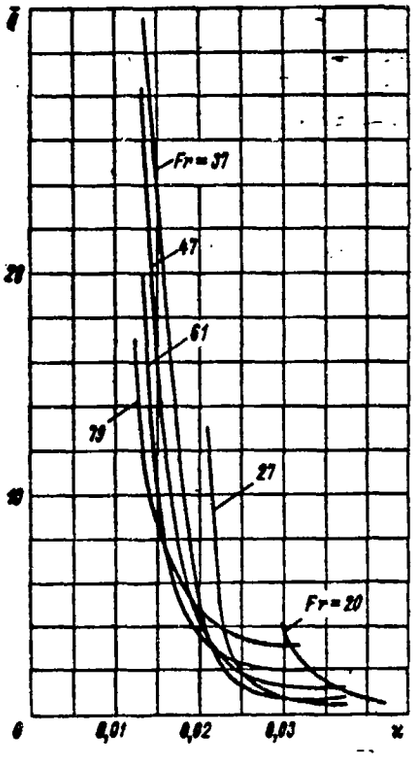

Fig. 59. Dependence of the coefficient of consumption $\bar{Q}$ on cavitation number $\varkappa$ for large Froude numbers.

CHAPTER V. APPLICATION OF DIMENSIONAL ANALYSIS THEORY TO PROBLEMS OF SUBMERGED HYDROFOIL MOTION

5.1. Special Features of Hydrofoil Performance Near the Free Surface

It is generally known that a change in the boundary conditions affects the flow around the body and therefore also affects the forces acting on the body. Specifically, the characteristics of a hydrofoil moving near a solid [130 baffle can be substantially different from the characteristics of the hydrofoil in an infinite fluid.

However, the influence of the free fluid surface, especially for small submergences, is combined with a number of particular additional phenomena, defined firstly by the specific features of the boundary, which deforms under the action of the pressure field produced by the hydrofoil, as well as under the effect of the wave processes related to gravity, and secondly by the entry of atmospheric air to the region of air rarefaction on the hydrofoil. The relative overlap and interweaving of these factors becomes additionally complicated in the region of high velocities when cavitational phenomena emerge.

If we analyze the hydrofoil moving near a free surface not as an isolated object, but as an element of a hydrofoil craft, it becomes necessary to consider also the presence of the supporting struts or the V-shaped tips of the hydrofoils intersecting the free surface, which very often serve as one of the channels for air passage to the surface of the hydrofoil.

The spread of hydrofoils along the length of a craft's hull makes it necessary to look not only into the effects of the enumerated factors on the performance of the hydrofoil itself, but also to study them even in those regions where this influence is absent. This, for example, pertains to deformation of the free surface or to determination of the position of the vortex filaments streaming off the hydrofoil. The deformed areas of the surface and vortex filaments (especially those filled with air) from the foil can have a substantial effect on the operation of the stern foil and the screw propellers. The formal application of the theory of dimensional analysis to the study of the above-mentioned phenomena does not produce effective results, and only slightly reduces the number of independent variables. Suppose we wish to determine the process of air entry toward the hydrofoil or the condition under which the cavity with the greatest depth behind the hydrofoil is

located at some specific distance behind it. The mathematic expression for the desired condition will have the form

$$F(l_1, \ldots, l_n, v, \nu, \sigma, \rho, g, p_0, p_d) = 0; \qquad (5.1)$$

where $l_1, \ldots, l_n$ - geometric dimensions defining the given distance, span l, chord b and other dimensions of the hydrofoil and struts, submergence h, angle of attack α, etc.;

ρ, ν, σ - correspondingly the density, kinematic coefficient of viscosity and surface tension coefficient, i.e., the parameters which determine the properties of the medium;

g - acceleration of gravitational force;

v - velocity of hydrofoil motion;

p_0 - pressure at the free surface;

p_d - pressure of the saturated vapors.

The use of dimensional analysis theory makes it possible to reduce the number of variables by three and reduce (5.1) to the form

$$f\left(\frac{l_2}{l_1}, \ldots, \frac{l_n}{l_1}; \frac{p_0 - p_d}{\frac{\rho v^2}{2}}; \frac{vl_1}{\nu}; \frac{\sigma}{\frac{\rho v^2}{2} l_1}; \frac{v}{\sqrt{gl_1}}\right) =$$

$$= f\left(\frac{l_2}{l_1}, \ldots, \frac{l_n}{l_1}, \varkappa, \mathrm{Re}, \mathrm{We}, \mathrm{Fr}\right). \qquad (5.2)$$ [1

Relationship (5.2) contains n + 3 terms (even in the simplest case of the flat plate n = 4) and not only does not allow us to draw any conclusions with respect to the question under consideration, but also does not provide any hope of devising a feasible experiment, because even if we restrict every parameter of the problem to the four values, it would still require a minimum of $4^7 \approx 16{,}000$ experiments for its evaluation.

In order to obtain the needed relation it is necessary to analyze the problem in more reduced, concrete form, and to apply, along with the theory of dimensional analysis, physical and mathematical considerations and evaluations, as well as experimental and theoretical information.

However, we would like to emphasize that these considerations and evaluations by themselves do not make it possible to solve the problem and are valid only when used together with the theory of dimensional analysis. We will

not discuss here in any great detail the known problems with respect to the forces exerted by the fluid on the hydrofoil. In contrast to the characteristics of a hydrofoil in an infinite fluid, the values C_y, C_x and C_M of a submerged hydrofoil will also depend on its relative submergence h/b and the Froude number $Fr_b = \frac{v}{\sqrt{gb}}$. For practically used regimes of $Fr_b > 5$ the effect of the Froude number on C_y, C_x and C_M is usually made negligibly small, but as will be shown below, for some other factors it is always significant.

5.2. Deformation of the Free Surface Behind the Hydrofoil

From experiments by the author [52, 63], V. T. Sokolov and others it has been established that behind a hydrofoil, moving near the free surface with a positive lifting force, there develops a cavity with a width approximately equal to the span of the hydrofoil. For small submergences of the hydrofoil the edges of this cavity form almost perpendicular walls. The bottom of the cavity is flat with a slight bulge in the diametral region. With an increase in submersion the steepness of the walls decreases and the bottom becomes trough-shaped. Farther from the hydrofoil the cavity becomes narrower and finally turns into a crest. The cavity formed behind a hydrofoil is shown schematically in Fig. 60, while in Fig. 61 a photograph of one of the cavities is illustrated.

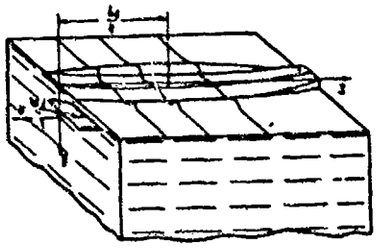

Fig. 60. Schematic presentation of free surface deformation above the hydrofoil.

The longitudinal, diametral cross section of the free surface behind the hydrofoil closely approaches a sinusoidal curve in the region of 1/4-1/3 of its wave length L_β. In this region the bottom can be considered to be flat in the first approximation. Thus, we will characterize the cavity by its diametral cross section, whose shape approximates a section of a sine curve with wave length L_β and amplitude y_0. Let us analyze how the wave length

[133

Fig. 61. Photograph of the cavity behind a hydrofoil. Needles for measuring the profile of the diametral cross section of the cavity are seen. Hydrofoil $\lambda = 2$.

depends on the parameters that define the medium, the conditions of motion, and the shape and position of the hydrofoil. Let us note first of all that in the given problem some properties of the medium can be eliminated from analysis, such as viscosity and surface tension. The unimportance of friction stresses in the wave processes is considered to be due to the low viscosity of water and the small velocity gradients along the normal to the stream lines. [132

Evaluating the order of the friction stresses τ for the orbital motion of particles with velocities $u = \omega r$, and considering that for the waves produced by the hydrofoil $\omega = \frac{g}{v}$, we have

$$\tau \sim \mu \frac{\partial u}{\partial r} \sim \mu\omega \sim \frac{\rho v g}{v}.$$

Comparing these stresses with the magnitude of hydrostatic pressures for the level variation of Δh, we find that

$$\frac{\rho v g}{v} \sim \rho g \Delta h,$$

from which, by relating everything to the chord of the hydrofoil, we find that the variation of wave ordinates because of viscosity is

$$\frac{\Delta h}{b} \sim \frac{v}{\omega b} = \frac{1}{Re}.$$

The unimportance of the surface tension is brought about by the relatively large wave length, which exceeds the chord of the hydrofoil by many times the range of Froude values of practical interest, and therefore exceeds the wave length of the capillary waves, which is 1.72 cm. Even in the cross-sectional areas of the cavity, for curvature radii of the fluid surface on the order of 1 cm the capillary forces can change the level by about 1 mm.*

---

*The performed evaluations indicate that the considerations discussed are valid not only for full-size hydrofoils, but also for small models with a chord of only a few centimeters.

Further, since we are interested in the region of flow far from the hydrofoil, the hydrofoil can be substituted by a Π-shaped vortex which is characterized by the circulation value Γ, span l and submergence depth h. Taking the above comments into account, we can write

$$L_0 = F(h, l, \Gamma, v, g). \tag{5.3}$$

The quantity Γ determines the amplitude of the wave, and within the linear formulation of the problem should have no effect on the length (see Sect. 2.1). The same statement can be made with respect to the submergence depth of the vortex. In Fig. 62 experimental results [63] are presented which confirm the condition of independence of [134
the wavelength from the circulation (coefficient of the lifting force) and the submergence. Thus, we have

$$L_0 = F(l, v, g). \tag{5.4}$$

Designating l and g as units of measurement we find

$$\frac{L_0}{l} = f_1\left(\frac{v}{\sqrt{gl}}\right) \tag{5.5}$$

or, returning from the vortex to the hydrofoil and introducing its chord b and the span-chord ratio λ, we obtain

$$\frac{L_0}{\lambda} = f\left(\frac{Fr_b}{\sqrt{\lambda}}\right). \tag{5.6}$$

[133

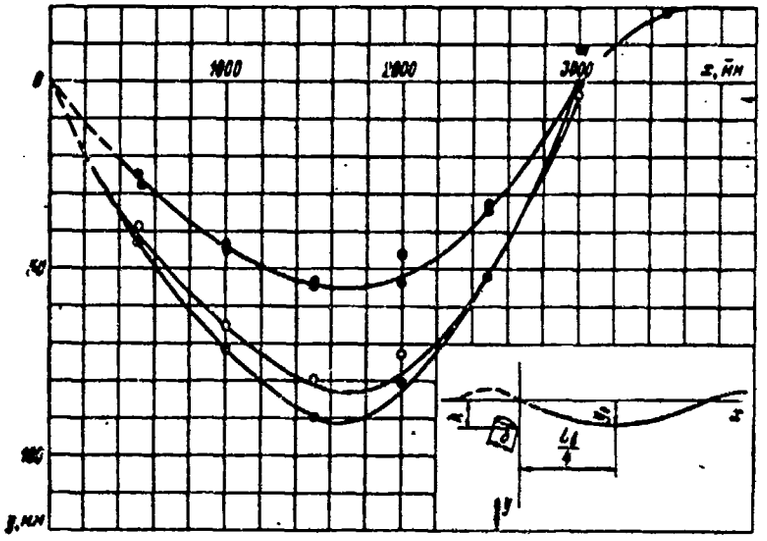

Fig. 62. Test results confirming the independence of the length of the wave cavity behind the hydrofoil from its submergence h and angle of attack α.
b = 200 mm; λ = 4; v = 6 m/sec; ● - α = = 0, $\bar{h} = \frac{h}{b} = 0.7$; o - α = 3°, $\bar{h} = 0.2$; ● - α = 3°, $\bar{h} = 0.7$.

[134

Here $\bar{L}_0 = \frac{L}{b}$ and $Fr_b = \frac{v}{\sqrt{gb}}$.

Thus, we can conclude that for all profiles, span-chord ratios and Froude numbers there must exist a universal dependence (5.6). In the event of a two-dimensional problem, i.e., with $\lambda = \infty$. we have for the length of the wave located far behind the hydrofoil the known formula

$$L_0 = \frac{2\pi v^2}{g}.$$

Dividing both parts of this equation by b and λ we obtain for this particular case the following form of the right part of function (5.6):

$$\frac{\bar{L}_0}{\lambda} = 2\pi \left(\frac{Fr_b}{\sqrt{\lambda}}\right)^2. \qquad (5.7)$$

In order to find the universal dependence (5.6) with $\lambda \neq \infty$ it is sufficient to conduct experiments with one arbitrary hydrofoil with any small value of submergence and

Note to final editor =

See the legend to Fig. 63.

Is it really "$0 - \lambda = -2$?

minus ?

Is that a minus sign or a typo - perhaps a second equals sign. I don't remember seeing any other negative λ numbers in this text. Dick Baker

angle of attack, and with several values of Froude number.

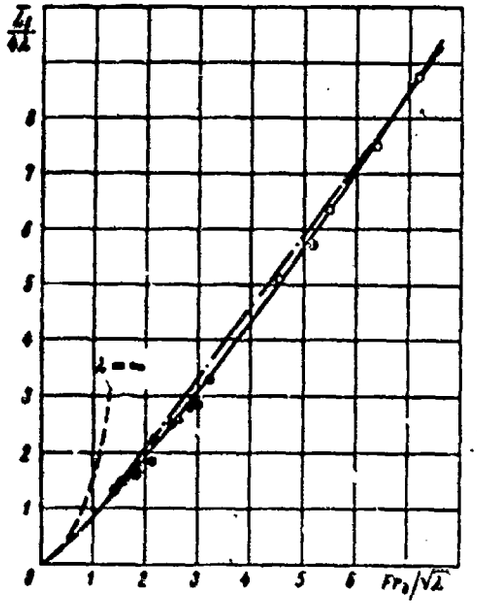

[135

Fig. 63. Graph showing the plot of the dependence of $\frac{\overline{L}_a}{4\lambda}$ on the ratio $\frac{Fr_b}{\sqrt{\lambda}}=\frac{v}{\sqrt{gl}}$. o - $\lambda = -2$; ● - $\lambda = 4$; ● - $\lambda = 6.5$; ø - $\lambda = 8$; Δ - $\lambda = 10$. ---- theoretical calculation for $\lambda = \infty$; -·-·-·- approximated linear dependence.

In Fig. 63 the curve of $\frac{\overline{L}_a}{4\lambda}\left(\frac{Fr_b}{\sqrt{\lambda}}\right)$ is shown, which was [134
plotted using the experimental data obtained by Sokolov and [63]. In the region $\frac{Fr_b}{\sqrt{\lambda}}\to 0$ the dependence $\frac{\overline{L}_a}{\lambda}$ has been drawn in accordance with formula (5.7) and is represented in Fig. 63 by the dotted line. In the range of $1<\frac{Fr_b}{\sqrt{\lambda}}<8$ the universal graph can be approximated by the linear relationship (dash-dot curve)

$$\frac{\overline{L}_a}{4\lambda}=1{,}25\frac{Fr_b}{\sqrt{\lambda}}-0{,}5. \qquad (5.8)$$

from which the abscissa of the cavity will be determined [135
by the formula

$$\frac{l_a}{4}=1{,}25\,Fr_b\sqrt{\lambda}-0{,}5\lambda. \qquad (5.9)$$

The maximum depth of the cavity y_0 depends on the same values as the wave length in formula (5.3). Selecting l and v as the units of measurement we obtain

$$\frac{y_0}{l} = f\left(\frac{h}{l}, \frac{\Gamma}{vl}, \frac{gl}{v^2}\right). \qquad (5.10)$$

If the boundary conditions on the free surface are linearized, then, taking into consideration the linear character of the Laplace equation and concepts discussed in [62], it can be affirmed that the amplitude of deformation of the free surface will be proportional to the disturbances that cause these deformations. In the case under discussion the intensity of the disturbances is determined by the circulation value, and therefore, replacing gl/v^2 with the value $Fr_l = \frac{v}{\sqrt{gl}}$, instead of (5.10) we can write

$$\frac{y_0}{l} = \frac{\Gamma}{vl} f\left(\frac{h}{l}, Fr_l\right). \qquad (5.11)$$

Expanding the function f in powers of the small value of h/l (submergences of the hydrofoil are considered within the limits of its chord and the span-chord ratio $\lambda > 2$), we have

$$\frac{y_0}{l} = \frac{\Gamma}{vl}\left[a_0'(Fr_l) + \frac{h}{l} a_1'(Fr_l) + \ldots\right]. \qquad (5.12)$$

Since with small submergences, right up to the point of planing, or with large span-chord ratios, deformation of the free surface does exist, then $a_0' \neq 0$ and represents in this region the main term of the expansion. We will limit ourselves in the future to two terms of expansion. Relating the circulation value to the lifting force coefficient of the hydrofoil and its chord by the known formula* [1

*In [63] it is shown that in practice it is also retained near the free surface.

$$\Gamma = \frac{C_y b v}{2},$$

we obtain instead of (5.12)

$$\frac{\bar{y}_0}{C_y} = a_0\left(\frac{Fr_b}{\sqrt{\lambda}}\right) + \frac{\bar{h}}{\lambda} a_1\left(\frac{Fr_b}{\sqrt{\lambda}}\right). \qquad (5.13)$$

From the above it follows that in order to find the dependence of the depth of the cavity on the values of C_y,

Fr_b, λ and $\bar{h}$ for a hydrofoil of any profile it is sufficient to test one hydrofoil of any type for one angle of attack, several velocities, and two different submergences, and then by plotting the curves $\frac{\bar{y}_0}{C_y}=f\left(\frac{Fr_b}{\sqrt{\lambda}}\right)$ with $\bar{h}=\bar{h}_1$ and $\bar{h}=\bar{h}_2$ to find a_0 and a_1. Let us note that in the event $\frac{Fr_b}{\sqrt{\lambda}}=0$ (for finite Froude numbers this corresponds to an infinite span), the values $\bar{y}_0/C_y$ with $\bar{h}$ = const depend on the Froude number. According to the theoretical solution by M. V. Keldysh and M. A. Lavrent'yev [12], for the vortex we have

$$\frac{\bar{y}_0}{C_y}=e^{-\frac{\bar{h}}{Fr^2}}. \tag{5.14}$$

In practice, for Fr > 4 and $\bar{h}$ < 1 this value differs little from unity.

In Fig. 64 experimental points $\frac{\bar{y}_0}{C_y}\left(\frac{Fr_b}{\sqrt{\lambda}}\right)$ have been plotted, based on the experiment presented in [63]; in the same work a_0 and a_1 were determined from these curves:

$$a_0=0{,}5\frac{Fr_b}{\sqrt{\lambda}}+0{,}65; \tag{5.15}$$
$$a_1=-3.$$

The calculated dependences based on formula (5.13) and the given values of a_0 and a_1 are represented by the curves in this graph. The dotted curves indicate the assumed approach of the curves in the region of small $\frac{Fr_b}{\sqrt{\lambda}}$ to to the theoretical value of (5.14). The satisfactory agreement between experiments and calculations indicates that the formulas presented above may be used in the range of $1<\frac{Fr_b}{\sqrt{\lambda}}<3$, which ordinarily encompasses the entire range of Froude numbers and span-chord ratios that are of practical [137 interest. If the wave amplitude and length are known at the diametral cross section of the cavity behind the hydrofoil, we can write the equation for the corresponding profile as follows:

$$\frac{\bar{y}}{C_y}=\left(0{,}5\frac{Fr_b}{\sqrt{\lambda}}+0{,}65-3\frac{\bar{h}}{\lambda}\right)\sin\frac{2\pi\bar{x}}{5Fr\sqrt{\bar{x}-2}}. \tag{5.16}$$

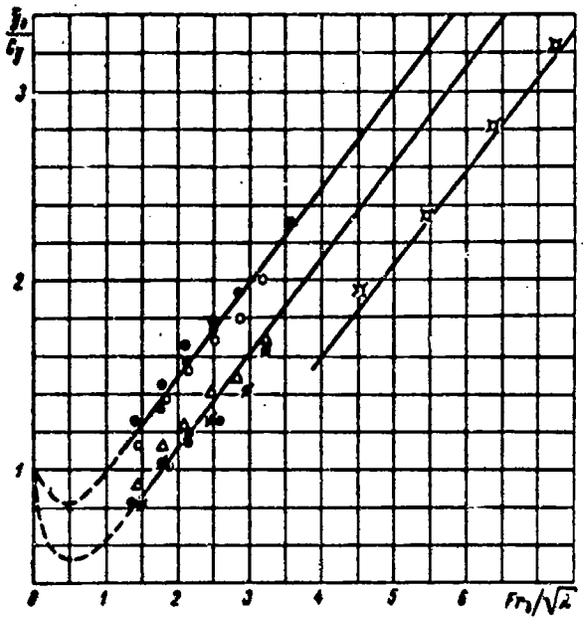

Fig. 64. Dependence of $\frac{\bar{y}_0}{C_y}$ on the relationship $\frac{Fr_b}{\sqrt{\lambda}} = \frac{v}{\sqrt{gl}}$. The dotted curve shows the assumed direction of the curves toward a point which corresponds to the solution of a two dimensional problem.
Hydrofoil $\lambda=4$: ●●○○ – $\bar{h}=0.2$; △⊖ ● – $\bar{h}=0.7$; ⊖ – $\alpha=1°$; ● – $\alpha=0°$; ○⊖ – $\alpha=3°$; ○● – $\alpha=6°$.
Hydrofoil $\lambda=2$: ⊡ – $\alpha=10°$; $\bar{h}=0.7$.

The maximum slope angle is

$$\alpha_{i_{max}} = 2\pi \frac{0.5\frac{Fr_b}{\sqrt{\lambda}} + 0.65 - 3\frac{\bar{h}}{\lambda}}{5\,Fr_b\sqrt{\lambda} - 2} C_y; \qquad (5.17)$$

with an increase in Fr_b it approaches the constant value

$$(\alpha_{i_{max}})_{Fr_b=\infty} = 0.2\pi\frac{C_y}{\lambda} \approx 2\frac{C_y}{a\lambda}. \qquad (5.18)$$

5.3. Cavitation in the Vortex Filaments Trailing the Finite-Span Hydrofoil [13

For a very long time the problem of determining the flow velocity at which cavitation on the hydrofoil begins

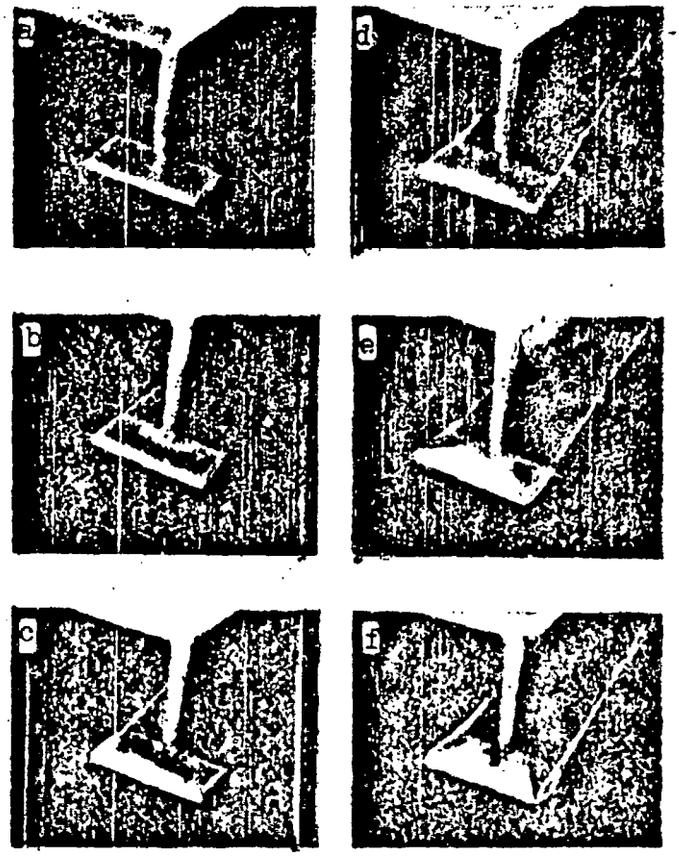

Fig. 65. Photograph of cavitation in vortex filaments trailing a hydrofoil of finite span during testing in a test basin: a) v = 7.5 m/sec; b) v = 8.9 m/sec; c) v = 9.0 m/sec; d) v = 10 m/sec; e) v = 11 m/sec; f) v = 12 m/sec. Hydrofoil with chord b = 60 mm, $\lambda = 2$, $\alpha = 18^{\circ}$.

was considered to be solvable provided the distribution of pressure along the corresponding profile at the given submergence is known. The critical cavitation number $\varkappa_{kp}$ was equated to the minimum value of the pressure coefficient with an opposite sign

$$\varkappa_{kp} = -\bar{p}_{min},$$

and v_{kp} at which the cavitation begins was found from the determination of $\varkappa = \frac{p_\infty - p_d}{\frac{\rho v^2}{2}}$ with known $p_\infty = p_a + \gamma h$ (p_a = [139

= atmospheric pressure) and p_d.

This approach for determining the velocity v_{kp} was based on the inconclusive assumption that cavitation is generated at the middle part of the hydrofoil, where experiments in which the pressure distribution is measured usually indicate the greatest rarefaction and where also the distribution of pressures approaches that on the profile.

In [54] it was shown that in a number of cases cavitation can occur considerably earlier than predicted by the above calculation, and it will start not at the middle, but at the ends of the hydrofoil, in vortex filaments trailing it.

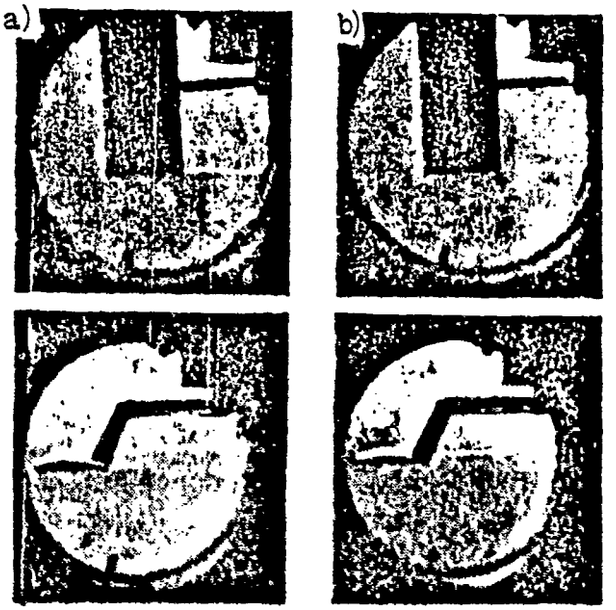

Fig. 66. Photographs of cavitation in vortex filaments trailing a hydrofoil of finite span during experiments in a cavitation tunnel: a) $\chi = 0.82$; b) $\chi = 1.35$.

Figures 65 and 66 are photographs from [54] of cavitation in vortex filaments obtained in a test basin and a cavitation tunnel. The experiments were conducted with hydrofoils with various span-chord ratios and shapes in plan and profile. The rounding off of the hydrofoil tips was also investigated. Also tested was a scale series of three hydrofoils of segmented profile, with relative

thickness c = 0.15, span-chord ratio $\lambda = 5$ and chords b = = 30 mm, 60 mm and 120 mm. During tests the angles of attack and the velocities were varied. The submergence constituted basically three chords. The lifting force was measured and a visual determination was made of the condition of the beginning of cavitation in vortices, i.e., the state at which the vortices became visible. The direct results of the tests were plotted as the dependence $C_y(v)$ with $\alpha = \text{const}$. The experimental points where the vortices were visible were darkened and then the boundary was drawn separating the black points from the white. An example of such a graph is shown in Fig. 67.

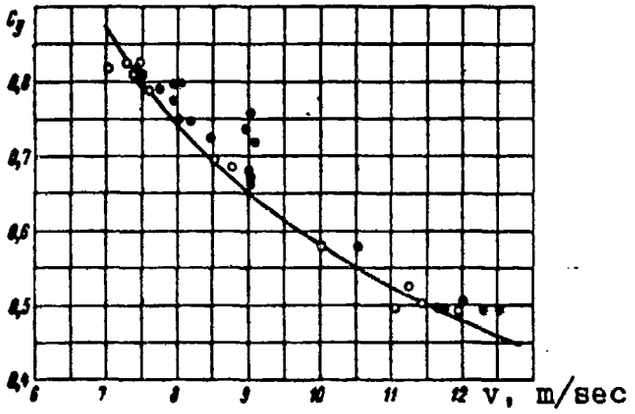

Fig. 67. Sample of the graph for determining the beginning of the cavitation regime in vortex filaments trailing a finite-span hydrofoil with chord b = 120 mm, $\lambda = 5$; o - filaments not visible; ● - filaments visible.

In the case of the theoretical determination of the emergence of cavitation in vortex filaments, it was only natural to employ the known work of L. Prandtl [79], who, representing the vortex cores according to Rankine's scheme, determined the radius of the core r_0 and the pressure on its axis. Prandtl based his evaluation on the condition of equality of the induced drag X_i and kinetic energy T_1 of the fluid enclosed between two flat plates located far behind the hydrofoil, perpendicular to the velocity and separated by a unit of distance. Since the kinetic energy T_1 is proportional to the square of circulation Γ and $\ln\frac{l_1}{r_0}$,

$$F(\alpha_{кр}, \bar{\Gamma}_1, \mathrm{Re}_1) = 0 \qquad (5.21)$$

or

$$\alpha_{кр} = f(\bar{\Gamma}_1, \mathrm{Re}_1). \qquad (5.22)$$

The circulation is related to the chord of the hydrofoil b, velocity v and the lifting force coefficient C_y by the known relationship

$$\Gamma = \frac{C_y b v}{2}. \qquad (5.23)$$

Substituting this expression into (5.22) and considering (5.20) we obtain

$$\alpha_{кр} = f_1\left(\frac{C_y}{\lambda}, \mathrm{Re}_1\right). \qquad (5.24)$$

As has already been mentioned, the experiment demonstrates that $\alpha_{кр} \neq C_y^2$. However, it follows then from (5.24) that if the effect of Re_1 is ignored, then $\alpha_{кр} \neq \frac{1}{\lambda^2}$, i.e., the same result which was derived from the stated theory, while the experiment did not produce any noticeable dependence of $\alpha_{кр}(\lambda)$. How, then, can we explain the closeness of the results derived from the theory based on Prandtl's calculations on the one hand, and on the presented theoretical concepts of the dimensional theory and the experimental data on the other? [142

It is not difficult to determine that out of the two prerequisites of the theory based on Prandtl's computations--the vortex scheme of the core as defined by Rankine and the determination of the dimensions of the core from the equality between the induced drag and the kinetic energy of a single layer--the closeness of the results is really defined by the second prerequisite, which in the process of applying dimensional analysis theory is reflected in the choice of the defining linear dimension l_1 between the vortices. However, it is natural to consider that this dimension is insignificant, because it is difficult to assume that the forming of the core of one vortex will be influenced by the other vortex, especially for large span-chord ratios. On the basis of these remarks, and utilizing the dimensional analysis theory, it is expedient to formulate this problem somewhat differently and examine it in the following way: there is a semi-infinite hydrofoil with

chord b, moving at velocity v; at the free end there is a trailing vortex with circulation Γ. Similarly to (5.20) the dimensionless terms now become

$$x = \frac{p_\infty - p_d}{\frac{\rho v^2}{2}}; \quad \Gamma_b = \frac{\Gamma}{vb} \text{ and } \mathrm{Re}_b = \frac{vb}{\nu}, \tag{5.25}$$

and instead of (5.24) we obtain

$$x_{кр} = f(C_y, \mathrm{Re}_b) \tag{5.26}$$

or according to experimental results

$$x_{кр} = C_y^2 f(\mathrm{Re}_b). \tag{5.27}$$

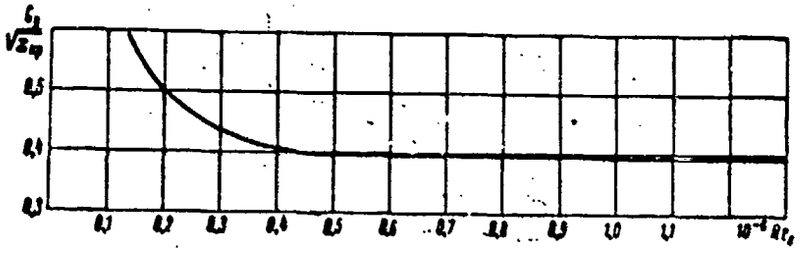

Fig. 68. Averaged dependence of $\frac{C_y}{\sqrt{x_{кр}}}$ on the Reynolds number $\mathrm{Re}_b = \frac{vb}{\nu}$ obtained during experiments in a basin and a cavitation tunnel. Rectangular hydrofoils $2 \leqslant \lambda \leqslant 5.7$, $0.3 \leqslant C_y \leqslant 1$; with chords 7 mm $\leqslant b \leqslant$ 120 mm.

An averaged dependence of $\frac{C_y}{\sqrt{x_{кр}}} = \frac{1}{\sqrt{f(\mathrm{Re}_b)}}$ on Re_b, based data of several experiments [54], is shown in Fig. 68. It can be seen from this figure that beginning with the values of $\mathrm{Re}_b \geqslant 5 \cdot 10^4$, $f(\mathrm{Re}_b) = \text{const} = 6.2$ and, consequently, the calculations of $x_{кр}$ with $\mathrm{Re}_b \geqslant 5 \cdot 10^4$ can be performed by the formula

$$x_{кр} = 6.2 C_y^2. \tag{5.28}$$

It is interesting to note that $x_{кр}$ depends not on the intensity Γ itself, but rather on Γ/bv. The physical meaning of this lies in the fact that the pressure drops at the upper and lower surfaces of the hydrofoil are the

chord b, moving at velocity v; at the free end there is a trailing vortex with circulation Γ. Similarly to (5.20) the dimensionless terms now become

$$\varkappa = \frac{p_\infty - p_d}{\frac{\rho v^2}{2}}; \quad \Gamma_b = \frac{\Gamma}{vb} \text{ and } \mathrm{Re}_b = \frac{vb}{\nu}, \tag{5.25}$$

and instead of (5.24) we obtain

$$\varkappa_{kp} = f(C_y, \mathrm{Re}_b) \tag{5.26}$$

or according to experimental results

$$\varkappa_{kp} = C_y^2 f(\mathrm{Re}_b). \tag{5.27}$$

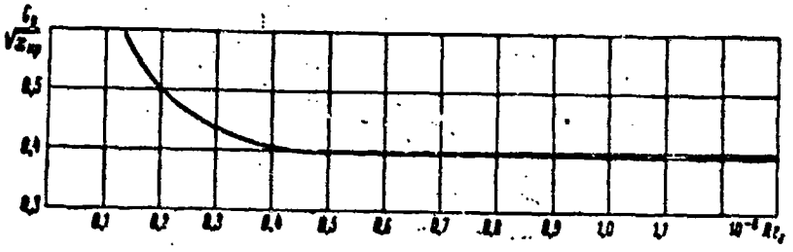

Fig. 68. Averaged dependence of $\frac{C_y}{\sqrt{\varkappa_{kp}}}$ on the Reynolds number $\mathrm{Re}_b = \frac{vb}{\nu}$ obtained during experiments in a basin and a cavitation tunnel. Rectangular hydrofoils $2 \leqslant \lambda \leqslant 5.7$, $0.3 \leqslant C_y \leqslant 1$; with chords 7 mm $\leqslant b \leqslant$ 120 mm.

An averaged dependence of $\frac{C_y}{\sqrt{\varkappa_{kp}}} = \frac{1}{\sqrt{f(\mathrm{Re}_b)}}$ on Re_b, based data of several experiments [54], is shown in Fig. 68. It can be seen from this figure that beginning with the values of $\mathrm{Re}_b \geqslant 5 \cdot 10^5$, $f(\mathrm{Re}_b) = \mathrm{const} \approx 6.2$ and, consequently, the calculations of $\varkappa_{kp}$ with $\mathrm{Re}_b \geqslant 5 \cdot 10^5$ can be performed by the formula

$$\varkappa_{kp} = 6.2 C_y^2. \tag{5.28}$$

It is interesting to note that $\varkappa_{kp}$ depends not on the intensity Γ itself, but rather on Γ/bv. The physical meaning of this lies in the fact that the pressure drops at the upper and lower surfaces of the hydrofoil are the

determining factors. We can expect a substantial effect on $\varkappa_{kp}$ at the curved tip of the hydrofoil, while variation in circulation due to variation of the chord will have no influence on $\varkappa_{kp}$. For hydrofoils moving near the free surface, when the hydrostatic pressure can be disregarded, a simple expression can be given for the relationship of the rate of emergence of cavitation in the vortex with C_y [143

$$v_{kp} = \frac{5.5}{C_y} \text{ [m/sec]}. \qquad (5.29)$$

Let us return to formula (5.28) and compare it with the formula for the critical cavitation number that was obtained in Rankine's study of a vortex with a core. The pressure p_1' at the boundary of the core can be found from the Lagrange-Cauchy integral for potential motion outside of the core

$$p_1' = p_\infty - \rho \frac{u^2}{2},$$

where

$$u = \frac{\Gamma}{2\pi r_0} = \omega r_0.$$

The pressure p_1 at the axis of the core can be conveniently found by employing a system of coordinates rotating with the core. Bernoulli's equation, considering the potential centrifugal forces, produces

$$p_1 = p_1' - \frac{\rho\omega^2 r_0^2}{2} = p_\infty - \frac{\rho\Gamma^2}{4\pi^2 r_0^2}; \qquad (5.30)$$

the relationships for the moment of the beginning of cavitation $p_1 = p_d$, and by taking (5.23) into account we obtain the formula

$$\varkappa_{kp} = \frac{\Gamma^2}{2\pi^2 v^2 r_0^2} = \frac{C_y^2 b^2}{8\pi^2 r_0^2}. \qquad (5.31)$$

Comparing it with (5.28) we will find [144

$$r_0 \approx 0{,}045b, \qquad (5.32)$$

i.e., the radius of the vortex core amounts to approximately 5% of the hydrofoil's chord and does not depend on C_y.

In Fig. 69 the values $\frac{C_y}{\sqrt{\kappa_{kp}}}$ corresponding to the beginning of cavitation on the segmented profile $\bar{c} \approx 15\%$ (based on experiments [77] and [78]) are compared to similar values for the beginning of cavitation in the vortices (based on experiments [54]). Cavitation in vortices with $C_y > 0.3$ begins at considerably smaller $\frac{C_y}{\sqrt{\kappa_{kp}}}$, i.e., at correspondingly smaller velocities than on the profile.

Similar results were obtained later on by McCormack [20]; the data obtained by him are basically in close agreement with [54].

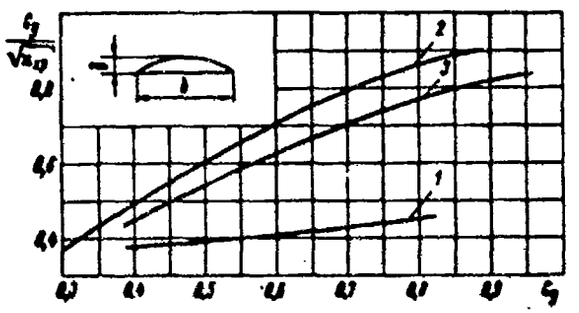

Fig. 69. Comparison of regimes of the beginning of cavitation on the profile and in trailing vortices: 1. cavitation in vortices, hydrofoil $\lambda = 5$, $\delta/b = 0.15$; 2. cavitation on the profile $\delta/b = 0.1475$; 3. cavitation on the profile $\delta/b = 0.12$.

5.4. Simulation of the Conditions of Air Entry to the Hydrofoil and to Bodies Intersecting the Free Surface

As is indicated by the analysis [52], air entry to the hydrofoil is a complex problem, i.e., it is not defined by some simple process, but rather consists of a series of various phenomena, each of which requires a separate study. The knowledge of all these phenomena separately is not sufficient for explaining conditions of air entry; analysis of their interaction is also necessary. Initially, we will divide the problem under consideration into two separate areas: air entry along vortex filaments and air entry along elements intersecting the free surface. [145

There are a great number of descriptions of cases of air entry along vortex filaments (see, for example, [6, 7]). In comparing and analyzing observations and evaluations performed by various authors on this phenomenon, a number of inconsistencies were observed. According to one group of observations and evaluations, at first hollow tubular vortices are formed which, while floating upward, create the channels through which atmospheric air reaches the hydrofoil. According to other observations, it is just the opposite--vortex filaments are not visible (and

therefore they can not be hollow) in the region adjacent to the hydrofoil, but can be seen only in the region departing from the free surface far from the hydrofoil.

Some authors consider that loss of lifting force occurs as soon as the visible part of the vortex reaches the hydrofoil. According to the repeated observations of others, the air that reaches the hydrofoil along the vortex is not distributed along its surface and does not cause any changes in the flow around the hydrofoil and in the action of the fluid force on the hydrofoil.

What is the real character of the phenomena which cause the drop in the lifting force due to the entry of atmospheric air along vortex filaments?

First of all, we should note the unfitness of the popular hypothesis that air entry into the vortex filament for shallow submergences of the hydrofoil takes place due to the surfacing of the vortex filament, which, in turn, is the result of cavitation and the filling of the vortex filament with the air dissolved in water.

As was shown in the previous section, cavitation in vortex filaments begins at sufficiently large velocities $v = \frac{5.5}{C_y}$ m/sec, which for the values $C_y = 0.2\text{-}0.3$ typical for hydrofoils correspond to $v = 18\text{-}25$ m/sec. At the same time, air entry to the hydrofoil is very often observed under simulation conditions with $v = 3\text{-}4$ m/sec. In addition, direct observations through a perisocpe [52] have shown that the cavitating vortex filaments at a distance on the order of 40 chords from the hydrofoil do not float up, but rather sink deeper, which is in complete agreement with the direction of induced velocities and with the insignificant role played by hydrostatic forces at large Froude numbers.

We have elaborated especially on the criticism of the "theory of surfacing vortices" because this theory, which at first glance appears to be probable and even seems to be correct for the case of deeply submerged hydrofoils, is used to explain the phenomenon of air entry for shallowly submerged hydrofoils for which this phenomenon is more important, and also mainly because from this theory follow incorrect conclusions with respect to the laws of simulation and the scale effect. Actually, if the existence of cavitating vortices was necessary for the process of air entry, then it would mean that for all models, the scales

and velocities of which would correspond to conditions without cavitation, there would be no entry of air along vortex filaments. However, when going over to full size the emergence of cavitation will lead to the entry of air. [1

But if the air entry does not depend on the surfacing of vortices, how can the vortices communicate with the atmosphere?

According to research [52], this occurs due to the specific deformation of the water surface behind the hydrofoil. The character of this deformation is described in Section 2 of this chapter. The axes of the vortex filaments pass in the immediate vicinity of the nearly vertical walls that confine the cavity, and during convergence with them there arises the possibility of the entry of atmospheric air into the vacuum region of the vortex filament. Thus, it is not the vortices that approach the free surface, but rather the free surface of the fluid deforms and approaches the vortices. Figure 70 is a photograph of the air entry to the vortex through the side boundary of the cavity formed behind the hydrofoil.

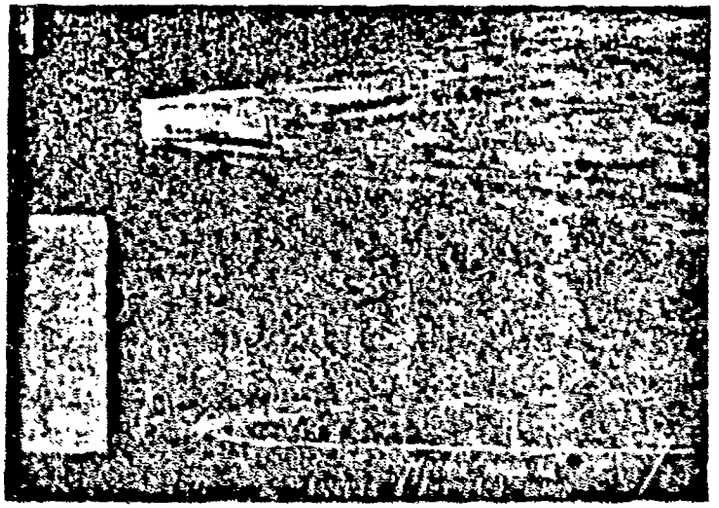

Fig. 70. Photograph of the moment of the beginning of air entry across the boundary of the deformed water surface into the trailing vortex filament.
Segmented hydrofoil with a relative thickness of 15%; b = 120 mm; λ = 5; $\alpha = 0^{\circ}$; v = 5 m/sec. Depth of submergence is 23 mm. The white line is the wave from the strut.
*Point of air entry to the vortex filament.

Under conditions at which the air from the free surface does not yet penetrate into the vortices, its penetration can be achieved artificially. In experiments it was sufficient to touch with the tip of a needle the vertical boundaries of the cavity in the region where the vortex may be expected to pass.

The suction of air into the region of the vortex does [14
not depend on its surfacing or on the cavitation phenomenon, but is stipulated by the shape of the water surface which, for similar hydrofoils with equal angles of attack and relative submergences, is determined by inertia forces, depends partially on the Froude number, and is practically independent of the Reynolds number. For small submergences the point of air penetration into the vortex filament is located relatively close to the hydrofoil (5-10 chords). This area of the free surface remains virtually unchanged for large Froude numbers. From this we must draw the conclusion that for large Froude numbers the air entry to the vortices depends on neither the Froude number nor the Reynolds number.

From Section 2 of this chapter it follows that the forces of surface tension do not have any effect on the shape and dimensions of the water surface. However, they can have a substantial effect on the phenomena connected with the breaking of the water surface (penetration of air into the vortex filaments) and with the separation of the fluid from the surface of the hydrofoil. The latter case is also related to the wettability of the material of the hydrofoil.

Depending on the cavitation number and C_y, the visible vortices of a cavitational nature at the ends of the hydrofoil can either exist or be absent; however, independently from this, at a certain submergence (for a given hydrofoil and conditions of motion) atmospheric air penetrates into the region of the vortex.

Thus, the contradictory observations, which indicate [1
in one case that the visible vortices begin from the hydrofoil, and in another that they begin from the surface, can be explained by the fact that they belong not to the same, but to different phenomena, related to the above-noted nature of the visibility of vortices. The entry of air, which produces changes in the hydrodynamic characteristics, is determined not by the cavitation of the vortex, but rather by the penetration of atmospheric air due to deformation of the water surface. The presence of waves or

[147

Fig. 71. P ɔgraph of the head portion of a cavity ing toward the hydrofoil. For hydrofoil data see the legend to Fig. 70; $\alpha = 5^\circ$; v = 5.1 m/sec.

ripples always facilitates air entry and reduces the scale [148 effect of capillarity.

Thus, due to the deformation of the water surface behind the hydrofoil the vacuum region in the vortex core connects with the atmosphere and air rushes toward the hydrofoil. The process of air displacement requires special attention. According to [6] and [7], cited above, this process was presented in the form of air flow along some "tubular conduit" created by the hollow vortex. These presentations, however, proved to be too primitive; they correspond to reality only for deep submergences, while for the shallow submergences which are of interest to us, they do not reflect the true phenomenon.

With small submergences the air penetrates toward the hydrofoil, forming either a characteristic spindle-shaped cavity with one or several constrictions, the leading part of which moves, according to the conducted computations, at a velocity (0.1-0.3)v from the free surface toward the hydrofoil* (Fig. 71-72), or (this usually happens with very

*The velocity is given in a system of coordinates related to the hydrofoil.

shallow submergences, when air has easy access into the

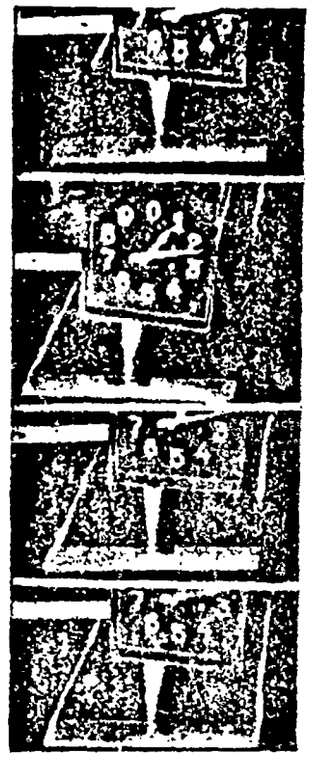

Fig. 72. Frames from a movie of the process of convergence of the air-filled regions of the vortex filaments with the hydrofoil. In the second and third frames one can see the leading region of the air-filled vortex filament approaching the hydrofoil from the right.
Hydrofoil $\lambda = 5$; $b = 60$ mm; $\alpha = 2^{\circ}$; $v = 11$ m/sec; $h = 30$ mm.

cavity) a conical cavity, which, as has been noted in previous works, is established at a certain distance from the hydrofoil and in the process of its motion oscillates randomly in the axial direction, catching up with the hydrofoil and then lagging behind again. Conditions also exist under which the conical cavity comes into contact with the tips of the hydrofoil with its front end.

Cavities of this type are shown in Figures 73 and 74.

A question arises as to why the cavities, the stream boundaries of which could be replaced by solid walls, move forward with velocities equal to or greater than those of the hydrofoil, and therefore have either zero or negative drag.

In ordinary stream flows the cavity (the region of constant pressure) also has no drag; however, its leading region, for example a cone, behind which it is formed, experiences increased pressures. The absence of drag at the cavity visible in Figures 73 and 74 is explained by the rotary motion of the fluid.

We will analyze this problem in more detail for the

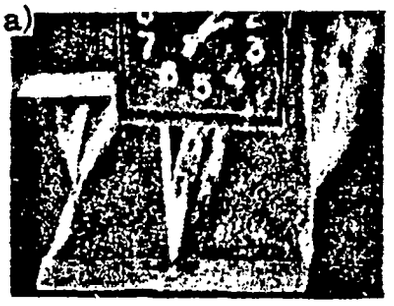

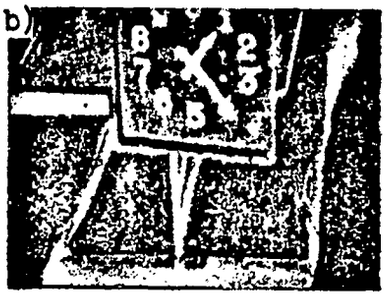

Fig. 73. Photograph of cavities in trailing vortex filaments with small submergences: a) h = 8 mm, v = 8.2 m/sec; b) h = 15 mm; v = = 7.1 m/sec.
Segmented hydrofoil $\lambda = 5$; b = = 60 mm; $\alpha = 8^{\circ}$.

Fig. 74. Photograph of cavities in vortex filaments for small submergences of the hydrofoil. The conical cavities have reached the tips of the hydrofoil, but the air is not rushing toward its surface. The lifting force of the hydrofoil has not changed. Segmented hydrofoil $\lambda = 5$; b = 60 mm; $\alpha = 5^{\circ}$; v = 12.4 m/sec; h = 23 mm.

[1

case of a cavity in a rotating fluid flow enclosed in a cylindrical pipe. We will determine the drag of a body with a stream flow around it using a potential flow of an ideal, weightless, incompressible fluid enclosed in a cylindrical pipe with a radius R which, in addition to forward motion, is also rotating near the axis of the pipe (Fig. 75).

Let us designate the axial fluid velocity by v and the circumferential velocity by u. We will consider that at the cross sections 0-0 and 1-1 the axial velocities are constant and the circumferential velocities are

$$u = \frac{\Gamma}{2\pi r}. \qquad (5.33)$$

We will consider the pressure inside the pipe with radius r_0 to be constant. Designating the drag of the

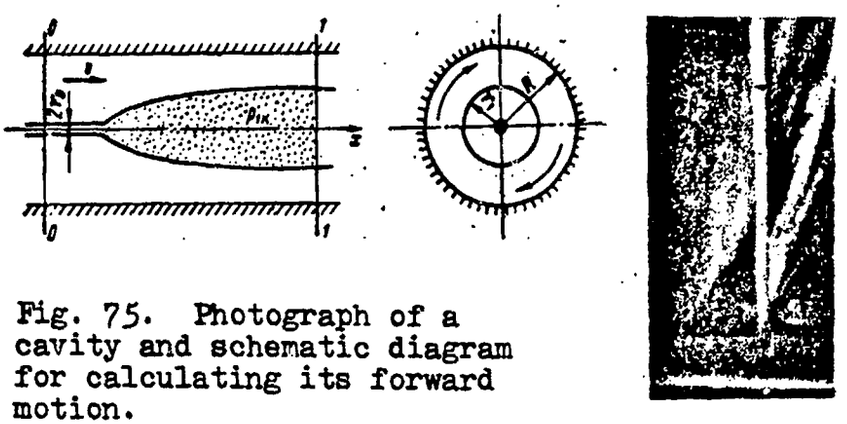

Fig. 75. Photograph of a cavity and schematic diagram for calculating its forward motion.

body by X, we apply the law of momentum to the volume confined within the cross sections 0-0 and 1-1,

$$X = -\rho\pi\left[(R^2-r_1^2)v_1^2-(R^2-r_0^2)v_0^2\right]+$$
$$+2\pi\int_{r_0}^{R} rp_0(r)\,dr+\pi r_0^2 p_0(r_0)-2\pi\int_{r_1}^{R} rp_1(r)\,dr-\pi r_1^2 p_1(r_1). \qquad (5.34)$$

In the future we will consider the value r_0 to be small and ignore r^2_0 as compared to r^2_1 and r^2; then, taking the continuity equation into account, we can rewrite (5.34) as follows:

$$X = -\rho v_0^2\pi R^2\left(\frac{R^2}{R^2-r_1^2}-1\right)+$$
$$+2\pi\left[\int_{r_0}^{R} rp_0(r)\,dr-\int_{r_1}^{R} rp_1(r)\,dr-\frac{r_1^2}{2}p_1(r_1)\right]. \qquad (5.34')$$

Applying Bernoulli's equation to the stream lines in contact with the pipe walls, we obtain, keeping in mind that $u_0(R) = u_1(R)$,

$$p_0(R)+\frac{\rho v_0^2}{2}=p_1(R)+\frac{\rho v_1^2}{2}, \qquad (5.35)$$

from which

$$p_1(R)=p_0(R)-\frac{\rho v_0^2}{2}\left[\frac{R^4}{(R^2-r_1^2)^2}-1\right].$$

Applying Bernoulli's equation at sections 0-0 and 1-1 [151 we obtain, taking into consideration that v_0 and v_1 are constant along the cross section,

$$p_0(r)+\frac{\rho u_0^2(r)}{2}=p_0(R)+\frac{\rho u_0^2(R)}{2}; \qquad (5.36)$$

$$p_1(r)+\frac{\rho u_1^2(r)}{2}=p_1(R)+\frac{\rho u_1^2(R)}{2}$$

or by considering (5.33) and (5.36)

$$p_0(r)=p_0(R)-\frac{\rho\Gamma^2}{8\pi^2R^2}\left(\frac{R^2}{r^2}-1\right);$$

$$p_1(r)=p_0(R)-\frac{\rho v_0^2}{2}\left[\frac{R^4}{(R^2-r_1^2)^2}-1\right]-\frac{\rho\Gamma^2}{8\pi^2R^2}\left(\frac{R^2}{r^2}-1\right). \qquad (5.37)$$

Substituting the new expressions into (5.34') and then denoting $\bar{r} = r/R$, $p_0(R) = p_0$ and $p_1(r_1) = p_k$, we find

$$\frac{X}{\pi R^2}=-\frac{\rho v_0^2}{2}\frac{2\bar{r}_1^2}{1-\bar{r}_1^2}+2\int_{\bar{r}_0}^{1}\left[p_0-\frac{\rho\Gamma^2}{8\pi^2R^2}\left(\frac{1}{\bar{r}_1^2}-1\right)\right]\bar{r}d\bar{r}-$$

$$-2\int_{\bar{r}_1}^{1}\left\{p_0-\frac{\rho v_0^2}{2}\left[\frac{1}{(1-\bar{r}^2)^2}-1\right]-\frac{\rho\Gamma^2}{8\pi^2R^2}\left(\frac{1}{\bar{r}^2}-1\right)\right\}\bar{r}d\bar{r}-\bar{r}^2p_k. \qquad (5.38)$$

Integrating and introducing the designations

$$C_{x_k}=\frac{2X}{\rho v_0^2\pi r_1^2}; \qquad (5.39)$$

$$\varkappa=\frac{p_0-p_k}{\frac{\rho v_0^2}{2}}, \qquad (5.40)$$

after some simple transformations we obtain

$$C_{x_k}=-\frac{\bar{r}_1^2}{1-\bar{r}_1^2}+\varkappa-\frac{\Gamma^2}{2\pi^2r_1^2v_0^2}\left(\ln\frac{r_1}{r_0}-\frac{\bar{r}_1^2}{2}\right). \qquad (5.41)$$

Assuming that at increased R the value $\bar{r}_1$ can be made sufficiently small, and ignoring $\bar{r}^2_1$ compared to unity, we find

$$C_{x_k}=\varkappa-\frac{\Gamma^2}{2\pi^2r_1^2v_0^2}\ln\frac{r_1}{r_0}. \qquad (5.42)$$

If there is no body and we are dealing with the

steady-state motion of one cavity only in a rotating fluid flow, then the drag, and hence C_{x_k}, must be equal to zero and the condition of steady-state motion of the cavity behind the hydrofoil will become [152

$$\varkappa - \frac{\Gamma^2}{2\pi^2 r_1^2 v_0^2} \ln \frac{r_1}{r_0} = 0. \tag{5.43}$$

Expressing Γ through C_y by the known formula

$$\Gamma = \frac{C_y b v_0}{2} \tag{5.44}$$

(where b is the chord of the hydrofoil), we will obtain instead of (5.42)

$$C_{x_k} = \varkappa - \frac{C_y^2}{8\pi^2} \frac{b^2}{r_1^2} \ln \frac{r_1}{r_0}. \tag{5.45}$$

Formula (5.45) allows us to observe the influence of various factors on the motion of the cavity.

Suppose that under certain conditions the steady-state motion of a cavity is present, i.e., $C_{x_k} = 0$. If the supply of air into the cavity now stops or diminishes, then the value p_k will decrease, $\varkappa$ will increase, C_{x_k} will become greater than zero and the cavity will start to lag behind. On the contrary, passage of air into the cavity and increased p_k will lead to accelerated cavity motion, and it will begin to catch up with the hydrofoil. Air enters into the cavity through its trailing tip where, due to the pulsating action of the converging streams, communication with the astmosphere becomes either facilitated or hindered, which, as we can see, must cause longitudinal pulsations of the cavity, which are in fact observed.

According to (5.45), deeper submergence of the hydrofoil, i.e., an increase of p_0, should lead to the falling behind of the cavity, and it actually does. A similar effect will be produced by decrease in the velocity of the hydrofoil, although at first glance it seems that a decrease in hydrofoil velocity will enable the cavity to catch up to it.

According to (5.45), increase in C_y will cause an acceleration of cavity motion, while a decrease in C_y will

cause it to lag behind. This is in complete agreement with the existing ideas about the necessity to use small values of C_y in order to move air entry farther away.

Since $\varkappa$ is a positive value, then from (5.42) it follows that C_{x_k} can be equal to zero only in the presence of rotational motion, i.e., when $\Gamma \neq 0$; by decreasing Γ it is possible to slow down the forward motion of the cavity. If we lower a plate into the water behind the hydrofoil near the vortex axis (Fig. 76), this plate will hinder the rotational motion of the fluid (at least in the area of its location) and the cavity will not be able to advance ahead of the plate.

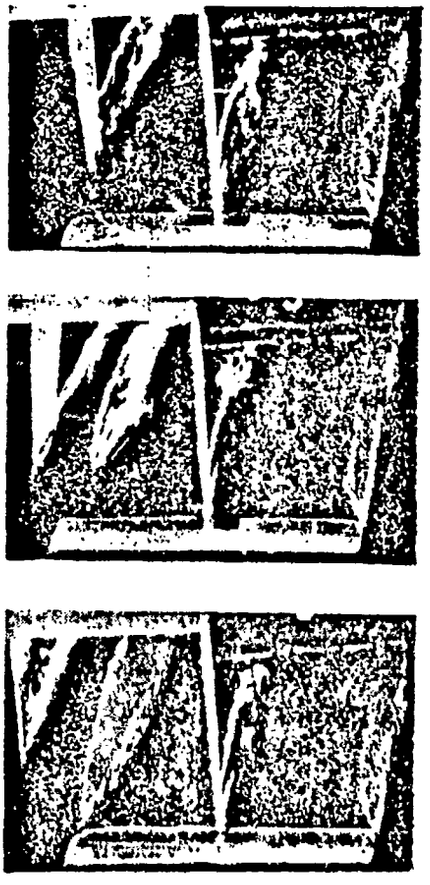

Fig. 76. A flat plate placed behind the hydrofoil and passing through the axis of the vortex prevents motion of the cavity toward the hydrofoil. After shifting the plate to the side (middle frame) the cavity tends to approach the hydrofoil and reaches it in the lower frame.
Segmented hydrofoil $\lambda = 5$; $b = 60$ mm; $\alpha = 8^\circ$; $v = 5.04$ m/sec; $h = 15$ mm.

The experiments conducted support this assumption. In Fig. 76, where motion picture frames are presented, it can be seen that from the side where the plate is located (on the right with respect to motion) the vortex cavity in front of it is absent and on the left side it has approached the hydrofoil. In the following frames it can be seen that by moving the plate farther away the cavity tends to approach the right tip of the hydrofoil.

Cavities located along the vortex filaments do not always change the character of the flow around the hydrofoil, even in those cases where they come in contact with the hydrofoil. Figure 74 shows a photograph of a hydrofoil with cavities which adjoin its tips and do not lead to air penetration to its upper side. Such conditions virtually do not reflect on the lifting force or the drag of the hydrofoil and do not create the instability described above. This is explained by the presence of increased pressure under certain conditions between the vacuum region on the hydrofoil and the vortex cavity.

However, as follows from Figures 70 and 71, vortex cavities are not steady-state cylindrical or conical cavities. They are twisted into spiral cavities, they intersect each other and are in a continuous state of pulsating motion with respect to the hydrofoil (the reason for this type of pulsation with the closing of partial cavity regions was discussed above). As a result of these pulsations, which are partially dependent on the instability of the spiral cavities and partially on the weak perturbances of the free surface, there arises the probability of reduction and even elimination of the above-mentioned high-pressure region, and at that moment air from the cavity at the end rushes in toward the hydrofoil*. The process of the

---

*This air entry, similarly to cavitation in vortices, substantially depends on the shape of the tip. Roundness of the tip accelerates the entry.

---

distribution of the cavity along the hydrofoil is shown in Fig. 77.

Depending on the depth of submergence, the shape of the hydrofoil, its angle of attack and its velocity, two types of flow around the hydrofoil can emerge when the hydrofoil is fixed at a certain depth. For relatively great depths and small angles of attack the existence of the cavity on the foil itself depends on the final volume of the penetrated air, whereby after change in the character of flow and decrease of the lifting force, the intensity of the vortices changes and further supply of air from the end cavities stops, and the vortices disappear. Air hitting the foil is carried off by the flow and the initial conditions of flow around the hydrofoil are re-established; the vortices appear again and the entire process is repeated.

With low velocities and small angles of attack and

Fig. 77. Motion picture frames showing the cavity approaching the hydrofoil and the entry of air to the surface of the hydrofoil. Hydrofoil with a symmetrical profile $\lambda = 2$; $b = 60$ mm; $\alpha = 18^{\circ}$; $v = 7.65$ m/sec; $h = 27$ mm.

with large submergences the probability of air entry is low. Air entry can be observed on one out of several dozens of frames and it quickly disappears. On the contrary, with large velocities and large angles of attack and with small submergences the instances of air entry follow one after another and remain for a prolonged time. Noting these qualitative regularities we should stress that the frequency with which entry occurs for the given condition does not remain constant and is subject only to statistical regularity.

In addition to the periodic air entry described above, a stationary entry can be present, leading to pure stream flow around the hydrofoil with the formation of a thin water arch above the foil. This second type of flow develops when air penetrates into the region above the hydrofoil not only through the vortex cavity, but also directly through the formed water arch or its edges. This type of entry, later to be referred to as the arched type, is the most characteristic type for large angles of attack, sharp leading edges and small submergences. Photographs of arched entry are shown in Fig. 78.

The described phenomena emerge for the rigidly fastened hydrofoil. If surfacing of the hydrofoil is unrestricted and the hydrofoil is carrying a certain [15
load, then after the entry it will fall down, the air in the cavity will be carried off by the stream flow, the lifting force at this depth becomes greater than the load, and the hydrofoil is thrown above the water level. As the hydrofoil again submerges the disruption occurs and the process is repeated. This process is periodical with a constant period of oscillation for a given object and conditions of motion.

The development of air entry itself for a hydrofoil with free vertical movement is somewhat accelerated due to

Fig. 78. Process of entry leading to stream flow around the hydrofoil and to the formation of an arch made of water streams above the hydrofoil.

Hydrofoil with a symmetrical profile $\lambda = 2$; $b = 60$ mm; $\alpha = 18^{\circ}$; $v = 7.65$ m/sec; $h = 14$ mm.

interaction between the pulsating cavities and the natural oscillations of the hydrofoil; moreover, the hydrofoil oscillations and the cavity pulsations are mutually interrelated. Thus, for example, the envelopment of the hydrofoil region by the cavity leads to its submergence and the submergence in turn is reflected on the vortex cavities. There are cases when this interaction leads to resonant oscillations of the hydrofoil, which, intensifying, cause air entry.

In order to simulate the entry phenomena which depend on oscillations, it is necessary to additionally provide dynamic similarity. The analysis and considerations presented above with respect to the simulation of air entry phenomena along vortex filaments are supplemented by the tests of a scale series of the hydrofoils described in Section 3 of this chapter. These tests, described in detail in [52], consisted in the towing of hydrofoils which were capable of surfacing freely with various angles of attack, velocities and loads. The boundaries of the regimes for which air entry and the dipping of the hydrofoil occurred were sought. There was no cavitation of the hydrofoil.

Assuming that the phenomenon being analyzed depends on b, l, l_1, ..., l_n, α, ρ, ν, σ, v, g, Δ (in the indicated formulation instead of the submergence the weight Δ is introduced, which is equal to the lifting force Y), it is possible, using ordinary techniques of dimensional theory, to express the regime of air entry by the expression [156

$$F\left(\lambda, \frac{l_1}{b}, \ldots, \frac{l_n}{b}, \alpha, \frac{vb}{\nu}, \frac{v}{\sqrt{gb}}, \frac{Y}{\frac{\rho v^2}{2} bl}\right) = 0 \qquad (5.46)$$

or for all similar hydrofoils

$$C_{y_{кр}} = f(\alpha, Fr_b, Re_b, We_b). \qquad (5.47)$$

Rewriting the last expression in the form [see (1.55)]

$$C_{y_{кр}} = f_1(\alpha, Fr_b, \Pi, K), \qquad (5.48)$$

it can be seen that with constant values of ρ, g, ν and σ the last two terms depend on b only and thus the number of terms can be reduced

$$C_{y_{кр}} = f_2(\alpha, Fr_b, b). \qquad (5.49)$$

Let us emphasize that this formula is valid only for ρ, g, ν and σ corresponding to the conditions of the conducted experiments, i.e., specifically for water bordering with air.

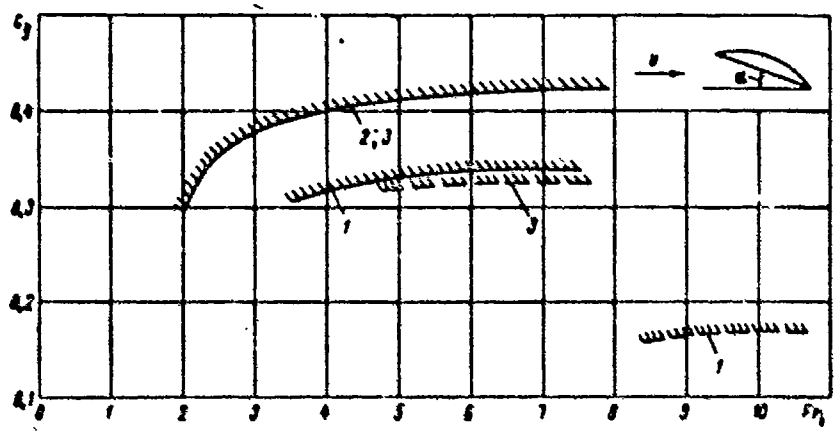

Fig. 79. Boundary of the regime of air entry to a flat hydrofoil in coordinates C_y and $Fr_b = \frac{v}{\sqrt{gb}}$. Profile of a segment; $\delta/b = 15$; $\lambda = 5$. ——— $\alpha = 8^0$; ----- $\alpha = 4^0$; 1. b = = 30 mm; 2. b = 60 mm; 3. b = 120 mm.

Figure 79 shows dependences $C_{y_{kp}}$ (Fr_b) with α = = const and b = const plotted according to results of tests of a scale series. Completely in agreement with the above analysis, it turned out that in the case of large Froude numbers and hydrofoils with chords of b > 60 mm, the conditions for air entry depend neither on the Froude number nor on the Re and We numbers. Therefore, based on physical considerations, as well as on the test results from the

scale series, it is possible to draw the conclusion that until the beginning of cavitation on the profile for hydrofoils of sufficiently large dimensions (for the experiments under discussion starting with b = 60 mm) there is no scale effect of air entry. For hydrofoils with a chord b > 60 mm it is possible with sufficient accuracy to also omit simulation with respect to the Froude number, if $Fr_b > 5$, preserving only geometric similitude, equality of the angles of attack and similitude in immersion or load coefficients.

For small hydrofoils (b = 30 mm) the influence of the scale effect proved to be of significance, which means that a decrease in hydrofoil dimensions leads to the air entry phenomenon shifting toward higher velocities. The nature of this influence is, probably, the result of the action of surface tension forces, which impede the breaking of the fluid surface and thus resist air penetration into the vortex filaments. The surface tension also hinders the formation of separating flow, i.e., the penetration of air from the vortex to the hydrofoil. According to the experiments conducted, the scale effect increases with decrease in angles of attack (see Fig. 79). This is in agreement with the suggested hypothesis concerning the role of surface tension forces, since a specific portion of these forces increases with decrease in the angle of attack.

The technical possibilities of analyzing air entry are hampered under conditions of cavitation. This makes it necessary to limit the study to an analysis of the physical considerations and to schematized experimentation in a basin, using relatively high velocities and a small, thick hydrofoil with large angles of attack.

First of all, it should be expected that cavitation of the vortex filaments will have little effect on the penetration of atmospheric air into them and may even delay this phenomenon somethat. The following considerations support the above opinion:

-- Prior to the emergence of cavitation in the vortices the pressure difference between that in vortices and at the fluid surface varies in direct proportion to the square of the velocity. After cavitation begins, with further increase in velocity this difference ceases to increase and remains constant.

-- Air penetration into the vortex filaments occurs not from the horizontal water surface, as was previously assumed, but rather from the vertical walls of the cavity

developed behind the foil. Therefore, the surfacing of the hollow packs of vortex filaments virtually does not draw them nearer to the free surface. For an evaluation of the height of the surfacing motion we can look at Fig. 80, where the tip of a foil with a hollow vortex of circular cross section is shown schematically. Assuming that every element of the vortex rises toward the surface independently of its remainder, and disregarding the mass of the air and the vapors confined within the pipe, it is possible to write the equation of motion for an element as follows:

$$\pi r_0^2 dx \rho \ddot{y} = \pi r_0^2 dx \rho g. \qquad (5.50)$$

where the coefficient for $\ddot{y}$ in the left part of the equation expresses the attached mass of the element, while the right side expresses its buoyancy force. [158

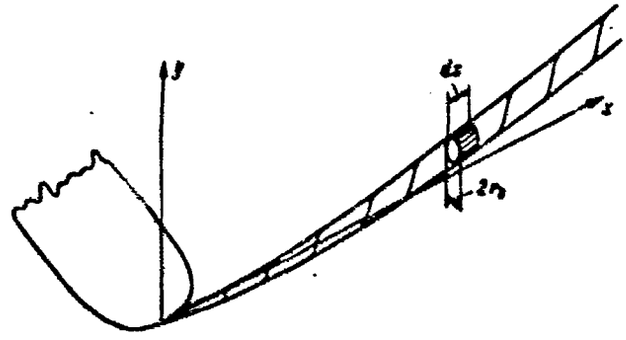

Fig. 80. Schematic presentation for calculating the surfacing of a cavitating vortex filament.

From (5.50) it follows that

$$\ddot{y} = g. \qquad (5.51)$$

Since the distance x from the element to the tip of the hydrofoil can be expressed in the form

$$x = vt, \qquad (5.52)$$

where v is the velocity of wing motion and t is the time elapsed from the moment the tip of the foil passes the plane in which the cross section of the element is located, then equations (5.51) and (5.52) become similar to equations of the free falling body thrown with a horizontal velocity v. The trajectory of the vortex filament will be determined by the equation

$$y = \frac{gx^3}{2v^2} \qquad (5.53)$$

or in the dimensionless form

$$\frac{y}{b} = \frac{\left(\frac{x}{b}\right)^3}{2Fr_b^2}. \qquad (5.54)$$

For example, for a hydrofoil with a chord equal to 60 mm, at a velocity v = 10 m/sec and with the cross section under consideration at a distance of five chords away from the foil, we obtain a rise of y = 4.5 mm; at a distance of 20 chords y = 72 mm.

Here we should make the reservation that for deeply submerged foils with a relative submergence on the order of one chord and greater, when the vortex filaments in non-cavitational flow do not pass near the free surface, the [1
presence of cavitation in the vortex can actually cause its surfacing and consequent suction of atmospheric air. Cavitation on the profile can influence the air entry to the hydrofoil itself, if the air has reached the tip of the hydrofoil along the vortex filament. This is explained by the redistribution of pressures along the profile typical for cavitation and by the pulsations characteristic of it.

As a result of analysis of the problems of simulation and the series of experiments conducted on geometrically similar hydrofoils, it was established that for small hydrofoils, with the chord b = 30 mm, a considerable scale effect takes place, and that the velocity at which air entry occurs is substantially higher than for the large hydrofoils in simulation according to Froude's law of similitude.

The scale effect was not detected for hydrofoils with a chord b = 60 mm, and when $Fr_b = \frac{v}{\sqrt{gb}} > 5$ we can dispense with Froude simulation, preserving only geometric similarity and the similarity of the inertia forces. This condition can substantially facilitate some analyses. From the above discussion it follows that the disagreement between experiments with models in a basin and experiments with full-size objects under actual conditions can be due to the scale effect for small hydrofoil models. If the hydrofoils are of sufficient dimensions, with a chord on the order of 100 mm, we should not expect any pronounced scale effect in the absence of cavitation. It should be noted

that a major source of disagreement may be the schematization adopted for the simulation tests: the absence of drift, heeling, real waves, wind, etc.

The phenomenon of air entry on objects which intersect the free surface [5, 72, 86, 88] (struts, tips of the foil) has its own characteristics and the reasons that cause it are different from those that lead to the entry along vortex filaments discussed above.

Even though a great number of publications have been devoted to analysis of air entry near objects intersecting the free surface, there is so far no rational theory nor clear scheme for this phenomenon. Apparently correct but very general concepts have been presented which indicate that entry is caused by, in addition to decrease in the ambient pressure on the object to atmospheric, phenomena of the separation of the boundary layer and--with small dimensions of objects--by the forces of surface tension.

According to the observations and the experiments carried out by the author, the nature and character of air entry near objects intersecting the free surface are not identical for the so-called well and poorly streamlined bodies. To the first category belong struts and hydrofoils with small relative thickness and small angles of attack or drift, while to the second category belong objects with large relative thickness and any struts or hydrofoils with large (supercritical) angles of attack.

Let us describe, first of all, the outer side of this [16
phenomenon. The level of the free surface in the region of its intersection with the body rises in the zone of increased pressure and drops slightly in the region of vacuum on the body. With small angles of attack the level drop is not great and does not progress substantially with increased velocity. It is obvious that on the deformed free surface the pressure is equal to atmospheric, while on the submerged body elements the emerged vacuums increase with increase in velocity. As a result, there occur conditions where $\frac{\partial p}{\partial y} < 0$ on a portion of the body (the y axis is directed downward).

Beginning at some velocity, individual air cavities in the shape of cones with the apex directed toward the leading edge appear on the submerged part of the body. The appearance of these cavities occurs due to the passage of portions of air from the region of lower water level where fluid separation from the strut sometimes occurs.

After their appearance the cavities exist for a certain time, sometimes jumping over from one place to another, disappearing depending on the amount of air loss and being replaced by new ones. All the factors which lead to increase of rarefaction--increased velocity, angle of attack, etc.--lead to enlargement of the region occupied by cavities, which propagate depthwise and, finally, envelop the entire span of the inclined hydrofoil or strut. Increase of velocity and angle of attack causes the separate cavities to merge, and finally leads to the formation of a common cavity, i.e., to transition to the stream-flow condition.

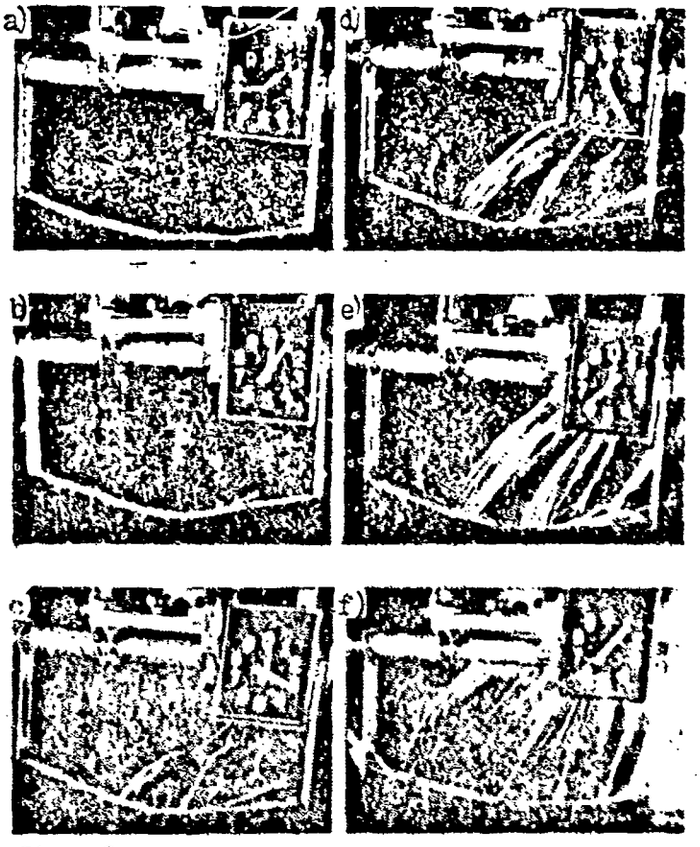

Fig. 81. Photographs illustrating the effect of velocity on the character of the flow around a submerged V-shaped hydrofoil intersecting the free surface (b = 50 mm): a) v = 1.5 m/sec; b) v = = 2.0 m/sec; c) v = 2.5 m/sec; d) v = = 3.5 m/sec; e) v = 4 m/sec; f) v = 7 m/sec.

The entire cycle of air entry development is illustrated in the example of the V-shaped hydrofoil with a low

deadrise (Fig. 81). For bodies positioned at a large angle of attack, particularly ones with sharp edges, the process of air penetration into the vacuum region is different. With an increase in velocity the region with the lowered surface level behind the body gradually increases lengthwise and depthwise and, as a rule, becomes filled with foam. With velocity increase the depression-cavity behind the body reaches its lower edge and is eventually cleared of the foam.

Thorough experimental studies of the phenomenon of air entry to vertical cylindrical struts that intersect the free surface were performed by D. Wetzel [88]. He analyzed the dependence of the condition under which air entry occurs on a large number of parameters. The diameter of the cylinder d (0.8-50 mm) and the relative depths of submergence $\bar{h}=\frac{h}{d}$ (from 1-20) were varied within a wide range. During the course of the experiments the viscosity of the water ν, the surface tension coefficient σ, and the strut materials were varied.

The principal results of experiments are presented in [88] in the form of the relationships between the relative submergence and the Froude numbers $Fr_h=\frac{v}{\sqrt{gh}}$ and $Fr_d=\frac{v}{\sqrt{gd}}$ [161] (Fig. 82a, b) at which air entry occurs, down to the lowest point on the metal strut. In Fig. 83 these results are compared with the results obtained during similar tests of struts coated with teflon, an evidently nonwettable material.

In his conclusions, Wetzel indicates that two types of "ventilation," or the suction of air into the vacuum region behind the body, were observed: instantaneous, when the air penetrated along the entire depth of the submerged strut, and gradual, when the cavity behind the body moved deeper with increase of the Froude number, while its lower [163] portion was filled with foam. Ventilation of the first type was predominant for thin struts without coating and was characterized by substantial hysteresis, i.e., by the difference of the Froude numbers that corresponded to its formation and its disappearance.

In the discussion of Wetzel's article, as well as in the discussion of K. Wadlin's work [86], in which Wetzel's data are cited, along with statements on the relation of viscosity and surface tension to the phenomenon under consideration there are several attempts to present specific

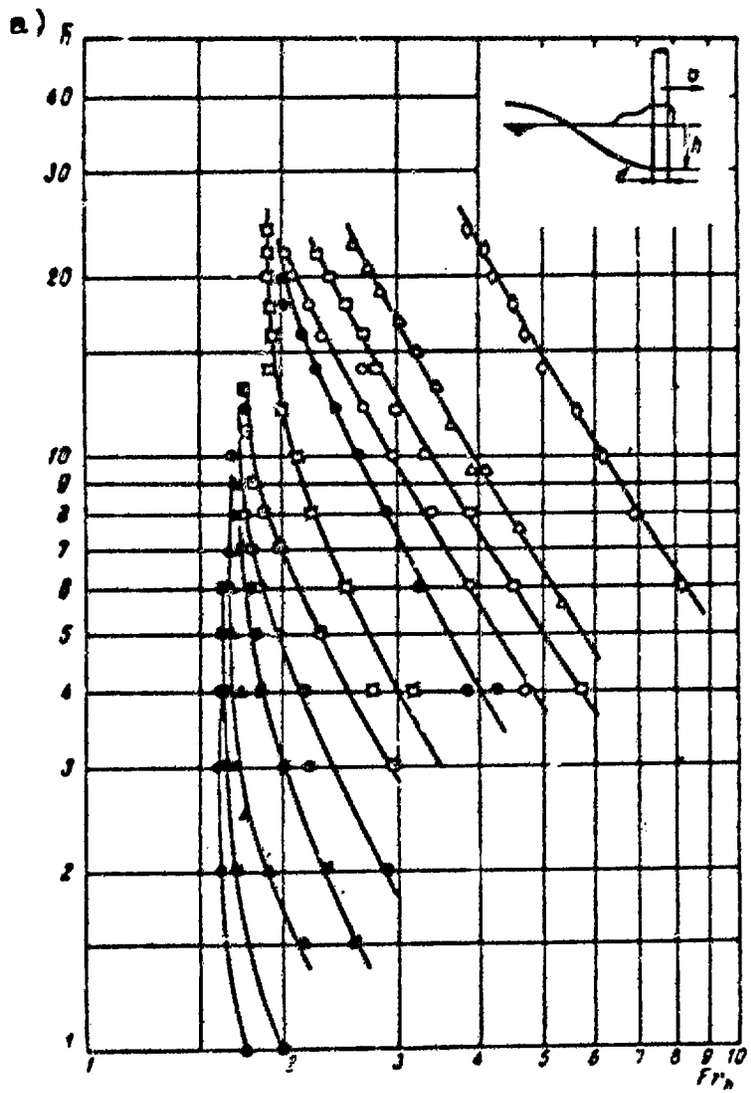

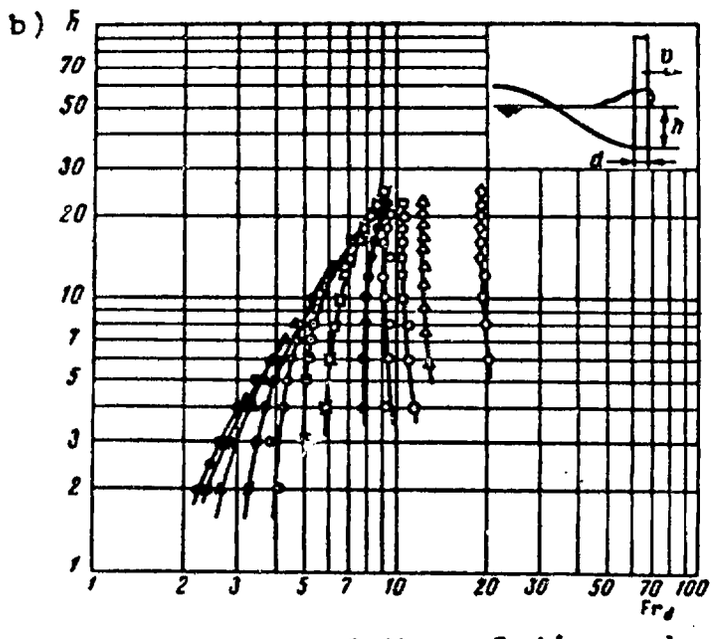

Fig. 82. Dependence of the relative submergence $\bar{h}$ and the Froude number for conditions under which the air penetrates to the lower end of a round strut which intersects the free surface [88]: a) Froude number plotted along the abscissa with respect to submergence $Fr_h = \frac{v}{\sqrt{gh}}$; b) Froude number plotted along the abscissa with respect to diameter $Fr_d = \frac{v}{\sqrt{gd}}$.

○ — d=0,8 мм; △ — d=1,27 мм; □ — d=1,57 мм; ○ — d=1,98 мм; ⊕ — d=2,41 мм; ⊡ — d=3,15 мм; ⊡ — d=4,76 мм; ⊕ — d=6,35 мм; ⊕ — d=12,7 мм; ▲ — d=25,4 мм; ■ — d=38,1 мм; ● — d=50,8 мм.

[162/163]

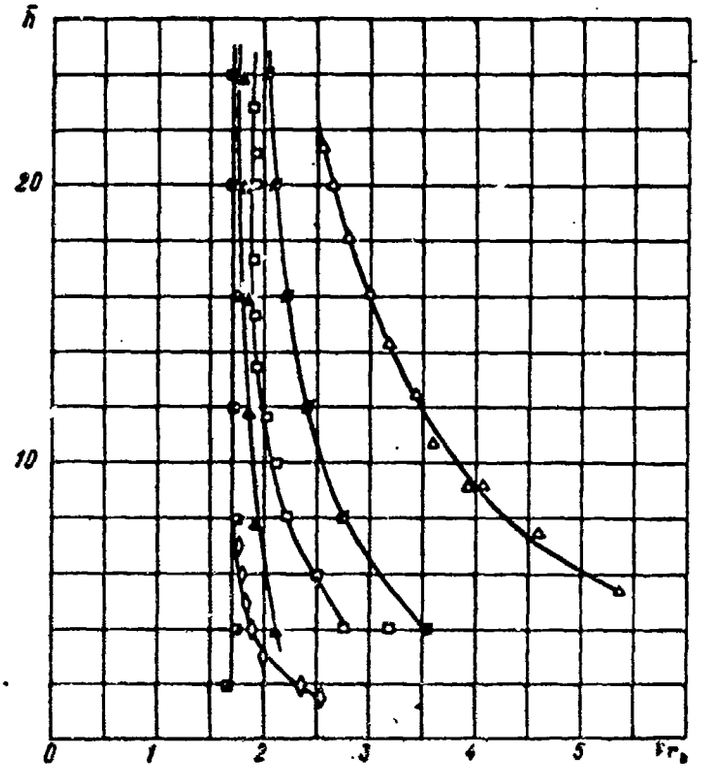

Fig. 83. Effect of teflon coating on the condition of air entry to the lower end of a round strut intersecting the free surface [88].

Metal struts: Δ - d = 1.27 mm; □ - d = 3.15 mm; ◇ - d = 12.7 mm.
Teflon-coated struts: ⌀ - d = 1.32 mm; ▲ - d = 3.22 mm; ■ - d = 12.7 mm.

calculations and explanations. Thus, E. R. Tinny suggests that we determine the conditions of entry by equating the value of the greatest vacuums on the cylinder to the hydrostatic pressure at the level of the submerged edge. From the relationship

$$-\bar{p}_{min}\frac{\rho v^2}{2} = \rho g h \qquad (5.55)$$

he finds

$$Fr_h = \frac{v}{\sqrt{gh}} = \sqrt{\frac{2}{-\bar{p}_{min}}} \qquad (5.56)$$

and, assuming that $\bar{p}_{min} = -0.8$ for the range of $1.5 \cdot 10^3 <$

$< Re < 1.5 \cdot 10^5$, he gets $Fr_h = 1.58$, a value that is close to the limiting value $Fr_h = 1.6\text{-}1.7$ for large cylinders (see Fig. 82a). For small-diameter cylinders Tinny suggests an empirical formula $Fr_h = 1{,}6 + \frac{1{,}8 \cdot 10^4}{\bar{h}\, Re^{3/4}}$, i.e., he relates the air entry only to the relative submergence and the Reynolds number.

Wadlin [86] rearranged the data of [88] in the form of the relationship Fr_h with respect to the absolute submergence h and obtained the relationship shown in Fig. 84 by employing formula (5.56). He writes the following: "...this figure indicates that for a depth of submergence exceeding two inches the pressure coefficient at the lower end is constant. However, at depths of less than two inches the pressure coefficient at the lower edge rapidly decreases." Wadlin attributes this decrease to the influence of the free surface and indicates that in accordance with formula (5.56) a decrease in $(\bar{p})$ leads to an increase in Fr_h. [166

Considerable attention in [86] and others is paid to analysis of the relationship of ventilation to phenomena in the boundary layer. Thus, Garner considers that "accumulation of material of the boundary layer and negative pressures in the zone of separation" serve as the prerequisites for ventilation. In [86] special studies of the boundary layer are described, where an oil film was applied on the body being towed, after which the surface was viewed under ultraviolet light.

Under closer analysis it became evident that the suggested explanations of the experimental results in [86] and others are inconsistent.

In Fig. 85 the distribution of pressure on cylinders for various Re values from 2800 to $\sim 2 \cdot 10^5$ are shown [34]. From this figure it follows that the values of greatest rarefactions are on the order of $/\bar{p}_{min}/ \sim 1$ only for Re = = 2800, but for such cylinders $Fr_h > 10$; while as far as the cylinders are concerned for which $Fr_h > 1.6\text{-}1.7$, the values are $Re \sim 10^5$ and $/\bar{p}_{min}/ \sim 2$.

Wadlin's explanations, based on the influence of the free surface on $\bar{p}_{min}$ for submergences of less than two

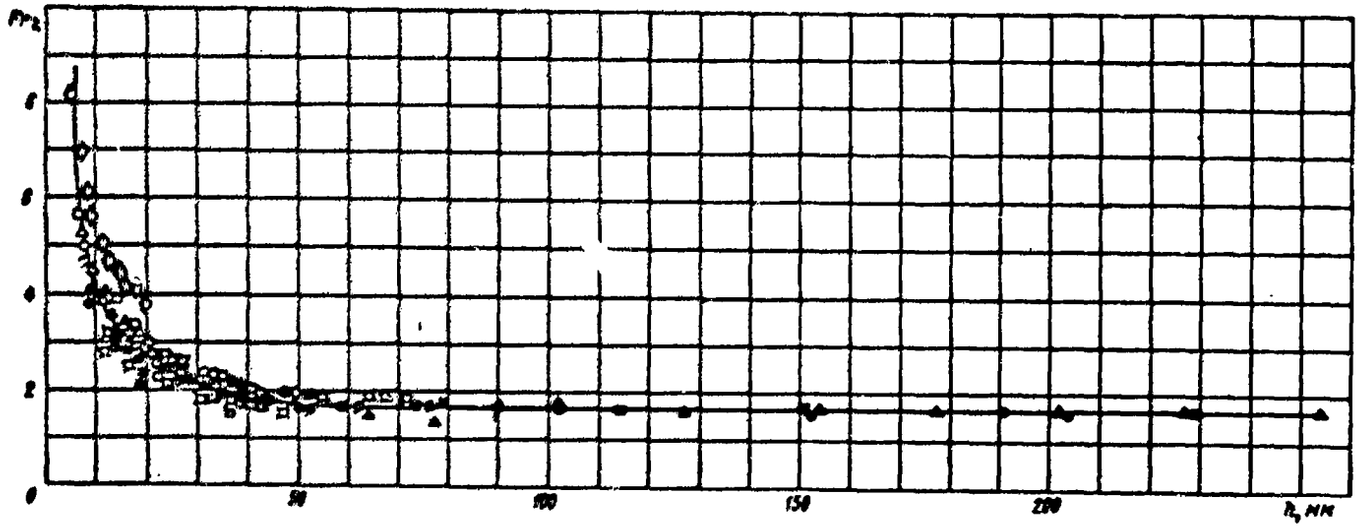

Fig. 84. Graph from the work of Wadlin [86]. Dependence of the Froude number $Fr_h = \frac{v}{\sqrt{gh}}$ on the lower end of a round strut that does not intersect the free surface (for diameter designations see Fig. 82).

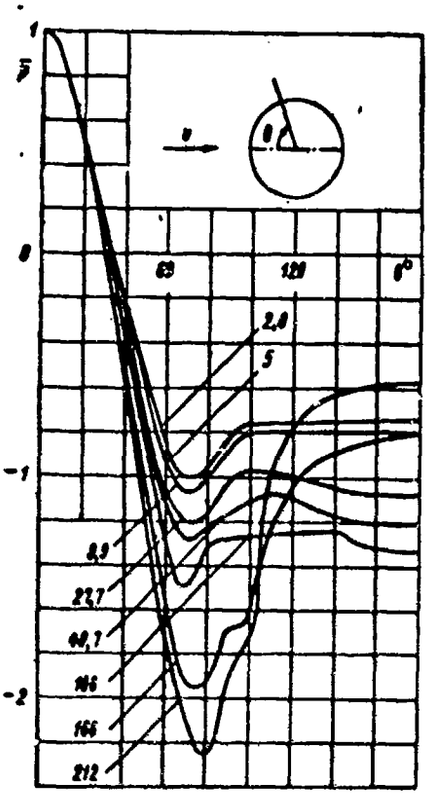

Fig. 85. Distribution of pressure in the cylinder for various values of Re [34]. Re values in thousands are indicated on the curves.

inches, are at least strange, since the effect of the free surface on the pressure near the lower end of the strut must be reflected through the relative submergence which, for thin struts, was sufficiently large (4-20). [166

What are the real causes of air entry, and specifically, the causes that define the character of the dependences shown in Fig. 82?

As in many cited examples, formal adaptation of dimensional theory to the complex phenomenon being studied produces no effect. We can write that the condition for air entry depends on: the diameter of the cylinder d and the depth of its submergence h; the properties of the fluid--density ρ and viscosity ν; the surface tension coefficients at media boundaries σ_{12}, σ_{13}, σ_{23}; the gravitational acceleration g; and on the velocity of motion v [167

$$F(d, h, \rho, \nu, \sigma_{12}, \sigma_{13}, \sigma_{23}, g, v) = 0$$

or, after reducing to dimensionless form and retaining only $\sigma = \sigma_{12}$

$$f\left(\frac{h}{d}, \frac{vd}{\nu}, \frac{v}{\sqrt{gd}}, \frac{\sigma}{\rho v^2 d}\right) = 0.$$

Four independent terms also require for their analysis an extensive number of experiments, a part of which was conducted in [88]. In order to obtain effective results the phenomenon must be subdivided into elements and additional considerations should be utilized.

Let us first examine a more simple case for cylinders with large diameters, with respect to which we can expect that the role played by viscosity and surface tension will be negligibly small. For this type of cylinder, according to the observations, the cavity gradually deepens proportionally to the increase of the velocity (Fig. 86), and

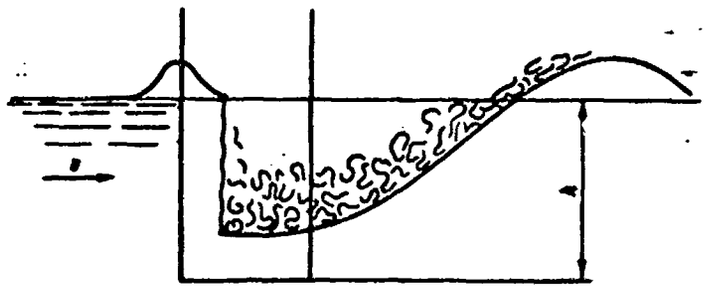

Fig. 86. Schematic diagram of cavity formation for flow around a round cylinder of large diameter intersecting the water surface. The lower part of the cavity is filled with foam.

finally, at a certain critical velocity, approaches the lower end of the cylinder. However, the regimes of flow that exist under these conditions, first of all, correspond to the conditions not of continuous, but of stream cavitation flow, and secondly, they are essentially related to the three-dimensional character of flow around the end of the cylinder.

Just as for all supercavitating flows, in this case too it should be considered that the motion regime virtually does not depend on the Reynolds number, and for the given relative submergence the critical value of Fr_h = = const must remain for any practical values of $Re > 5 \cdot 10^3$ (for smaller values of Re the flow can change slightly at the front part of the cylinder). In the first approximation* for qualitative analysis we can compare the phenome-

*The inaccuracy of such an approximation is due, firstly, to the fact that the values $Fr_d = v/gd$ are not small enough to replace the liquid surface with a solid wall, and secondly to the fact that the cavitation number is different at different flat cross sections.

non being considered to the cavitation flow around the end of a cylinder with a length of 2h/d for the cavitation number

$$\sigma = \frac{p_0 - p_n}{\frac{\rho v^2}{2}} = \frac{(p_0 + \gamma h) - p_n}{\frac{\rho v^2}{2}} = 2\frac{gh}{v^2} = \frac{2}{Fr_h^2}. \qquad (5.57)$$

where p_a is the atmospheric pressure; $\gamma = \rho g$ is the specific weight.

The critical value of $\varkappa_{kp}$ and the corresponding value of Fr_h will belong to the transitional regime from the initial cavitational state to the supercavitating condition. With a decrease of $\bar{h} = h/d$ the value $\varkappa_{kp}$ decreases and, therefore, $(Fr_h)_{kp}$ increases. In general $\varkappa_{kp} = f(\bar{h})$.

For large length-to-diameter ratios of the cylinder the flow around its end becomes independent of this ratio and $(Fr_h)_{kp}$ remains virtually constant. If the diameter of the cylinder is small, the surface tension forces are equivalent to the increase in external pressure. Considering that in its initial state the cavity which has enveloped the body does not yet substantially exceed the body dimensions and the radii of the cavity's boundary curvatures have the order of the radius of the cylinder*, we will find

---

*Generally speaking, a correction multiplier should be introduced, and instead of the $2\sigma/R$ term the value $m2\sigma/R$ should be used; correspondingly, $8m\sigma/\rho v^2 d$ should be used instead of $8\sigma/\rho v^2 d$.

---

that the exposure of the entire strut will correspond to the condition where

$$\varkappa_{kp} > \frac{p_0 + \gamma h + \frac{2\sigma}{R} - p_a}{\frac{\rho v^2}{2}} = \frac{2}{Fr_h^2} + \frac{8\sigma}{\rho v^2 d}. \qquad (5.58)$$

from where, after some simple transformations, we find

$$(Fr_d)_1 \geqslant \sqrt{\frac{2 + \frac{8\sigma}{\gamma d^2}\frac{1}{\bar{h}}}{\varkappa}} \qquad (5.59)$$

or

$$(Fr_d)_1 \geqslant \sqrt{\frac{2\bar{h} + \frac{8\sigma}{\gamma d^2}}{\varkappa_{kp}}}. \qquad (5.60)$$

Thus, we have found the expressions $(Fr_h)_1$ and $(Fr_d)_1$ for which the cavity formed behind the cylinder reaches its lower point.

Until now we have analyzed the conditions of equilibrium of the cavity already formed behind the strut in the region of its submerged end. Let us look now at the conditions under which such a cavity begins to form near the free surface. In the middle portion of the strut and behind it a region of vacuum exists, which at a certain point of the cylinder's surface may be characterized by the coefficient $\bar{p}$. Obviously, $\bar{p}$ depends on the dimensionless coordinates of the point θ and y/d, relative submergence of the cylinder $\bar{h}$, and also on the Froude number $Fr_d = v/\sqrt{gd}$ and Reynolds number $Re = vd/\nu$. At the locations of the greatest vacuum [169

$$\bar{p}_{min} = f(\bar{h}, Fr_d, Re). \qquad (5.61)$$

Let us note that $\bar{p}_{min}$ has nothing in common with $\varkappa_{kp}$.

The presence of vacuum will cause a drop of the water level and the inception of cavity formation behind the cylinder in the region of the free surface. Let us examine in more detail the shape of the free surface near the wall of the cylinder. If the boundary were to coincide with the fluid at rest, then, depending on whether the material of the cylinder walls gets wetted or not, the contour of the boundary would have the shape shown in Fig. 87a or b, respectively.

Equilibrium under conditions of a moving fluid will of course exist with another form of boundaries; however, it can be expected that at a small distance from the wall, where the velocities of the particles in the boundary layer are small, the character of the boundary outline shown in Fig. 87a will be preserved. This can be expected with even greater reason in the stagnation zone behind the cylinder.

Figure 87b shows the schematic diagram of a longitudinal section of the bottom of a developing cavity. Since the surface tension forces are directed toward the center of curvature, it follows from Fig. 87a that the capillary forces hinder the formation of a cavity for the case of a wettable wall. Thus, the forces that tend to form the cavity will be proportional to the value $\bar{p}_{min}\frac{\rho v^2}{2}$, while the

[170

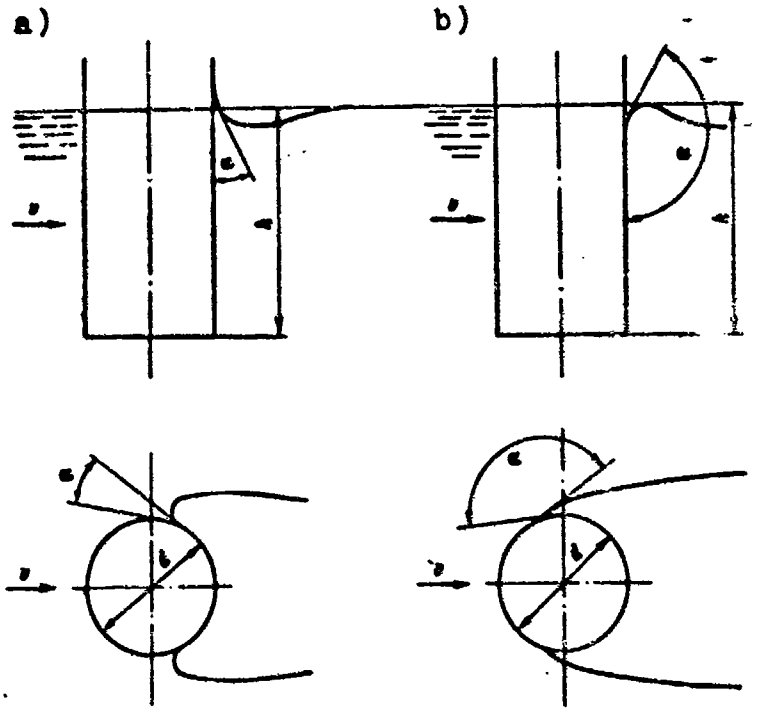

Fig. 87. Longitudinal and cross sections of the incipient cavity near the free surface behind a moving cylinder:
a) wall is wetted, contact angle $\alpha < \frac{\pi}{2}$;
b) wall is not wetted, contact angle $\alpha > \frac{\pi}{2}$.

[169

forces that hinder the cavity, to the value $\sigma\left(\frac{1}{R_1}+\frac{1}{R_2}\right)$, where R_1 and R_2 are the radii of curvature of the deformed fluid surface at the points of its contact with the body.

Assuming the radii of curvature to be proportional to the characteristic linear dimension of the body, i.e., to its diameter*, we can write the relationship for equilibrium

*This assumption would be too strict for this type of conditions under the action of inertia forces only. In this case the shape of the boundaries and, therefore, the radii of curvature of the incipient cavity. depend also on the forces of viscosity which govern the velocities in the boundary layer. The fluid's weight should not be reflected on the critical state of cavity formation, since the ini-

tial deformations may be considered to be small. Thus, we must consider that $R_1 = f_1(\mathrm{Re})d$ and $R_2 = f_2(\mathrm{Re})d$. The greater the value dv/dy in the boundary layer, the smaller the radii of curvature of contours of the free boundary, which, near the wall, where the velocities are close to zero, should form an angle of $\alpha < \pi/2$ with the wall. Since with increase of Re the velocity gradient along the normal increases, the constant must also increase.

---

among the forces acting on the formation of the cavity in the following form: [170

$$\bar{p}_{\min}\frac{\rho v^2}{2} = \mathrm{const}\,\frac{\sigma}{d}. \qquad (5.62)$$

In accordance with the note above, it is more accurate to consider that the constant is a function of Re.

Thus, we see that for wettable struts the regime of cavity inception can be written in the form of the relationship

$$\frac{\rho v^2 d}{\sigma} \geqslant \frac{C(\mathrm{Re})}{\bar{p}_{\min}(\bar{h}, \mathrm{Fr}_d, \mathrm{Re})}. \qquad (5.63)$$

For deep submergences $\bar{h}$ and large Froude numbers Fr_d the right side can be considered only a function of Re.

Expression (5.63) can be transformed into the form [171

$$(\mathrm{Fr}_h)_2 \geqslant \sqrt{\frac{C(\mathrm{Re})}{\bar{p}_{\min}}\frac{\sigma}{\gamma d^2}}\cdot\frac{1}{\bar{h}} \qquad (5.64)$$

or

$$(\mathrm{Fr}_d)_2 \geqslant \sqrt{\frac{C(\mathrm{Re})}{\bar{p}_{\min}}\frac{\sigma}{\gamma d^2}}. \qquad (5.65)$$

Let us sum up some results: if the Froude number values obtained from expressions (5.59) or (5.60) are greater than the ones computed by formulas (5.64) and (5.65), then the regime of strut exposure will be determined by (5.59) and (5.60) only, since the conditions of cavity inception near the surface have been met. In the worst case, i.e., if

$$(\mathrm{Fr}_d)_2 > (\mathrm{Fr}_d)_1 \text{ or } (\mathrm{Fr}_h)_2 > (\mathrm{Fr}_h)_1,$$

the beginning of this regime will be defined only by the relationships (5.64) and (5.65), and as soon as the Froude

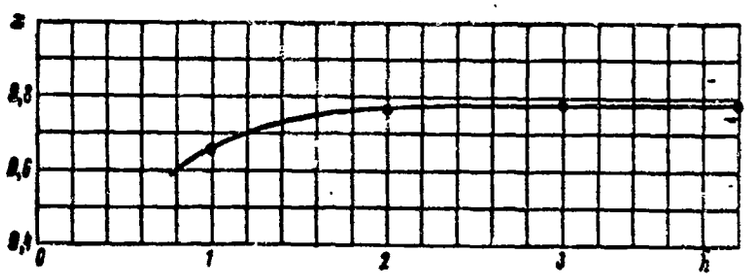

Fig. 88. Dependence of $\varkappa$ on the relative submergence $\bar{h}$ according to processing of data from experiments [88].

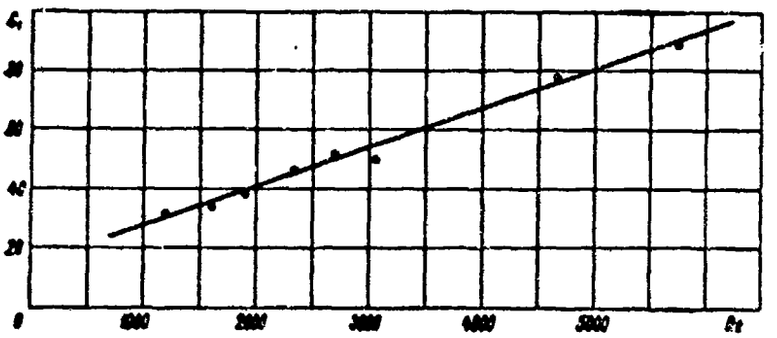

Fig. 89. Dependence of C_1 on the Reynolds number according to processing of data from experiments [88].

numbers reach the proper values exposure will occur immediately along the entire length of the strut. A section of a vertical line will correspond to the regime of entry in coordinates $\bar{h}$ and Fr_d for a constant diameter with accuracy of up to the influence of $\bar{h}$ on $\bar{p}$. [173

The boundary at which calculations based on formulas for $(Fr)_1$ must be replaced by calculations based on formulas for $(Fr)_2$ obviously corresponds to the condition of $(Fr)_1 = (Fr)_2$, from which

$$\bar{h} = \left[\frac{C(Re)}{\bar{p}_{min}} \cdot \frac{\varkappa}{2} - 4\right]\frac{\varkappa}{16}. \qquad (5.66)$$

For the calculations of the regimes of entry obtained in [88] it is necessary to know the two slowly varying dependences $\varkappa_{sp}\left(\frac{h}{d}\right)$ and $C_1(Re) = \frac{C(Re)}{\bar{p}_{min}}$. [174

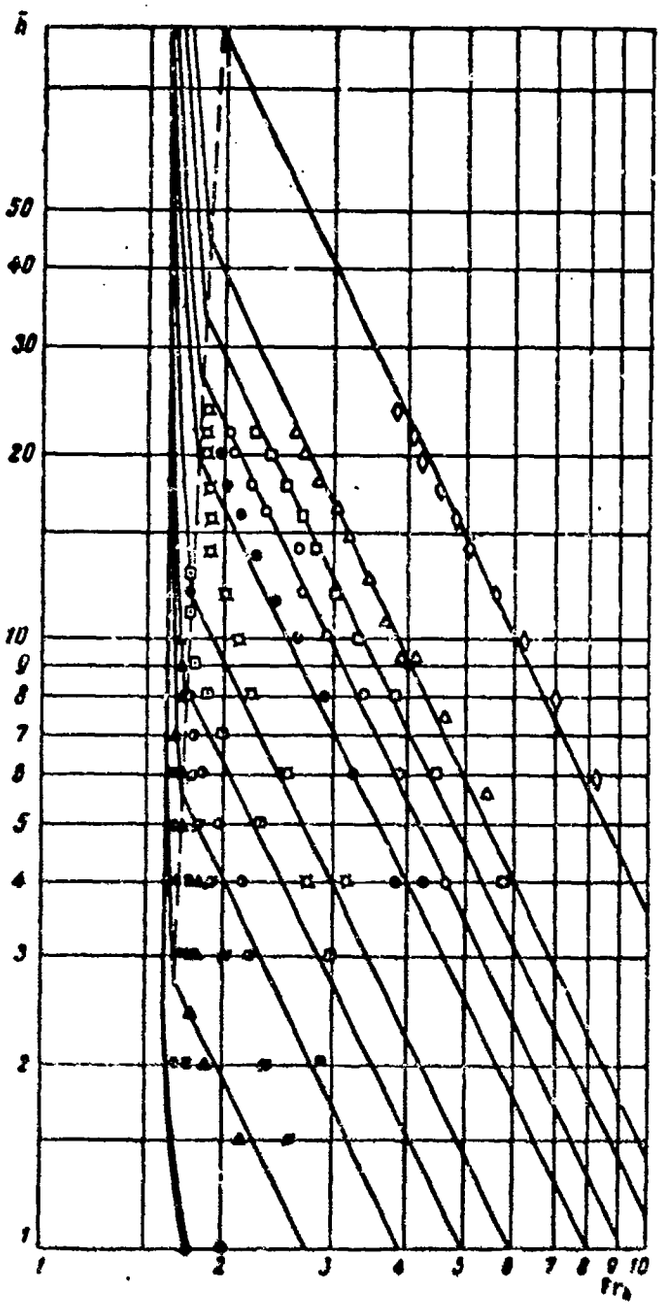

Fig. 90. Comparison of computations of air entry toward the end of round struts intersecting a free surface with experiments [88].
----- computed boundary between the regimes of gradual and sudden entry; ——— computations. Dots represent experimental data. For the designations of diameters see Fig. 82.

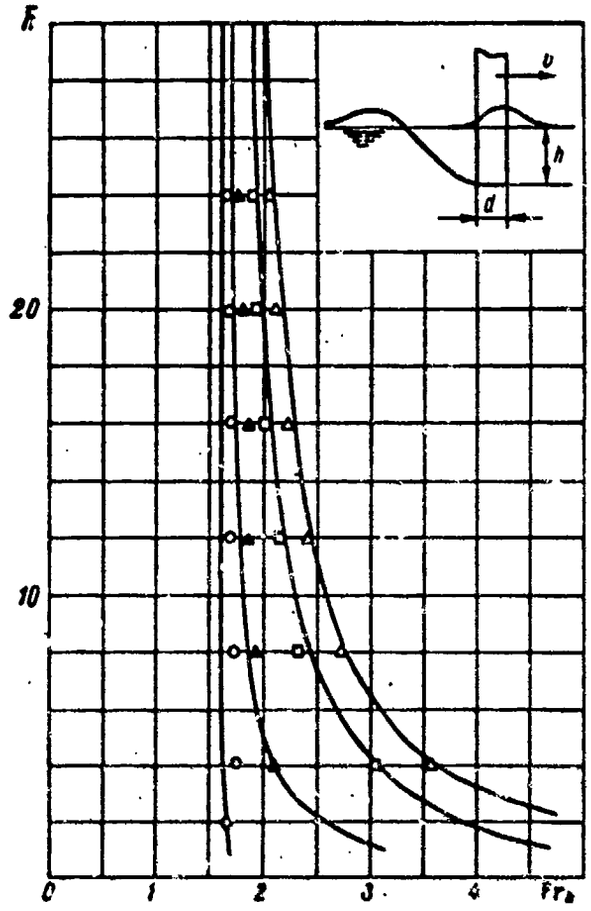

Fig. 91. Comparison of theoretical calculations with experimental data [88] for the regime of air entry toward the ends of circular struts with teflon coating intersecting a free surface. Lines represent values calculated by formula (5.59). Dots are plots of experimental data [88].

Δ - d = 1.32 mm; □ - d = 1.62 mm; ▲ - d = 3.88 mm; o - d = 19.1 mm.

The value of $\chi(\bar{h})$ for large diameters d = 50.8 and d = 34 mm we determine from experimental results [88] according to Fig. 82a and formula (5.59). The function $C_1(Re)$--for small diameters d < 5 mm--can be determined from Fig. 82b and formula (5.65). The relationships

obtained are shown in Figures 88 and 89.

The results of calculations for the regime of air entry from formulas (5.60), (5.65) and (5.66) with determined values of $\varkappa$ and C_1 are given in Fig. 90 (lines). The results of Wetzel's experiments are shown by dots. The close agreement between calculated and experimental data demonstrates the correctness of the above-stated considerations with respect to the nature of the air entry phenomenon and the formulas derived on their basis.

In general, the following phenomena can now be easily explained and evaluated: hysteresis at small struts, independence of the critical Fr_d from the relative submergence for small struts, and the effect of rippling, which disrupts the above-described stabilizing action of surface tension forces at the free surface.

The suggested computations are in agreement with experiments in which struts coated with teflon were examined. With nonwettable material the above-described phenomena which hinder cavity formation at the free surface do not occur and the calculations should be conducted only using formulas (5.59) or (5.60). The comparison of theoretical computations with experimental results for teflon struts is shown in Fig. 91.

The qualitative aspect of the suggested explanations of air entry to round struts also applies to profiled struts.

CHAPTER VI. CONCERNING SIMULATION OF CERTAIN PROBLEMS RELATED TO AIR-CUSHION MOTION

At the present time air-cushion vehicles (ACV) are still in the formative stage; nevertheless, there are many types and shapes of such vehicles. This is particularly related to the fact that by their principles of motion and areas of application they are at the junction of land, water and air transport.

In a number of cases it is difficult to determine whether a certain type of vehicle is ship, airplane, automobile or flying platform. A review of the various types of air-cushion devices can be found in [26].

Regardless of the design of the ACV, we will always encounter the problem of the interaction of gaseous streams with the water surface. The velocities of the gas under a chamber type vehicle are very small, and gas streams develop only in the area of outflow around the perimeter of the cushion. Nozzle type vehicles feature the direct action of slit gas streams on water, while in flying platform vehicles this action takes place practically under the entire vehicle. [17

Some aspects of the simulation of phenomena connected with the hovering of craft above water, with the escape of gas streams and their interaction with the water surface are analyzed in the first three sections of this chapter. The fourth section is devoted to simulation of flexible enclosures [skirts].

6.1. Calculation of the Regime of Hovering Above Water for a Device with the Chamber Type of Air Cushion

Let us analyze the steady-state condition of hovering above a solid screen of an ACV with the chamber system. The regime is well defined by the geometry of the craft, which in turn is defined by the linear dimensions l, l_1, ..., l_n, by excess subdome pressure Δp, by air density ρ' and by the position of the craft relative to the screen. Let us consider that the plane passing through the lower edge of the craft's dome is parallel to the screen; then the position of the craft will be defined by the hovering height, i.e., by the distance h from this plane to the screen. All other characteristics of the regime--air consumption Q, power used N, lifting force Y--will be functions of

$$l, l_1, \ldots, l_n, \rho', \Delta p, h. \qquad (6.1)$$

Since from the terms of (6.1) we can form only dimensionless combinations in the form

$$\frac{l_1}{l}, \ldots, \frac{l_n}{l}, \frac{h}{l}, \tag{6.2}$$

then for all geometrically similar craft all the dimensionless characteristics will become functions of h/l. Specifically, denoting the consumption of the gas refered to the perimeter by Q_1 we will obtain by employing ordinary methods

$$\frac{Q_1}{h}\sqrt{\frac{\rho'}{\Delta p}} = f\left(\frac{h}{l}\right). \tag{6.3}$$

In the case of a two-dimensional problem, when the dimensions of the craft are sufficiently large as compared to the area of gas outflow from under the edge of the dome, it is not possible to select a characteristic dimension l, and the dimensionless combination containing Q_1 must be a constant or a function of the angle of wall inclination θ, since from the terms remaining in (6.1)--ρ', Δp and h--it is not possible to form a dimensionless quantity. Thus,

$$\frac{Q_1}{h}\sqrt{\frac{\rho'}{\Delta p}} = f(\theta) \tag{6.4}$$

and

$$Q_1 = f(\theta) h \sqrt{\frac{\Delta p}{\rho'}} \quad \text{or} \quad h = \frac{Q_1}{f(\theta)}\sqrt{\frac{\rho'}{\Delta p}}. \tag{6.5}$$

The value $f(\theta)$ can be expressed through the so-called coefficient of pressure increase Ψ. Applying Bernoulli's equation to the two points A and B of the stream flowing out from under the dome (Fig. 92), we will find the velocity of the stream at point B: $v_B = \sqrt{\frac{2\Delta p}{\rho'}}$; designating the width of the stream by Ψh we will obtain the amount of consumption Q_1 in the form

$$Q_1 = \psi h v_B = \psi \sqrt{2} h \sqrt{\frac{\Delta p}{\rho'}}, \tag{6.6}$$

i.e.,

$$f(\theta) = \psi\sqrt{2}. \tag{6.7}$$

If the craft is hovering above the fluid surface,

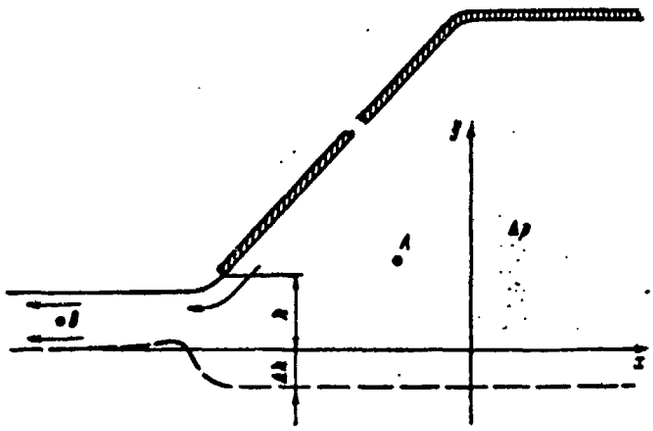

Fig. 92. Diagram for calculating the hovering height of a chamber-type ACV.

then the latter deflects under the craft to the distance

$$\Delta h = -\frac{\Delta p}{\gamma} \tag{6.8}$$

(Fig. 92) and the number of determining parameters will increase by the value γ, i.e., it will be

$$\rho', \Delta p, h, \gamma. \tag{6.9}$$

Now the coefficient of consumption formulated as

$$\bar{Q}_1 = Q_1 \gamma \sqrt{\frac{\rho'}{\Delta p^3}}, \tag{6.10}$$

will be a function of a single dimensionless value which can be formed from (6.9), i.e., from

$$\bar{h} = \frac{\gamma h}{\Delta p}. \tag{6.11}$$

It is not difficult to determine the character of the dependence of $\bar{Q}_1(\bar{h})$. It is more convenient to analyze the reversed dependence, i.e., $\bar{h}(\bar{Q}_1)$. Without disturbing the commonality of discourse, let us assume that the values γ, Δp, ρ' are fixed; then a small gap between the water surface and the edge of the dome will also correspond to very small consumptions Q_1, i.e. $h \to \Delta h = -\Delta p/\gamma$. Also, according to (6.11) $\bar{h} = -1$. The limiting case of large $\bar{Q}_1$ can

be analyzed as an increase of γ with constant Q_1, ρ' and Δp. Obviously, by increasing the value γ for a given Δp we will decrease the deflection of the free surface which, in the extreme case, will not be different from a solid screen, where the relationship between h and Q_1 is expressed by (6.6). According to (6.6), (6.10) and (6.11), we find that for large values of $\bar{Q}_1$

$$\bar{h} = \frac{1}{\psi\sqrt{2}}\bar{Q}_1, \tag{6.12}$$

i.e., the relationship $\bar{h}(\bar{Q}_1)$ will be asymptotic and will approach a straight line coming out of the origin of coordinates at an angle whose tangent is equal to $1/\sqrt{2}\psi$ and, as has been mentioned before, passing through the point $\bar{Q}_1 = 0$, $\bar{h} = -1$. In Figures 93-95 experimental results are presented concerning the relationships $\bar{h}(\bar{Q}_1)$, obtained by K. V. Zharinov, for $\theta = 45^\circ$, $\theta = 90^\circ$, $\theta = 135^\circ$ and various Δp. In the same figures there is a straight line plotted by formula (6.12) for a stiff screen; in the computations of this line the value Ψ is taken as a dependence on θ in correspondance with known data from theoretical evaluations [11].

For computations of the dependence $\bar{h}(\bar{Q}_1)$ the following semi-empirical formula can be suggested:

$$\bar{h} = \frac{1}{\psi\sqrt{2}}\bar{Q}_1 - \frac{1,5}{\bar{Q}_1 + 1,5}, \tag{6.13}$$

which satisfies the condition $\bar{h} = -1$ with $\bar{Q}_1 = 0$ and the asymptotic approach to (6.12), and which is basically in agreement with Zharinov's experiments (see dotted line in Fig. 93-95). Since the dimensions of ACVs are large with respect to the region of outflow, then by subdividing the perimeter of the craft into sections and by adopting the results of the two-dimensional problem to each of them, we will find that for the actual chamber-type craft it is sufficient, in the first approximation (for the evaluation of consumption Q), to multiply the consumption Q_1 by the perimeter of the dome Π, i.e., in accordance with (6.10)

$$Q = \bar{Q}_1\sqrt{\frac{\Delta p}{\rho}}\frac{\Pi\Delta p}{\gamma}. \tag{6.14}$$

[178

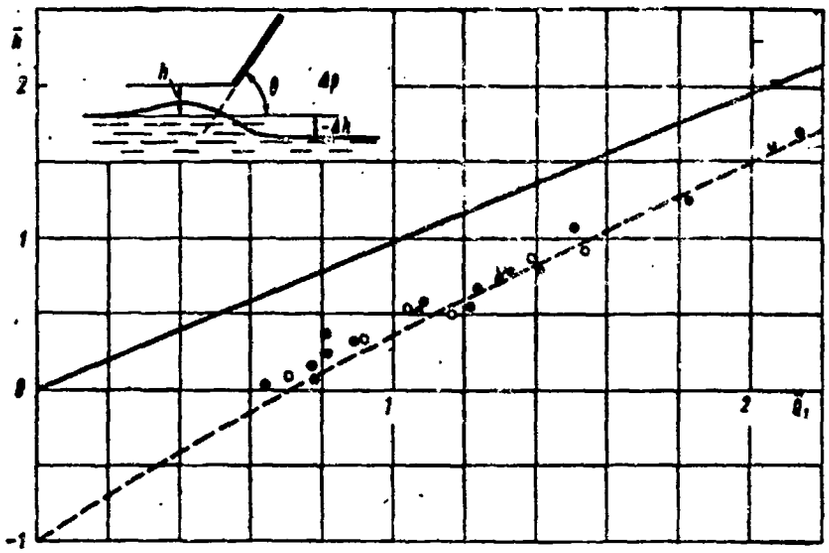

Fig. 93. Dependence of the dimensionless distance from the craft to the undisturbed water surface $\bar{h}=\frac{\gamma h}{\Delta p}$ on the dimensionless consumption $\bar{Q}_1=Q_1\sqrt{\frac{\rho'}{\Delta p^3}}$, $\theta=45°$. ——— dependence $\bar{h}(\bar{Q}_1)$ for a stiff screen; ------ theoretical computations by formula (6.13).

[179

The lifting force Y will obviously be equal to the product of the cushion area and the Δp value

$$Y = S\Delta p. \tag{6.15}$$

The power expended for suspension of the craft is

$$N = Q\Delta p. \tag{6.16}$$

The problem of spray formation is far more complex, even in a two-dimensional case. Due to tangential stresses the surface layer of the fluid becomes deformed, moves and disintegrates; the gaseous stream carrying away the wet particles forms the spray. It is no longer possible to disregard the fluid motion and the viscous and capillary stresses, and therefore instead of (6.9) we must write

$$\rho', \Delta p, h, \rho, g, \nu, \sigma, v'. \tag{6.17}$$

For analysis of a craft under the conditions of motion with velocity v, it is necessary, in addition to parameters

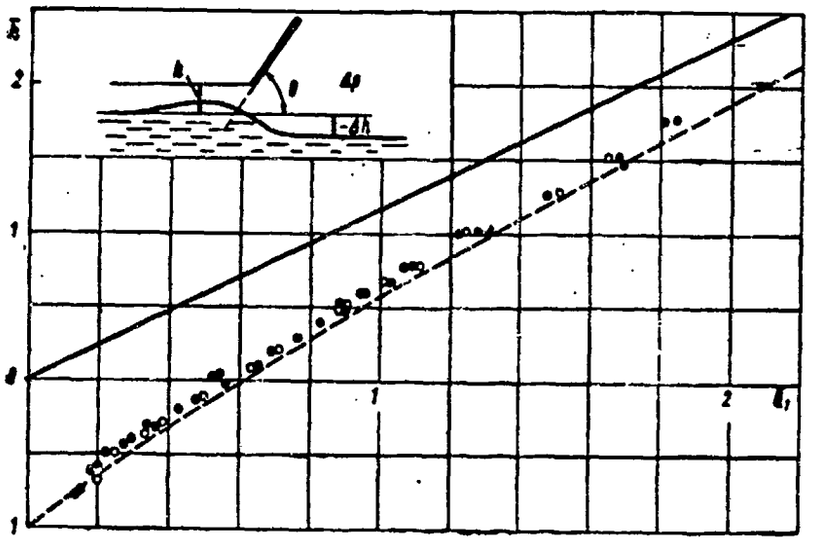

Fig. 94. Dependence of the dimensionless distance from the craft to the undisturbed water surface $\bar{h}=\frac{\gamma h}{\Delta p}$ on the dimensionless consumption $\bar{Q}_1=Q_{11}\sqrt{\frac{\rho'}{\Delta p^3}}$. $\theta=90°$. ——— dependence $\bar{h}(\bar{Q}_1)$ for a stiff screen; ------ theoretical computations by formula (6.13).

(6.17), to use the value of velocity v and the linear values $l, l_1, \ldots, l_n$, which characterize its shape and dimensions. For geometrically similar craft the following system of defining dimensionless parameters, for example, can be written

$$\frac{Q}{l^2}\sqrt{\frac{\rho'}{\Delta p}};\ \frac{\Delta p}{\gamma l};\ \frac{Q}{vl};\ \frac{\rho'}{\rho};\ \frac{\nu'}{\nu};\ \frac{\rho' Q^2}{\sigma l^3};\ \frac{v}{\sqrt{gl}}. \qquad (6.18)$$

6.2. Submerged Streams

Let us analyze the steady-state, two-dimensional or axisymmetrical stream of viscous, incompressible fluid flowing out from an opening of infinitely small width (from the pole) into a boundless region filled with the same fluid. Far from this jet the fluid is at rest. The mechanism of stream formation consists of the fact that escaping particles move through inertia, but are gradually slowed by the forces of friction with the surrounding fluid.

[179

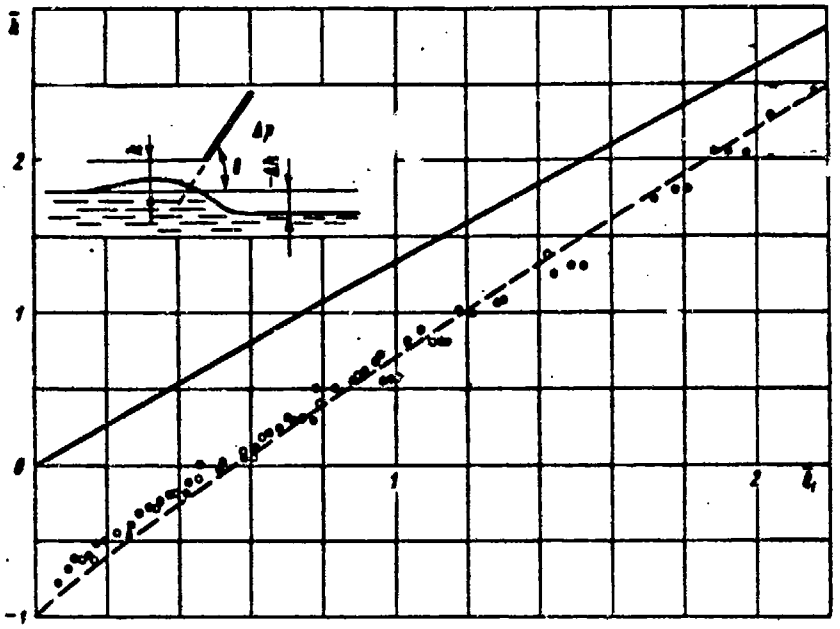

Fig. 95. Dependence of the dimensionless distance from the craft to the undisturbed water surface $\bar{h}=\frac{\gamma h}{\Delta p}$ on the dimensionless consumption $\bar{Q}_1=Q_1\gamma\sqrt{\frac{\rho'}{\Delta p^3}}$, $\theta=135°$. ——— dependence $\bar{h}(\bar{Q}_1)$ for a stiff screen; ------ theoretical computations by formula (6.13).

[180

Due to these friction forces, the particles of the surrounding fluid accelerate and become drawn into the stream, as a result of which the stream's mass increases with increase of the distance from the opening. A schematic representation of the submerged stream is shown in Fig. 96.

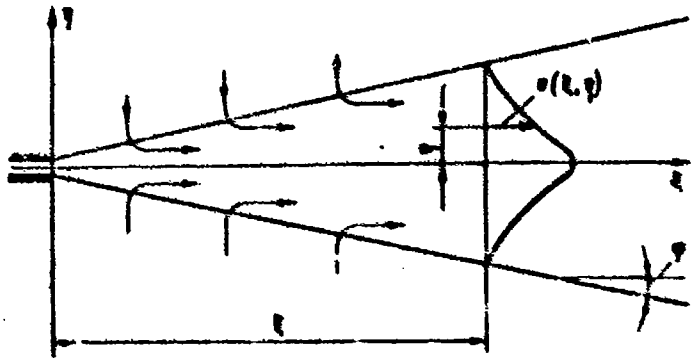

Fig. 96. Schematic diagram for evaluating a submerged stream.

We will consider that in spite of the infinitely small dimensions of the opening, a second's pulse I of the escaping stream remains finite. The velocity of the fluid particles at a certain point of the stream will depend, obviously, on the coordinates ξ and η of this point (see Fig. 96), on the magnitude of the pulse I and on the fluid's properties, which can, according to what we've said, be defined by the values of its density ρ and viscosity ν. Thus, we can write that

$$v = F(\xi, \eta, I, \rho, \nu). \tag{6.19}$$

Transforming into the dimensionless form, instead of (6.19) for the axisymmetric stream we obtain

$$v\sqrt{\frac{\rho}{I}} = f_1\left(\frac{\eta}{\xi}, \frac{I}{\rho\nu^2}\right), \tag{6.20}$$

from which [181

$$v = \frac{1}{\xi}\sqrt{\frac{I}{\rho}} f\left(\frac{\eta}{\xi}, \frac{I}{\rho\nu^2}\right). \tag{6.21}$$

In particular, it follows from (6.21) that for the given stream, i.e., for fixed values I/ρ and ν, the velocity at the axis of the stream ($\eta = 0$) varies in inverse proportion to the distance ξ from the opening (pole).

According to (6.21) the value

$$\frac{v(\xi, \eta)}{v(\xi, 0)} = \frac{f_1\left(\frac{\eta}{\xi}, \frac{I}{\rho\nu^2}\right)}{f_1\left(0, \frac{I}{\rho\nu^2}\right)}, \tag{6.22}$$

i.e., the ratio $v(\xi, \eta)/v(\xi, 0)$ with fixed $I/\rho\nu^2$, is determined by the ratio η/ξ only, and, thus, the geometric locus of points where the velocity is a definite portion of the velocity on the axis is formed by the rays $\eta/\xi = k = \text{const}$ emerging from the pole.

If we plot $v(\xi, \eta)/v(\xi, 0)$ along the ordinate axis and the relationship η/ξ along the abscissa axis, we can consider the graph obtained as the velocity profile at the cross section of the stream with the plane $\xi = \text{const}$. This profile, as shown by (6.22), will be universal for all ξ. It is common practice to plot along the abscissa axis instead of η/ξ a value η/η_0 proportional to it, where η_0 is the value at the points $v(\xi, \eta)/v(\xi, 0) = 0.5$.

Note: Dividing the numerator and the denominator of the relationship η/η_0 by ξ, we obtain

$$\frac{\eta}{\eta_0} = \frac{\eta/\xi}{\eta_0/\xi} = \frac{1}{k_0} \cdot \frac{\eta}{\xi}, \qquad (6.23)$$

where $k_0 = \eta_0/\xi$ is the tangent of the angle formed by the stream's axis and the ray passing through the points $v(\xi, \eta)/v(\xi, 0) = 0.5$.

For turbulent streams the tangential stresses in the fluid are determined by the turbulent agitation, and the parameter $I/\rho\nu^2$ becomes unimportant and must be excluded from equations (6.20)-(6.22).

In the case of the two-dimensional problem, the stream will be characterized by the pulse I_1 per unit length of of the opening. In accordance with this, instead of (6.20) we will obtain

$$v\sqrt{\frac{\rho}{I_1\xi}} = f_0\left(\frac{\eta}{\xi}, \frac{I_1\xi}{\rho\nu^2}\right). \qquad (6.24)$$

For turbulent streams we can drop the second term of the function f_2. Then

$$v = \frac{1}{\sqrt{\xi}}\sqrt{\frac{I_1}{\rho}} f_0\left(\frac{\eta}{\xi}\right). \qquad (6.25)$$

i.e., in the case of the two-dimensional flow the velocities along the rays η/ξ = const decrease in inverse proportion to the square root of the distance to the pole, and not in inverse proportion to the distance, as was the case for the axisymmetrical stream [formula (6.21)]. [182

For the two-dimensional turbulent stream, obviously, a relationship analogous to (6.22) takes place:

$$\frac{v(\xi, \eta)}{v(\xi, 0)} = f\left(\frac{\eta}{\xi}\right); \qquad (6.26)$$

the term η/ξ is also usually replaced by the proportional quantity $\frac{\eta}{\eta_0}$, which has the same meaning as in the three-

dimensional case. Figures 97 and 98 show experimental data from [84] and [75] which characterize the velocity fields of two-dimensional and axisymmetric streams. Based on the same data, the dependences [18

$$\frac{v(\xi, \eta)}{v(\xi, 0)} = f\left(\frac{\eta}{\eta_0}\right). \qquad (5.27)$$

are plotted in Figures 99 and 100.

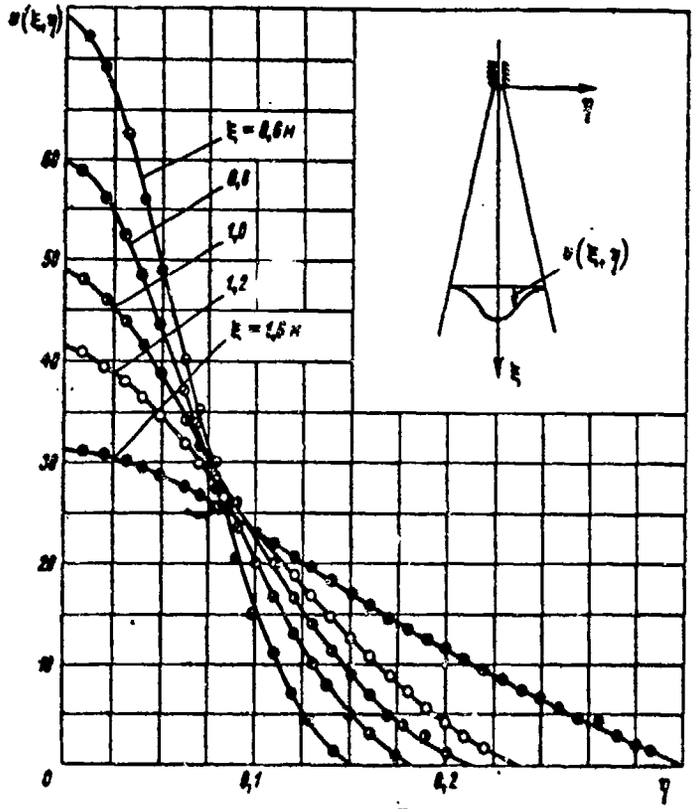

Fig. 97. Test data [75] concerning the velocity field in an axisymmetric submerged stream.

Thus, the law of self-similar stream expansion, universal for all cross sections, which was derived from the theory of dimensional analysis, is well supported by experimentation. [1

The experimental data are also in close agreement with the derived laws of decrease of axial velocity $v(\xi, 0)$ at increased distance from the pole. The width of streams, analagously to the thickness of the boundary layer, cannot

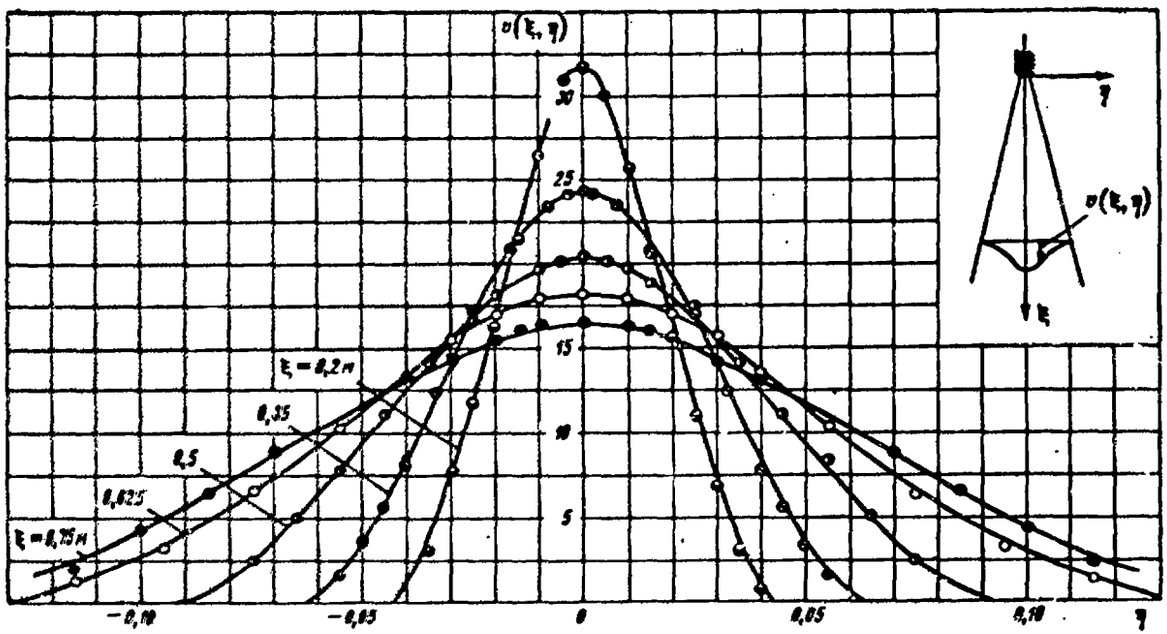

Fig. 98. Test data [84] concerning the velocity field of a two-dimensional submerged stream.

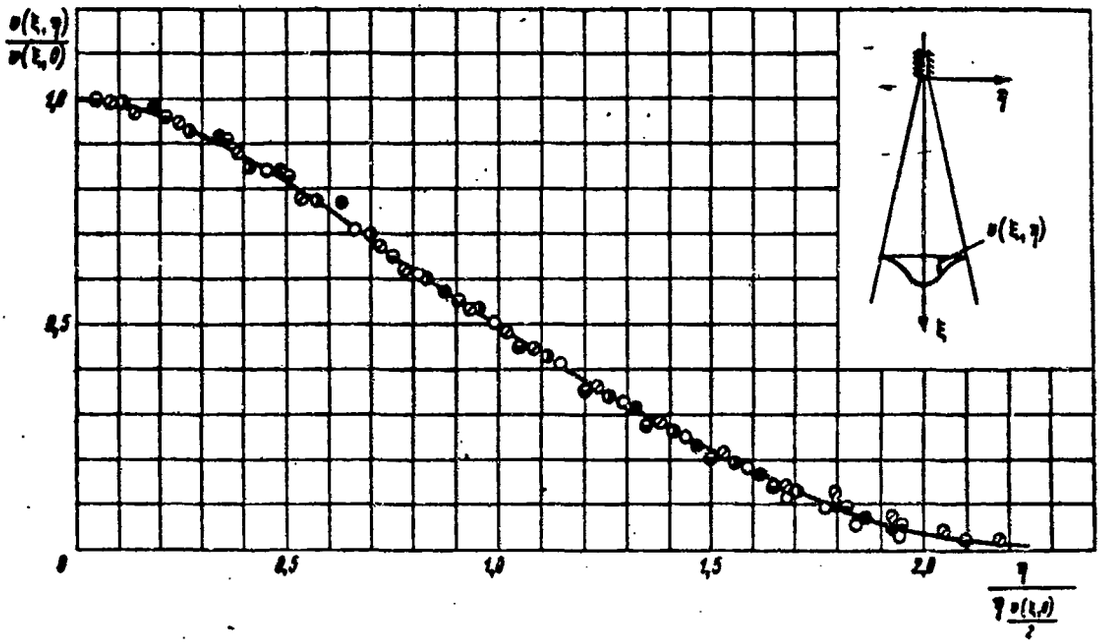

Fig. 99. A universal profile of velocities in an axisymmetric submerged stream, based on the data of Fig. 97.

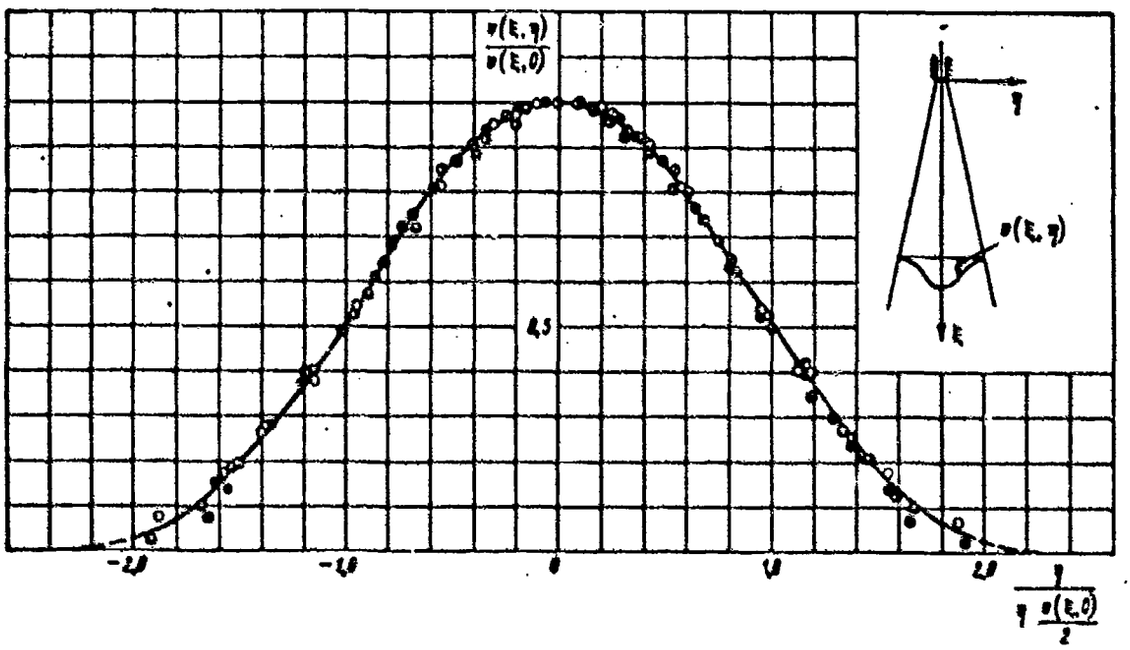

Fig. 100. A universal profile of velocities in a two-dimensional submerged stream based on the data of Fig. 98.

be determined precisely, since the velocity decreases asymptotically to zero at greater distances from the axis. If we use the data of Fig. 97 and 98 and adopt the character of universal relationships $f(\frac{\eta}{\eta_0})$ as it is in Figures 99 and 100, then the values k_0 and the tangents of the angle of inclination φ of the stream boundaries will be $k_0 \approx 0.1$, $\tan \varphi \approx 0.224$ for two-dimensional, axisymmetric streams.

6.3. On the Cavity Formed on the Surface of a Fluid Under the Action of a Vertical Gaseous Stream

For certain types of ACVs, as well as for other technical applications, the question of the cavity formed on a fluid's surface under the action of a vertical gaseous stream is of great interest.

Experiments show that with low-velocity heads of the gaseous stream and with great distances from the nozzle to the surface, a smooth, sloping cavity emerges, surrounded by a slight ring-shaped elevation. With an increase in the velocity head, all other conditions being equal, the cavity becomes deeper, a system of spreading ring-shaped waves develops on the surface, and then foam is formed on the bottom of the cavity, with spray flying out from its periphery. Figure 101 shows photographs of cavities obtained at various velocities of the gas stream. They represent an instantaneous picture, because actually the cavity is pulsating all the time, and its average shape and dimensions, which are of interest for practical applications, can be obtained by photography with a prolonged exposure. Figure 102 has several pictures of a cavity under constant conditions of the gas stream, but with short and long exposure.

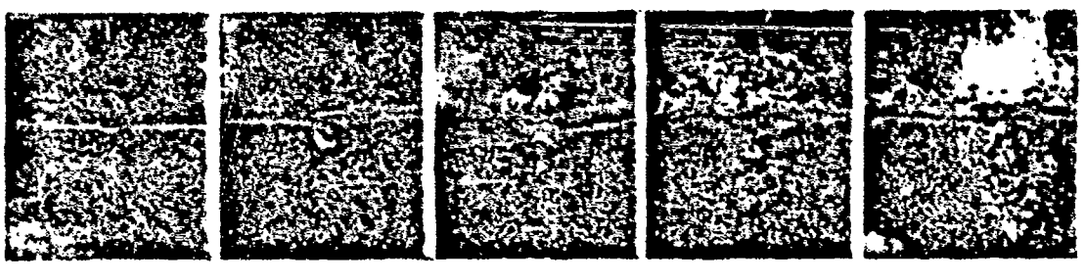

Fig. 101. Photographs of a deformed water surface under the action of a vertical gas stream. Nozzle diameter d_0 = 6 mm; distance of the nozzle from the surface l_1 = = 40 mm. Gas velocities at nozzle cutoff (from left to right): v_0 = 12.6, 25.2, 40, 69.4 and 86.7 m/sec.

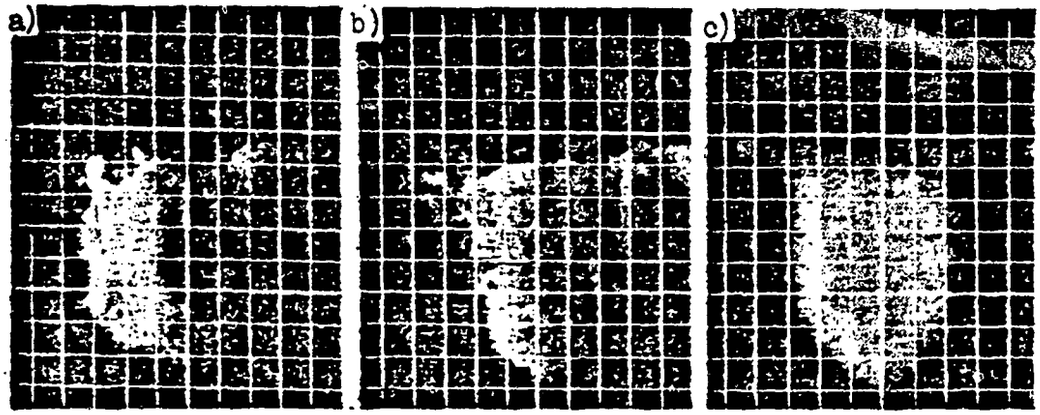

Fig. 102. Photographs of a cavity developing under the action of a vertical gas stream (d_0 = 12 mm, ξ_1 = 24 mm, v_0 = 74 m/sec): a) and b) two instantaneous photographs; c) photograph with an exposure of 15 seconds which enables us to determine the averaged contour of the cavity.

Let us analyze the problem of determining the dimensions of a cavity formed under the action of a vertical gas stream which is discharged at velocity v_0 from a nozzle with diameter d_0 suspended at a distance ξ_1 from the free surface. [186

In the process of solving this problem, it becomes possible to clearly illustrate the dependence of the effectiveness of results on the approach and on the utilization of certain simple physical concepts and experimental factors. Let us first apply general concepts of the theory of dimensional analysis and describe the factors which can take part in our problem. [188

It is obvious that among the values which have an influence, for example, on the depth of the cavity y_1, are primarily the parameters of the gas stream, defined by the physical properties of the ejected gas--its density ρ', viscosity ν' and temperature T', and also the diameter of the nozzle d_0, its profile and the characteristic velocity v_0 at the cutoff of the nozzle*.

*It is assumed that the law of distribution across the cross section of velocities and temperatures at the nozzle's cutoff is given.

Furthermore, before the gas stream has any effect on the fluid, it will become deformed as a result of interaction with the layer of gas located between the nozzle cutoff and the fluid. Therefore, among our parameters we must include the thickness of this layer, i.e., the distance ξ_1 from the nozzle to the water surface, and its physical properties: density ρ'', viscosity ν'' and temperature T''. The physical properties and the dimensions of the fluid medium must be indicated: its density ρ, viscosity ν, temperature T, the surface tension coefficient at the boundary between the fluid and the gas σ, the shape and overall dimensions of the container with the fluid, and, finally, the acceleration of gravity g. Thus,

$$y_1 = F(d_0, \xi_1, l_1, \ldots, l_n, v_0, \nu, \nu', \nu'', \rho, \rho', \rho'', T, T', T'', \sigma, g). \quad (6.28)$$

Here, $l_1, \ldots, l_n$ are the linear dimensions which define the shape of the nozzle and the container, as well as the dimensions of the latter.

In addition, if the temperature is expressed in independent units (degrees) it is necessary to introduce the gas constant or Boltzmann's constant into the parameters. Transformation to dimensionless values will reduce the number of parameters by four, but even then the number of them will remain n + 12, so the problem remains immense for practical purposes.

Let us simplify its formulation by employing additional assumptions. Let us assume that it is not necessary to consider compressibility, that the temperatures of all the media are the same, and that the stream is surrounded by gas with the same properties; then instead of (6.28) we can write

$$y_1 = F(d_0, \xi_1, l_1, \ldots, l_n, v_0, \nu, \nu', \rho, \rho', \sigma, g). \quad (6.29)$$

Experiments [69] have shown that for a wide range of limits the bottom and the walls of the container virtually are not reflected in the dimensions of the cavity (Fig. 103), which is explained by the almost completely undisturbed condition of the fluid, in which only weak circulation currents develop. Noticeable velocities are present only along the boundaries of the cavity and are directed along the tangent to its contour.

The described condition is illustrated by photographs made by the author, in which suspended particles introduced into the fluid are rendered in the form of dashes. The

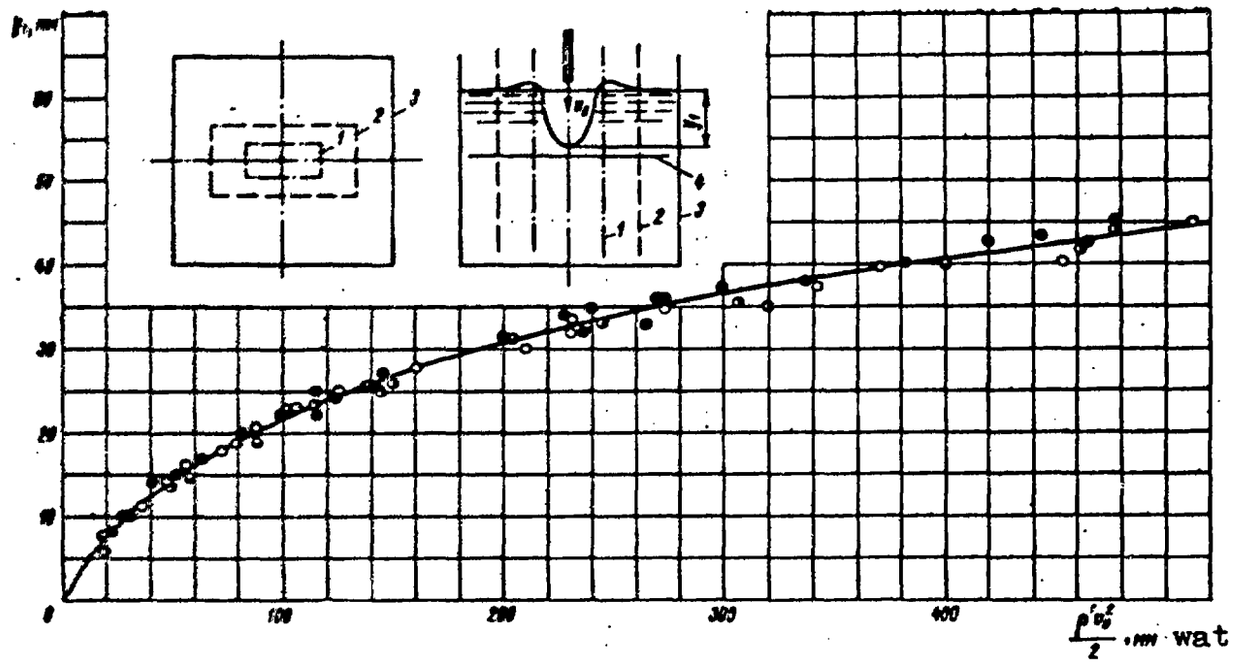

Fig. 103. Effect of the bottom and walls of a container on the depth of the cavity (d_0 = 3 mm).
● - 1 (container 50 x 25 mm); o - 2 (container 100 x 50 mm); ● - 3 (container 150 x 150 mm); ● - 4 (bottom of containers at depth of 46 mm).

length of these dashes is proportional to the velocity of the particles and the length of exposure. In Fig. 104 examples are shown of this type of photograph. [190

[191

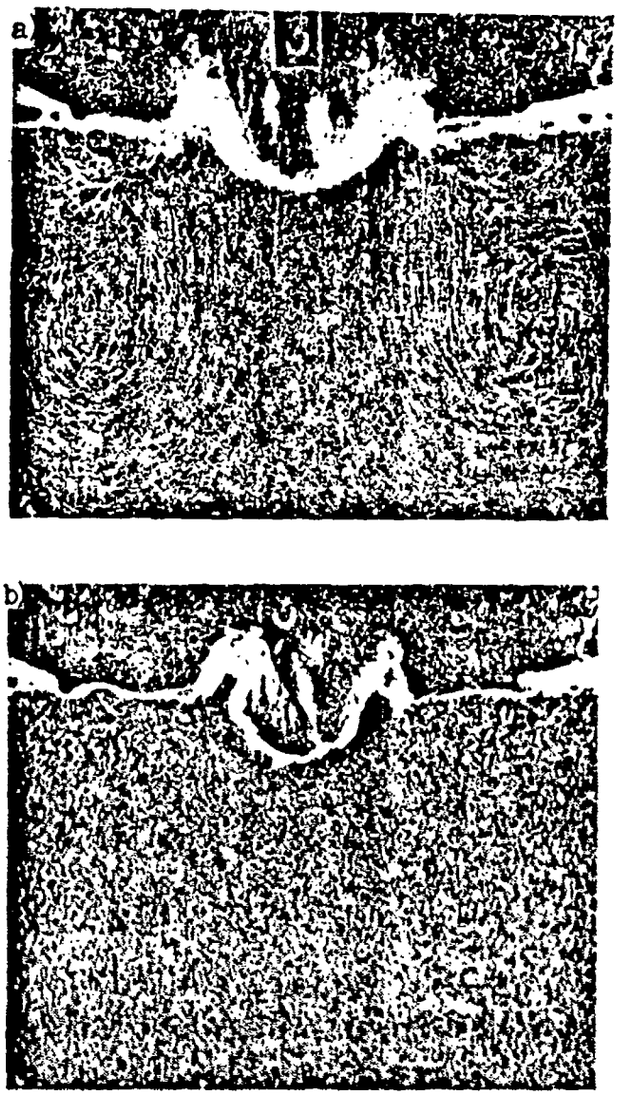

Fig. 104. Photographs illustrating the motion of the fluid which surrounds the cavity formed by the action of a two-dimensional gas stream (v_0 = 125 m/sec):
a) exposure 0.5 sec, the current lines are visibly marked by suspended particles;
b) exposure 0.03 sec, making it possible to determine the velocity field by means of the length of dashes marked by the suspended particles.

The information presented allows us to exclude from [190
(6.2) the values* $l_1, \ldots, l_n$, as well as ν; besides, since

*Let us also consider that the shape of the nozzle will provide a nearly uniform velocity field at its face.

the fluid can be considered practically at rest, then instead of ρ and g we can introduce the specific weight $\gamma = \rho g$. As a result, instead of (6.29) we obtain

$$y_1 = F(d_0, \xi_1, v_0, \nu', \rho' \sigma, \gamma_1). \qquad (6.30)$$

If we adopt some simple physical concepts, the number of variables can be additionally decreased. Actually, since the deflection of the surface is determined by the normal pressures, then instead of the parameters ρ' and v_0 their combination in the form of the product $\rho' v_0^2$ or the pulse of the stream $I = \frac{\pi d_0^2}{4} \rho' v_0^2$ within one second can be used. In a similar manner, ρ and g are combined in (6.30) by their product γ, since only the gravity manifests itself.

In addition, taking into account that only the regimes of a turbulent free stream are of practical interest, for which, according to current concepts, the flow is considered to be self-similar, we can exclude the parameter ν'. Thus, instead of the n + 9 parameters in (6.29), and the seven in (6.30), we now have only five:

$$y_1 = F(d_0, \xi_1, \rho' v_0^2, \gamma, \sigma). \qquad (6.31)$$

In transition to the dimensionless form, instead of (6.31) we obtain*

*We were able to form three dimensionless combinations from the five parameters in the right side of (6.31), because the dimension of time does not enter into these parameters, but only the dimensions of length and force, i.e., only two parameters with independent dimensions.

$$\frac{y_1}{d_0} = f\left(\frac{\rho' v_0^2}{\gamma d_0}; \frac{\xi_1}{d_0}; \frac{\sigma}{\gamma d_0^2}\right). \qquad (6.32)$$

For sufficiently large dimensions, when the capillary effects may be ignored, only two parameters will remain:

$$\frac{y_1}{d_0} = f\left(\frac{\rho' v_0^2}{\gamma d_0}; \frac{\xi_1}{d_0}\right). \qquad (6.33)$$

If we take instead of $\rho' v_0^2$ the pulse of the streams, we will obtain a relationship similar to (6.33):

$$\frac{y_1}{d_0} = f_1\left(\frac{I}{\gamma d_0^3}; \frac{\xi_1}{d_0}\right). \qquad (6.34)$$

It may appear that the problem has been reduced to the extreme limit. This simplification was accomplished through the use of the additional information and assumptions introduced in the process of the development of the problem. We can, however, indicate an approach which will lead to even greater reduction of the number of terms, even with fewer assumptions, i.e., in a formulation that [19
corresponds to (6.28).

Let us assume that the cavity is formed as a result of the action of the gas stream on the water surface and therefore will be determined if we will assign its characteristics in the cross section at a distance from the nozzle face the same as the undistrubed fluid surface. These characteristics are well defined by the pulse within one second I, by the radius of the stream r_1 at the cross section being considered, and the laws of velocity and temperature distribution in the cross section

$$\frac{v(\xi_1, \eta)}{v(\xi_1, 0)} = F_1\left(\frac{\eta}{r_1}, r_1\right); \qquad (6.35)$$

$$\frac{T'(\xi_1, \eta)}{T'(\xi_1, 0)} = F_2\left(\frac{\eta}{r_1}, r_1\right). \qquad (6.36)$$

If we now take into account the noted experimental fact in regard to the absence of any pronounced fluid motion, and consider that the cavity, especially its central part, depends on the normal pressures, then the system of defining parameters can be written in the form

$$y_1 = F\left[r_1, I, \gamma, v, F_1\left(\frac{\eta}{r_1}, r_1\right), F_2\left(\frac{\eta}{r_1}, r_1\right)\right]. \qquad (6.37)$$

In this formulation we have actually subdivided the

problem into two parts. The diameter of the stream, its density, temperature and viscosity at the face of the nozzle, the density, temperature and viscosity of the gas between the nozzle and the water surface, the distance of the nozzle from the water surface, etc.--all of these factors determine the radius of the stream and the fields of velocities and temperatures in the cross section under consideration.

Determination of the stream's radius, as well as of the fields of velocities and temperatures at a given distance from the face of the nozzle, is purely an aerodynamic problem, uncomplicated by hydrodynamic factors. Existing methods, such as those discussed in [1], can be successfully used for its solution.

The second part of the problem reflected in relationship (6.37) consists in finding the cavity's depth with given I, r_1, $F_1\left(\frac{\eta}{r_1}, r_1\right)$ and $F_2\left(\frac{\eta}{r_1}, r_1\right)$.

If we consider, as is usually done, that for the formed stream

$$F_1\left(\frac{\eta}{r_1}, r_1\right) = F_1\left(\frac{\eta}{r_1}\right); \tag{6.38}$$

$$F_2\left(\frac{\eta}{r_1}, r_1\right) = F_2\left(\frac{\eta}{r_1}\right), \tag{6.39}$$

and if we assume that these functions are universal and known, then

$$y_1 = F(I, r_1, \gamma, \sigma) \tag{6.40}$$

or in a dimensionless form [194

$$\frac{y_1}{r_1} = f\left(\frac{I}{\gamma r_1^2}; \frac{\sigma}{\gamma r_1^2}\right). \tag{6.41}$$

For a stream of sufficiently large diameter, when the influence of the surface tension forces can be disregarded, we have

$$\frac{y_1}{r_1} = f\left(\frac{I}{\gamma r_1^2}\right), \tag{6.42}$$

i.e., the dimensionless depth of the cavity is expressed through a single parameter.

The boundaries of the cold turbulent stream have the

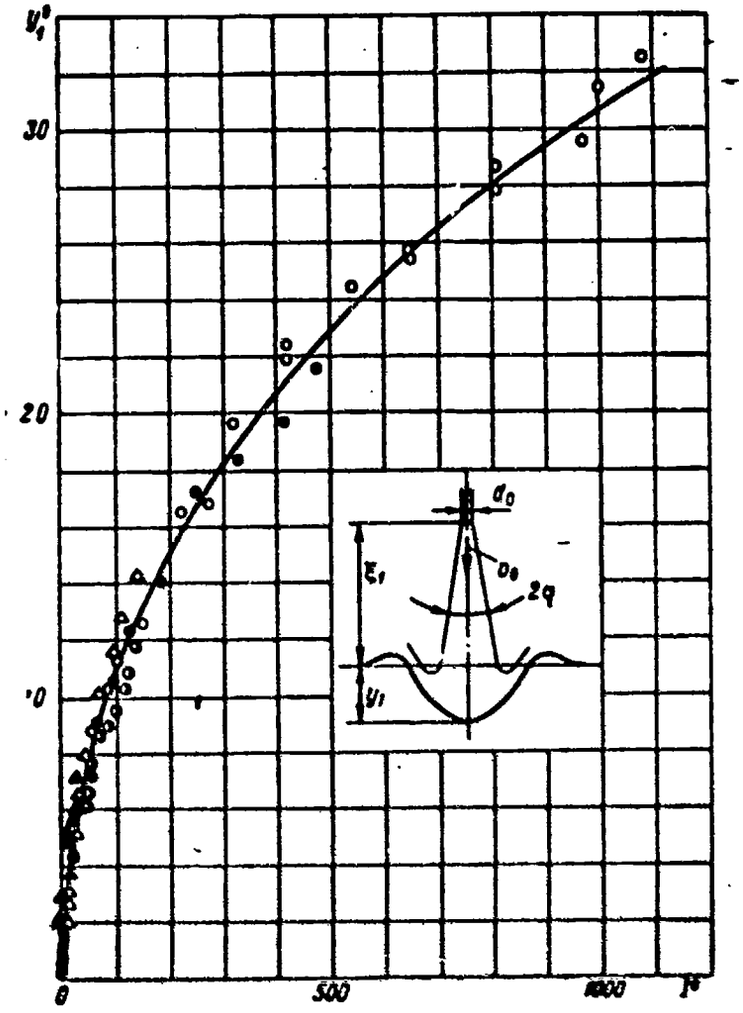

Fig. 105. Dependence of the dimensionless depth of the cavity $y^0 = \frac{y_1}{\xi_1 \operatorname{tg}\varphi + \frac{d_0}{2}}$ on the dimensionless pulse of the gas stream.

$$\bar{p} = \frac{p}{\left(\xi_1 \operatorname{tg}\varphi + \frac{d_0}{2}\right)^2}; \quad \operatorname{tg}\varphi = 0.224.$$

○ – $\bar{\xi}_1 = 2$; $d_0 = 35$ мм; ● – $\bar{\xi}_1 = 2$; $d_0 = 80$ мм;
◎ – $\bar{\xi}_1 = 2$; $d_0 = 100$ мм;
△ – $\bar{\xi}_1 = 10$; $d_0 = 35$ мм; ▲ – $\bar{\xi}_1 = 10$; $d_0 = 80$ мм;
⊙ – $\bar{\xi}_1 = 20$; $d_0 = 35$ мм.

form of straight lines inclined to the axis at an angle φ. [194
The radius of the stream can be expressed through the distance from the nozzle to the free surface ξ_1 -

$$r_1 = k\xi_1 + r_0. \qquad (6.43)$$

where k = tan φ, and $r_0 = d_0/2$ is the radius of the nozzle.

Thus,

$$\bar{y}_1 = \left(k\bar{\xi}_1 + \frac{1}{2}\right) f\left[\frac{\bar{I}}{\left(k\bar{\xi}_1 + \frac{1}{2}\right)^3}\right]. \qquad (6.44)$$

Here

$$\bar{I} = \frac{I}{\gamma d_0^3};\ \bar{\xi}_1 = \frac{\xi_1}{d_0};\ \bar{y}_1 = \frac{y_1}{d_0}. \qquad (6.45)$$

Figure 105 presents experimental data concerning the dependance between $y_1^0 = \frac{\bar{y}_1}{k\bar{\xi}_1 + \frac{1}{2}}$ and $I^0 = \frac{\bar{I}}{\left(k\bar{\xi}_1 + \frac{1}{2}\right)^3}$ for various ξ_1 and d_0 with k = tan φ = 0.224.

6.4. On Simulation of Flexible Enclosures for Air-Cushion Vehicles

The higher the body of the vehicle is lifted up by the air cushion, the greater are the obstacles (on land) or waves (on water) which the vehicle can overcome. However, as we have seen in Section 6.1, any increase in the gap requires greater air consumption and more power, which are proportional to the size of the gap. Application of the nozzle-type system makes it possible to lift the body of the vehicle somewhat higher for equal power; however, it leads to structural complications while producing relatively small effect.

A substantial improvement in the passability of ACVs is achieved through the use of special flexible enclosures, the so-called skirts. Flexible enclosures are of quite [195
diversified design, but with the same purpose: to remove the vehicle farther from the water or earth surface and to reduce air escape to a minimum. Their small inertia and their ready yielding to local deformations make vehicles fitted with skirts highly navigable on earth as well as on water.

There are three basic types of flexible enclosures:

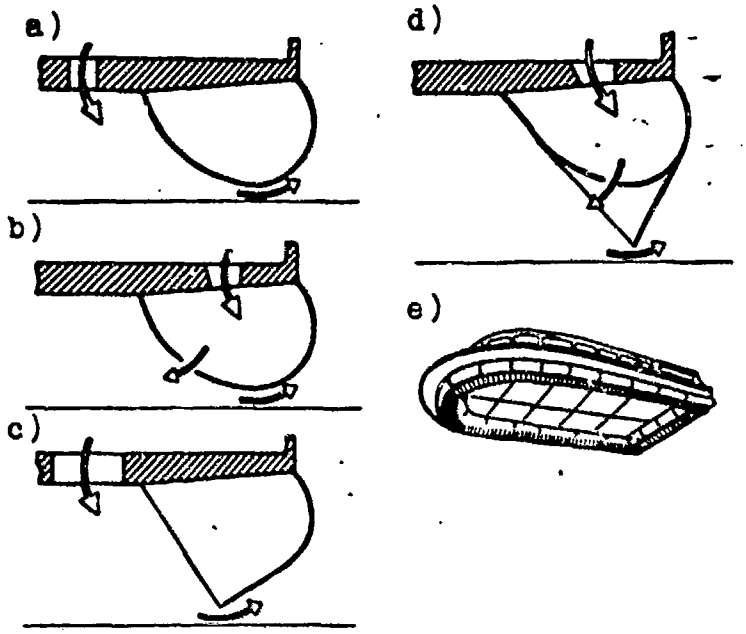

Fig. 106. Schematic drawing of the types of flexible skirts for ACVs: a) hermetically sealed flexible skirts; b) inflated bag skirt connected by channels with the receiver; c) open flexible skirt; d) combination flexible skirt; e) general composition of flexible skirts on a vehicle.

-- hermetically sealed; in the inflated state these are toroidal bodies usually located around the perimeter of the vehicle and having its shape in plan;

-- inflated bag type, but with the chamber connected by channels with a pressure air delivery system. Air, forced by the blowers, expands the bag skirt and runs out through special holes under the frame where it forms a cushion;

-- open, which take shape due to the effect of the pressure difference in the cushion and the outside area.

Variations of these types of skirts are shown in Fig. 106. They are used in various combinations and assume various configurations. A scheme for the arrangement of their elements on one of the vehicles [82] is shown in Fig. 106e. [196

The selection and analysis of the performance of the skirts under different conditions, including motion over

a seaway, is performed on models (for example, see [80]); however, the design of the flexible enclosures is a problem which has been studied little. Literature in regard to this problem practically does not exist. There is no clear concept, not only with respect to how to provide for similarity, but even which enclosures can be considered to be similar.

In analyzing regular ship models Froude's law is used and geometric similarity of outer shape is preserved. The difficulty with ACVs with flexible enclosures is the inability to specify the outer shape, since the shape is determined by the interaction of hydro-aerodynamic forces and by the weight and elastic properties of the enclosure itself.

Analyzing the steady-state motion problem first, let us consider that simulation can be accomplished if, taking into account the above-mentioned interaction, the exterior forms of the model and the full-size prototype are similar. It should be noted that similitude is not achieved in its usual concept here, but the problem under consideration narrows down to the well-studied problem of model analysis and recalculation of the data for full-size, ordinary ships.

Let us see which of the elements can be varied in order to achieve similitude. It is obvious that the following elements belong to this group: the thickness of the walls of the flexible enclosures, as well as the weight and the elastic properties of the materials from which they are made. Further, let us analyze what kind of forces will produce deviation of the shape of the flexible enclosure from geometric similitude. Of the external forces, we should first of all examine the viscosity forces, since with the adopted law of Froude's similitude and identity of the media and gravitational acceleration, the Reynolds numbers for the model and the prototype will be different. The usual influence of the Reynolds numbers on the drag of the ship is not meant here, but rather the influence which would affect the shape of the flexible enclosure if similitude with full size were attained in the thickness of the walls, the weight and the elastic characteristics.

The effect of the difference in Reynolds numbers is stipulated by the difference of the internal and external flows, with the greatest error to be expected in the diffuser regions of the stream, especially in the case where the model and the prototype are located on different sides of the critical Reynolds number. In Fig. 107 is a drawing of an example of the effect of Reynolds numbers on the

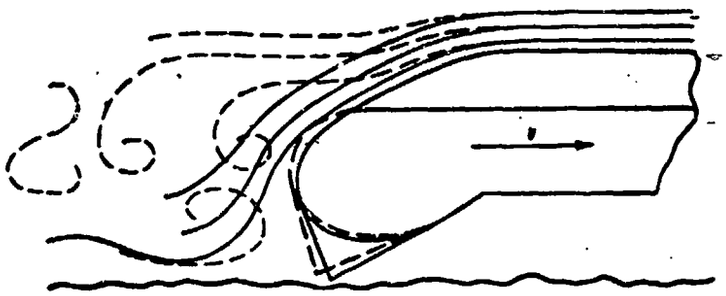

Fig. 107. Schematic presentation of variation of the shape of a flexible enclosure under the action of changes in the flow around the ship at subcritical (dotted lines) and supercritical Reynolds numbers.

geometry of a vehicle. If the configuration of the vehicle and the conditions of motion under analysis are such that the indicated influences are unessential, then the differences between the Re numbers may be disregarded.

In the case of small models, wettability can also play a role. If we ignore the above-mentioned effect of the Reynolds numbers and the surface tension forces and provide a wall for the flexible enclosure of the model in accordance with its scale from material with a specific gravity equal to the specific gravity of the walls of the enclosure for the prototype, and if the elastic characteristics are such that the Cauchy number of the model and the prototype are maintained equal, then geometric similitude of the outline of the flexible enclosures* will be fulfilled. This

*It is assumed that the layout and attachment of the flexible enclosures are similar.

approach, however, would be strictly formal and the fulfillment of these conditions presents many technical difficulties.

It is necessary to clarify whether there are other ways of simulation which provide sufficient accuracy in the preservation of similitude without setting stiff requirements on the thickness of the walls and the material of the enclosure. Let us evaluate the effect of weight and elastic properties on the shape of the enclosure. The weight of the wall varies within relatively wide limits,

but judging, for example, by prospectuses from the Hovercraft Company, it does not exceed a few kilograms per square meter. The projection of this force onto the normal to the area under consideration will constitute an even smaller value, which can be considered negligibly small in comparison to the pressure drops in the cushion $\Delta p \approx 100\text{-}400$ kg/m^2.

In most cases the elastic deformations that are related to flexure of the wall surfaces, as well as to its expansion, are not important. The possibility of analyzing the walls of a flexible enclosure as having zero-moment is based on their small thickness, comprising, usually, a fraction of a millimeter or a few millimeters, while the size of the radii of curvature is two or three orders greater. The tensile stresses σ_p in a shell of thickness δ with excess internal pressure Δp can be expressed as follows:

$$\sigma_p = \frac{\Delta p}{\delta} \cdot \frac{1}{1/R_1 + 1/R_2} < \Delta p \frac{R_1}{\delta}, \qquad (6.46)$$

where R_1 and R_2 are the radii of curvature of the shell at the given point; $R_1 < R_2$. With values of Δp typical for contemporary vehicles ($\Delta p < 400$ kg/m^2) and $\frac{R_1}{\delta} < 1000$, from (6.46) we obtain $\sigma_p < 0.4$ kg/mm^2. [1

Corresponding to these values* of σ_p are the elonga-

*Designs can exist, for the individual elements of which the presented evaluations of flexibility are not valid. This can take place for nearly flat regions, where R_1 is very large, and also for isolated guy wires, where considerable stresses and deformations occur. These separate elements can and should be simulated from the condition of deformation similitude by including specially selected elastic inserts.

tions of the material, which do not exceed 2-3%. The effects of variations in the shape of the flexible inclosure specified by this type of deformations lie within the limits of accuracy and virtually do not affect the hydrodynamic characteristics of the vehicles being investigated.

Thus, the preparation of the model for the steady-state condition of the flexible enclosure must satisfy only unilateral limitations: the weight with respect to the

cubed linear dimensions and the elastic relative deformations of the walls of the flexible enclosure of the model must be smaller than or equal to the corresponding values of the full-size prototype. These conditions are easily satisfied, since according to Froude's law the stresses in the model must decrease in the same proportion as its dimensions. In accordance with the stresses the relative deformations will also decrease, and this in turn makes it possible, changing to smaller relative thickness, to obtain necessary values for the relative weight of the enclosure, even when heavier materials are used.

The problem of simulation becomes substantially more difficult in analyzing unsteady motion--impact against a wave or an obstacle, auto-oscillations while hovering above a screen, etc. In these problems the similitude must be achieved among the inertia and elastic forces. The means for achieving these requirements depend on the type of enclosure used.

Let us first analyze the hermetically sealed enclosure shown in Fig. 106a. Let us formulate the first problem as follows: the bag is made from an unstretchable, zero-moment shell containing gas under excess pressure Δp. The shell is surrounded by the same gas under pressure p_0. It is necessary to find the conditions of similitude for the case of restoration by the shell of its former shape after deformation as a result, for example, of impact against a wave.

Let us first of all establish the factors on which depends the motion of the wall of a shell which has thickness δ and density ρ_c. The inertia forces, along with the linear dimensions l, l_1, ..., l_n, which characterize the shell and the deformation, and the values δ and ρ_c, will be related to the associated inertia and hence to the density ρ' of the air. Since the excess pressure Δp inside the shell is small as compared to the ambient pressure p_0, the density of the air inside and outside the bag can be assumed to be equal. The ability of the shell to restore its original shape will be determined by the forces of excess pressure Δp, as well as by the additional increase in pressure dp due to the decrease in volume caused by the deformation of the bag. This increase in pressure is expressed in terms of the modulus of buoyancy of the air E and the relative volumetric deformation dV/V [199

$$dp = -E\frac{dV}{V}. \qquad (6.47)$$

If we consider that the temperature of the gas in the bag varies little, then $E \approx p_0$. Thus, the system of defining parameters can be written in the form

$$l, l_1, \ldots, l_n, \delta, \rho_c, \rho', \Delta p, p_0. \tag{6.48}$$

Below, instead of the two values δ and ρ_c it is advantageous to introduce the unit of mass of the shell surface

$$m_1 = \rho_c \delta, \tag{6.49}$$

since the inertia properties are specifically defined by the value m_1, while the density and the thickness of the shell do not enter into any other relationships.

Any quantity which characterizes the process under analysis is a function of the parameters (6.48); specifically, the time τ, during which a shell deformed by the impact of a wave is restored to its former shape, can, with consideration of (6.49), be written in the form

$$\tau = F(l, l_1, \ldots, l_n, m_1, \rho', \Delta p, p_0). \tag{6.50}$$

For similar shapes of the bag and initial deformations we obtain from (6.50)

$$\frac{\tau}{l}\sqrt{\frac{\Delta p}{\rho'}} = f\left(\frac{m_1}{\rho' l}, \frac{\Delta p}{p_0}\right). \tag{6.51}$$

Expression (6.51) demonstrates that in order to achieve similitude it is necessary to maintain the constancy of the values $\frac{m_1}{\rho' l}$ and $\frac{\Delta p}{p_0}$. At the same time the corresponding increments of time for the model τ_M and for the prototype τ_H will be expressed as follows:

$$\frac{\tau_M}{\tau_H} = \frac{l_M}{l_H}\sqrt{\frac{\rho_M \Delta p_H}{\rho_H \Delta p_M}}. \tag{6.52}$$

Taking into consideration that from the conditions of similitude $\frac{\Delta p_H}{\Delta p_M} = \frac{p_{0H}}{p_{0M}}$ and that according to the equation describing the state of the gas

$$\frac{p_0}{\rho'} = BT, \tag{6.53}$$

where B is the specific gas constant, and T is the absolute temperature, we can write instead of (6.52) [200

$$\frac{\tau_M}{\tau_H} = \frac{l_M}{l_H}\sqrt{\frac{T_H}{T_M}\cdot\frac{B_H}{B_M}}. \qquad (6.54)$$

If we analyze the deformation of the bag not as an isolated problem, but rather as one integral to the air-cushion vehicle, and consider that simulation of the motion of these vehicles is done on the basis of Froude's law of similitude, then as an additional condition we should require that $\frac{\tau_M}{\tau_H} = \sqrt{\frac{l_M}{l_H}}$. Precisely in this relationship are the intervals between encounters of the ship with waves for the model and the prototype. From this additional condition it follows that with $B_M = B_H$

$$\frac{T_H}{T_M} = \frac{l_H}{l_M}, \qquad (6.55)$$

i.e., the absolute temperature of the gas that surrounds and fills the bag should change during simulation proportionally to the linear dimensions. This conclusion could have been obtained immediately if we would have included into the parameters of (6.48) the value of the gravitational acceleration, which, even though it does not participate in the process under consideration, should be taken into account, considering the combination of the phenomena connected with the motion of an ACV*.

---

*Unfulfillment of the condition (6.55) will lead to the emergence of the scale effect, which consists in the fact that the shape of the shell after the impact will be restored quicker in the model than in the full-size prototype. This can be demonstrated by the following simple example: let the pressure Δp_H in the prototype be 300 kg/m^2 and the value of the relative deformation $\frac{\Delta V}{V}$ = 1%; then the additional pressure stipulated by compressibility will be $dp_H = p_0 \frac{dV}{V}$ = 100 kg/m^2, and the restoration of the original shape will start under the action of excess pressure $\Delta p_H + dp_H$ = 400 kg/m^2. For the model with the scale 1:10 the pressure in the cushion, set up on the basis of Froude's law, will be Δp = 30 kg, while $dp_M = dp_H$, and therefore

$\Delta p_M + dp_M = 130$ kg instead of 40 kg, as it should have been in accordance with Froude's law of similitude. If the pressure in the cushion is similated according to (6.51) then $\Delta p_M + dp_M = 400$ kg.

For open type enclosures the complications in simulation stipulated by the condition (6.55) are virtually eliminated, because the parameter p_0 becomes unessential. Excluding p_0 from (6.50) and introducing, according to the above considerations, g, we will obtain instead of (6.50)

$$\tau = F(l, l_1, \ldots, l_n, m_1, \rho', \Delta p, g) \qquad (6.56)$$

and instead of (6.51)

$$\frac{\tau}{l}\sqrt[3]{\frac{\Delta p}{\rho'}} = f\left(\frac{m_1}{\rho' l}, \frac{\Delta p}{\rho' g l}\right). \qquad (6.57)$$

Since during simulation $\rho'_M = \rho'_H$ and $g_M = g_H$, then [201
from (6.57) it follows that the mass of a unit area of the wall m_1 and the excess pressure Δp must vary in proportion to the linear dimensions, and in addition

$$\tau = \text{const}\sqrt{l}.$$

If we analyze the flexible enclosure shown in Fig. 106b, it is easy to see that with very small channel dimensions and clearances we will arrive at the case of the hermetically sealed enclosure, while for channels with large dimensions, at the case of an open enclosure.

The obtained expression for the recalculation of the time of recovery of a shell deformed as the result of an impact will hold for any other characteristic time. The arguments of the function in the right side of (6.56) will define not only the time but also any other characteristics of the motion of the walls of an enclosure not in contact with water. If the hydrodynamic forces are taken into account, then to the terms of (6.56) would be added the density ρ and the viscosity ν of the water, as well as the velocity v. Correspondingly, the number of dimensionless combinations will increase by three as follows: the relationship ρ'/ρ will appear, as will the Reynolds number $\mathrm{Re} = vl/\nu$ and Froude number $\mathrm{Fr} = v/\sqrt{gl}$. The second of these

is fulfilled automatically, the simulation in Froude numbers was foreseen from the very beginning, while unfilfillment of similitude with respect to the Reynolds numbers will result in a scale effect related to the unidentical (for the model and the full size) deformations of the enclosure under the action of friction forces in water.

Summarizing the considerations with respect to the simulation of flexible enclosures, we can formulate the following basic concepts: in a geometrically similar layout the mass (or weight) of a unit area of the wall and the pressure in the cushion should vary proportionally to the linear dimensions. The elastic properties of the material may, as a rule, be ignored. The properties of the enclosure wall should approach those of a zero-moment, unstretchable shell; its thickness, as such, plays no role. In the case of elements of an open type enclosure and with large sizes of channels and clearances, fulfillment of these conditions is provided (with precision to the influence of the Reynolds numbers) by similitude of the external shape of the enclosure for steady-state or unsteady motion. With enclosures in the form of hermetically sealed bags the scale effect appears, which is caused by the absence of similitude in the compressibility of the gas in the bag and which leads, specifically, to decrease of the corresponding time intervals for the model (as compared to intervals under Froude's law of similitude). If the enclosures have air passages, then the mentioned scale effect will decrease with increasing cross-sectional area of the air passages*.

---

*All the channels which connect the area of the cushion with the atmosphere, and specifically the channels of the fan, are among the elements of air passages.

BIBLIOGRAPHY

1. Abramovich, G. N. Teoriya turbulentnykh struy [The Theory of Turbulent Streams]. Moscow, Fizmatgiz, 1960.

2. Alabushev, P. M. et al. Teoriya podobiya i razmernostey, modelirovaniye [Theory of Similitude and Dimensional Analysis--Simulation]. Moscow, Vysshaya shkola, 1968.

3. Basin, A. M. Khodkost' i upravlyayemost' sudna [Ship Sailability and Maneuverability], Part 1. Transport, 1968.

4. Birkhoff, G. and E. Sarantonello. Strui, sledy, kaverny [Streams, Wakes, Cavities]. Moscow, Mir, 1964.

5. Blyumin, V. I., Experimental Analysis of Hydrodynamic Forces Acting on a Partially Submerged Vertical Strut, Technical Reports of TsAGI, No. 186, 1960.

6. Vladimirov, A. N., Lifting Force of the Hydrofoil Near the Free Surface, Sudostroyeniye, No. 6, 1937.

7. Vladimirov, A. N., Concerning the Motion of Hydrofoil Ships, Sudostroyeniye, No. 7, 1938.

8. Voytkunskiy, Ya. I., R. Ya. Pershits and I. A. Titov. Spravochnik po teorii korablya [Handbook on the Theory of Ships]. Leningrad, Sudpromgiz, 1960.

9. Voytkunskiy, Ya. I. Soprotivleniye vody dvizheniyu sudov [Water Resistance to Ship Motion]. Leningrad, Sudostroyeniye, 1964.

10. Volynskiy, M. S., Concerning Break-up of Drops in an Air Stream, DAN SSSR, Vol. 12, No. 3, 1948.

11. Gurevich, M. I. Teoriya struy ideal'noy zhidkosti [Theory of Streams of an Ideal Fluid]. Moscow, Fizmatgiz, 1961.

12. Keldysh, M. V. and M. A. Lavrent'yev, Concerning the Motion of a Hydrofoil Under the Surface of a Heavy Fluid, IN: Transactions of the Conference on the Theory of Wave Drag, TsAGI, 1937.

13. Kirpichev, V. L. Besedy po mekhanike [Discussions on Mechanics]. Moscow-Leningrad, GITTL, 1951.

14. Kotlyar, L. I. and A. G. Terent'yev, A Nonlinear Problem on Cavitation Flow of a Weighable Fluid Around a Plate,

IN: "Ship Propulsion Devices and Cavitation," Materials on the Exchange of Experience, No. 106, Leningrad, Sudostroyeniye, 1968.

15. Kochin, N. Ye., I. A. Kibel' and N. V. Roze. Teoreticheskaya gidromekhanika [Theoretical Hydromechanics], Part 2. Moscow, Fizmatgiz, 1963.

16. Krylov, V. V., Experimental Materials Concerning the Carrying Away of Gas from a Cavity Formed by the Method of Additional Blowing, IN: "Articles Concerning the Problems of Cavitation Flows," Transactions of TsAGI, No. 824, 1961.

17. Kuznetsov, B. G., V. N. Shepelenko and N. N. Yanenko, Calculation of the Cavity Shape with Consideration of the Gravity and Surface Tension Forces, IN: Tretiy vsesoyuznyy s"yezd po teoreticheskoy i prikladnoy mekhanike [Third All-Union Conference on Theoretical and Applied Mechanics], Annotations of Papers, Moscow, 1968.

18. Logvinovich, G. V., Flows with Developed Cavitation, Inzhenernyy zhurnal, Vol. 1, No. 1, 1961.

19. Logvinovich, G. V., Hydromechanics of Flows with Free Boundaries, Transactions of TsAGI, No. 935, 1965.

20. McCormick. Cavitation Caused by the Free Vortex Trailing the Carrying Surface, Transactions of the American Society of Mechanical Engineers, Series D, Tekhnicheskaya mekhanika, Vol. 84, No. 3, 1962.

21. Nogid, L. M. Teoriya podobiya i razmernostey [The Theory of Similitude and Dimensions]. Leningrad, Sudpromgiz, 1959.

22. Oshima, R., Theory of the Influence of the Scale Effect on the Inception of Cavitation on Axisymmetric Bodies, Transactions of the American Society of Mechanical Engineers, Series D, Tekhnicheskaya mekhanika, Vol. 83, No. 3, 1961.

23. Pavlenko, G. Ye. Soprotivleniye vody dvizheniyu [203
sudov [Water Resistance to Ship Motion]. Moscow, Morskoy Transport, 1956.

24. Pernik, A. D. Problemy kavitatsii [Problems of Cavitation], 2nd edition, Leningrad, Sudostroyeniye, 1966.

25. Prandtl, L. Gidroaeromekhanika [Hydro-aeromechanics]. Moscow, IL, 1949.

26. Ruzhitskiy, Ye. I. Vozdushnyye vezdekhody [All-Terrain Hovercraft]. Moscow, Mashinostroyeniye, 1964.

27. Sedov, L. I., Steady-State Planing, Sudostroyeniye No. 2, 1937.

28. Sedov, L. I., Two-dimensional Problem of Planing Along the Surface of a Heavy Fluid, IN: "Proceedings of the Conference on the Theory of Wave Drag," Publishing House TsAGI, Moscow, 1937.

29. Sedov, L. I., Concerning Scale Effect and the Most Advantageous Relationships for Gliding, Transactions of TsAGI, No. 439, 1939.

30. Sedov, L. I., Planing Along the Water Surface, Tekhnika vozdushnogo flota, No. 4-5, 1940.

31. Sedov, L. I. and A. N. Vladimirov, Planing of a Flat-Keeled Plate, DAN SSSR, Vol. 33, No. 2, 1941.

32. Sedov, L. I. and A. N. Vladimirov, Stability of Planing of a Keeled Plate, DAN SSSR, Vol. 33, No. 3, 1941.

33. Sedov, L. I. Metody podobiya i razmernosti v mekhanike [Methods of Similitude and Dimensions in Mechanics], 3rd edition. Moscow, GITTL, 1954.

34. The State of the Art of the Hydro-Aerodynamics of Viscous Fluid, ed. by Goldshteyn, trans. from English under the editorship of N. Ya. Fabrikant, Vol. 2. Moscow, GIIL, 1948.

35. Spravochnik aviakonstruktora [Aircraft Designer's Handbook], Vol. 2. Moscow (Central Aero-hydrodynamic Institute), 1937.

36. Teoreticheskaya mekhanika [Theoretical Mechanics], ed. N. V. Roze, Part 1. Moscow-Leningrad, GTTI, 1932.

37. Khaskind, M. D., Hydrodynamic Theory of Ship Rolling and Pitching on Rough Sea, PMM, Vol. 10, No. 1, 1946.

38. Khaskind, M. D. and I. S. Riman, Methods of Determining Characteristics of Ship Rolling and Pitching, Izv. AN SSSR, OTN, No. 10, 1946.

39. Hall, D. U. and G. E. Vislisenus, Size Effect in Cavitation, IN: Transactions of the American Society of Mechanical Engineers, Series D, Tekhnicheskaya mekhanika, Vol. 83, No. 3, 1963.

40. Chaplygin, Yu. S., Planing of a Flat Plate of Infinite Span Along the Surface of Heavy Fluid, Transactions of TsAGI, No. 508, 1940.

41. Epshteyn, L. A., Vibrations of a Cylinder in Viscous Fluid, Transactions of TsAGI, No. 233, 1935.

42. Epshteyn, L. A., Some New Experimental Data Concerning the Phenomenon of Planing, DAN SSSR, Vol. 26, No. 8, 1940.

43. Epshteyn, L. A., New Experimental Materials Concerning Planing of Thin Plates, Transactions of TsAGI, No. 508, 1940.

44. Epshteyn, L. A., Scale Effect of Waves and Sprays Formed by Planing Ships, Transactions of TsAGI, No. 469, 1940.

45. Epshteyn, L. A., Stability of Planing, Transactions of TsAGI, No. 500, 1941.

46. Epshteyn, L. A., On Possibilities for the Theoretical Study of Cavitation Considered as the Motion of a Special Type of Compressible Fluid, DAN SSSR, Vol. 49, No. 6, 1945.

47. Epshteyn, L. A., Inception and Development of Unidimensional Cavitation Flows, Izv. AN SSSR, No. 6, 1946.

48. Epshteyn, L. A., The Effect of the Transverse Profile of a Hydroplane Boat Bottom on Stability, Transactions of TsAGI, No. 583, 1946.

49. Epshteyn, L. A., Cavitation and the Possibility of its Theoretical Study Considered as the Supersonic Flow of a Compressible Hypothetic Fluid, Transactions of TsAGI, 1946; Transactions of TsAGI, No. 656, 1948.

50. Epshteyn, L. A., Inception and Development of Cavitation (Dissertation, 1946), Transactions of TsAGI, No. 656, 1948.

51. Epshteyn, L. A., Determining Characteristics of Ship Propellers with Small Cavitation Numbers, Transactions of TsAGI, No. 689, 1956.

52. Epshteyn, L. A., Analysis of the Conditions of Air Entry and the Simulation of Hydrofoil Motion, Technical Reports of TsAGI, No. 143, 1958.

53. Epshteyn, L. A., Experimental Analysis of Axisymmetric Cavitation Flows in a Test Basin, Transactions of TsAGI, No. 710, 1958.

54. Epshteyn, L. A., On Inception of Cavitation in Vortex Filaments Trailing a Finite-Span Hydrofoil, Transactions of TsAGI, No. 716, 1958. [204

55. Epshteyn, L. A., Flows Near Bodies of Revolution at Small Cavitation Numbers, Transactions of TsAGI, No. 817, 1961.

56. Epshteyn, L. A., Inception and Development of Cavitation (Paper presented at the First All-Union Conference on Theoretical and Applied Mechanics, 1960), Transactions of TsAGI, No. 824, 1961.

57. Epshteyn, L. A., V. I. Blyumin and P. S. Starodubtsev, Effect of the Cavitation and Froude Numbers on the Size of the Cavity and the Amount of Air Necessary for its Existence, IN: "Collection of Articles on Cavitation Flows," Transactions of TsAGI, No. 824, 1961.

58. Epshteyn, L. A., On Surfacing of the Cavitating Cavity in Heavy Fluid, ibid.

59. Epshteyn, L. A., Determining the Amount of Gas Necessary to Maintain the Existence of a Cavity Behind a Body Moving Horizontally with Small Froude Numbers, ibid.

60. Epshteyn, L. A. and G. M. Kryukov, Analysis of an Operating Model of a "Rotating Tunnel," Technical Reports of TsAGI, No. 204, 1961.

61. Epshteyn, L. A., V. I. Blyumin and A. P. Fadyushin, Experimental Determination of the Amount of Gas Carried Away and of the Length of the Cavity Behind Cones, Transactions of TsAGI, No. 1100, 1968.

62. Epshteyn, L. A., Solution of Thompson's Problem Concerning Ship Waves with the Aid of the Theory of Dimensional Analysis, Transactions of KTIRP, No. 15, 1962.

63. Epshteyn, L. A., Deformation of the Free Surface Behind a Hydrofoil, Transactions of TsAGI, No. 932, 1964.

64. Epshteyn, L. A. and V. I. Blyumin, Concerning the Effect of the Shape of the Body on the Cavity Formed Behind This Body and on the Gas Carried Away, Materials on the Exchange of Experience, 1965, No. 106, Leningrad, Sudostroyeniye.

65. Epshteyn, L. A., On the Effect of the Froude Number and the Submergence on the Size of the Cavity and on the

Carrying Away of Gas, Transactions of TsAGI, No. 950, 1965.

66. Epshteyn, L. A. and V. I. Klyumin, Studies of Developed Cavitation Flows in a Rotating Tunnel, Transactions of TsAGI, No. 950, 1965.

67. Epshteyn, L. A., V. I. Klyumin and A. P. Fadyushin, Analysis of the Carrying Away of Gas from the Cavity Behind a Disc at Large Froude Numbers, IN: Papers for the 16th Scientific-Technical Conference on the Theory of the Ship (Krylov's Lectures), Leningrad, 1966 (NTO Sudprom, No. 73).

68. Epshteyn, L. A., On the Minimum Cavitation Number and the Width of the Cavity in Two-dimensional and Axisymmetric Canals, Izv. AN SSSR, MZhG, No. 5, 1966.

69. Epshteyn, L. A. and I. E. Vol'grot, Concerning the Cavity Formed Under the Action of a Vertical Gas Stream Against the Surface of a Fluid, Transactions of TsAGI, No. 1061, 1967.

70. Epshteyn, L. A., Consideration of the Effect of the Canal Walls on the Size of the Middle of the Cavity, Izv. AN SSSR, MZhG, No. 2, 1968.

71. Epshteyn, L. A. and V. I. Klyumin, Some Problems of Hydrodynamics of Hydrofoils, Transactions of TsAGI, No. 1103, 1968.

72. Birkhoff G., Plesset M. and Simmons N. Wall effects in cavity flow.— Quarterly of applied mathematics, vol. 8, N 2, 1950, vol. 9, N 4, 1952.

73. Campbell I. and Hilborne D. V. Air Entrainment Behind Artificially Inflated Cavities. Second Symposium of Naval Hydrodynamics, Washington, 1958.

74. Cox R. N. and Clayden W. A. Air Entrainment at the rear of a steady cavity.— Cavitation in Hydrodynamics, London, 1956.

75. Förtmann E. Über die turbulente Strahlausbreitung.— Ingenieur-Archiv, vol. 5, N 1, 1934.

76. Kermeen R. W., Mc Graw J. T. and Parkin B. R. Mechanism of Cavitation Inception and the Related Scale-Effects Problem.— Transactions of the ASME, vol. 77, N 4, May 1955.

77. Martyrer E. Kraftmessungen an Wiederstandskörpern und Flügelprofilen im Wasserstrom bei Kavitation.— Hydromechanische Probleme des Schiffsantriebs, Hamburg, 1932.

78. Numachi F. Kraftmessungen an vier Flügelprofilen bei Hohlsog.— Forschung auf dem Gebiete des Ingenieurwesens, Band 11, Nr. 6, 1940.

79. Prandtl L. Tragflügeltheorie, Band 2. Aus den Nachrichten der K. Gesellschaft der Wissenschaften zu Göttingen. Mathematisch-physikalische Klasse, 1919.

80. Rapson J. E. Research and Development International Hovercraft Conference 1968.— Aircraft Engineering, May 1968.

81. Sottorf W. Versuche mit Gleitflächen.— Werft—Reederei—Hafen, N 21, 1929; N 19, 1932.

82. Stanton-Jones R. The Future Development of Hovercraft. International Hovercraft Conference, 1968.— Aircraft Engineering, May 1968.

83. Streeter Victor L. Handbook of Fluid Dynamics. New York, Toronto, London, 1961.

84. Trupel T. Über die Einwirkung eines Luftstrahles auf die umgebende Luft.— Zeitschrift für das gesamte Turbinenwesen, N 5—6, 1915.

[205

85. Vennard I. Nature of Cavitation. Proceedings American Society of Civil Engineers, V. 71, N 7, September, 1945.
86. Wadlin K. L. Mechanics of ventilation inception. Second Symposium of Naval Hydrodynamics, 1958, Washington, 1960.
87. Walchner O. Profilmessungen bei Kavitation.— Hydromechanische Probleme des Schiffsantriebs, Hamburg, 1932.
88. Wetzel I. M. Ventilation of bodies piercing a free surface. Second Symposium of Naval Hydrodynamics, 1958, Washington 1960.